In Vitro Human Cell Transplantation for Engineering the Hard-Soft Tissue Interface: A Soluble Phosphate Based Glass Fibre Scaffold System

Malak Bitar

UCL Eastman Dental Institute,
256 Gray's Inn Road
London
WC1X 8LD

This thesis is submitted in fulfilment of the
requirements for the degree of PhD
University of London

ProQuest LLC
789 East Eisenhower Parkway
P.O. Box 1346
Ann Arbor, MI 48106-1346

November 2005

To Nicoletta,
My wife...
My love...
My home...

To Daniele Antonio,
My son...
May a smile always shine on your face...

"Imagination is more important than knowledge"
A Einstein

Declaration

I declare that all the experiments in this thesis were carried out by the author, Malak Bitar, unless otherwise stated:

The results outlined in Chapter Four, Section 4.3.2.3, were obtained by Dr Iolo ap Gwynn at the Institute of Biological Sciences, The University of Wales.

Summary: Abstract

This work investigated the biocompatibility of soluble phosphate based glasses as scaffolds for supporting the *in vitro* morphogenesis the hard-soft tissue interface (enthesis) as an approach dealing with ligaments and tendons clinical problems.

The short term response of human oral osteoblasts (HOB), oral fibroblasts (HOF) and flexor tendon fibroblasts (HTF) was assessed on glass discs of various compositions, and different dissolution rates, of the generic ternary form $(CaO)_{0.0x}$-$(Na_2O)_{0.0y}$-$(P_2O_5)_{0.5}$ through evaluating the maintenance of the seeded cell attachment, survival, proliferation and phenotype by using SEM, immunocytochemistry and the CyQUANT cell density kit. Subsequently, the most biocompatible ternary glass compositions were utilised for fibre production.

The effect of fibre diameter of cell adhesion and survival was determined and quaternary glass fibres, of the generic composition $(CaO)_{0.46}$-$(Na_2O)_{0.0x}$-$(Fe_2O_3)_{0.0y}$-$(P_2O_5)_{0.50}$, where characterised in terms of diameter and solubility profiles.

Three-dimensional scaffolds were produced from these fibres and the long term viability, morphology and population growth of the seeded HOB and HOF cells were determined using immunocytochemistry and direct cell count. This was coupled with application of qPCR experiments to evaluate the maintenance of differentiation of the seeded cell population.

The role of extrinsic factor inclusion in enhancing *in vitro*, scaffold associated, tissue morphogenesis was also investigated by stimulating osteogenic differentiation in the seeded HOB cell population. An open lamellar flow bioreactor providing nutrients, oxygen and waste perfusion to the cell-scaffold culture was deigned and assessed. The feasibility of simulating the anatomical architecture of the enthesis has also been addressed as cells were seeded in co-culture on a continuous fibre arrangement.

In this study, quaternary phosphate based glass fibre scaffolds containing 3 mol% iron oxide (Fe_2O_3), of approximately 30 μm in diameter, and of the composition $(CaO)_{0.46}$-$(Na_2O)_{0.01}$-$(Fe_2O_3)_{0.03}$-$(P_2O_5)_{0.50}$ have been shown to support HOB and HOF attachment, well spread morphology, survival and proliferation with no negative impact of cell differentiation. Induction of osteogenesis in the scaffold culture has resulted in up-regulating HOB related gene transcription and the flow culture system, at certain flow rates, has been verified for future use. The Co-culture system design has been successfully implemented as HOB and HOF cells were seeded with an acellular separation zone across the fibre scaffold arrangement.

Papers/Communications

Papers

Bitar, M., Salih, V., Mudera, V., Knowles, J.C. and Lewis, M.P. (2004).
Soluble phosphate glasses: *in vitro* studies using human cells of hard and soft tissue origin. Biomaterials.*25*,2283-92.

Bitar, M., Knowles, J.C., Lewis, M.P., Salih, V. (2005).
Soluble Phosphate Glass Fibers for Repair of Bone-Ligament Interface. Journal of Materials Science: Materials in Medicine. *16*, 1131 – 1136.

Published abstracts

Bitar, M., Ahmed, I., Knowles, J.C., Salih, V. and Lewis, M.P.
Development of novel soluble glasses for tissue engineering of hard tissue. European Cells and Materials, Vol. 4. Suppl. 2, 2002 (pages 138-139) ISSN 1473-2262

Bitar, M., Knowles, J.C., Salih, V. and Lewis, M.P.
Biocompatible phosphate glass fibre scaffolds: Engineering of the hard/soft tissue interface. European Cells and Materials Vol. 7. Suppl. 1, 2004 (page 26) ISSN 1473-2262

Oral Presentations

September 2002. Cell adhesion and migration: the Interface with Tissue Engineering. The University of Nottingham, Centre for mathematical Medicine
Bitar, M., Knowles, J.C., Salih, V. and Lewis, M.P. Development of Novel Soluble Glasses for Hard Tissue Engineering.

September 2005. European Society for Biomaterials Conference, Sorrento, Italy.
Bitar, M., Knowles, J.C., Salih, V. and Lewis, M.P. Phosphate-Based Glass Fibre System: An Inductive Approach to the Hard-Soft Interface Repair.

Poster presentations

September 2002. Tissue and Cell Engineering Society (TCES) 2002. The University of Glasgow.
Bitar, M., Ahmed, I., Knowles, J.C., Salih, V. and Lewis, M.P.
Development of novel soluble glasses for tissue engineering of hard tissue.

Acknowledgements

I would like to thank my primary supervisor, Dr Mark Lewis, for leading this project and providing me with mentorship, excellent scientific advice and academic support throughout. Most of all, I thank him for encouraging creativity and independent thinking.

I would also like to express my sincere gratitude for my supervisor, Dr Vehid Salih, for granting me training and prompt scientific advice; for his tremendous help in editing this thesis and most of all; for his encouragement when motivation was needed.

I greatly appreciate the help of Professor Jonathan C Knowles, Dr Iftikhar Ahmed, Andrea A Sinanan and Nicky Mordan whose contribution was vital for the conduct of this work.

I acknowledge the help of Dr Chris Irwin at Queen's University, Belfast, in providing the primary oral fibroblasts and that of Dr Vivek Mudera at The Institute of Orthopaedics and Musculo-Skeletal Science, UCL, in providing the primary human tendon fibroblasts.

Finally, I thank Dr Iolo ap Gwynn at the Institute of Biological Sciences, The University of Wales, for kindly performing the SEM analysis of the glass fibres.

This project was funded by The EPSRC and The Lord Dowding Fund.

Table of Contents

List of Abbreviations

°C	Degrees Celsius, temperature
µg	Microgram, weight
µl	Microlitre, volume
µM	Micro molar, concentration
µm	Micrometer, length
AA	Ascorbic acid
ACL	Anterior cruciate ligament
ANOVA	Analysis of variance
BMP	Bone morphogenic protein
BSA	Bovine serum albumin
BSP	Bone Sialoprotein
CaO	Calcium oxide
Cbfa-1	Core binding factor alpha 1
cDNA	Complementary DNA
CMFDA	5-chloromethylfluorescein diacetate
CO_2	Carbon dioxide
COL1A1	Collagen type I alpha polypeptide 1 subunit
COL-I	Collagen, type 1
C_T	Threshold Cycle
Cy3	Carbocyanine 3
DAPI	4',6-Diamidino-2-phenyindole
dH_2O	Distilled water
D-MEM	Dulbecco's Modified Eagles Medium
DMSO	Dimethylsulphoxide
DNA	Deoxyribonucleic Acid
dNTP	Deoxynucleotide
ECM	Extracellular matrix
EDI	UCL Eastman Dental Institute
EDTA	Ethylenediaminetetraacetic acid
EGF	Epidermal growth factor
Em	Emission
Ex	Excitation
Fab	fragment antigen binding
FAM	Fluorescent reporter dye fragment
FCM	Fibroblast conditioned medium
FCS	Fetal calf serum
FDA	Food and Drug Administration (USA)
Fe_2O_3	Iron oxide
FITC	Fluorescein isothiocynate
Gla	gamma-carboxyglutamate
GM	General medium
h	Hour, time
HA	Hydroxyapatite
HOB	Human osteoblast
HOF	Human oral fibroblast
HTF	Human tendon fibroblast
Hz	Hertz, frequency

IGF	Insulin-like growth factor
IgG	Immunoglobulin G
IL	Interleukin
IU	International unit, drug potency
min	Minute, time
ml	Millilitre, volume
mm	Millimetre, length
mM	Millimolar, concentration
mRNA	Messenger RNA
MSCs	Mesenchymal stem cells
N	Newton, force
NCP	noncollagenous protein
nm	Nanometer, length
OC	Osteocalcin
ON	Osteonectin
OP	Osteopontin
P-4-H	Prolyl-4-hydroxylase
P4HA3	Prolyl-4-hydroxylase alpha polypeptide III subunit
PBS	Phosphate buffered saline
PDGF	Platelet derived growth factor
PI	Propidium iodine
PLA	Polylactic acid
PLAGA	Polylactide-co-glycolide acid
qPCR	Quantitative polymerase chain reaction
r/min	Revolution per minute, rotational speed
Re	Reynolds number, flow characteristics
RGD	Arginine-glycine-aspartate (Arg-Asp-Gly)
RNA	Ribonucleic acid
RQ	Relative quantification
RT	Room temperature
SD	Standard Deviation
SE	Secondary electron
sec	second, time
SVCT1	Sodium-dependent vitamin-C transporter 1
TCP	Tricalcium phosphate
TGF	Transforming growth factor

List of Figures

List of tables

CHAPTER ONE

INTRODUCTION

1.1 Introduction

The hard-soft tissue interfaces, whether osteotendinous or osteoligamentous, are integral units supporting the posture and mobility of the musculoskeletal system. The soft connective tissue components of the interface, i.e. ligaments and tendons, undergo injury, disease and degradation throughout life leading to a wide range of medical conditions.

1.2 Aetiology and mechanisms of injury

1.2.1 Overuse Injuries

As dense connective tissue structures, and owing to considerable tensile strength, tendons and ligaments transmit physical loads and forces with minimal energy loss between muscle/bone and bone/bone respectively providing the necessary framework crucial for movement and skeletal stability. Tendons and ligaments are also elastic and capable of extending 4-8% beyond their resting length, thus preserving their structural integrity when higher levels of activity are to be met. Loss of elasticity may occur however, when the tissue is subjected to stresses exceeding its resistance capacity. As seen from Figure1.1, a tendon or a ligament commences longitudinal elongation as strain surpasses a certain level at a point termed the "toe" region after which, resistance to the increasing stress follows a linear (Ng et al., 2004). It is at strain levels above 4%, and beyond the elasticity threshold, that permanent loss of functional structure and injury may occur.

Such acute overloading is of common occurrence in strenuous exercises resulting in the partial or complete rupturing of, for example, the Achilles tendon or the anterior cruciate (ACL) ligament of the knee. Tissue injury may also result from repetitive strain a phenomenon often associated with athletic exercise. Chronic repetitive microtrauma frequently leads to the formation of multiple microscopic cracks within the tendon matrix, where the eventual coalescence of these micro-defects will culminate in various forms of tendinopathies. Exercise mediated overuse injuries have shown to be exacerbated when combined with the presence of certain intrinsic

contributing factors. Table 1.1 summarises the risk factors associated with overuse injuries of tendons and ligaments.

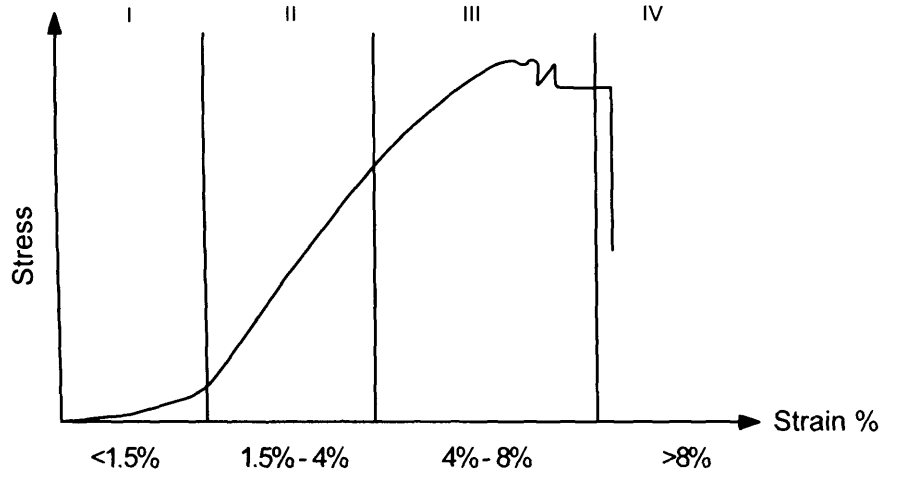

Figure 1.1 Typical stress-strain curve for tendons and ligaments

Toe region (I), linear region (II) and failure region (III and IV) (Goh et al., 2003; Ng et al., 2004)

Table 1.1 Risk Factors That Contribute to Overuse Injuries

(O'Connor et al., 1997)

Intrinsic	Extrinsic
Malignant	Training errors
Muscle imbalance	Equipment
Inflexibility	Environment
Muscle weaknesses	Techniques
Instability	Sport-acquired deficiencies

1.2.2 Aging and limited mobility

Elderly individuals are susceptible to ligament, Tendon and other musculoskeletal injuries at a rate similar to those in the young (Goh et al., 2003; Dressler et al., 2005). Age associated biomechanical changes, however, increase the tissue susceptibility to physical damage and pose a negative impact on its healing capacity. Aging tendons and ligaments undergo degenerative quantitative and qualitative changes in terms of both, collagenous and noncollagenous components of the extracellular matrix (ECM). This might be attributed to the slow metabolic rate of the cellular component contributing to the matrix turnover and an increasingly limited vascularisation resulting, ultimately, in stiffness and the loss of elasticity. The lack of physical stimuli required to maintain an efficient structure through functional homeostasis whether associated with aging or due to disability and disease, will also increase the predisposition of tendons and ligaments to injuries, particularly those of the chronic nature (Kjaer, 2004). It has been reported that immobilisation of the Achilles tendon induced the thinning and disorientation of collagen fibres and decreased the strength and resistance capacity by 20% (Matsumoto et al., 2003).

1.2.3 Endogenous factors

Various pathological conditions may either directly generate deficiencies in ligaments and tendons, or indirectly predispose such structures to acute or chronic traumatic injury. Familial hypercholesterolemia, a common hereditary condition (Descamps et al., 2001), induces the formation of tendon xanthomata where tissue structure is altered by the presence of lipid deposits (Tall et al., 1978). Various genetic disorders such as ochronosis, mucopolysaccharidoses and osteogenesis imperfecta are associated with collagen synthesis deficiency thus directly causing connective tissue abnormalities (Jozsa et al., 1981; Jarvinen et al., 1997; Misof et al., 1997; Cortes and Maloney, 2004). Chronic inflammatory conditions, primarily rheumatoid arthritis, lead to the occurrence of degenerative changes in tendons and ligaments via the inflammation of the synovial envelope. Again, this is followed by an increased vulnerability to microtrauma (Kramer et al., 2003; Bring et al., 2005). Other

infectious, iatrogenic, endocrine, metabolic and tumorogenic factors may also contribute to the induction of tendons and ligaments pathology (Hayem, 2001).

1.3 Pathology and healing

Trauma to the tendon or ligament, whether acute or chronic, usually results in the complete or partial tearing of the structure. Following injury, a predominantly intrinsic repair process is initiated and can be divided into several overlapping phases where the duration of each phase is dependant on the nature and location of the defect. Associated with pain, swelling, heat and redness the first phase, immediately preceding injury, is characterised by an inflammatory response (Weintraub, 2003). This is instigated, and ensuing blood vessel rupture, by haematoma formation and the injury site infiltration by inflammatory cells and macrophages and followed, at later stages, by angiogenesis and the invasion of fibroblasts, tissue constituting proteins and tissue growth factors from the surrounding structures so that the formation of a new ECM is initiated (Fenwick et al., 2002). The second phase of the repair process is dominated by the presence of a disorganised matrix of granulation tissue, the proliferation of fibroblasts and the synthesis of collagen as the main constituting protein of the fibre structure. Within the granulation tissue, stimulated by mechanical stress and induced by the presence of transforming growth factor-β (TGF-β) and finbronectin, fibroblasts undergo differentiation into protomyofibroblasts and subsequently differentiate into mature myofibroblasts (Lygoe et al., 2004). This differentiation process has been shown to be primarily controlled by the formation of TGF-β/αv intergin complexes on the cell membrane followed by the activation of differentiation mediated by Smad proteins (Smad2 in particular) (Lan, 2003). Myofibroblasts express smooth muscle cell characteristics expressing alpha smooth muscle actin (α-SM actin, an actin isoform) and play a major role in adult wound healing, wound contraction and scar formation (Grinnell, 1994; Hakkinen et al., 2000; Van Beuerden et al., 2005). The final stage of repair, and scar formation, is the remodelling and maturation process where the fibroblasts assume a round morphology and slow their metabolic rate; the newly formed fibrils are cross-linked and oriented parallel to the ligament or tendon longitudinal axis; and the fibrils constituting collagen is converted to a type similar to that of the normal tissue (Lin et al., 2004).

Figure 1.2 illustrates the healing process and the approximate duration of each phase. The scar tissue, however, is of inferior biomechanical properties when compared to the uninjured structure (Ferguson and O'Kane, 2004). The healed tissue is increasingly hypercellular and collagen fibrils are characterised by distorted cross linking and orientation, small diameter and composed largely of Type III collagen thus greatly compromising the function and stress resistance of the structure (Maffulli et al., 2002). Furthermore and due to the presence of blood clotting associated fibrin, during chronic injury and prolonged healing, adhesion formation among tissue layers may occur thus contributing to the loss of functional elasticity (Kader et al., 2002; Weintraub, 2003).

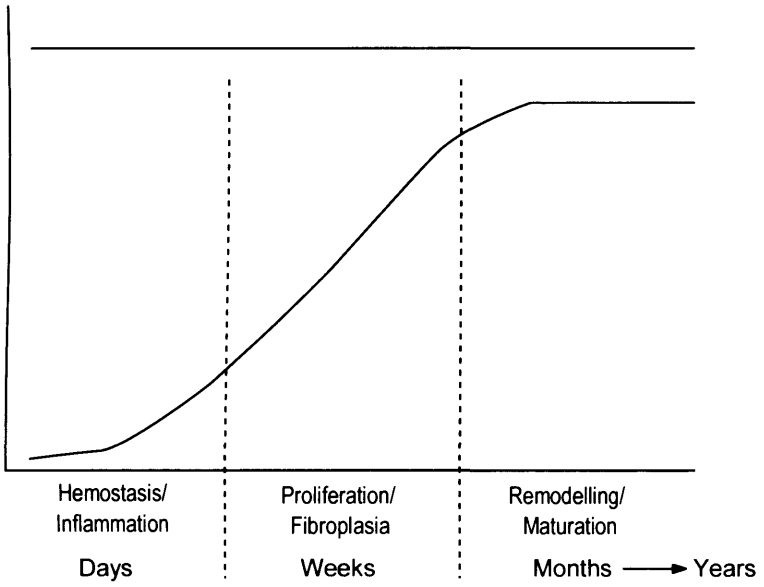

Figure 1.2 Wound healing mechanism and response in tendons and ligaments (Lin et al., 2004).

1.4 Conventional surgical intervention

Ensuing injury and intrinsic repair, tendons and ligaments may never regain their original functional structure and surgical reconstruction, in a considerable number of cases, is an inevitable choice when attempting to replace the damaged tissue. This is highlighted by the fact that in the United States, surgical reconstruction is performed on almost 50% of all ACL injury cases (Kartus et al., 2001; Herrington et al., 2005). In 1993, the number of patients undergoing surgery to repair deficient tendons and ligaments was estimated at 120,000 annually (Langer and Vacanti, 1993). The extent and form of the operative procedure is related to the nature, site and severity of injury (Coleman et al., 2000). Partial or complete ruptures are directly sutured whereas in chronic injury conditions, open tenetomy is conducted by making multiple longitudinal incisions in the structure (Maffulli, 1999; Kader et al., 2002). This is conducted to detect intratendinous lesions; to remove fibrotic adhesions and degenerated tissue formations; and to restore vascularity. Surgical reconstruction using variety of graft material is another approach aimed at completely replacing dysfunctional structures (Figure 1.3). Various anatomical sites can be utilised as sources for autogenic or allogenic graft tissue such as the gracilis muscle ligament, the hamstring muscle ligament and the patellar tendon of the knee. Synthetic alloplast material has also been used or evaluated for repair purposes. These include polymer-carbon fibre composites as non-degradable scaffolds to aid tissue growth, Gore-Tex (polytetrafluoroethylene-PTFE) as permanent prosthesis (Roolker et al., 2000; Kimura et al., 2003); Dacron (polyethylene terepthalate) as both permanent prosthesis and graft augmentation supporting device (Wredmark and Engstrom, 1993; Brekke and Toth, 1998; Kimura et al., 2003); Marlex mesh (Polypropylene) (Choksey et al., 1996); ligament augmentation devices (polypropylene) (Van Kampen, 1994; Steenbrugge et al., 2001); and collagen prosthesis (Kato et al., 1991).

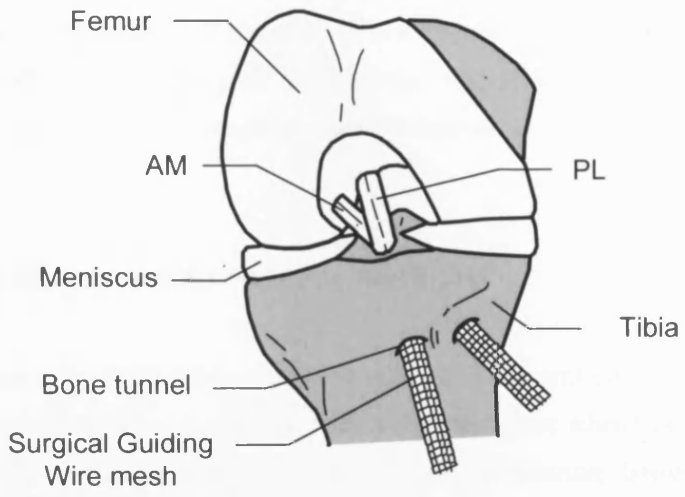

Figure 1.3 Schematic illustration of surgical reconstruction of the anterior cruciate ligament (posterior view)

The anteromedial (AM) and posterolateral (PL) bundles of the ACL were replaced using hamstring tendon autografts. (Yasuda et al., 2005)

1.5 Disadvantages of surgical management

1.5.1 Significant failure rate and surgical complications

Surgical management of chronic tendon and ligament lesions, particularly where extended chronic degradation is present, have been shown to be associated with an unpredictable outcome. Previous studies have concluded that as high as 29-54% of patients suffered poor results following surgery and several re-operation procedures, therefore, may need to be conducted (Coleman et al., 2000; Cook et al., 2002; Kader et al., 2002). Full recovery however, even with prolonged post operative rehabilitation strategy, is not guaranteed as in many patients the return to normal function and activity level is less than satisfactory (Cook et al., 2002). The high incidence of complications associated with, or ensuing, surgery may also compromise the

outcome. Such complications may include delayed wound healing, deep infections, necrosis and re-rupture of the repaired tissue and adherence of tissue to skin (Nistor, 1981). Failure of the tendon/ligament graft integration into bone, following surgery, is another common complication. It has been shown that the inferior bonding between the hard and soft tissues, at the graft augmentation site, often resulted in structural laxity and in many cases, failure of treatment (Martinek et al., 2002; Song et al., 2004).

1.5.2 Autograft associated donor site morbidity

Despite advances in developing alternative allograft and artificial replacements, autograft augmentation remains the most widely used technique when treating tendon and ligament defects (Kartus et al., 2001). Secondary complications however, due to the damage inflicted on the donor tissue, are evident in many cases. It has been suggested that the use of muscle tendons as graft sources resulted in reduced strength, compromised extensor mechanisms and nerve damage (Comley and Krishnan, 1999; Kartus et al., 2001; Soon et al., 2004). The use of patellar tendon grafts, to reconstruct the ACL, has also been shown to be associated with pain and discomfort, reduced range of motion of the knee and altered mechanical function (Kartus et al., 2000; Eriksson et al., 2001). The presence of such complications was detected up to two years following surgery (Kartus et al., 1999). Histopathology findings confirmed the presence of hypertrophic scar formation in the donor tissue. Manifested by poorly aligned collagen fibrils, increased cellular content and hypervascularity the histological appearance of the regenerated tissue, at the harvest site, was markedly different from normal (Berg, 1992; Linder et al., 1994; Proctor et al., 1997; Sanchis-Alfonso et al., 1999).

1.5.3 Allograft availability and limitations of use

When, in some cases, allograft augmentation is the only option at hand, a familiar scenario emerges. The demand simply exceeds availability. Many of the patients on the transplant waiting lists will die before a transplant organ or tissue is available for them (Vacanti et al., 1998; Alberto, 2004).Allograft use is also associated with the

risk of infectious disease transfer and unreliable graft incorporation (Brekke and Toth, 1998). Furthermore and being genetically alien to the host tissue, allografts are extremely liable to immunorejection and the use of immunosuppressant agents is a requirement.

1.5.4 Alloplast mechanical failure and short lifetime

Synthetic materials used as augmentation devices lack the fundamental capacity of normal tissues to self-repair and to adapt to biomechanical stimuli. Despite continuous efforts to improve both morphological and biological fixation properties of these devices, long term clinical outcome remains poor and the in vivo lifetime is unpredictable (Hench, 1998). Whether as a result of poor abrasion resistance or mechanical mismatch, alloplasts are susceptible to fatigue failure and limited integration into normal tissue (Cooper et al., 2005).

1.6 Development, Structure and biomechanical properties

1.6.1 Introduction

Ligament, tendon and bone, components of the hard-soft interface, are all connective tissue structures and all follow closely related developmental pathways. During early foetal life, and by the end of the second week in utero, the embryonic structure is formed by three distinct germ layers: the ectoderm, the mesoderm and the endoderm. The middle layer, the mesoderm, will eventually give rise to skeletal, connective and muscle tissues of the body (Figure 1.4A) (Mitchell and Sharma, 2004). By the end of the third week, the paraxial (medial) regions of the mesoderm undergo differentiation and paired tissue blocks, or somites, are formed on either side of the primitive neural tube. The somites undergo further development whereby cell populations aggregate into sclerotomes evolving later into axial bone and cartilage; and dermomytotomes from which the skeletal muscles and connective tissue are to be formed (Figure 1.4B). The distal parts of the mesoderm, or the lateral plate, will form the basis of the musculoskeletal system of the limbs. The somites and the lateral plate are composed by a loose connective tissue network, the mesenchyme, formed by the mesoderm cells except for the head region where it is, entirely, induced by the invasion of neural crest cells migrating from the ectoderm (Armitage et al., 1990). As well as their primary function forming fetal structures, the pluripotent stellate-shaped cells of the embryonic mesenchyme persist in the adult bone marrow, and various other tissue structures, as multipotent mesenchymal stem cells capable of differentiating into connective tissue cells (Winslow, 2001).

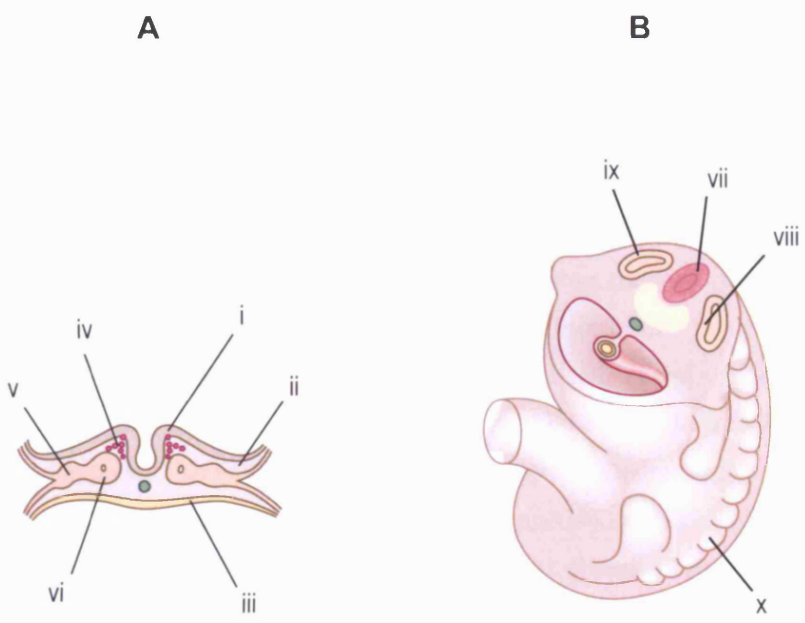

Figure 1.4 Transverse Sections of the Human embryo at 20 days (A) and 4 weeks (B) in utero

(i) Ectoderm, (ii) Mesoderm, (iii) Endoderm, (iv) Neural crest cells, (v) Lateral plate mesoderm, (vi) Medial plate mesoderm, (vii) Neural Tube, (viii) Sclerotome, (ix) Dermomyotome and (x) a Somite. (Mitchell and Sharma, 2004).

1.6.2 Bone

1.6.2.1 Fetal bone formation

During morphogenesis, bone development in the embryo occurs via two different processes. Commencing by the second month of development and stimulated by various factors, FGF (fibroblast growth factor) in particular, endochondral ossification is preceded by the formation of mesenchymal cell condensations (Orintz, 2005). Within the condensed matrix, the mesenchymal cells undergo differentiation into highly proliferative chondroprogenitor cells that later differente into cartilage synthesising cells. This process is preceded by the activation of transcription factors Sox 9, Sox 5 and Sox 6 whereby the cells, highly expressing collagen type II, form the cartilaginous template (anlagen) of the future bone (Orintz, 2005 ; Tuan, 2004). Following peripheral capillary proliferation, the peripheral cells of the anlagen adopt an osteoblastic fate and a "collar" of bone is thereby formed around the middle of the cartilaginous template. This process is highly regulated by bone morphogenic proteins 2 and 7 (BMP2, BMP) and characterised by an up-regualtion in cbfa1 and collagen type I expression by the cells (Forriol and Shapiro, 2005). Simultaneously, centrally located chondroblasts undergo hypertrophy, the cartilaginous structure becomes increasingly vascularised and several ossification centres begin to emerge within the hypertrophic cartilage (Zelzer and Olsen, 2003). The hyaline cartilage is gradually replaced by bone except for the growth plate regions where post-natal longitudinal growth occurs. The cancellous tissue nature at the centre of newly formed bones permits the hosting of the bone marrow (Sommerfeldt and Rubin, 2001; Zelzer and Olsen, 2003). Intramembranous ossification takes place in the head region mesenchyme, and throughout the development of the skull, maxilla and mandible. This type of bone formation is initiated by the aggregation and condensation of clusters of mesenchymal cells differentiating directly into bone forming cells or osteoblasts (Sommerfeldt and Rubin, 2001). An ossification centre is hereby formed where the osteoblasts begin the synthesis of the bone matrix (osteoid) which, in turn, undergoes mineralisation within days. As the new formed bone continues to grow around the embryonic blood vessels the surrounding mesenchyme undergoes fibrous condensation so that the precursor structure of the periosteum is laid (Sommerfeldt

and Rubin, 2001). Maturation into compact bone ensues at the peripheral level whereas a cancellous, central zone housing the haematopoietic marrow tissue persists. Figure 1.5 summarises the endochondral and intramembranous ossification processes.

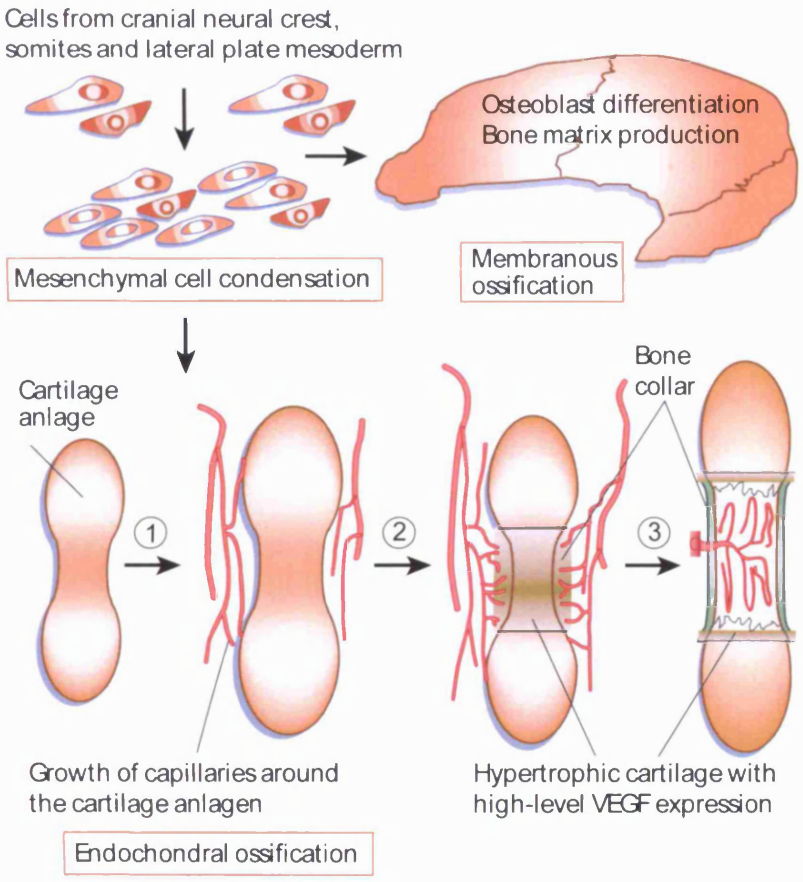

Figure 1.5 Schematic illustration of endochondral and intramembranous bone formation (Zelzer and Olsen, 2003).

1.6.2.2 Bone cells

Osteoprogenitor cells originate from the multipotent mesenchymal stem cells of the bone marrow. The process by which MSC commitment to the osteoblastic monopotent progeny is conducted is not fully understood however, certain factors appear to play a major role in regulating such an event particularly the TGF-β superfamily (including BMPs) and parathyroid hormone (PTH) (Abuin et al., 1995). Osteoprogenitor cells give rise to preostoblasts that are of distinct elongated morphology and commonly located near bone surfaces which, in turn, undergo differentiation into osteoblasts(Weiss, 1983). The osteoblast expresses several stages of differentiation generating the bone matrix through collagen type I synthesis and regulating bone mineralisation (Gay et al., 2000; Sommerfeldt and Rubin, 2001). Osteoblasts are of cubodial morphology and are located at the bone surface and once active can be characterised for synthesising osteopontin (OP), bone sialo protein (BSP), osteonectin (ON), alkaline phosphatise (ALP) and osteocalcin (OC). Additionaly, osteoblasts have been shown to be capable of producing BMP where his appears to be directly linked to the activation of differentiation pathways of osteoprogenitor cells into osteoblasts (Mackie, 2003). Osteoblasts lay down an estimated 0.5-1.5 μm of osteoid every day (Weiss, 1983) and once entrapped in the newly synthesised bone matrix, changes in cell morphology and function take place giving rise to what is commonly referred to as the mature bone cell, the osteocyte. Characterised by a rounded morphology, a relatively large nucleus and a low content of cytoplasmic organelles, osteocytes are the most abundant cells in the mature and mineralised bone (Weiss, 1983; Sommerfeldt and Rubin, 2001). Osteocytes reside in lacuni and communicate with one another, and with other cells at the bone surface, via an extensive network of cytoplasm processes running through pre-mineralisation formed canals, the canaliculi. Being part of this three dimensional syncitium is what defines the function of osteocytes as regulators of bone matrix maintenance. It has been suggested that by responding to external mechanical signals transmitted through the lacuno-canalicular network, osteocytes orchestrate the recruitment of cells in bone construction and resorption (Sikavitsas et al., 2001). Playing an active role in mineralised bone resorption, the osteoclast is third bone-associated cell type. Unlike osteoblasts, osteoclasts originate from haematopoietic, as opposed to stromal,

mesenchymal stem cells of the marrow (Gay et al., 2000). Osteoclasts differentiate from mononuclear monocytes and macrophages that migrate, in response to hormonal or physical stimuli, towards the bone remodelling site. Osteoclasts are located in resorption pits, or Howship's lacunae and can be microscopically distinguished by their large size, multinucleated cytoplasm and high motility rate (Sambrook et al., 2001).

1.6.2.3 Bone structural properties and architecture

Newly laid osteoid consists mainly of organic substance, primarily collagen Type I, which forms 95% of the bone ECM. Following the onset of mineralisation however, this structure is gradually replaced by an inorganic mineral, hydroxyapatite (HA). The mature calcified bone is made up from 25% organic substance including collagen, cells and water; and 70% inorganic HA crystals (Sikavitsas et al., 2001; Sommerfeldt and Rubin, 2001). Collagen fibrils, whether in osteoid or mineralised bone, are linked together in regular alignment thus providing bone with structural cohesion and stability; shape; and tensile and compression resistance. This is achieved by the presence of proteoglycan (PG) protein species. In bone, PGs are synthesised by the osteoblasts in the two major forms PG-I and II (biglycan and decorin respectively). The PG core protein is covalently attached to one or more glycosaminoglycans (GAG) chains and to oligosaccharides at the N- and O- ends (Grzesik et al., 2002). PGs non-covalently bind to collagen via the sugar group and GAG chains form duplex GAG complexes between two adjacent collagen molecules (Scott, 2003). Several groups of bone-associated transmembrane proteins and soluble factors are present in the matrix and are of extreme importance for the maintenance and function of bone (Sikavitsas et al., 2001; Hing, 2004). A brief description of the most important of these molecules and their role in coordinating bone and cell function is outlined in table 1.2. It should be also noted that most of these transmembrane proteins, growth factors in particular, play similar role in regulating fibroblast function and matrix turnover in the soft connective tissue.

Architecturally, bone can be classified as either cortical (also referred to as compact) or cancellous (also referred to as trabecular or spongy). The two types are histologically and biochemically identical but differing in their structural organisation,

porosity and soft tissue content. Cortical bone forms 80% of the skeleton and is present mainly in the diaphyses of long bones. Whilst, forming only 20% of the skeletal structure, trabecular bone is found principally in the epiphysis of long bones, cranium and vertebrae (Weiss, 1983). At a microscopic level, mineralised bone can be subdivided into two structural categories, woven and lamellar. Woven or immature bone is rich in osteocytes and generally exhibiting disorganised structural arrangement where collagen fibrils are small, irregular and disorientated. It is primarily formed in the embryo, during fracture healing and at the sites of certain pathologic conditions where rapid bone formation occurs (Sommerfeldt and Rubin, 2001). Woven bone however, will eventually be remodelled and replaced by the more organised, structurally superior, lamellar bone. Lamellar bone is less mineralised and generated at a slower rate than woven bone and is characterised by the presence of structural subunits, the lamellae, which are arranged in adjacent layers. Collagen fibres are preferentially orientated and extend between adjacent lamellae thus contributing to the structural strength of bone (Weiss, 1983).

Table 1.2 ECM proteins and factors involved in bone remodelling and cell function

(Sikavitsas et al., 2001).

Osteocalcin (OC)	May inhibit mineralisation and participates in resorption.
Osteonectin (ON, SPARC)	A mineralisation nucleator with high affinity to both collagen and HA.
Osteopontin (OP)	Mediates cell attachment to the bone matrix.
Bone Sialoprotein (BSP)	Mediates cell attachment to the bone matrix.
Alkaline Phosphatase (ALP)	Promotes mineral crystal formation
Fibronectin	Mediates cell attachment to collagen and fibrin
Calcitonin	Osteoclast function inhibitor.
Biglycan (PG-I)	Affects collagen fibre growth and diameter.
Decorin (PG-II)	Affects collagen fibre growth and orientation.
Bone morphogenic Proteins (BMP)	Stimulate chondrocyte and osteoblast proliferation and ECM synthesis. Induce MSCs differentiation into osteoblasts.
Fibroblast growth factors (FGF)	Stimulate MSCs differentiation, chondrocyte and osteoblast proliferation. May induce angiogenesis.
Insulin-like growth factor (IGF)	Stimulate chondrocyte and osteoblast proliferation and ECM synthesis.
Transforming growth factor-	Induce chondrocyte differentiation and osteoblast

β (TGF-β)	proliferation. May act as a bone remodelling regulator.
Epidermal growth factor (EGF)	Stimulates chondrocyte proliferation. Inhibits ECM synthesis.
Platelet-derived growth factor (PDGF)	Stimulates osteoblast differentiation. May stimulate bone resorption
Prostaglandin	Regulates osteoclast differentiation, proliferation and function.
Interleukin-I (IL-I)	Stimulates preosteoclast differentiation
Parathyroid hormone	Both stimulates and inhibits osteoclast differentiation
Thyroxin	Stimulate osteoclast mediated resorption
Estrogen	Resorption inhibitor. Remodelling regulator
Dexamethasone	Induces endochondral ossification
Vitamin D	Regulator of bone associated protein synthesis. Bone remodelling regulator.

In cortical bone (Figure 1.6), the lamellae are arranged in concentric layers around central capillaries forming cylinders of 200-300 μm in diameter. These arrangements are referred to, and depending on the pattern of development, as either osteons or Haversian systems where up to 20 lamellar plates surround a central canal (Haversian canal) containing blood vessels, nerves and connective tissue (Weiss, 1983). Communication among Haversian canals, the periosteum and bone marrow is conducted via oblique or transverse channels termed Volkmann's canals. Each Haversian system is surrounded by a cement line, a noncollagenous interface of mineralised mucopolysaccharides (Sambrook et al., 2001). In cancellous bone the trabeculae are formed by the incorporation of trabecular segments, or packets, where each packet comprises several horizontally arranged lamellae. Several osteon-like structures can also be seen throughout cancellous bone. All bones irrespective of structure and form are covered with periosteum except joint surfaces, which are covered with articular cartilage. The periosteum is permeated by blood vessels and nerve fibres that pass into the bone via Volkman's canals. The periosteum may also serve as an osteogenic layer as the presence stromal and haematopoietic mesenchymal stem cells has been detected (Weiss, 1983).

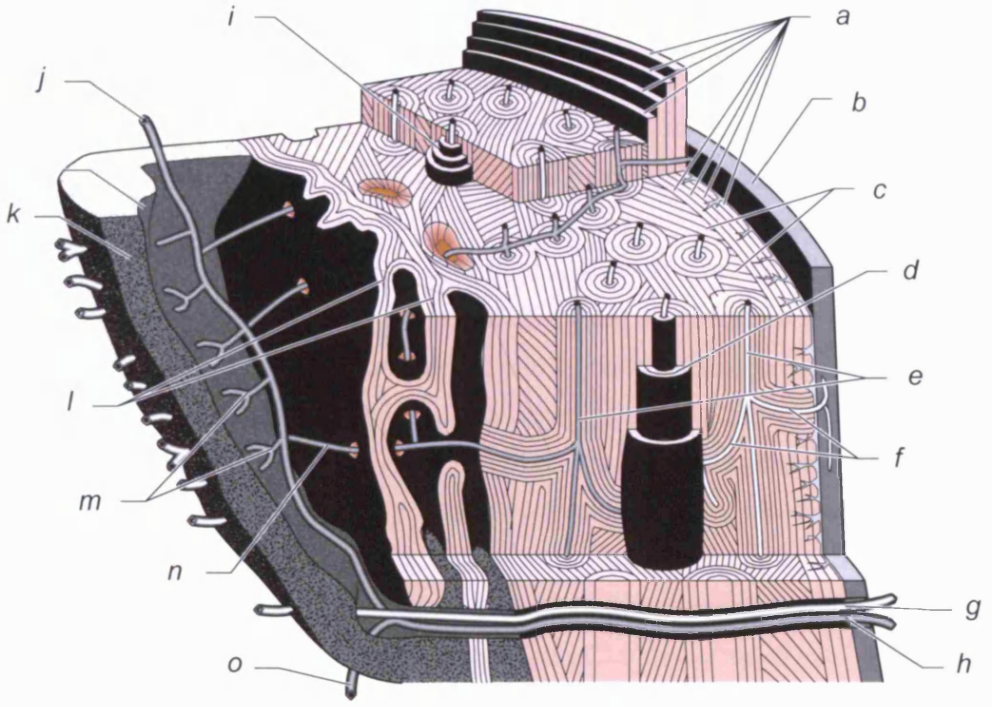

Figure 1.6 A three dimensional reproduction of lamellar bone architecture

(a) Subperiosteal outer circumferential lamellae, (b) Periosteum, (c) Interstitial lamellae, (d) Concentric lamellae of osteon (haversian system), (e) Capillaries in haversian canals, (f) Capillaries in Volkmann's canals, (g) vein, (h) Nutrient artery, (i) Concentric lamellae of osteon (Haversian system), (j) Nutrient artery, (k) Marrow meshwork (Containing haematopoietic/ stromal stem and fat cells), (l) Trabeculae, (m) Central arteriolar branches of nutrient artery, (n) Peripheral arteriolar branch of nutrient artery gives rise to capillaries that enter Volkmann's canals of cortical (compact) bone and, (o) Nutrient artery eventually anastomoses with distal metaphyseal arteries. (Sambrook et al., 2001).

1.6.2.4 Bone mineralisation

Mineralisation can be simply defined as the formation and growth of HA ($[Ca_{10}(PO4)_6(OH)_2]$) crystals within the collagenous ECM of bone. This process is preceded by local pH changes and increases in mineral ion concentration levels. The exact mechanisms by which the precursors of bone mineral are introduced to the matrix are poorly understood. It is believed nonetheless that this involves the release, by the osteoblasts, of matrix vesicles and mitochondrial granules containing phosphatases (ALP), phospholipids, and calcium ions (Sikavitsas et al., 2001; Sommerfeldt and Rubin, 2001). HA deposition is initiated by a process of nucleation during which an amorphous mineral nucleus is formed so that crystal growth, around the nucleus, can proceed. Nucleation appears to be closely related to certain molecular groups capable of binding calcium and phosphate ions to the matrix. These include among various others, phosphorelated amino acid residues such as serine (present in collagen and osteonectin); carboxyl groups of glutamic and aspartic acides (present in collagen); and carboxyl groups of hexose or hexoseamines (present in proteoglycans) (Hauschka et al., 1989; Hing, 2004). Also, the precise arrangement of collagen molecules within the collagen fibrils of the bone ECM plays a major role in initiating nucleation and HA crystal growth. Collagen molecules are arranged in a quarter-stagger/ end-overlap manner whereby the "gap" present between collagen molecule ends provide the sites for crystal nucleation (Knott et al, 1997; Landis 1999). In response to mechanical stimuli and metabolic demands, bone is constantly subjected to remodelling throughout which, a balance is struck between the two processes of absorption and formation thus maintaining, under normal conditions, a state of functional haemostasis.

1.6.2.5 Bone remodelling

Understanding the mechanisms involved in the remodelling process might provide an excellent insight into the differentiated function of bone cells. Bone is normally maintained in a resting state where the bone surface is lined with the inactive, quiescent bone specific precursor cells. Initiated by various factors such as the parathyroid hormone (PTH), osteoclast differentiation and recruitment are induced

primarily by several factors produced by the osteoblasts located at bone remodelling sites. Activation of preosteoclasts from the precursor pool is initiated via a direct interaction between RANK-L (osteoblast transmembrane receptor) and RANK (osteoclast precursor receptor) and mediated; by macrophage colony-stimulating factor (M-CSF) secreted by the osteoblast. This formation of receptor-ligand complexes on the preosteoclast membrane is followed by the translocation of differentiation transcriptional factors into the nucleus (Sambrook et al., 2001). Such a process can also be inhibited by the presence of osteoprotegrin (OPG), a protein produced by the osteoblasts, blocking and subsequently deactivating the role of RANK-L receptors (Mackie, 2003; Sommerfeldt and Rubin, 2001). As the resorption phase begins the osteoclast adhere to the bone surface creating a sealed zone with the corresponding cell membrane characteristically exhibiting several folds thus creating a ruffled border. This is followed by the onset of phagocytosis, a local drop in pH value creating a favourable environment for the activation of several released enzymes, mainly tartrate-resistant acid phosphatise, leading eventually to the degradation of HA crystals and the enzyme mediated breakdown of collagen(Gay et al., 2000; Sommerfeldt and Rubin, 2001). Once the resulting cavity (Howship's lacuna or cutting cone) has reached 60-100 μm in depth the reversal stage commences. As the osteoclasts disappear, preosteoblasts differentiate into active osteoblasts and a cement, or reversal, line is formed encasing the resorption border and aiding the adherence of the newly formed bone at a later stage (Sambrook et al., 2001). Subsequently, and with the onset of the formation phase, the invading osteoblasts synthesise the collagenous (primarily collagen Type I) ECM which undergoes mineralisation once approximately 20 μm of osteoid has been deposited. The combined ECM formation-mineralisation process continues until the appropriate volume of bone has been formed and the resting state is finally reached. A bone remodelling unit (BRU) is schematically illustrated in Figure 1.5.

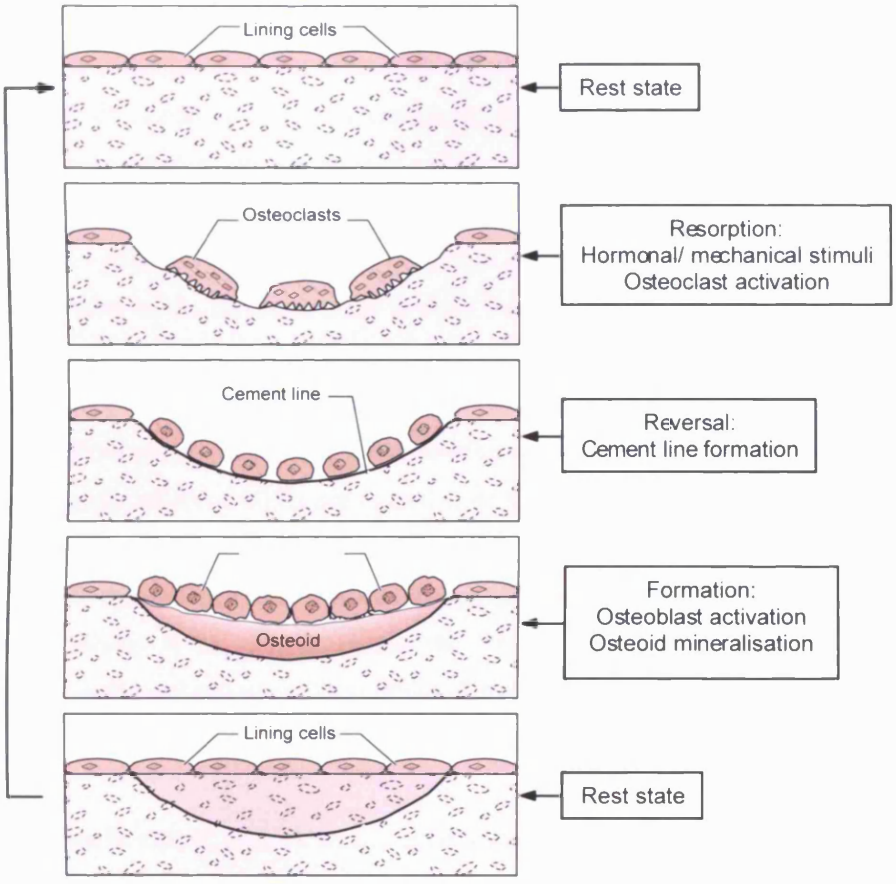

Figure 1.7 Schematic illustration of Bone Remodelling Unit (BRU) (Sambrook et al., 2001).

1.6.3 Ligaments and tendons

1.6.3.1 Development

During embryogenesis precursors of tendon and ligament formation appear as condensations of mesodermal mesenchyme cells closely adjacent, and inserted into, the bone forming hyaline cartilage (Birk and Trelstad, 1986; Wolfman et al., 1997). Within these mesenchymal aggregates cell differentiation into fibroblasts occurs and collagen fibrils continuously and increasingly form within the extracellular space. Fibrillogenesis takes place within extracellular compartments (Birk and Trelstad, 1986) the formation of which is regulated by the fibroblasts and can be divided into three distinct phases. Firstly, collagen molecules are assembled extracellularly and in close proximity to the cell membrane to form immature fibril intermediates. This is followed, and during the second phase, by the linear growth of the collagen fibrils where collagen intermediates assemble end to end forming the first structurally functional fibril units. Finally, and characterising the third phase, lateral fibril growth occurs whereby adjacent fibrils are cross-linked through certain enzymatic function, particularly that of lysyl oxidase, forming larger fibril bundles that eventually coalesce into the collagen fibre units of the mature tendons and ligaments (Kadler et al., 1996; Zhang et al., 2005). Hierarchal arrangement of the structure is also established in the embryo as collagen fibrils, fibroblasts and extracellular components become arranged in subunits or fascicles.

1.6.3.2 Biochemical and structural properties

Ligaments and tendons are microscopically and morphologically identical however, minor biochemical and structural differences are present between the two tissue types. Despite studies attempting to estimate collagen weight in tendons reporting variable results, it is clear that collagen contribution to the dry weight of the structure is in the region of 80%. This is mainly formed by collagen Type I although other types, in much smaller amounts, such as types III, V, XII and XIV have also been detected (Kadler et al., 1996; Kannus, 2000; Lin et al., 2004; Zhang et al., 2005). Tendons also contain 1-2 % elastin, a major constituent of elastic fibres, and proteoglycans of which

decorin is predominant at 1% of the dry mass (Gosline et al., 2002). Water constitutes approximately 80% of the wet weight of tendons (Lin et al., 2004). Ligaments contain similar amounts of collagen, with Type I being also predominant, and water contributes to 60 % of the wet weight (Frank, 2004). Ligaments however are more active metabolically and contain more cells and higher DNA content than tendons (Goh et al., 2003). Noncollagenous proteins can also be traced biochemically in both structures and appear to provide a binding function between cells, polypeptide macromolecules and various ECM components. Among these fibronectin, thrombospondin, tenascin-C, and undulin have been identified (Kannus, 2000). The description of the tendon structural arrangement can be applied to ligament, with a slight variation in nomenclature, as the two structures are virtually identical. In tendons collagen fibres group together in primary fibre bundles or subfascicles which, in turn, form larger secondary fibre bundles identified as fascicles. Fascicles are grouped into tertiary bundles, several of which make up the structure of the tendon proper (Lin et al., 2004; Zhang et al., 2005). Fibre bundles, of all categories, and starting from the subfacicle are enclosed and separated by a connective tissue structure, the endotenon, containing the nerve and vascular supply networks (Cook and Khan, 2001). Surrounding the tendon, and continuous with the endotenon, is a dense collagen fibril network termed the epitenon and the entire structure, in most anatomical sites, is enclosed in a loose areolar connective tissue, the paratenon, containing types I and II collagen and elastic fibrils(Kannus, 2000). Figure 1.8 illustrates the hierarchal arrangement of the various subunits. Collagen fibres are preferentially arranged to provide the maximum functional strength and adaptation to rotational forces. This is achieved through longitudinal, horizontal and transverse crossing of adjacent fibres resulting in the formation of plaits and spirals (Culav et al., 1999). Depending on the anatomical location and the position within the structure, collagen fibres can measure up to 300 μm and exhibit a wavy, or crimped, appearance that can be easily distinguished under the microscope as periodic cross-striations or bands across the fibre width (Figure 1.9). This pattern provides the elasticity and stress resistance in tendons and ligaments and is attributed to proteoglycan cross-linking between adjacent areas on the fibre surface. When the structure is stretched in response to physical strain collagen fibres become increasingly straight only to return to the wavy appearance of the resting state once the tensile load is removed (Kannus, 2000; Lin et al., 2004).

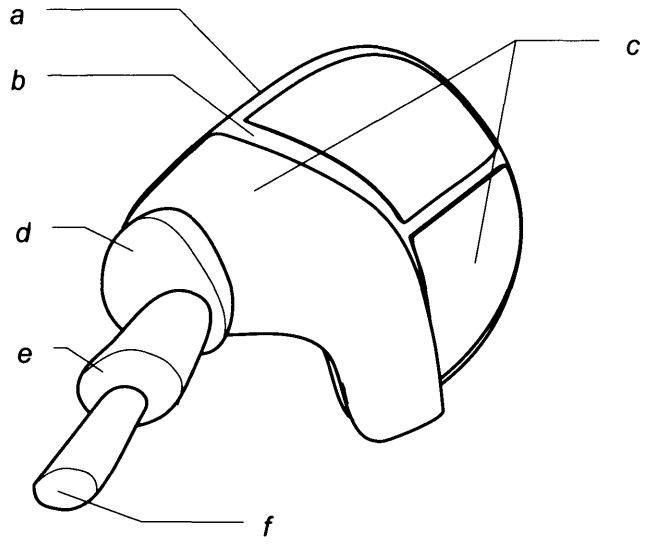

Figure 1.8 Schematic of the hierarchal arrangement of the tendon subunits

(a) Epitendon, (b) endotendon, (c) tertiary fibre bundle, (d) Secondary fibre bundle (fascicle), (e) Primary fibre bundle (subfascicle) and (f) Collagen fibre.

Figure 1.9 X128000 Transmission Electron Microscope image of Tendon collagen fibrils

Reprinted, Electron Microscopy Centre, Babes Bolyai University, Romania.

1.6.3.3 The fibroblast, ECM turnover and collagen synthesis

Similar to osteoblasts, fibroblasts originate from the stromal stem cells of the bone marrow following several steps of differentiation (Baksh et al., 2004) and despite the presence of endothelial and mast cells in the tendon and ligament ECM, fibroblasts remain the predominant cell population composing almost 3% of the dry weight of the structure (Hayem, 2001). These cells are elongated, arranged in longitudinal rows in close proximity to collagen fibres and contain spindle-shaped nuclei (Kim et al., 2002; Claudepierre and Voisin, 2005). Fibroblasts also exhibit numerous, sheet-like, cytoplasmic processes extending into the extracellular space and it has been demonstrated that adjacent cells communicate via theses processes, and through the presence of gap junctions, thus forming an elaborate three-dimensional network which may potentially act as a coordinator of cellular and metabolic responses of the tissue (Frank, 2004; Claudepierre and Voisin, 2005; Kjaer et al., 2005). In the normal resting state fibroblasts appear quiescent however; certain cellular functions are reactivated as the ECM is constantly remodelled in response to physical activity, immobilisation and injury (Hayem, 2001). Subjected to *in vitro* mechanical stretch and cyclic loading, fibroblasts have expressed increased DNA transcription levels and up-regulated collagen synthesis (Kim et al., 2002; Gough et al., 2003). Fibroblasts are also responsible for matrix degradation via the breakdown of collagen molecules, particularly during rapid remodelling as in tissue damage of inflammation, either via intracellular lysosomal phagocytosis or extracellularly by the action of secreted enzymes, the matrix metalloproteinases (MMPs) (Federman et al., 2002). Collagen synthesis is preceded by the increase of interstitial concentration of several growth factors including FGF, IGF, TGF-β and several interleukin types (Kjaer, 2004; Kjaer et al., 2005). These proteins bind to certain receptors/integrins on the cell membrane promoting the transcription of preprocollagen nuclear DNA sequence into the corresponding messenger RNA (mRNA). Subsequently, the polypeptide α-chains of procollagen are translated, by ribosomal action, from the mRNA strands and relocated to the endoplasmic reticulum where the assembly of the triple helix of collagen molecule takes place. This action is mediated by several enzymes such as prolyl-4-hydroxylase (P-4-H), and it is well described that P-4-H activity levels increase and decrease in correspondence with collagen synthesis rates (Kjaer, 2004; Kjaer et al.,

2005). Procollagen molecules are then transported into the extracellular space, via the Golgi apparatus, where the conversion into fibrillar collagen and fibril assembly is conducted. Firstly, The 300 nm long procollagen molecule is modified by the removal of two N and C ends propeptides (by the action of N and C-protinases respectively) into collagen molecules that spontaneously self-assemble into end-overlapped/ cross-striated fibrils. These fibrils are then stabilised by covalent cross linking mediated by the enzyme lysyl oxidase (Kadler et al., 1996; Kjaer, 2004; Zhang et al., 2005; Kjaer et al., 2005). As in hard tissue, cross linking of adjacent collagen molecules is achieved by the presence of PG-GAG complexes (Section 1.6.2.3). Intracellular collagen synthesis is outlined in Figure 1.10.

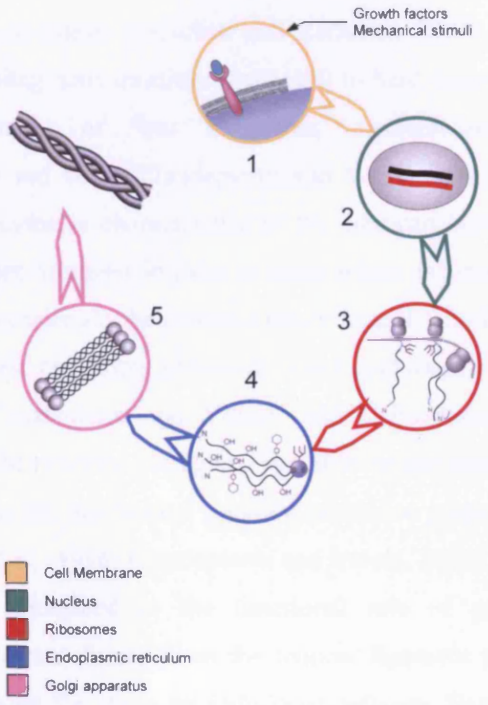

Figure 1.10 Schematic of the mechanisms involved in collagen Synthesis

(1) Signalling molecule-receptor complex formation and collagen synthesis activation, (2) collagen gene transcription into mRNA, (3) Ribosomal mRNA transcription into polypeptide α-chains, (4) Procollagen molecule assembly and (5) Extracellular Procollagen molecule transport. Some elements of the illustration adopted from (Nelson and Cox, 2004).

1.6.4 The enthesis: The hard-soft tissue interface

Entheses are the insertions of tendons, ligaments, joint capsules or fascia into bone. Soft tissues attachment to bone occurs via a transitional zone composed of histologically distinct layers and depending on the developmental mechanisms involved, this zone may assume a fibrous or fibrocartilaginous nature (Claudepierre and Voisin, 2005; Doschak and Zernicke, 2005). Tendons and ligaments attach to bone mainly through fibrocartilaginous entheses the development of which is an integral part of the endochondral embryonic bone formation. In a process coinciding with ossification of the hyaline cartilage anlagen, cells within the tendon/ ligament matrix undergo differentiation into metaplastic chondrocytes and commence fibrocartilage matrix synthesis (Doschak and Zernicke, 2005). By the end of this process, the fibrocartilaginous transition from soft to hard tissue is composed of the continuous arrangement of four structures; ligament/tendon, fibrocartilage, mineralised cartilage and bone (Claudepierre and Voisin, 2005) (Figure 1.11). The presence of chondrocytes is characteristic of the fibrocartilaginous layer, whereby these rounded cells are arranged in pairs or rows within lacunae in the ECM. Also, collagen fibres can occasionally be detected penetrating the cartilaginous zone, in the form of Sharpey fibres, providing additional direct anchorage of the soft tissue into the bone surface (Claudepierre and Voisin, 2005). Biochemical analysis of the fibrocartilaginous ECM revealed collagen Type II to be the predominant component largely contributing to the mechanical pressure resistance properties of the structure (Sagarriga Visconti et al., 1996; Claudepierre and Voisin, 2005). The structure of the enthesis is greatly committed to the functional role of gradually distributing mechanical load and shear forces from the tendon/ ligament proper into the bone surface, thus minimising the stress on individual collagen fibres (Goh et al., 2003; Doschak and Zernicke, 2005). Additionally, the combined mineralised/non-mineralised nature of this structure provides both, stress concentration stiffness and compression stress tolerance (Benjamin et al., 2000; Doschak and Zernicke, 2005).

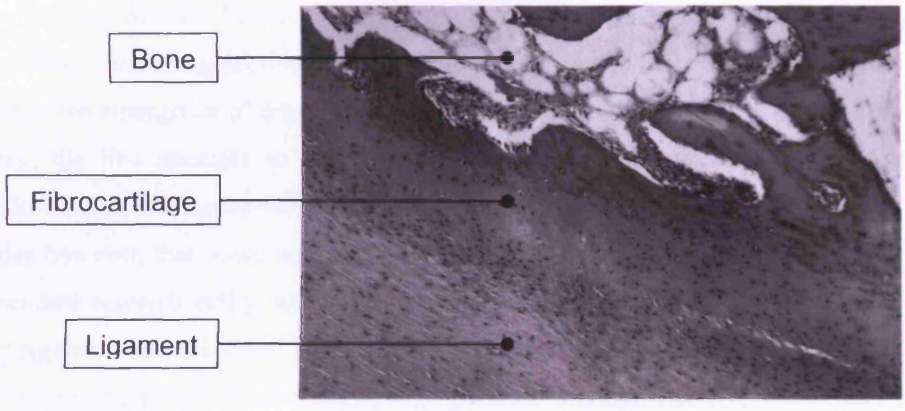

Figure 1.11 Histological Sections through an enthesis

Insertion of the vastus lateralis on the greater trochanter. X 100 (Claudepierre and Voisin, 2005).

1.7 Tissue Engineering: Repair through regeneration

1.7.1 Introduction

In 1993 in Science magazine, and possibly for the first time in scientific literature, Langer and Vacanti defined tissue engineering research as "an interdisciplinary field that applies the principles of engineering and the life sciences toward the development of biological substitutes that restore, maintain or improve tissue function." This definition however, was first used by F. C. Fung of University of California, San Diego in 1985 in a proposal for establishing an engineering research centre submitted to the National Science Foundation (NSF) in the USA (Langer and Vacanti, 1993). Historically, tissue engineering is deeply rooted in clinical medicine and can be related to the emergence of organ transplantation where, and at beginning of the 20th century, the first attempts to replace deficient tissue structures were carried out (Toledo-Pereyra and Lopez-Neblina, 2003; Aviles et al., 2004). It was in the last two decades however, that tissue engineering was conceptualised and well defined as an independent research entity, as a shift from the emphasis on tissue replacement to tissue regeneration took place (Hench, 1998). Such a shift was based upon the fact that conventional tissue replacement through grafting, although effective, is limited by various factors accentuating the need of developing an alternative approach. An approach that combines the use of biocompatible and bioactive matrices as scaffolds guiding or supporting tissue growth; the utilisation of the host cells as means of synthesising the ECM components; and the application of several extrinsic signalling and biomechanical factors so that the in vivo environment necessary for tissue formation can be simulated (Berg, 1992; Braddock et al., 2001).

1.7.2 Conductive tissue regeneration

Through the use of acellular biocompatible material configurations, guided tissue regeneration aims at reconstructing the deficient structure and preventing the invasion of non-functional scar tissue (Fujihara et al., 2005). Providing that the appropriate morphogenetic factors are delivered to the site, these biocompatible matrices may serve firstly as pathways for cell migration from the adjacent, intact and healthy tissue

towards the void and secondly, as scaffolds providing the biomechanical support for new tissue formation, vascularisation and integration into the host body (Burg et al., 2000). This approach is being assessed extensively, and in conjunction with use of grafts, for the surgical treatment of periodontal disease (Alberto, 2004). Recent studies reported on the potential use of biodegradable copolymers, alginate calcium membranes and polymer/calcium phosphate composites as periodontal pocket filling and graft supporting constructs as these materials have been shown to support cell invasion, proliferation and differentiated function (Hokugo et al., 2004; Fujihara et al., 2005). Demineralised bovine and porcine matrices, polymer and polymer/ ceramic composites were also evaluated as scaffolding systems for the in vivo regeneration of large bone defects and have been proven to be reasonably biocompatible and, most importantly, possess osteoinductive qualities (Burg et al., 2000). The success of guided tissue regeneration, however, remains dependent on the availability of a viable and well vascularised host bed and strongly related to the critical size of the tissue loss as large defects, greater than 4 cm, cannot be regenerated unless combined with a grafting procedure (Harakas, 1984; Croteau et al., 1999; Gugala and Gogolewski, 2002).

1.7.3. The inductive approach

Frequently referred to as cell transplantation, the concept of inductive tissue regeneration can be accurately described as bioengineering an autograft. This concept evolved around developing a cell/ matrix system as a nucleus for the *in vitro* morphogenesis of tissue (Vacanti et al., 1998). Host cell populations, either differentiated or mesenchymal stem cells (MSCs) can be isolated, expanded and seeded onto biocompatible and biodegradable scaffold constructs so that matrix synthesis mechanisms can be invoked leading, ultimately, to the *in vitro* formation of de novo tissue units. These units can be subsequently transplanted into the area of need where integration into the deficient site may occur restoring structure, volume and function (Alsberg et al., 2001) (Figure 1.12). Capitalising on this inductive strategy, naturally derived and synthetic materials fabricated into three dimensional and porous scaffolds have been utilized for bone regeneration. It has been shown, in numerous studies, that scaffold invasion by the seeded cells and the ensuing

mineralised tissue formation can be successfully induced (Bruder and Fox, 1999; Laurencin et al., 1999; Holy et al., 2000; Salgado et al., 2004). Bioengineered replacement systems for the repair of tendons and ligaments, in the form of fibroblast seeded collagen matrices and polymer fibre scaffolds, are also the subject of constant development (Laurencin et al., 1999; Goh et al., 2003; Cooper et al., 2005).

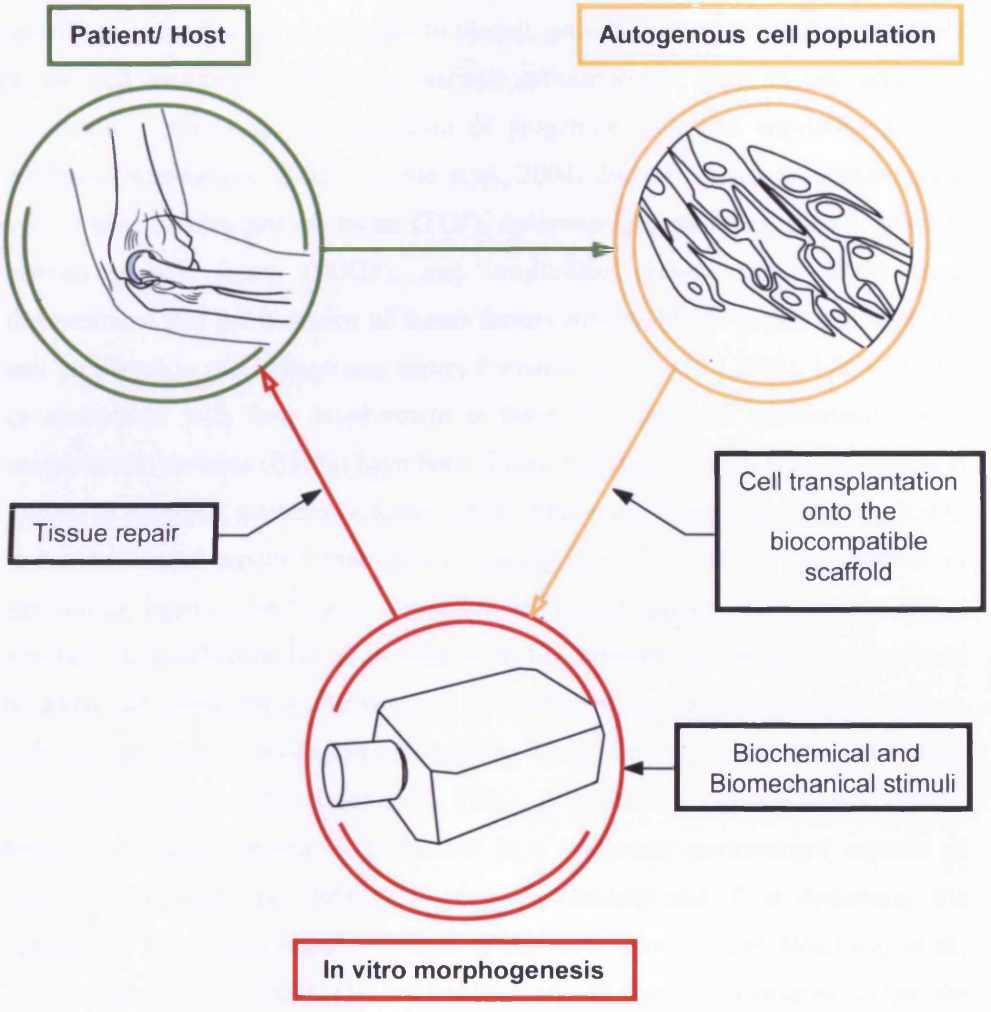

Figure 1.12 The concept of inductive tissue engineering

1.7.5 The role of extrinsic factors and culture environment

As tissue engineering attempts at recreating the biological mechanisms by which tissue formation is induced, it is critical that the relevant *in vitro* culture environment is supplemented with the appropriate growth, regulatory, hormonal and mechanical factors. Growth factors play an important role in the formation of tissue and organs during embryogenesis, postnatal growth and tissue remodelling in adulthood. As signalling molecules and in response to stimuli, growth factors bind to their receptors on the cell membrane influencing various cellular events such as cell adhesion, proliferation, migration, differentiation of progenitor cells and regulating protein synthesis (Schliephake, 2002; Salgado et al., 2004). *In vitro* studies investigating the role of transforming growth factor (TGF), epidermal growth factor (EGF), platelet-derived growth factor (PDGF), and insulin-like growth factor (IGF) have demonstrated that the inclusion of theses factors enhanced both tendon and ligament cell proliferation and collagenous matrix formation (Goh et al., 2003). Likewise and in accordance with their involvement in bone formation and maintenance, bone morphogenic proteins (BMPs) have been shown to induce *in vitro* bone formation if present in sufficient quantities (Boden, 1999; Burg et al., 2000; Vogelin et al., 2000). It has been also reported that BMPs, namely types 13 and 13, are capable of stimulating ligament-like tissue formation in animal models (Goh et al., 2003). Similarly, biomechanical forces in influencing cell function and tissue formation must be taken into consideration. Sensing and responding to mechanical and shear stresses, cells activate adaptive biological processes as tissues undergo remodelling (Braddock et al., 2001; Oakes, 2004; Kjaer et al., 2005). It is therefore imperative that *in vitro* tissue regeneration should be conducted in a bioreactor environment capable of delivering, through the application of cyclic loading and fluid dynamics, the appropriate mechanical stimuli (Frangos et al., 1987; Brown, 2000; Botchwey et al., 2001; Salgado et al., 2004). This environment should also be constructed so that the adequate and uniform diffusion of nutrients, waste and scaffold degradation by-products can be achieved by implementing a continuous flow culture design (Grabowski et al., 1993; Botchwey et al., 2001; Navarro et al., 2001)

1.7.6 The biocompatible scaffold

1.7.6.1 Introduction

The nature of scaffold forming material enables the fabrication of matrices of appropriate shape and form so that *in vitro* cell invasion is permitted in a uniform manner throughout the entire structure and the efficient delivery of nutrients, growth and regulatory proteins is facilitated (Brekke and Toth, 1998). Mechanically, the material must be capable of withstanding the hydrostatic pressures and mechanical loads once implanted into the host and of a volume, shape and size matching those of the structure to be replaced (Salgado et al., 2004; Cooper et al., 2005). The chemical and biological properties of the constituting material however, remain critical for the success of this material in supporting cell function and tissue formation.

1.7.6.2 The concept of biocompatibility

When under consideration for tissue engineering, biocompatibility of a certain material is related to the nature of reaction this material provokes in both, the seeded cells and the recipient host tissue. The scaffold material must support and maintain the processes involved in cell attachment, differentiated function and long term synthesis of ECM proteins (Ahmad et al., 1999; Cooper et al., 2005). When implanted into the host the scaffold material is considered biocompatible if the following criteria have been met (Brekke and Toth, 1998),

- The material elicits low tissue reaction and limited inflammatory response.
- The material is non-immunogenic as foreign body chronic giant cell reaction, and the ensuing implant rejection, must not occur.
- The material is non-toxic.
- The material must be free of transmissible disease.
- If the material is degradable, the degradation must yield biocompatible by-products that can be removed by metabolic means.

1.7.6.3 The in vivo bioactivity

Bioactivity is the ability of the scaffold material to induce a specific biological response at the interface with the host tissue leading to the formation of a biological bond between the material and the adjacent tissue structure (Thompson and Hench, 1998). Bioactivity may also identify the capacity of this material in stimulating cell migration towards the scaffold (Burg et al., 2000). The formation of a bioactive bond at the scaffold-tissue interface has been attributed to the deposition, and growth, of a dense mineralised layer composed mainly of nano-scale HA crystals that bind strongly to collagen fibres (Hench, 1998). It has been shown that the strength of bioactive bonding, to both hard and soft tissue interfaces, is equal to or greater than the binding forces in the normal tissue (Hench, 1998). Bioactivity therefore is vital for in vivo integration of the scaffold, and must be evaluated when electing certain material for the biocompatible scaffold fabrication.

1.7.6.4 The importance of biodegradability

The total biodegradation of the scaffold forming material eradicates the problems associated with chronic foreign body reaction in the host. In the long term, functional dependency on the prosthetic device, fatigue properties and the possible mechanical failure of the material are all gradually decreased, and eventually eliminated, as the scaffold degrades (Alsberg et al., 2003; Cooper et al., 2005). It is important however, that the material solubility characteristics can be controlled and optimised in a manner corresponding to ECM deposition so that a linear relationship is established between the rate of scaffold degradation on one hand, and the pace of functional tissue formation on the other (Alsberg et al., 2003; Salgado et al., 2004).

1.8 Biomaterials for tissue engineering

1.8.1 Naturally derived polymers

Biopolymer-based cellular systems, whether animal or vegetal in origin, have attracted wide interest due to their low immunogenic potential, unlimited source and the capacity of interacting with the host tissue (Salgado et al., 2004). Collagen, fibrinogen, chitosan, starch, hyaluronic acid, and poly (hydroxybutyrate) are examples of the many biopolymers currently in use among which, fibrillar collagen is broadly considered the material of choice (Novikova et al., 2003). This material is considerably bioactive, can be biochemically formulated so that it approximates the host tissue's collagen type and, through the application of purification techniques, can be rendered nonimmunogenic (Cancedda et al., 2003). Collagen is also structurally versatile allowing the production of various scaffold configurations such as membranes, fibres and foams (Cancedda et al., 2003). The assessment of collagen scaffolds, as porous foams and fibre meshes, has demonstrated a promising potential in supporting bone, ligament and tendon tissue regeneration (Itoh et al., 2001; Goh et al., 2003). Despite being considerably bioactive, collagen derived material is low on mechanical strength and integrity hence necessitating structural modification, through incorporating calcium phosphate for example, to improve the in vivo functional resistance (Burg et al., 2000). Also, several issues concerning the risk of xenogenic factor transmission and the long term *in vitro* stability of collagen may prove to be challenging in relation to tissue engineering (Burg et al., 2000; Lee et al., 2001).

1.8.2 Synthetic polymers

Belonging mainly to the polyester family of organic compounds, soluble synthetic polymers are the most commonly assessed substrates in the biomedical engineering filed. Polylactic acid (PLA), polyglycolic acid, (PGA) and copolymers, polylactide-co-glycolide (PLAGA) are all derivatives of the poly (α-hydroxy acids) species and their use in human subjects is approved by the FDA (Cooper et al., 2005). This class of materials can be moulded into porous and fibre mesh structures that have been shown, in several animal models, to be potentially suitable as cell delivery

biocompatible systems (Burg et al., 2000; Holy et al., 2000; Goh et al., 2003; Cooper et al., 2005). Structurally, the suitability of synthetic polymers as scaffold material is undermined by their inherent mechanical weaknesses, and structural reinforcement into composites is often a requirement (Mooney et al., 1996). The release of the α-hydroxy carbonic acids degradation products, lactic and glycolic acids in particular, is associated with the induction of an acute toxicity inflammatory reaction in the host (Meikle et al., 1994; Martin et al., 1996; Winet and Bao, 1997). This toxicity may also negatively influence cell proliferation and function compromising the critically important in vivo integration of the implanted cell/ scaffold complex (van Sliedregt et al., 1992; van Sliedregt et al., 1994).

1.8.3 Ceramics and bioactive glasses

Bioceramics have been repeatedly nominated as fulfilling almost all the requirements of an ideal implant material. Ceramics are nearly biologically inert, can be fabricated into porous structures, can be biodegradable and considerably bioactive (Thompson and Hench, 1998). The interest in such materials probably emerged by observing their bioactive properties when, and in the 1970s, HA coating of stainless steal orthopaedic devices resulted in a significantly enhanced bonding to bone (Ducheyne and Qiu, 1999). Nonetheless, the highly organized crystalline structure, brittle nature and the extremely slow in vivo degradation of HA limit its application as tissue engineering scaffold material (Ducheyne and Qiu, 1999; Sikavitsas et al., 2001).This has led to incorporating HA with soluble tricalcium phosphate slats (TCP, bone ash) producing degradable HA/TCP composites (Verdonschot N et al., 2001; Cancedda et al., 2003). Solubility trends of TCP, on the other hand, are potentially unpredictable as rapid breakdown of the salt crystals, ensuing osteoclastic activity, may compromise the scaffold mechanical integrity and induce cytotoxicity as extracellular concentrations of calcium and phosphate are increased (Salgado et al., 2004). It was not until a new generation of material emerged, that the bioactive qualities of calcium phosphate based ceramics were truly incorporated in an appropriate biodegradable setting. This class A bioactive, silica based glass material form is based on the SIO4-4 building block combining structural flexibility with biodegradable properties (Thamaraiselvi and Rajeswari, 2004). This glass material is based on the generic form SiO_2–Na_2O–

$CaO–P_2O_5$ and is extremely versatile as modifying the glass structure, by varying the contribution of the constituent components, will affect the solubility rates and mechanical properties (Hench, 1998). The most commonly evaluated form of silica glasses is commercially available Bioglass ®45S5. Bioglass contains 45% SiO2 and have been shown to induce *in vitro* bone cells proliferation and function and crucially, to bind to collagen in both hard and soft tissues (Hench, 1998; Xynos et al., 2000). Due to an extremely brittle nature, the use of silica based glasses as scaffold material in load bearing sites is limited and structure enhancing methods, by incorporating polymer matrices, may produce non-soluble composites (Thompson and Hench, 1998).

1.9 Phosphate based glasses

1.9.1 Chemical and physical characteristics

The phosphate glass species polymeric network is formed around the tetrahedral phosphate anion and in the ternary form, $CaO\text{-}Na_2O\text{-}P_2O_5$, calcium and sodium oxides (CaO and Na_2O respectively) are added as modifiers (Ahmed et al., 2004b) (Figure1.13). Clear phosphate glasses can be generated at relatively low melting points and transition temperatures providing that the phosphorous pentoxide (P_2O_5) content is above 40 mol% in the ternary composition (Uo et al., 1998). Solubility measurements indicated that the degradation trends of these glasses are predictably stable and, by individually modifying each precursor's contribution within the glass generic form, extremely controllable (Knowles et al., 2001). This flexibility allows the creation of specific solubility profiles that may correspond to the in vivo scaffold degradation-tissue formation balance. Solubility rates of these glasses appeared to be primarily dependent on the inhibitory effect of the CaO content as, in several studies, increasing the CaO mol percentage resulted in reduced glass solubility (Franks et al., 2000; Ahmed et al., 2004a; Ahmed et al., 2004b). This phenomenon has been attributed to the saturation of the local environment with the ions released from the least soluble glass constituent, CaO in this case. However, a more plausible explanation may lie in the fact that the Ca cations can form cross links between oxygen atoms in different molecular chains within the glass (Uo et al., 1998).

Another advantage of the phosphate glass chemical structure is the ability to incorporate various additional elements, to produce more complex quaternary compositions, thus further enhancing the physical properties. For example, the introduction of iron oxides to the glass network may lead to more favourable solubility trends and mechanical strength (Wen et al., 1998; Franks et al., 2001). When the in vivo application is targeted, overcoming the mechanical limitations imposed by the glass brittle nature is achievable using phosphate based glasses. With the low melting temperature as an aiding factor and through reasonably uncomplicated processes, phosphate glasses can be drawn into fibres of considerable tensile strength and flexible physical features so that scaffold systems of suitable shapes and volumes can be constructed (Pahler and Bruckner, 1982; Ahmed et al., 2004a; Ahmed et al., 2004b). Hence the use of soluble phosphate based glass fibres, doped with various inorganic ions, have been highlighted in several reports as reinforcement scaffold material for orthopaedic devices (Choueka et al., 1995; Charvet et al., 2000; Navarro et al., 2001).

1.9.2 Bioactivity and biocompatibility

As in vivo scaffolds, phosphate based glasses are expected to exhibit bioactive features. The breakdown of these glasses is followed by the release of Na+ and Ca2+ cations which are both implicated, as catalysts, in the cascade of events leading to the formation of the material-tissue bioactive bonding (Hench, 1998). Salih and co-workers (Salih et al., 2000)studied the effect exerted by the degradation substrates of a series of ternary glass on the morphology, proliferation and protein synthesis of human osteoblastic cell lines and concluded, that the incubation in these substrates resulted in no negative impact on cell shape, growth and function. On the contrary, the presence of the substrates stimulated an osteogenic response in the targeted cells as expression of several ECM associated proteins was up-regulated (Salih et al., 2000). These results were in line with similar experimental studies that attempted to evaluate the biocompatibility of binary phosphate-calcium/ sodium glasses as scaffold material. Seeded macrophages, as manifested by morphology and cell activity, expressed low levels of activation as these glasses provoked limited inflammatory responses (Gough et al., 2002). Human osteoblasts adhered to these glasses, and

exhibited the appropriate functional morphology, in a manner indistinguishable from those cells seeded on control surfaces and in the long term, cells were capable of maintaining the expression of proteins directly involved in the ECM synthesis (Gough et al., 2002; Gough et al., 2003). In fact, and within 28 days in culture, the formation of a collagenous matrix did take place on the glass surface.

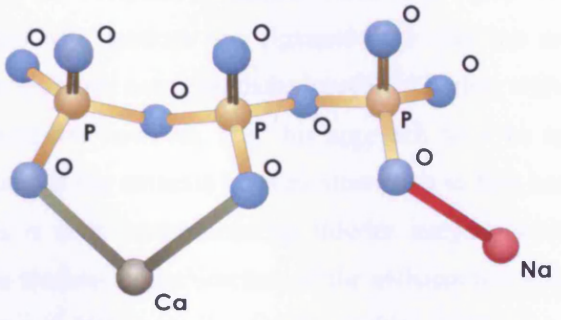

Figure 1.13 Basic molecular unit of a ternary phosphate based glass composition ($CaO\text{-}Na_2O\text{-}P_2O_5$)

Atoms: Phosphorous (yellow), Oxygen (blue), Calcium (green) and Sodium (red)

1.10 Summary: A Glass fibre scaffolding system for the hard-soft interface repair

As the conventional strategies aiming to replace defective structures suffer many limitations, inductive tissue engineering may present the ideal solution by generating autogenic de novo tissue units of biological, histological and biomechanical properties matching those of the recipient structure. Following injury or disease, clinical problems associated with tendons and ligaments are common and the cell-matrix tissue regeneration approach can potentially succeed in dealing with such problems. It is important to recognize however, that this approach must be applied so that the structure is generated at the enthesis level as attempting to fuse hard and soft tissues by surgical means is often undermined by inferior integration and in some cases, failure. Taking the anatomical architecture of the entheses into consideration, and in order to combine two histologically diverse entities so that an interface can be established, and evolve, the constituting cells must be seeded separately on one continuous incorporating scaffolding system whereby this continuity will later guarantee the establishment of a functional bond between the two tissue elements. Fibre-based matrices are therefore structurally suitable when providing the contiguous base for a co-culture cell transplantation strategy. Further to the physical configuration, the scaffold structure must be generated from a biocompatible and biodegradable material in a manner that guarantees the survival and function of the seeded cells on one hand; and the functional integration into the host tissue on the other. Owing to their biocompatibility and structural properties, phosphate based glasses have been shown as potentially excellent scaffold material for tissue engineering and it is important at this stage, that this potential is further investigated and developed towards a primary human cell seeded, fibre-based scaffolding system.

1.11 Aims of this study

(i) To evaluate the biocompatibility of a range of ternary phosphate based glass compositions by investigating the seeded primary human osteoblast and fibroblast attachment, morphology, survival and expression of phenotypic protein synthesis so that a base composition can be elected for glass fibre production.

(ii) To investigate the need of further enhancing the biocompatibility of the ternary glass form by adding a forth modifier to the glass network; and to produce glass fibre scaffolds of suitable configuration for biocompatibility testing.

(iii) To asses the suitability of glass fibre scaffolds as in supporting osteoblast and fibroblast long term survival, population growth and the expression of the differentiated cell function in maintaining both, hard and soft tissues ECM.

(iv) To investigate the feasibility of incorporating some of the extrinsic factors necessary for tissue formation within the cell-scaffold culture through stimulating osteogenesis in the fibre seeded osteoblasts; and the design of an open laminar flow bioreactor to provide nutrient, oxygen and waste perfusion to the scaffold culture on the other.

(v) Finally, to produce a co-culture system whereby osteoblasts and fibroblasts can be seeded separately on a contiguous fibre arrangement so that the hard-soft tissue interface can potentially be generated.

CHAPTER TWO

MATERIALS AND METHODS

2.1 Cell Culture

2.1.1 The *in vitro* cell culture environment

All cultured cells were maintained in a humidified atmosphere, in 5% CO_2 and at 37° C. The standard growth medium (GM) used was prepared from Dulbecco's Modified Eagle's Medium (D-MEM) supplemented with 10% (v/v) fetal calf serum (FCS), 2mM L-glutamine, 100 U/ml penicillin and 100 μg/ml streptomycin (all from Invitrogen, Paisley, UK). Cells were grown in 10 ml of GM using 80 cm^2 cell culture flasks (BD Biosciences, Oxford, UK) with gas-permeable caps.

2.1.2 Isolating primary human cells

Human osteoblasts (HOB) were isolated by both enzyme treatment and explant culture methods. Alveolar bone fragments were obtained from routine third molar extractions at the Eastman Dental Hospital and placed immediately in transport medium consisting of α-Minimal Essential Medium (α-MEM) supplemented with 100 U/ml penicillin, 100 μg/ml streptomycin, 2 mM L-glutamine, 10% FCS and 25 μg/ml fungizone (all from Invitrogen, Paisley, UK). Bone fragments were cut into small pieces (~ 2 mm^3) using no. 10 surgical blades and washed twice in sterile phosphate buffered saline (PBS; Invitrogen) to remove blood cells. The bone pieces were then digested using 0.02% (v/v) EDTA (Ethylenediaminetetraacetic acid)-trypsin and 10,000 IU collagenase (both from Sigma-Aldrich, Poole, Dorset, UK) for 1 h at 37°C and the digest was centrifuged, resuspended in GM and incubated in 25 cm^2 cell culture flasks. For explant culture, bone pieces were placed in 6 wellplates (BD Biosciences), incubated in a small volume of GM and left undisturbed for 7-10 days. Cells from confluent digest and the explant cultures were then harvested and pooled together to establish the primary cell stock. The osteoblastic characteristics of these cells, by the ability to form mineralised nodules in vitro, were confirmed by Salish and co-workers (Salih et al., 2001). In this work, passages 4 and 5 of HOB cells were used (Figure 2.1A).

Human tendon fibroblasts (HTF) were prepared by direct explant technique (obtained by Dr. V. Mudera, Institute of Orthopaedics & Musculo-Skeletal Science, UCL, UK).

Briefly, tissue taken from the flexor tendon of the hand was rinsed twice in PBS and cut into pieces (2mm x 2mm x 2mm). These pieces were placed in culture dishes for 2 h in a dry incubator to facilitate tissue adherence to culture dishes and GM subsequently added. Sub-confluent primary cultures were propagated in GM and experiments were performed using cells between passages 2 and 4.

Human oral fibroblasts (HOF) were isolated, as above, by direct explant culture of 4 mm punch biopsies of the buccal oral mucosa (obtained by Dr. C.R. Irwin, Queen's University Belfast, UK) (Irwin et al., 2002). Passages 14, 15 and 16 were used throughout the work.

2.1.3 The MG-63 cell line

MG-63 transfected human osteosarcoma cells were used to conduct initial biocompatibility experiments. This cell line was selected as it has been shown to possess osteoblastic properties (Clover and Gowen, 1994), and an easy to access stock is readily available within the Eastman laboratories.

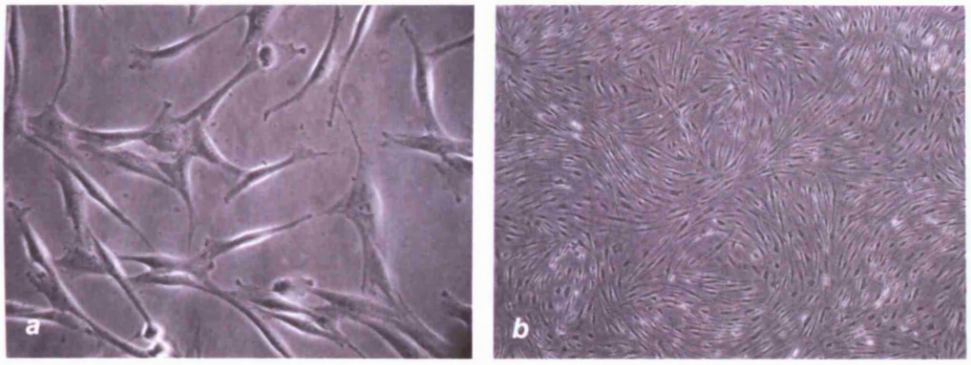

Figure 2.1 Primary cells in culture

Phase contrast light microscope images of *(a)*, Human craniofacial osteoblasts (HOB, X20 objective) and, *(b)*, Human oral Fibroblasts (HOF, X4 objectice).

2.1.4 Expanding the primary cell population

Primary cell populations were expanded via the regular passage of culture. At near confluence, GM was aspirated and adherent cells washed once in 5ml of PBS. This washing step was carried out to remove any traces of the trypsin inhibitor containing FCS. A 2.5 ml volume of Trypsin-EDTA solution (Invitrogen) was added and the cells were incubated for 10min to detach. The enzymatic action was inactivated by adding 7.5 ml of GM and the cell suspension was collected and transferred into a 15ml tube which was, subsequently, centrifuged at 1000 r/min for 5 min. The supernatant was later aspirated; the formed cell pellet disrupted; the cells resuspended in 10 ml of fresh GM; and the cell population was split 1:4.

2.1.5 Establishing primary cell stocks

Confluent cell populations were harvested as above however, the cell pellet was resuspended in 1 ml freezing medium of FCS containing 10% (v/v) dimethyl sulfoxide (DMSO, Sigma-Aldrich). The DMSO acts as a cryoprotectant preventing ice formation and ice-crystal cell damage. The cells, in freezing medium, were then immediately placed in a 1.5 ml cryovial and cooled gradually in an isopropanol container, overnight, to -70° C. The vials were later cryopreserved in liquid nitrogen, at approximately -196° C, until required. Cell stocks were resurrected by thawing the vial, at 37° C, in a water immediately bath after which, the cell suspension was transferred into 10 ml of pre-warmed GM in a 15 ml tube. The tube was then centrifuged as previously described, and the cell pellet resuspended in fresh GM.

2.1.6 Cell seeding considerations

To determine the appropriate cell concentration required for a certain seeding density, the suspended cells were counted using a counting chamber (Neubauer hemocytometer). The Neubauer hemocytometer 0.1 mm deep and subdivided into 9 main squares, each of 1 mm^2 surface area. and covered using a glass coverslip (Figure 2.2), At least 10µl of the sample was collected and pipetted under the coverslip and uniformly spread by capillary action. Using an X4 objective light microscope

objective, the cells were systematically counted in the 0.0625 mm^2 unit subdivided four primary squares. Cells contacting, or falling within, the lower and right boundaries of the main square were disregarded from the count. The average cell number, for the 1 mm^2 defined chamber volume (1 x 0.1 = 0.1 µl) was determined by dividing the total cell number by the number of counted squares, i.e. 4. This value was then multiplied by 10^4 so that cell density, in 1 ml of medium, was established.

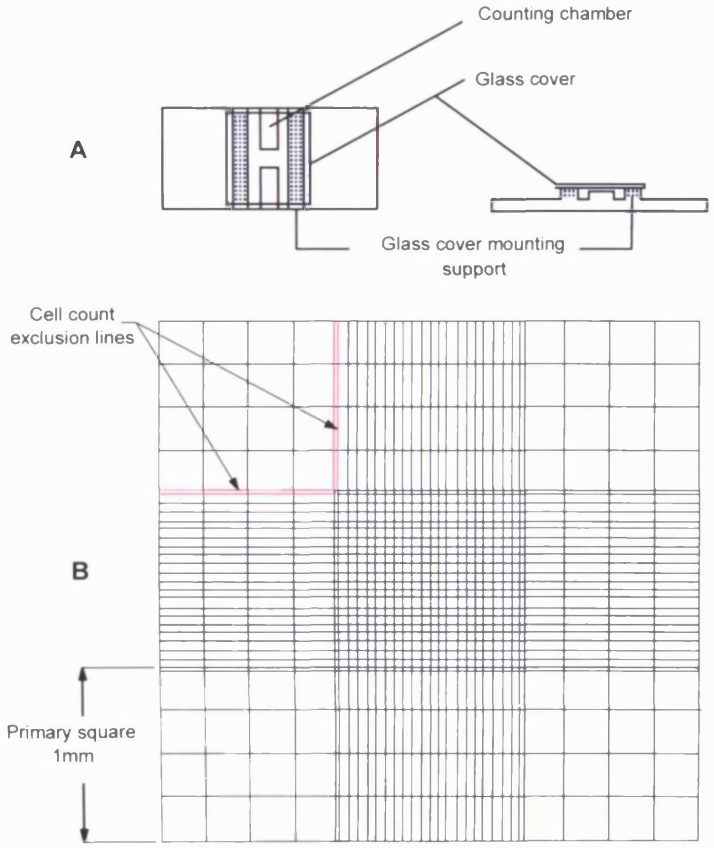

Figure 2.2 The haemocytometer

(a), Top and side views, *(B)*, the counting chamber surface.

Cell seeding density may influence the subsequent cell population behaviour in terms of proliferation and colonisation of the biocompatible scaffold (Wiedmann-Al-Ahmad

et al., 2002) however, and in this study, the main criterion for adopting certain cell seeding density was the limited stock of primary human cells. Mg-63 cells were accordingly seeded on borosilicate coverslips at a density of 5 x 10^3 cells in 1 ml of GM (3.2 x10^3 cell /cm^2), in 24 wellplates, and later investigated for protein synthesis (Section 2.7.3). Fluorescence microscopy evaluation 24 h in culture have shown positively stained and uniformly distributed population with cells exhibiting well spread morphology (Section 3.3.2). The seeding density of 3.2 x10^3 cell /cm^2 was therefore adopted for all biocompatibility assessment procedures for cells seeded on glass discs, fibres and control surfaces. This density was increased ten fold, to 3.2 x10^4 cell /cm^2, when conducting qPCR experiments in order increase total RNA yields thus improving qPCR efficiency and accuracy. The latter density was also adopted when seeding the co-culture configuration, and due to the short life span of the live staining assay, to maximize results. *In vitro* work on glass discs took place in 24 wellplates (BD Biosciences, Oxford, UK); and on glass fibre scaffolds in 55 mm petri dishes (Bibby Sterilin, Staffordshire, UK). All control experiments were conducted in 24 wellplates (BD Biosciences; and Orange scientific, Belgium).

2.2 Preparation of glass substrates

2.2.1 Introduction

At the melting point, the fusion of the crystalline glass forming precursor oxides forms a viscous slurry. As temperature increases, the crystal forming molecules increasingly vibrate around their solid state positions in the structural network until, and at the first order phase transition, a complete breakdown of the crystalline structure occurs and the molecules begin to flow. This shift from the solid to the liquid state of the matter is reversible if the liquid is gradually cooled to below the melting point so that crystal nucleation sties are formed, as viscosity increases, and the forming molecules are reorganised in an orderly fashion. This thermodynamic transition into the energetically favourable crystalline structure may not occur however, if the liquid is rapidly cooled so that low viscosity is maintained as temperature decreases thus inhibiting crystallisation. This kinetic transition, a second order phase transition, will result in glass formation as an amorphous solid of disordered molecular arrangement but with enough cohesion to maintain a rigid structure. Glass structural properties, density in particular, are strongly related to the temperature at which the transition takes place. At a slower cooling rate, glass transition is conducted at a lower temperature and higher viscosity, and a denser glass structure is therefore produced (Figure 2.3). Structural properties can be further enhanced by cooling the glass at an optimised temperature, and in a uniform manner, thereby releasing the internal residual stresses and inducing a minimum energy molecular arrangement. This annealing process has been shown to yield less brittle glass forms. For phosphate based glasses, and as described in Section 1.9.1, the P_2O_5 content plays a major role in the glass formation through affecting the glass transition phase. In this study, and for all glass compositions generated, the P_2O_5 content was fixed at 50 mol% as attempts to produce glass fibres using a lower content of P_2O_5 resulted in crystallisation and glass formation failure.

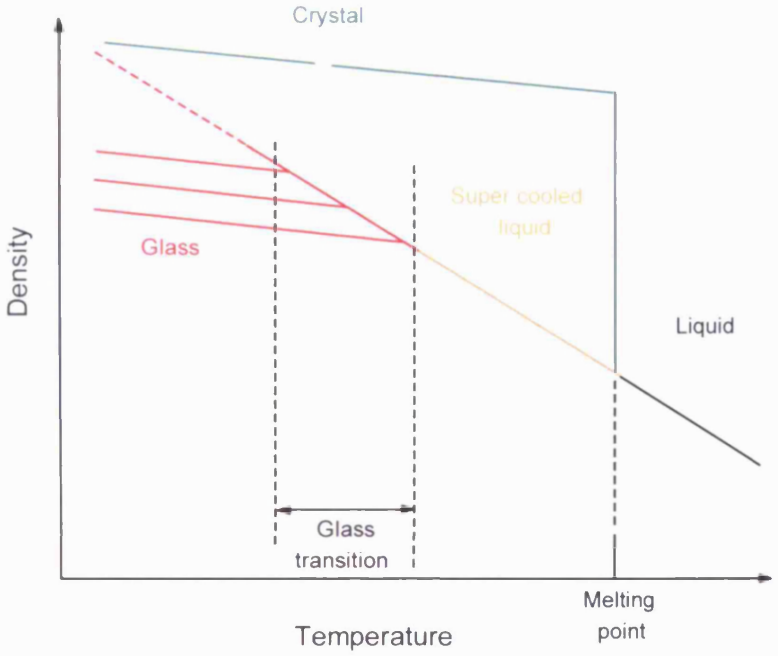

Figure 2.3 Density as a function of temperature in the phases of glass formation (Gibbs, 1996)

2.2.2 Glass batch calculations

The glasses were annotated in such a way that a glass composition, for example, of 40 mol % CaO, 10 mol % Na_2O and 50 mol % P_2O_5 was referred to as $(CaO)_{0.4}$-$(Na_2O)_{0.1}$-$(P_2O_5)_{0.5}$. In order to calculate the weight of each precursor oxide required to produce a particular glass form, the molecular weights of the components produced by this precursor were first determined. These values were then divided by the precursor's molecular weight and the component-precursor ratio was established. The amount of precursor needed, so that a particular molar contribution by this component to the final glass form is achieved, was calculated as follows:

(Component mol fraction x component molecular wt)/ component-precursor ratio

For example, and to produce the ternary $(CaO)_{0.3}$-$(Na_2O)_{0.2}$-$(P_2O_5)_{0.5}$ glass form, precursors calcium carbonate ($CaCo_3$), sodium dihydrogen orthophosphate (NaH_2Po_4)

and phosphorus pentoxide (P_2O_5) were used. During the glass melting process, the batch decomposition reaction of NaH_2Po_4 will yield the three components sodium oxide (Na_2O), phosphorus pentoxide (P_2O_5) and hydrates as detailed below.

	Precursor	Released components		
	2 NaH_2Po_4	Na_2O	P_2O_5	2 H_2O
Molecular weight g/mol	240	62	142	36
Component-precursor ratio		0.258	0.59	0.15

The amount of NaH_2Po_4 needed so that Na_2O contribution to the glass composition was 20 mol% (0.2 mol fraction) therefore was,

$$(0.2 \times 62)/ 0.258 \approx 48 \text{ g of } NaH_2Po_4$$

It is important to recognize however, that 48 g of NaH_2Po_4 will also contribute to the glass composition by approximately 20 mol% of P_2O_5 as,

$$(48 \times 0.59)/142 \approx 0.2 \text{ mol fraction of } P_2O_5$$

This value must be taken into consideration whereby a 30 mol% based batch calculation for the precursor P_2O_5, and due to NaH_2Po_4 contribution, is conducted. Hence, and as the component-precursor ratio for P_2O_5 is 1, the amount of phosphorus pentoxide required was ((0.3 x 142)/ 1) 42.6 g. Similarly, $CaCo_3$ decomposition results in the release of CaO and CO2 as components,

	Precursor	Released components	
	$CaCo_3$	CaO	CO2
Molecular weight g/mol	100	56	44
Component-precursor ratio		0.56	0.44

Accordingly, and for 30 mol% CaO contribution, the amount of $CaCo_3$ required was ((0.3 x 56)/ 0.56) 30 g.

Similarly, batch calculations for quaternary glasses were conducted with the inclusion of iron oxide (Fe_2O_3) as the fourth precursor.

Tables 2.1 and 2.2 detail the ternary, and quaternary, glass compositions generated throughout this study and the weights of the relevant precursors used. It should be noted however, and due to the volume capacity of the melting crucible, that the weight values are half of those established by the batch calculation process.

Table 2.1 Precursor weights for ternary glass production

Glass code	Precursor weight (g)		
	NaH_2Po_4	$CaCo_3$	P_2O_5
$(CaO)_{0.3}$-$(Na_2O)_{0.2}$-$(P_2O_5)_{0.5}$	24	15	21.3
$(CaO)_{0.3}$-$(Na_2O)_{0.18}$-$(P_2O_5)_{0.5}$	21.6	16	22.7
$(CaO)_{0.34}$-$(Na_2O)_{0.16}$-$(P_2O_5)_{0.5}$	19.2	17	24.1
$(CaO)_{0.36}$-$(Na_2O)_{0.14}$-$(P_2O_5)_{0.5}$	16.8	18	25.9
$(CaO)_{0.38}$-$(Na_2O)_{0.12}$-$(P_2O_5)_{0.5}$	14.5	19	26.9
$(CaO)_{0.4}$-$(Na_2O)_{0.1}$-$(P_2O_5)_{0.5}$	12.02	20	28.39
$(CaO)_{0.42}$-$(Na_2O)_{0.08}$-$(P_2O_5)_{0.5}$	9.61	21	29.81
$(CaO)_{0.44}$-$(Na_2O)_{0.06}$-$(P_2O_5)_{0.5}$	7.2	22	31.2
$(CaO)_{0.46}$-$(Na_2O)_{0.04}$-$(P_2O_5)_{0.5}$	4.8	23	32.6
$(CaO)_{0.48}$-$(Na_2O)_{0.02}$-$(P_2O_5)_{0.5}$	2.4	24	34.08

Table 2.2 Precursor weights for quaternary glass production

Glass code	Precursor weight (g)			
	NaH_2Po_4	$CaCo_3$	Fe_2O_3	P_2O_5
$(CaO)_{0.46}$-$(Na2O)_3$-$(Fe2O3)_1$-$(P2O5)_{0.50}$	3.6	23	0.8	33.37
$(CaO)_{0.46}$-$(Na2O)_2$-$(Fe2O3)_2$-$(P2O5)_{0.50}$	2.4	23	1.6	34.08
$(CaO)_{0.46}$-$(Na2O)_1$-$(Fe2O3)_3$-$(P2O5)_{0.50}$	1.2	23	2.4	34.8

2.2.3 Glass disc production

Using an analytical balance and in accordance with the desired composition, glass starting materials were weighed and thoroughly homogenised into a mix in a sealable plastic envelope as a homogenous precursor mix is critical for successful glass production. The precursor mix was then placed into a Pt/10% Rh crucible (Johnson Matthey, Hertfordshire, UK) which, in turn, was inserted in a preheated RTF 1500 furnace (Carbolite, Derbyshire, UK) at +1200° C for 75 min. The molten slurry was subsequently poured into a preheated graphite mould and placed in a Dicor furnace (Dentsply, Surrey, UK) at + 420° C for 60 min. The graphite mould was then left to cool overnight, inside the Dicor furnace, as the glass annealing process took place. The resulting 50 mm long glass rod was later cut, using a Testbourne diamond saw (Testbourne Ltd., Hampshire, UK) and water as coolant, into 1.5 x 13 mm discs (Figure 2.4) which were polished on a Knuth-rotor 6X using 1200 grit silicon carbide paper (6.5 μm average grain size). All glass discs, and prior to *in vitro* experimental procedures, were sterilised by dry heat at +180° C for 120 min and soaked in cell culture medium for 24 hours. The latter procedure was conducted to contain an initial surge of Ca^{2+} and Na^{+} ion release and, on the other hand, to allow the precipitation of dissolution products on the glass surface leading to more linear solubility patterns particularly for the highly soluble compositions (Franks et al., 2000).

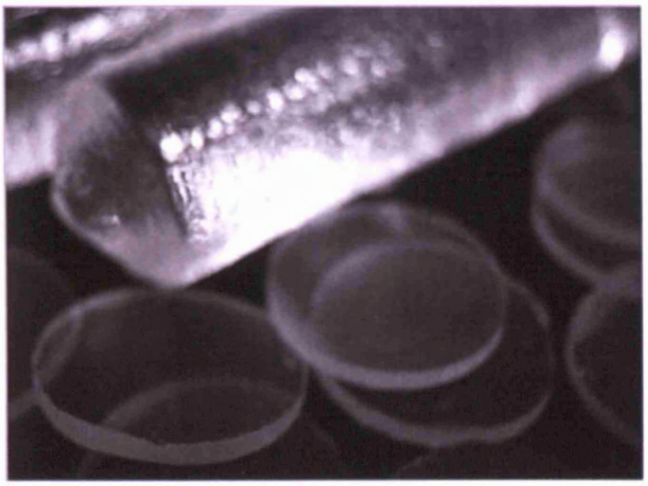

Figure 2.4 Glass rods and polished glass discs prior to *in vitro* assessment

2.2.4 Glass fibre fabrication

As detailed in Section 2.2.4 and excluding the annealing step, glass compositions were produced and the glass melt was poured directly onto a stainless steel plate to cool at room temperature (RT). Glass batches were then placed in a Lenton furnace incorporated Pt/10% Rh crucible to melt and homogenise, at approximately 1300° C, for 60 min. Situated below the furnace, and in close proximity to the crucible, a rotating stainless steel drum of 1 m circumference was used as fibre pulling device (Figure 2.5). Connected to a controller motor, the drum could be spun with precision at various rotational speeds thus granting the ability of producing various fibre diameters as at higher rotational rates; fibres of smaller diameters are generated. At a certain temperature specific to each composition, within the 1230° C to 1270° C range, an appropriate melt viscosity was reached and emerging through a 1mm funnel-like outlet in the crucible base, the slow formation of a glass droplet could be observed. Using a pointed-end ceramic rod, a fibre precursor was quickly drawn from the droplet onto the rotating drum surface where fibre bundle formation can henceforth be seen. The appropriate, temperature controlled, viscosity plays a major role during this process as a continuous and regular glass flow is vital for an uninterrupted, and successful, fibre production.

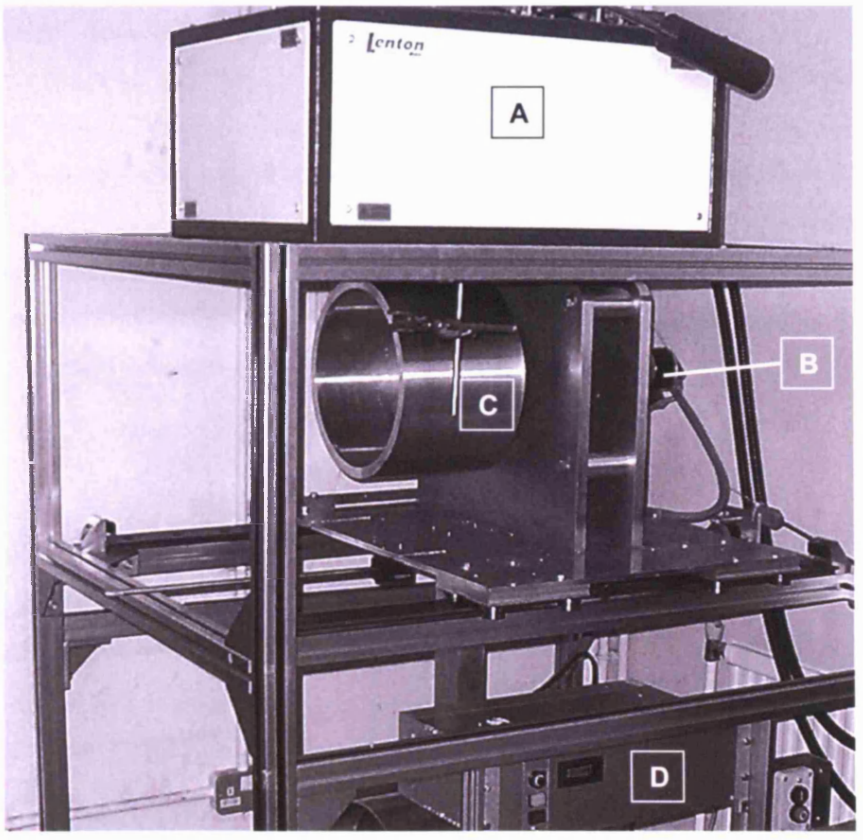

Figure 2.5 The glass fibre rig

(A) The melting furnace, (B) the rotor motor, (C) the fibre drum and (D) The rotational velocity control unit.

2.2.5 Glass fibre scaffold preparation

The fibre-based scaffolds must be designed so that fibres are arranged in a uniform and consistent fashion, thus eliminating the experimental variability related to random arrangement of the scaffold and ensuring, at this stage, that glass composition variability is the main investigated biocompatibility factor. This can be achieved if the fibres were laid, during production, in a manner that guarantees the presence of controllable fixed distances between alternating fibres.

For this purpose, the fibre rig was modified to allow a combined rotary-horizontal motion of the fibre drum. The drum was mounted on a horizontally movable plate which was, in turn, connected to a stepper motor via a driving centre shaft (Figure 2.6). The stepper motor was cyclically controlled, via a sweep-function generator, so that at 1 Hz frequency 32 steps per minute were generated and the drum mounting plate moved horizontally by 160 mm. The desirable value of the horizontal shift (v), in mm and in 1 min, was obtained from the equation,

$$v=[(d+s)k]/10^3$$

Where d is the fibre diameter value (μm); s is the desired distance between two adjacent fibres (μm); and k is the drum rotational frequency (r/min). Therefore, and assuming that at a drum rotational frequency of 800 r/min the generated fibre diameter is 20 μm; a desired gap of 10 μm for every revolution can be achieved by a horizontal shift value of ([(20+10)800]/10^3) 24 mm. Accordingly, the stepper motor frequency was adjusted to ((24 x1)/160) 0.15 Hz. The fibre configuration was carefully transferred, using adhesive tape, onto 32x32 mm custom made stainless steel frames and fibre ends were fixed using cyanoacrylate glue gel (product 01-06854, Henkel UK Ltd., Hertfordshire, UK). To prevent non-fibre associated cell adhesion and cyanoacrylate-medium contact, the 4 mm frame edges were coated with cell-repellent biocompatible RTV 118 silicone (Techsil Ltd. Warwickshire, UK) which was left to set overnight (Figure 2.7). A monolayer mesh and single parallel configurations were produced corresponding to bone and ligament tissue architecture respectively. Scaffolds were sterilised in 70% aqueous ethanol and immersed in GM for 24h prior to seeding.

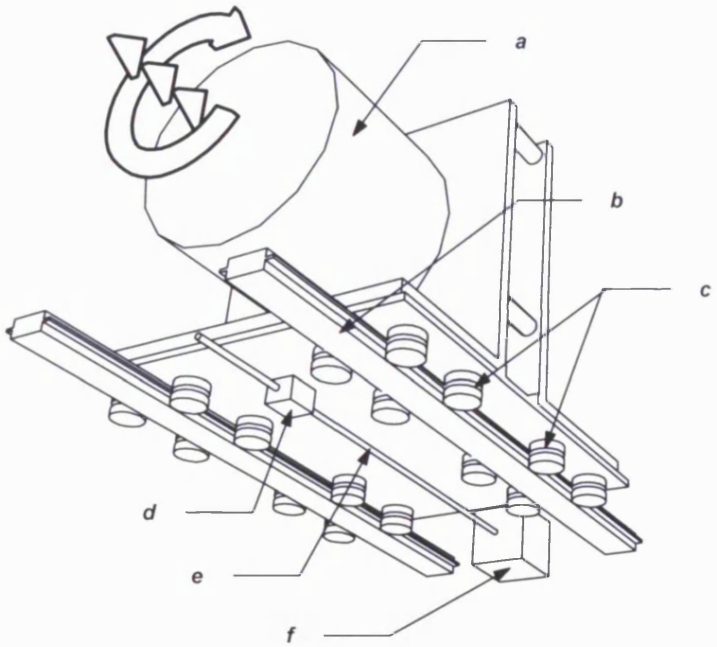

Figure 2.6 A schematic illustration of the stepper motor mechanism

(a) The fibre drum, *(b)* The plate track, *(c)* Metal bearings, *(d)* lockable turnbuckle, *(e)* Driving shaft, and *(f)* Stepper motor.

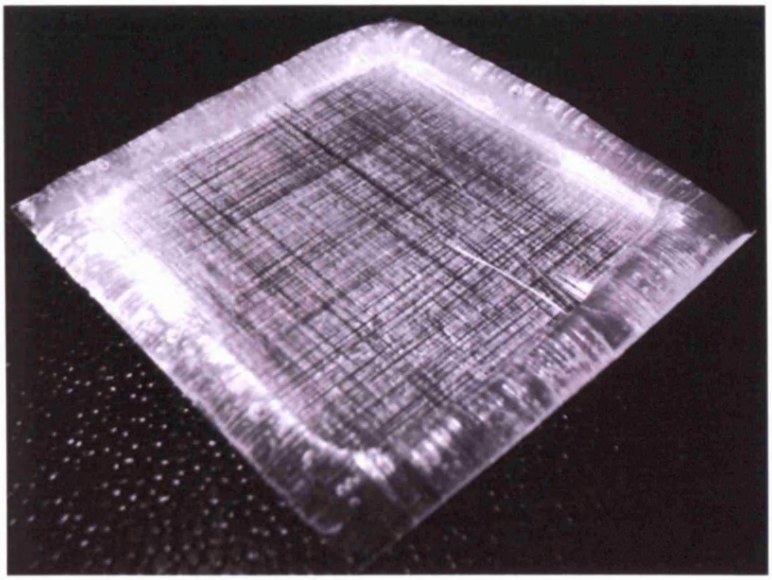

Figure 2.7 A monolayer mesh glass fibre scaffold

2.3 Co-culture scaffold system

In order for a continuous scaffold design to accommodate the separate seeding of two cell populations, a barrier configuration must be applied across the fibre arrangement. This barrier must prevent the mixing of the seeding media on either side during the time required for cell adhesion. Furthermore, the barrier must be removable so that any interference with the culture environment is eliminated. When in contact with an absolutely dry fibre arrangement, drop formation of tissue culture medium can be sustained and it has been hypothesised therefore, that a minimum dry separation zone may permit the segregated presence of two liquid drops in close proximity. A 100 μm dry space barrier, define by two 100 μm thickness glass coverslips, was therefore applied vertically across the fibre arrangement and fixed to the scaffold frame during the RTV 118 silicone application process (Figures 2.8a and b). When assessed for co-culture purpose, the 300 μm separation supported simultaneous, and separate, drop formation on either side.

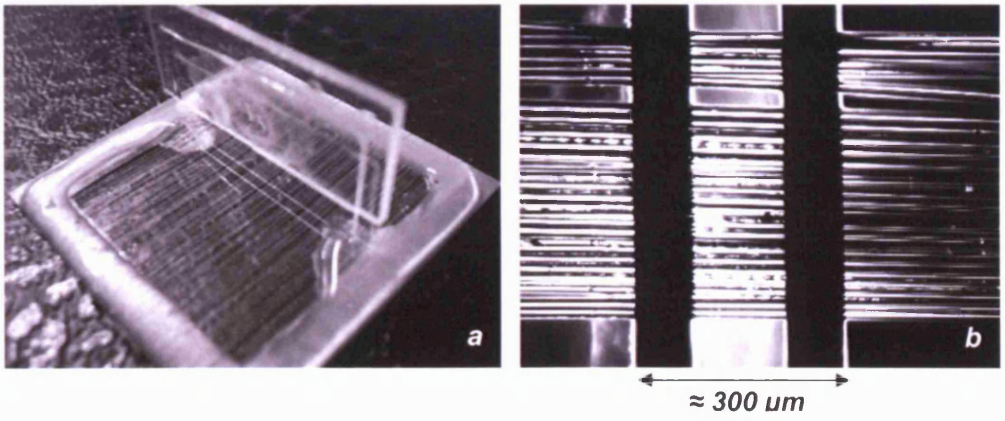

Figure 2.8 Co-culture scaffold design

(a) the glass-air-glass barrier across the fibre arrangement and , *(b)* An X20 objective microscope light image of the barrier.

2.4 Glass fibre characterisation

2.4.1 Solubility measurement

To ensure consistency with the cell culture environment, all solubility tests were carried out in GM. 30 mm long fibre bundles of 100 mg weight were placed in 6 well-plates (Orange Scientific), incubated in 5 ml GM to insure consistency with *in vitro* culture conditions and at days 1, 4, 7 and 10 fibres were dried and weighed. The medium was replaced at 2 day intervals.

2.4.2 Assessment of fibre diameters

Fibres were embedded in epoxy resin (SpeciFix-20, Struers Ltd., Glasgow, UK) blocks via a two-step mounting process. For both steps a resin-curing agent mix (7:1 weight/weight) was thoroughly stirred for 3 min and left to set for 2 min before use. Firstly, fibre bundles were placed in a 3 x 3 x 20 mm PTFE mould, embedded and the resin mix left to cure overnight at RT. The fibre bundle was placed in a MultiForm mounting cup using supporting clamps, embedded as described above and 30 mm cylindrical resin blocks were produced. The block was later cut (Testbourne diamond saw), perpendicular to the fibre axes, and sequentially polished on a combined LaboForce/ LaboPol Modular Preparation System (Struers Ltd.)as follows,

Surface	Medium/ Lubricant	Force (N)	Speed (r/min)	Duration (min)
SiC 220	Water	30	300	2
MD-Largo	Dp-Susspension, P (9 μM)	25	150	5.5
MD-DAC	Dp-Susspension, P (3 μM)	25	150	4.5
MD-NAP	Dp-Susspension, P (1 μM)	25	150	1.5

Digital light images of fibre Sections, at X20 magnification, were acquired and diameter values of 50 fibre Sections were obtained using Image-Pro® Plus software4.0 (Media Cybernetics UK, Berkshire, UK); exported into spread sheets; and analysed to determine the average fibre diameter.

2.4.3 Scanning electron microscopy

Glass fibres were mounted, in their dry state, on aluminium stubs and coated with 4nm platinum/palladium (80/20) using a high-resolution sputter coater (Agar Scientific, Stansted, UK). Samples were later imaged using a Hitachi S-4700II field emission scanning electron microscope (Hitachi High Technologies, Berkshire, UK) operated in ultra-high resolution mode at an accelerating voltage of 1.0kV(Hughes et al., 2005).

2.5 The flow culture system

2.5.1 Introduction

The flow culture system aimed at providing the perfusion of nutrients, and the removal of waste and glass degradation products throughout the scaffold. Therefore, and as simulating the physiological shear stresses are at this stage beyond the scope of this work, the near zero shear stress of 1.56 x 10^{-3} dyne/ cm^2 was adopted as a benchmark value (Navarro et al., 2001).

2.5.2 The flow cell

A study by Bakker et al., using particle image velocimetry, has shown that fluid flow inside a parallel plate chamber occurs at different hydrodynamic velocity profiles where the inlet and outlet conditions, and the chamber design, dictate the overall flow stability(Bakker et al., 2003). It has been concluded that in configurations where the inlet and outlet are horizontal, and at right angles with the flow plane, stable flow can be induced over a larger surface area (Figure 2.9). Stability has also been enhanced where a smooth transition between the various parts of the chamber is present. Accordingly, the geometrical characteristics of the flow cell were based on a parallel plate chamber design by Wan and co-workers (Wan et al., 2003); with an inner width of 35 mm so that the 32 x 32 mm fibre scaffold can be accommodated. This particular configuration was adopted in order to provide a central region of stable fluid flow across the cell seeded scaffold. The chamber was fabricated from a 3 mm thick rectangular stainless steel plate within which, an irregular hexagonal volume was subtracted. The 1 mm inlet and outlet ports were drilled through each side of the plate centrally, and along the long axis. The underside of the chamber consisted of a permanently fixed clear glass sheet. The top aspect was covered with a removable glass cover fixed with a rubber O-ring; and sealed with a 1 mm thick, water tight, silicon gasket bringing the total chamber height to 4 mm (Figure 2.10).

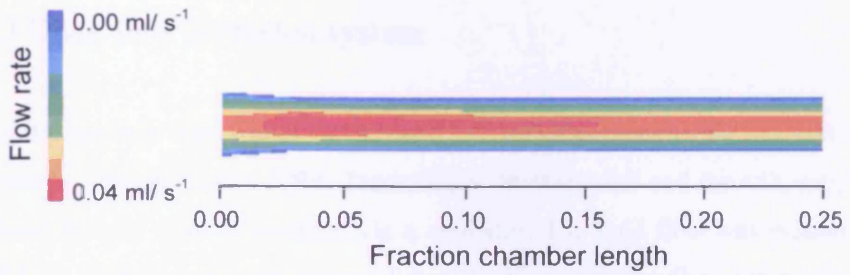

Figure 2.9 Confocal scanning laser microscope image of velocity profiles in a flow chamber

This longitudinal cross Section shows a transition from turbulent to steady flow occurring, and starting from the inlet, at approximately 15% of the chambers' length. The assessed chamber was geometrically hexagonal with both, inlet and outlet tubes parallel to the flow plane. (Bakker et al., 2003)

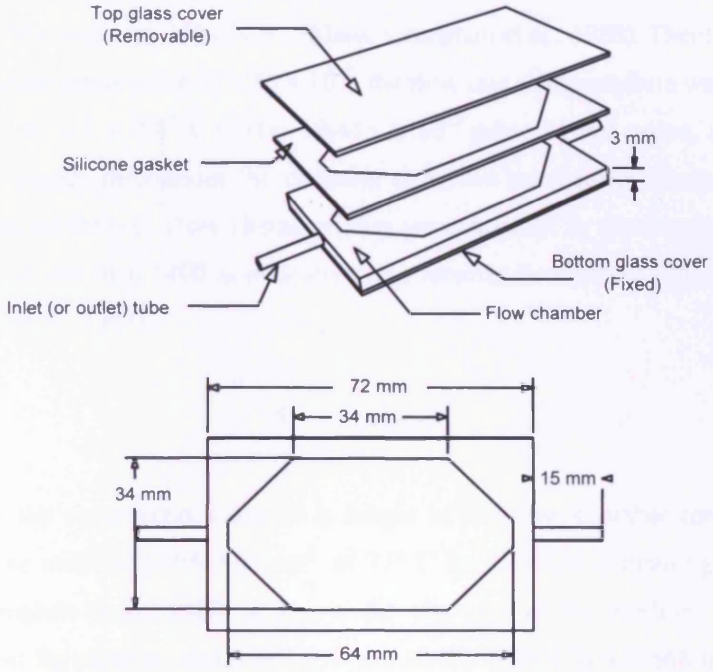

Figure 2.10 Components and dimensions of the flow chamber

2.5.3 Open flow perfusion system

A culture medium reservoir (1380 ml total volume) was prepared by linking two gas-permeable 150 cm^2 flasks (TPP, Trasadingen, Switzerland) and the CO_2 supply was perfused directly into the medium via a regulator. The fluid flow was induced using an IPS-12 multi-speed roller pump (Sotax, Basel, Switzerland) as the medium was drawn from the reservoir and passed sequentially through the flow cell, the roller pump and into the waste container(Figures 2.11 and 2.12). The flow cell was placed in a Shellab 2123-2 incubator and linked to the system via an access port (Figure 2.13). Based on maintaining a near zero shear stress, the medium flow rate value was obtained using the equation (Frangos et al., 1987),

$$Q = (T \times bh^2)/6\mu \text{ ml/s}$$

Where T is the shear stress (dyne/ cm^2), b and h are the width and height of the flow chamber (cm) respectively and μ is the viscosity of the medium (0.0075 g/cm/s, at 37° C for D-MEM containing 10% FCS) (Shane Croughan et al., 1988). Therefore, and to maintain a shear stress value of 1.56 x 10^{-3}, the flow rate of the medium was estimated at ([0.00156 x (3.5 x 0.4^2)]/ 0.045) 19,413 x 10^{-3} ml/s. At this value, the flow of medium is laminar throughout the chamber thus; the subsequent disruption to cell attachment is minimised. Flow characteristics are expressed by the Reynolds number (Re) which, at less than 1400 is indicative of a laminar flow nature. The Re is given by (Frangos et al., 1987),

$$Re = T(h^2p/\mu^2)$$

Where T is the shear stress value, h is height of the flow chamber (cm), p is the density of the medium (1.0045 g/ cm^2, at 37° C for D-MEM containing 10% FCS) (Shane Croughan et al., 1988) and μ is the viscosity of the Medium (as above). Therefore, an Re value of (0.00156 [(0.4^2 x 1.0045)/ 0.0075^2]) 4.77568 indicates the laminar nature of the flow. The flow chamber and medium reservoir were sterilised by exposure to UV light, over night, and the flow tubing system was sterilised by sequentially injecting 70% ethanol, whilst the pump was operational, followed by

flushing with sterile PBS. Glass fibre scaffolds were loaded, inside the cell culture (laminar flow) hood, into the flow chamber which was, in turn, covered and linked to the flow circuit inside the incubator. Samples were later processed so that the medium flow effect on gene regulation was assessed using quantitative polymerase chain reaction (qPCR).

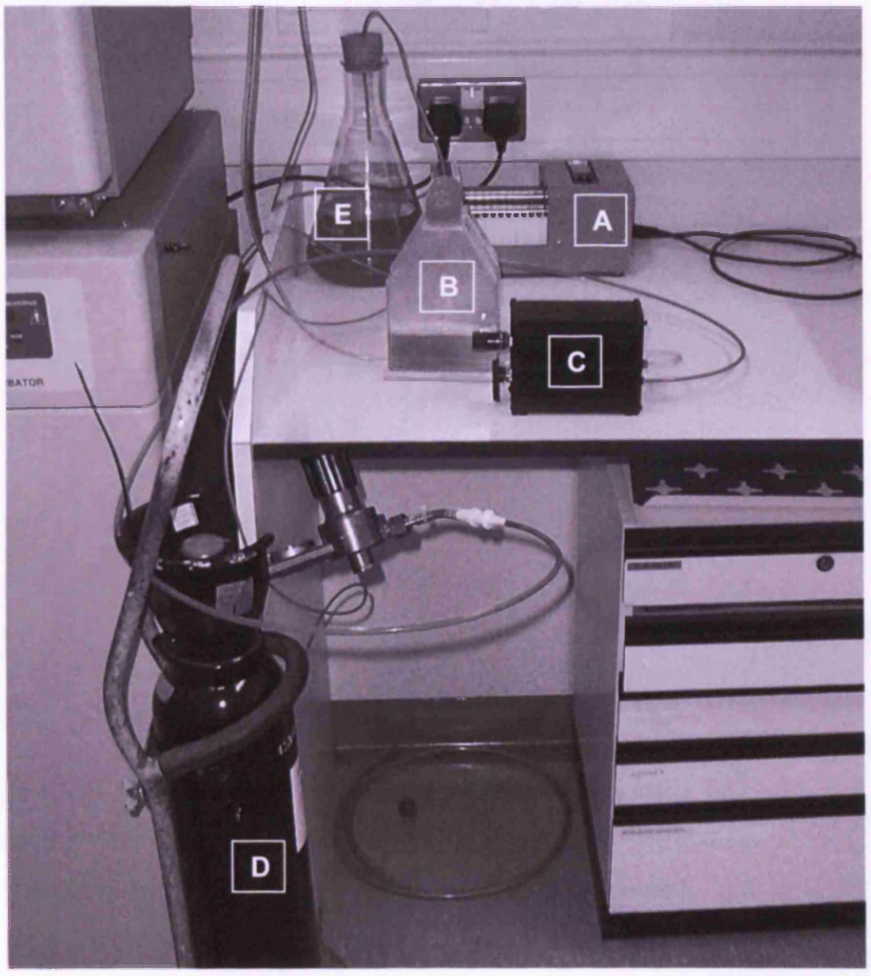

Figure 2.11 The open flow culture system

(A) Roller pump, (B) Medium reservoir, (C) CO2 Regulator, (D) CO2 supply, and (E) Waste container.

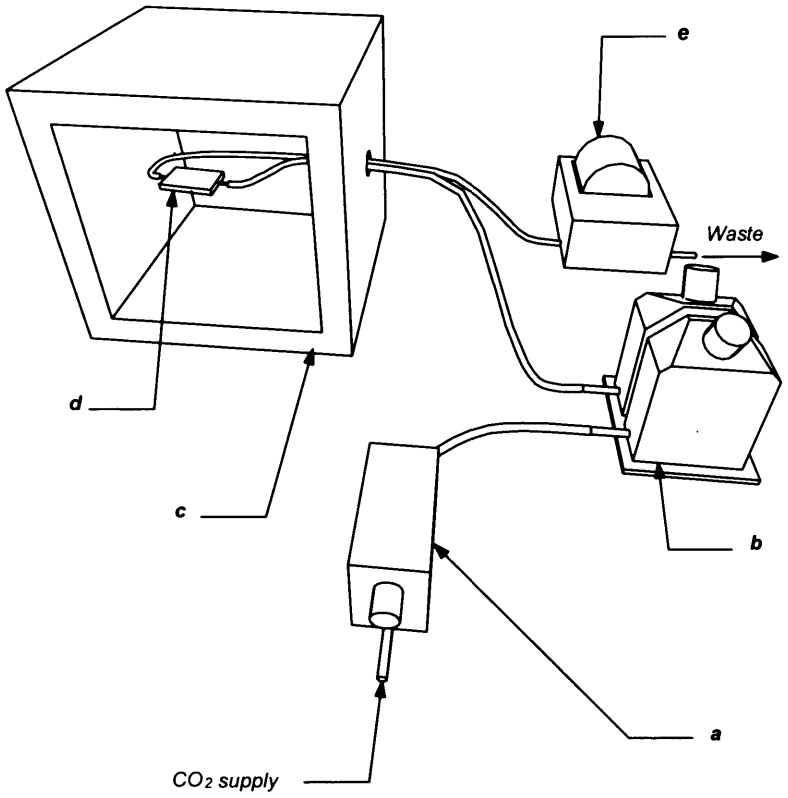

Figure 2.12 The open flow culture system unit configuration

Following flow direction: CO_2 supply, *(a)* CO_2 regulator, *(b)* Medium reservoir, *(c)* Incubator, *(d)* Flow chamber, *(e)* Roller pump, and waste outlet.

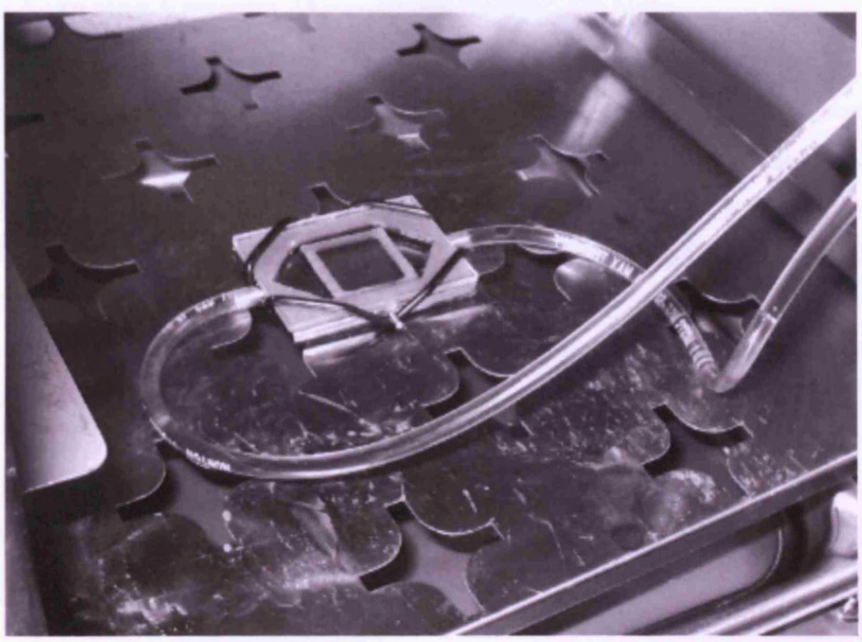

Figure 2.13 The flow chamber-scaffold arrangement inside the incubator

2.6 Cell viability assessment

2.6.1 Introduction

The viability of the seeded cell is a major indicator of the scaffold biocompatibility. Cell survival and proliferation were therefore assessed, on glass discs and fibres, using various techniques with the main variants being glass composition, fibre diameter and time in culture.

2.6.2 Scanning Electron Microscopy

MG63 cells were seeded on glass discs of various compositions and the scaffold cultures were fixed, after 24 hours in culture, using 3% glutaraldehyde (Agar Scientific Ltd., Essex, UK) in 0.1M sodium cacodylate buffer (Agar Scientific Ltd.)at +4° C overnight. Specimens were later sequentially dehydrated in 20%, 50%, 70%, 90% and 100% ethanol then critical point dried for 5 min following the application of hexamethyldisilazane (Taab Laboratories Ltd., Berkshire, UK). Discs were mounted, placed in a Polaron E5 100 sputter coater (Quorum Technologies, East Sussex, UK) and coated with gold-palladium. Images were obtained using a Stereoscan 90B electron microscope (Cambridge Instruments Ltd., Cambridge, UK).

2.6.3 The CyQUANT cell viability kit

2.6.3.1 Introduction

Using the CyQuant cell proliferation assay kit (Molecular Probes Europe BV, Leiden, The Netherlands), cellular nucleic acids are labelled with green fluorescein dye which, when excited, emits at an intensity directly related to the number of cells present. The unsymmetrical cyanine fluorescent CyQUANT GR dye (Ex/Em, 480/520 nm) can be detected, and depending on the cell type, in as little as 10-50 cells.

2.6.3.2 Assay preparation

Glass discs of various compositions were placed in 24-well sterile Optiplates (PerkinElmer Life Sciences, Cambridge, UK).Only 1 ml of GM was used per well and the medium changed at 1-2 day intervals. The generic configuration of the disc-well arrangement is illustrated in Figure 2.14. At the appropriate time points (Section 3.2.1), GM was gently aspirated and the cells were washed once in 500 µl PBS to remove non-adherent cells and any traces of phenol red that may interfere with the GR dye detection. The PBS was, in turn, aspirated and the Optiplates were stored at -70° C for at least 1 week to enhance the efficiency of the cell lysis buffer. This may be attributed to fracture formation between the two lipid layers of the cytoplasmic membrane, during the freezing process, lading to increased membrane permeability (Wolfe and Bryant, 1999). To perform the quantitative assay, the CyQUANT reagent was prepared in distilled water (dH_2O) by firstly adding the cell lysis buffer (1:20), then the CyQUANT GR stock solution (1:400). The cells were allowed to thaw, and each well was incubated in 300 µl of the reagent, protected from light, for 2-5 min at RT.

2.6.3.3 Fluorescent evaluation of cell density

The Optiplates were placed in a Fluroskan Ascent plate reader (Labsystems, Helsinki, Finland) and emitting florescent values obtained, and interpreted, using the Ascent software. Based on the optiplate measurements, the number of wells and the well diameter; a template was firstly created and loaded via the plate setup process. The fluorescence exposure area, within each well, was then defined by nine central points. A new step was next created and the preset excitation and emission values, approximating those of the GR dye, were elected (458 and 510 nm respectively). The plate was finally loaded into the plate reader (using the Fluroskan plate loader), and emission rates were sequentially obtained from wells and exported into spread sheets. It has been noticed however, that the background fluorescence values obtained for the negative (blank) controls varied for each well plate (assessed for fluorescence intensity at each time point). Accordingly, and in order to compare the data obtained from various well plates, percent normalisation was performed (De Luca et al., 1997;

Lemkin et al., 1999). The average negative control value for each well plate was first calculated, and these values were later normalized to the lowest control value and differences, as percentage increase or decrease, were obtained and applied to the corresponding positive value readings.

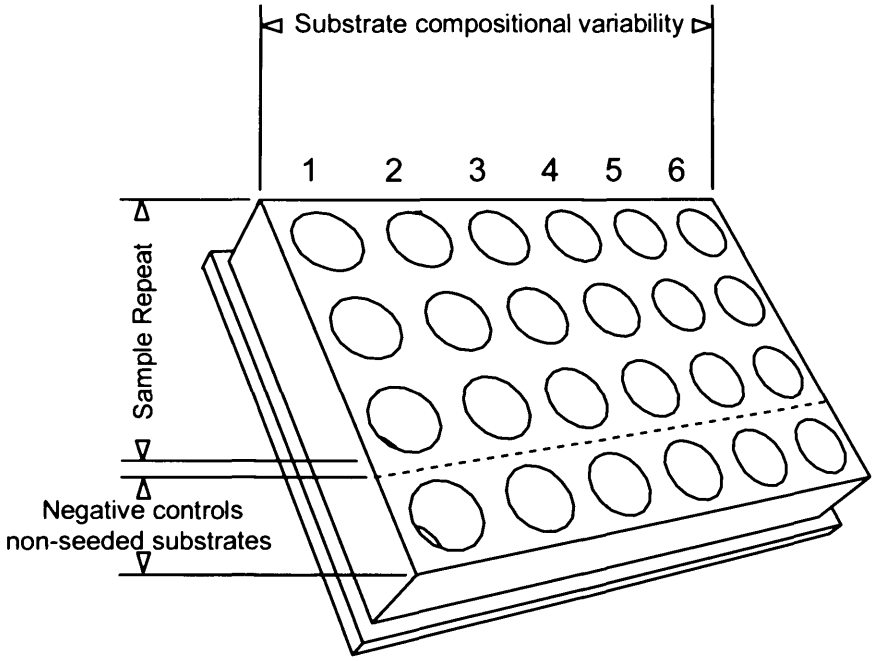

Figure 2.14 Generic configuration of glass discs for CyQUANT cell viability assay

2.6.4 Direct cell count

Glass fibre scaffold seeded cells were fixed at several time points in 70% ice cold methanol, nuclear DNA stained with 1:1000 concentration of propidium iodide (Ex/Em, 493/630 nm, Sigma-Aldrich) in PBS for 30 minutes. Samples were then sandwiched between two 24 x 24 mm glass coverslips in Citifluor mounting medium (Section 2.7.4). The nuclei were later visualised under the Leica DMIRB microscope where a minimum of 200 nuclei were directly counted(Mancini et al., 1997; Haverstick et al., 2000; Gabriella, V et al., 2000), at X20 magnification, in adjacent microscopic fields and the average cell number per field was established.

2.7 Fluorescence Immunocytochemistry

2.7.1 Introduction

Cytoplasmic proteins can be localised, and visualised, through the application of fluorescent staining. These proteins can be labelled with fluorescent dyes (fluorochromes) by exploiting antibody-antigen binding. Using a fluorescent microscope, fluorochromes can then be excited at a certain wave length and an image is formed by the emitted light at a certain, longer, wave length.

2.7.1.2 The function and structure of antibodies

Antibodies are immunoglobulins that are naturally produced, as part of the immune response, against invading pathogens (antigens) by immunoglobulin-producing B-lymphocytes. By injecting an animal with an antigen, several antibodies (clones) are produced which are capable of binding, with variable degrees of strength (affinity), to the multiple molecular binding sites (epitopes) of the antigen. The immunoglobulin molecular structure consists of two identical light polypeptide chains and two identical heavy polypeptide chains linked together via disulphide bonds (Figure 2.15). The antigen domain binding region of the antibody (fragment antigen binding, Fab), of 110-130 amino acids, is hypervariable thus corresponding to the diversity and specificity of the immunoglobulin-antigen interaction. Composed of the heavy chains, the other major component of the antigen is the constant Fc domain. This domain is antigenic in nature and responsible for compliment activation and the binding of, for example, natural killer cells and neutrophils to the antigen. Most of the antibodies used in biochemical assays belong to the immunoglobulin G (IgG) class and are used in both polyclonal and monoclonal forms. In the polyclonal form, a mixture of the various clones of the antibody is introduced binding, competitively, to several epitopes in the antigen. A more intense signal can therefore be obtained, however, with an increased potential for non-specific binding. Monoclonal antibodies on the other hand, are single immunoglobulin species produced specifically against single antigen epitopes. The use of monoclonal antibodies therefore greatly reduces background staining. This use, nonetheless, is sometimes associated with cross

reaction as the variable domain may bind to similar amino acid sequences on various antigens.

2.7.1.3 Immunocytochemical assay formats

In direct fluorescent labelling, the fluorochrome is covalently linked (conjugated) to the antibody which will then bind to its respective protein domain (Figure 2.16A). This method is often used as a rapid procedure and where great specificity, as non-conjugated antibody binding may occur, is not a major requirement. Indirect labelling is based on the capacity of the Fc fragment of the antibody to act as an antigen. Antibodies against a certain protein are produced in an animal, a mouse for example, and later introduced to a second species where secondary antibody formation, a goat-anti-mouse antibody for example, is induced. The secondary antibody is then conjugated to a fluorochrome so that a two-step immunolabelling can take place (Figure 2.16B). Using this method can significantly increase specificity as primary antibodies can be use in low dilutions and a strong fluorescent signal can be obtained, at a later stage, by the abundant application of the secondary conjugated antibody.

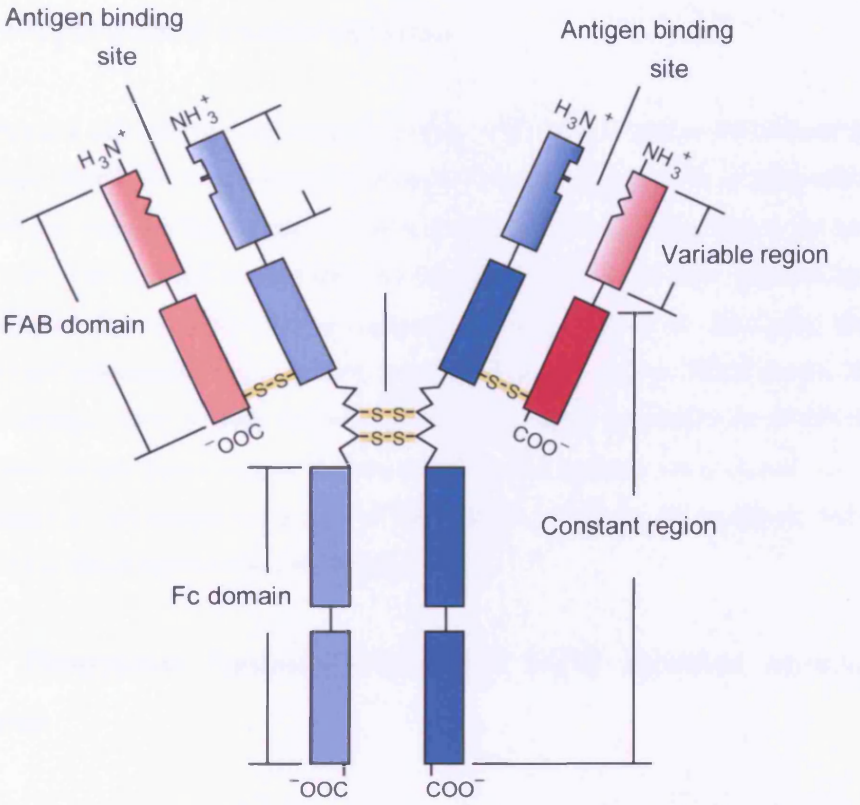

Figure 2.15 A schematic illustration of the antibody structure

The heavy chains are in blue and the light chains in red. (Nelson and Cox, 2004)

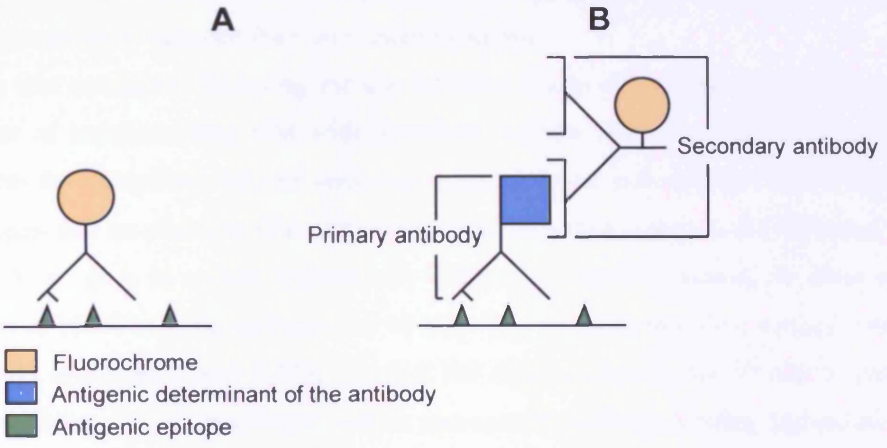

Figure 2.16 Immunocytochemical assay formats

A, Direct fluorescent immunolabelling and **B**, indirect fluorescent immunolabelling

2.7.2 Preparation of control surfaces

To maximise cell adhesion to control surfaces, the 13mm diameter borosilicate glass coverslips (BDH, UK) were coated with poly-l-lysine. The presence of this positively charged polymer has been shown to greatly enhance cell adhesion due to the strong interaction with the cell membrane anionic groups. The cover slips were soaked in 70% ethanol for 24 h to remove contaminants then, placed in glass petri dishes (Pyrex) and tissue culture grade water, sterilised using dry heat at 200° C for 2h. Next, the coverslips were placed sterile plastic petri dishes, incubated in 0.01% high molecular weight poly-l-lysine (Sigma-Aldrich) and agitated on a shaker for 3 h. Subsequently, coverslips were washed with dH_2O overnight, on a shaker, and air-dried in the tissue culture hood before use.

2.7.3 Fluorescent Immunolabelling of ECM turnover associated proteins

Prior to sample processing, HOB, HOF and HTF cells were incubated for 24 h in 1 μM monensin sodium salt (Sigma-Aldrich) to slow their metabolic rate and prevent the glycosylation of bone associated proteins. Monensin induces an increase of intracellular Ca^{2+} and subsequently inhibiting the terminal glycosylation of proteins (Mollenhauer et al., 1990). Consequently, these glycoproteins were accumulated in the cytoplasm to enhance their immunolocalisation.

This was conducted following the use of MG-63 cells as a model to investigate the effect of supplementing GM with monensin sodium salt on protein accumulation within the cytoplasm. MG-63 cells were seeded on the poly-l-lysine treated control surfaces and incubated in GM containing 1 μM monensin sodium salt (Thomas et al., 2001). At 24 h in culture, immediately following medium removal, the cells were fixed in 100% ice-cold methanol for 10 min. The samples were then washed 3 times in PBS and treated with 0.25% Triton-X100 (Sigma-Aldrich) for 10 min to further permeabilise the cell membrane, reduce non-specific antibody binding and reduce the samples' surface tension. Following a second triple wash with PBS, and to increase the immunolabelling specificity, secondary antibody non-specific binding was blocked incubating the samples in 10% denatured donkey serum albumin (Serotec,

Oxford, UK) in PBS for 30 min. The primary polyclonal antibody against osteonectin (ON) (1:100; all gift of Dr. L. Fisher, NIH, Bethesda, USA) (Fisher et al., 1995) was then applied, immediately after removing the PBS-donkey serum albumin solution, for 60 min. This was followed by the application of the secondary, FITC (Ex/Em, 480/530 nm)-conjugated, donkey anti-rabbit IgG (1:200, Jackson ImmunoResearch Laboratories, Inc., West Grove, PA, USA) for 30 min. The same experimental procedure was carried out using GM only (monensin sodium salt free) to incubate MG-63 cells. As an early marker for osteoblastic activity, ON synthesis is likely to be detected at an early time point (Dhore et al., 2001).

HOB cells seeded onto phosphate glass discs and control coverslips were fixed, treated exactly as above and labelled for primary polyclonal antibodies against bone sialoprotein (BSP), ON and osteopontin (OP) (1:100; gift of Dr. L. Fisher, NIH, Bethesda, USA) (Fisher et al., 1995) were applied for 60 min, whilst the negative control cells were incubated only in 10% denatured FCS in PBS. This was followed by the secondary labelling with FITC-conjugated, donkey anti-rabbit IgG.

HOF and HTF cell seeded samples were similarly treated however, primary labelling was conducted using mouse monoclonal anti-P-4-H (prolyl-4-hydroxylase) antibody (IgG1, clone 5B5, 1:50; Dako Ltd., Cambridge, UK) whilst negative control cells were incubated in a 1:50 dilution of mouse IgG1 (Negative control, Dako Ltd.) for the same period of time. Cells were subsequently incubated in 1:200 dilution of FITC-conjugated monoclonal donkey anti-mouse IgG (Jackson ImmunoResearch Laboratories). All immunocytochemistry reagents were applied in 50 µl volume aliquots using P200 pipette tips.

For all samples, DNA binding DAPI (Sigma-Aldrich) at 1:1000 dilution was included in the secondary staining procedure in order to visualise the nuclei. Glass disc samples were finally washed in PBS, and prepared for microscopic viewing by mounting the cell seeded surface, of both sample and controls, on 22 x 40 mm rectangular glass slides using AF2 antifadent aqueous glycerol solution (Citifluor Ltd., London, UK).

2.7.4 Fluorescent Immunolabelling of the cytoskeleton

To visualise and detect any cell morphology changes in relation to the phosphate glass substrates, the vimentin intermediate filament network was directly labelled with a fluorescent dye. At the appropriate time points the medium was aspirated and cells seeded on glass discs, and fibres, were fixed in 100% ice cold methanol for 10min. Samples were washed 3 times in PBS and incubated in 1:300 dilution of Cy3 (Ex/ Em, 530/590 nm)-conjugated mouse monoclonal anti-vimentin antibody (IgG1, clone V9, Sigma-Aldrich) for 30 min. A 1:1000 dilution DAPI solution was also included in the labelling step. All immunocytochemistry reagents were applied in 50 µl volume aliquots directly onto the disc samples whilst fibre scaffolds were treated with 300 µl reagent volume inside the petri dishes. Finally, the samples were washed and glass discs were mounted as described in Section 2.7.3 for microscopic assessment. Fibre scaffolds, on the other hand, were sandwiched between two 25 x 25 mm square coverslips in the AF2 aqueous mountant.

2.8 The CellTracker™ assay: Co-culture assessment

In order to observe migration patterns and morphology for both HOB and HOF cell populations, separately and over a period of time in culture, HOF cells were labelled with chloromethyl derivative reagent. The CellTracker green CMFDA probes (5-chloromethylfluorescein diacetate, Invitrogen) diffuse freely across the cell membrane and bind, through the chloromethyl group, to thiols on proteins or peptides thus becoming cell membrane-impermeant. Within 24 hours of loading into the cell and through the action of esterases, the acitate group is cleaved off releasing the fluorescent product (Ex/Em, 492/517 nm) (Boleti et al., 2000; Evans et al., 2003). These fluorescent properties are transferred through cell division and can be clearly detected, in culture, up to 72 h post incubation. As described in Section 4.3.5, a working concentration of 10 µM has been established as optimal when staining control surface seeded HOF cells.

2.8.1 Co-culture cell population identification

As a dry fibre arrangement is critical for the success of drop culture, fibre scaffolds were sterilised overnight under UV light. HOF cells were incubated in suspension at 37°C in pre-warmed, serum free, GM containing 10 μM of CMFDA dye for 45 min. The CMFDA medium was then replaced with fresh GM and the cells were carefully seeded, using a P1000 pipette tip, in a 250 μl drop culture on one side of the glass barrier. HOB cells were subsequently seeded on the opposite side and the configuration was incubated for 3 h to allow cell attachment to take place. The scaffold was then gently washed twice in GM to remove any non-adherent cells and all traces of CMFDA, 5 ml of GM added, and the barrier carefully removed using sterile disposable surgical scalpels and the culture re-incubated. At the desired time points, the medium was aspirated and the cells fixed in 100% ice cold methanol for 10 min. Subsequently, cells were washed twice in PBS and labelled using the combined anti vimentin-DAPI process as previously described. Finally, the mounting process in Citifluor was applied and the dual population seeded scaffold was assessed under the fluorescent microscope.

2.9 Fluorescence microscopy

Using a Leica DM-IRB inverted microscope (Leica Microsystems UK Ltd., Buckinghamshire, UK), a Hg^- lamp generated epifluorescent light induces the fluorescence of the antibody-conjugated fluorochromes. When a sample is excited, only the light emitting at a certain wave length (corresponding to the investigated fluorochromes' emission wave length, e.g. 530 nm for FITC) is allowed to pass through the objective, through an emission filter, to form an image (Figure 2.17). As emission filters of various spectra can be used, when viewing the same sample, images of several cell components can be composed as their labelling fluorochromes can be individually excited and captured. Images were captured via a CoHu CCD camera; through a Matrox Meteor-II monochrome frame grabber (Matrox Europe Ltd., Bucks, UK); and the Leica FW4000 software was used for digital image acquisition and pseudo colour application. Images of the various fluorochrome species of the sample were then composed using the Leica FW4000 software.

To ensure consistency, negative control cells were excited at the same fluorescence intensity used to detect positive staining.

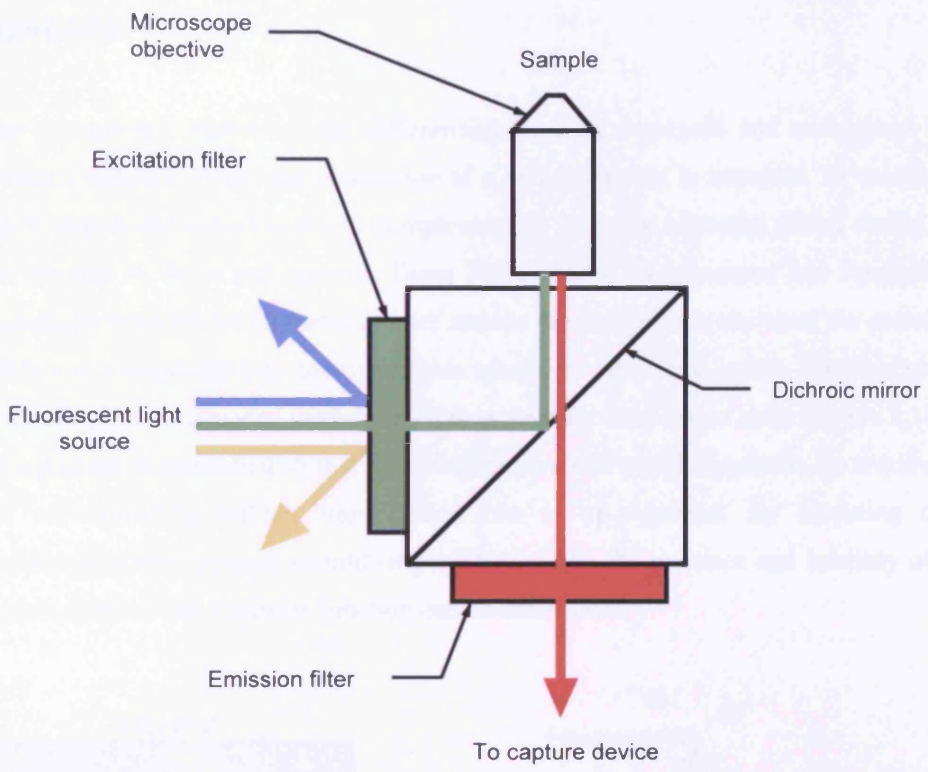

Figure 2.17 Excitation and emission light control in a fluorescent microscope

2.10 Quantitative polymerase chain reaction

2.10.1 Introduction: mRNA synthesis and function specific gene regulation

The committed function of the differentiated cell is expressed and maintained by protein synthesis. When the production of a certain protein is activated, its template DNA strands are transcribed into complementary (primary transcript) RNA chains in the nucleus by RNA polymerase. These RNA chains are processed into functional messenger RNA (mRNA) that will later encode the polypeptide chains of the protein. mRNA is transported into the cytoplasm where, by ribosomal action, the four base code of mRNA is decoded (translated) into protein forming amino acids (Figure 2.18). This process is controlled so that when higher levels of protein synthesis are required, the corresponding mRNA transcription rate is up-regulated. By assessing the transcription rate, through quantifying mRNA yields, the presence and intensity of a certain differentiated cellular function can be determined.

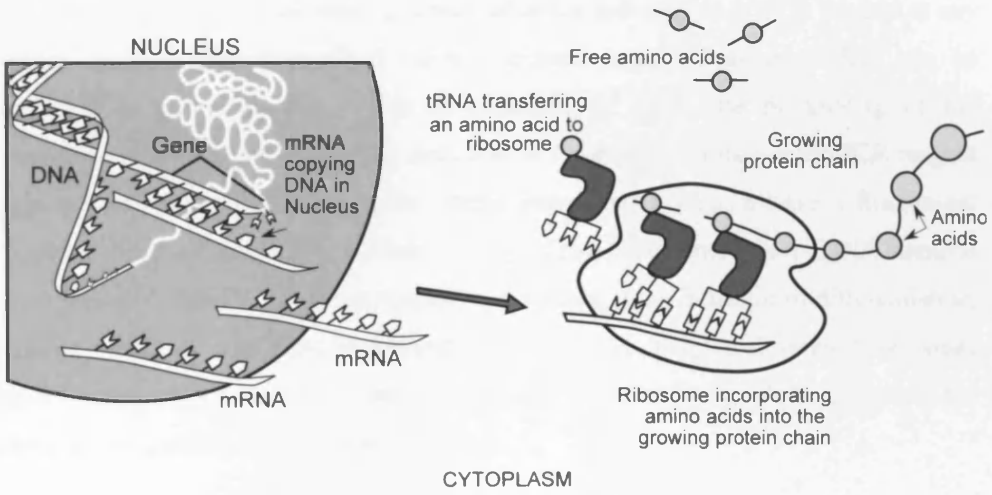

Figure 2.18 Gene transcription, mRNA synthesis and translation

The "central dogma" of molecular genetics: DNA codes for RNA and RNA codes for protein. The DNA to RNA step is transcription, and the RNA to protein step is translation. Modified, Primer on Molecular Genetics, DOE Human Genome Program, U.S.A Department of Energy, 1992.

2.10.2 Quantitative Polymerase Chain Reaction (qPCR): an overview

The transcription of a certain gene can be detected, and evaluated, by processing the resulting mRNA. When total RNA strands are extracted form the cell, complementary DNA copies (cDNA) maintaining the gene specific structure can be made (Figure 2.19.A). This cDNA can be then amplified into a detectable level using the Polymerase Chain Reaction (PCR) process. Heated to 95° C, the double-helix cDNA molecule is first denatured (melted) into two single strands. Next, and by lowering the temperature to 50-60°C, a synthetic oligonucleotide sequence (primer) complementary to the cDNA, and therefore the mRNA, sequence of interest is hybridized. The primers then act as starting sites for the extension of deoxynucleotides (dNTPs) bases and a double-stranded cDNA molecule is recompiled. Nucleotide annealing is induced by the presence of a temperature-resistant enzyme, Taq polymerase, and by increasing the temperature to an optimal 72 °C. Repeating this cycle of heating and cooling will lead to the exponential amplification of cDNA as with each cycle repeat, the primer associated nucleotide sequences are doubled (Figure 2.19B). As a quantitative relationship is present between the amount of the starting target sequence and amount of PCR product at any given cycle, highly transcribed mRNA sequences amplification profiles can be detected at earlier cycles. This is achieved by real time monitoring of the amplification progress through the inclusion of fluorogenic probes in the PCR reagent where these probes, and during the strand extension process, release a fluorescent reporter dye fragment (FAM, 6-Carboxyfluorescein) every time a new cDNA strand is synthesized (Figure 2.20). Gene regulation therefore, as an indicator of differentiation, can be monitored and most importantly, the regulation trend at different time points and under various culture conditions can be established by plotting against the constant expression of house keeping genes.

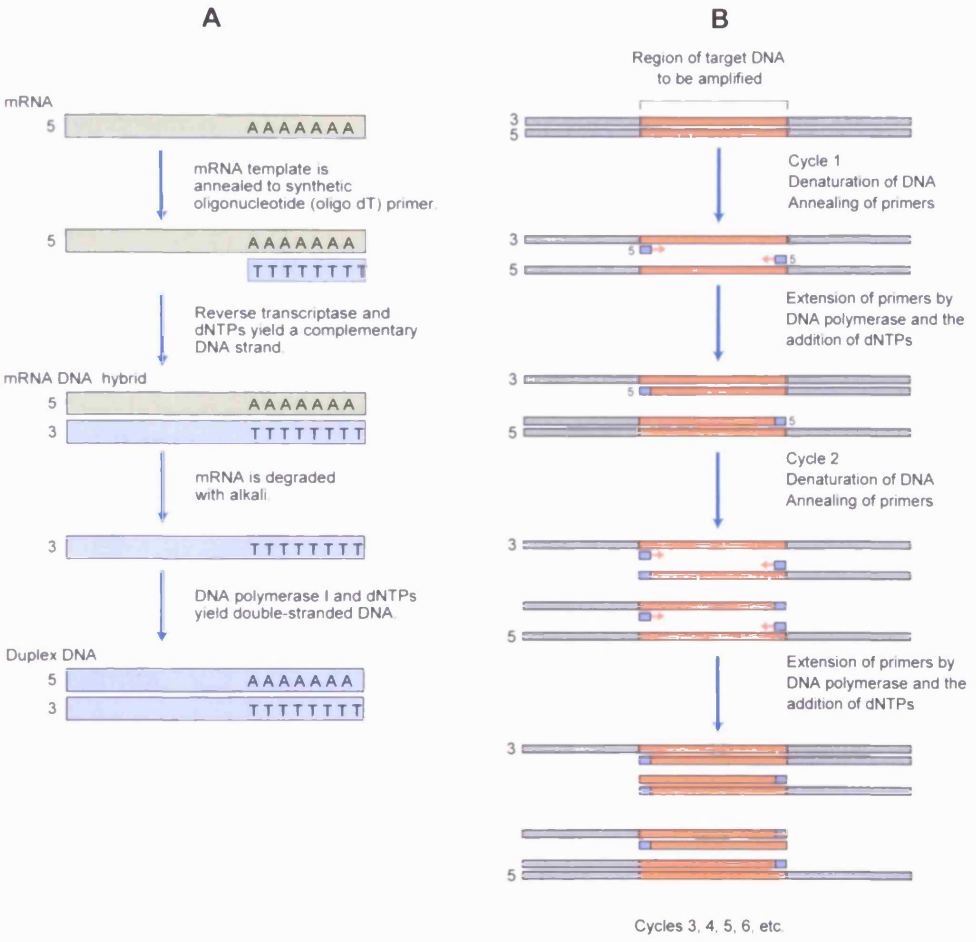

Figure 2.18 (A), cDNA synthesis from mRNA and (B), cDNA PCR amplification

(Lodish et al., 2004)

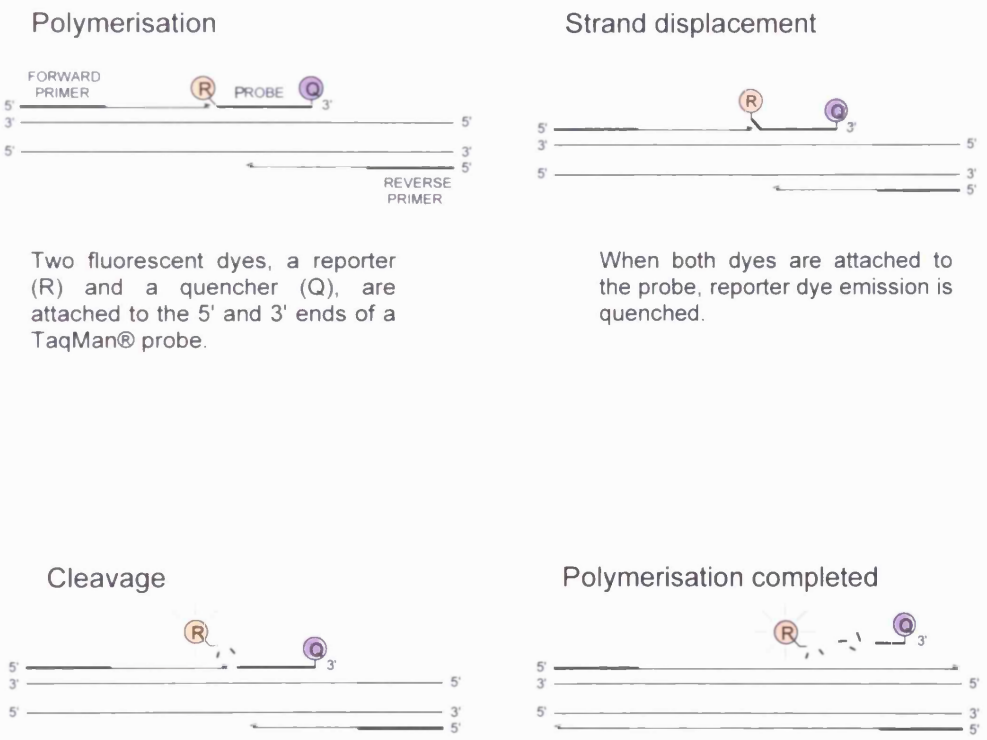

Figure 2.20 The TaqMan® probe function during PCR

Modified, User Bulletin #2, ABI PRISM 7700 Sequence Detection System, Applied Biosystems, 2001.

2.10.3 Total RNA extraction

The RNeasy Mini Kit (Qiagen Ltd., W Sussex, UK) was used to extract total RNA from Cells grown on glass fibres, and in the control 24 wellplates (Orange scientific, Belgium). The procedure was conducted according to the manufacturers' instructions as follows:

- Prior to use, the RLT cell lysis buffer was supplemented with β-Mercaptoethanol (β-ME) at1:100 (v/v) concentration. Similarly, one volume of PRE buffer was diluted in four volumes of near pure (99%) ethanol.
- At the desired time points, adherent cells from each sample were lysed directly using 350 µl of RLT buffer; the lysate collected with a P1000 pipette tip; and placed in a 1.5ml microfuge tube.
- In order to reduce viscosity, and to increase RNA yields, the lysate was passed 10 times through a 20-gauge needle fitted to a syringe to homogenise.
- 350 µl of 70% ethanol (in molecular biology grade, nuclease-free H_2O) was then added to the lysate and mixed thoroughly by pipetting.
- The 700 µl mixture was transferred into the RNeasy mini column and placed in a 2 ml collection tube and centrifuged, at 10000 r/ min, for 15 sec.
- The collection tube was reused and 700 µl RW1 buffer (700 µl) were added to the mini column and subsequently centrifuged, at 10000 r/ min, for 15 sec.
- The collection tube was replaced and RPE buffer (500 µl) was added and the mini column was centrifuged, at 10000 r/ min, for 15 sec.
- The latter step was repeated however, the mini column containing collection tube was centrifuged for 2min.
- The RNeasy mini column was finally placed in a 1.5ml collection tube, 30 µl of RNase-free H_2O added and centrifuged at 10000 r/ min, for 1 min.
- The eluant containing tube was then labelled, and stored at -70°C until required.

Prior to cDNA preparation, all RNA samples were verified for purity (RNA quality) as RNA may undergo contamination related degradation. RNA quality was assessed using Ultrospec 2000 UV spectrophotometer (Pharmacia Biotech, Cambridge, UK) where the spectrophotometer was firstly calibrated using a blank cuvette loaded with

dH_2O. Subsequently, RNA samples were loaded (1:100 in dH_2O) and assessed for quality by measuring the sample UV absorbance ratio at 260 and 280 nm wave lengths and the OD260/280 (optical density) ratio was obtained. OD260/280 is the ratio of absorbance for nucleic acid (260nm) to protein (280nm) and is a measure of protein contamination. RNA samples were considered to be of acceptable quality to perform qPCR When OD260/280 was $\geq$ 1.8(Xinmin et al., 2005).

To reduce contamination, qPCR related sample handling and processing were performed using PCR clean pipette tips (Fisher Scientific, Leicestershire, UK).

2.10.4 Preparation of cDNA

The extracted RNA was converted via reverse transcription (RT), using the High Capacity cDNA Archive kit (Applied Biosystems, Cheshire, UK), into single-stranded cDNA. The 2X RT master mix was prepared so that a similar volume of the RNA elute could be treated. Accordingly, and for 30 µl of RNA solution, the RT master mix components were mixed at the following volumes,

10X Reverse Transcription Buffer	6 µl
25X dNTPs	2.4 µl
10X random primers	6 µl
MultiScribe™ Reverse Transcriptase	3 µl
Nuclease-free H2O	12.6 µl

The master mix was prepared in 0.2 ml microfuge tube and the RNA solution was later added and pipetted twice to mix. The tubes were then placed in an Eppendorf thermal cycler (Mastercycler, Eppendorf UK Ltd., Cambridge, UK) and the RT reaction conducted at 25°C for 10 min, then at 37°C for 120 min. cDNA tubes were later stored at -70° for further analysis.

2.10.5 Relative quantification of gene expression and regulation

The qPCR assay took place using Optical 96-Well Reaction Plates (Applied Biosystems) at 25 μl per-well reaction volume. This volume was prepared by mixing 2.5 μl of the cDNA solution with various reagents as outlined below,

TaqMan Universal PCR Master Mix (2X)	12.5 μl
20X Assays-on-Demand™ Gene Expression Assay Mix (containing: TaqMan® probe; foreward and reverse primers)	1.25 μl
Nuclease-free H_2O	8.75 μl

The mix was then transferred into the 96-well reaction where three aliquots of each sample were processed (Figure 2.21). An endogenous control reaction, for the house-keeping rRNA (ribosomal RNA)-encoding 18S gene, was included in every well-plate so that relative quantification of gene expression, among various plates, can be performed. Consequently, TaqMan® probes for 18S were designated as an endogenous control during the plate setup process. The TaqMan® probes used to label the investigated genes cDNA are detailed in Section 5.2.3.

An example of the generic assay design adopted, assuming that four gene expression trends were to be quantified, is illustrated in Figure 2.21. The plates were loaded into the ABI PRISM® 7300 Sequence Detection System (Applied Biosystems) and cDNA amplification was conducted through 40 thermal cycles; at an assay volume of 25 μl. Relative quantification (RQ) took place using the 7300 SDS software whereby various plates, either time point or glass-composition related or both, were added to the RQ study. cDNA amplification curves for all target genes were normalised against the endogenous control expression of 18S. This Comparative C_T method was automatically preformed using the 7300 SDS software.

Firstly, the Baseline value (the average background fluorescence value detected at the early cycles) across the entire reaction plate was determined. Secondly, the Threshold representing the statistically significant numerical point above the Baseline value was calculated for the entire reaction plate. Finally, and for each sample well (target and endogenous), the C_T (Threshold Cycle) value where the florescence value for each

sample crosses the Threshold was obtained. Conducting Comparative C_T, the amount of target, normalised to the endogenous control was given by the equation,

$$2^{-\Delta\Delta C_T}$$

This equation was derived by determining the Threshold number (X_T) for each target gene using the target C_T value. A Threshold number (R_T) for the endogenous control was similarly obtained. X_T was then divided by R_T was to produce a constant value (K) which was used in the equation,

$$X_N = K \times (1 + E)^{-\Delta C_T}$$

Where X_N is the normalized amount of target, $^{\Delta C_T}$ is the difference between the target and endogenous control C_T values and E is the efficiency of probe cleavage. A calibrator (cb) sample was chosen against which all target amounts were compared thus,

$$X_N / X_{N,cb} = K \times (1 + E)^{\Delta C_T} / K \times (1 + E)^{\Delta C_{T,cb}} = (1 + E)^{-\Delta\Delta C_T}$$

Where $X_{N,cb}$ is the normalized amount of the calibrator. According to Applied Biosystems, the efficiency of probe cleavage (E) for TaqMan® probes can be considered to be equal to one (1) therefore, the amount of target normalised to the endogenous control and relative to the calibrator was $2^{-\Delta\Delta C_T}$.

To compare several well plates in a RQ study, the endogenous control fluorescence values were normalised first then the target gene values were normalised, in turn, to their corresponding endogenous control. The normalised amount for each target was obtained as an RQ (relative quantification) value.

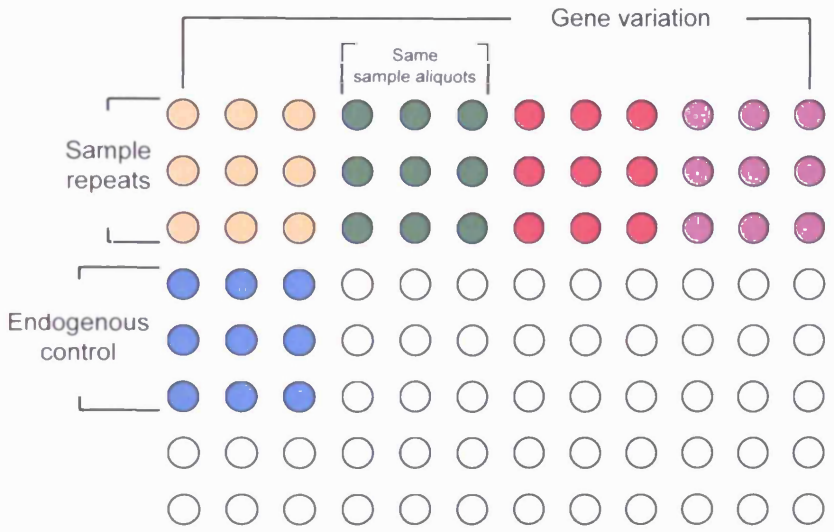

Figure2.21 Example of qPCR assay 96 well plate configuration to investigate the expression of four genes simultaneously

2.11 Statistical analysis

Statistical differences were obtained through applying a 1-way ANOVA test using SPSS for windows (release 11, SPSS UK Ltd. , Surrey, UK) followed by Tukey post-hoc analysis at 95% confidence interval. When $p<0.05$, data values differences were considered significant.

CHAPTER THREE

RESULTS ONE

3.1 Introduction

The short term biocompatibility of the ternary glass compositions was assessed by evaluating cell attachment, proliferation and maintenance of the osteoblastic and fibroblastic phenotypes. These glasses were evaluated in their disc form as changes in cell morphology and phenotype protein expression were visually assessed using fluorescence microscopy against the flat, borosilicate glass, control seeded cells. This was conducted in order to determine the relationship between each glass composition solubility trend and the seeded cell behaviour with the overall aim of electing the most appropriate ternary glass composition, or compositional range, as a base form for glass fibre production. As concluded by Salih et al.(Salih et al., 2000), incubating osteoblastic cell lines in glass substrates containing $\leq$ 28 mol% CaO content resulted in inhibiting cell proliferation and bone associated gene regulation therefore, and in this study, only glasses of $\geq$ 30 mol% CaO content were considered for biocompatibility assessment. Throughout this work, The P_2O_5 content for all glass compositions was fixed at 50 mol% as attempts to produce glass fibres from glasses containing less than 50% P_2O_5 were unsuccessful (Section 2.2.1). As described in Section 1.9.1, ternary phosphate based glasses solubility patterns are primarily dependant on the inhibitory effect of CaO as increasing CaO content resulted in reducing the corresponding glass dissolution rates (Franks et al., 2000; Franks et al., 2001; Knowles et al., 2001; Ahmed et al., 2004). Accordingly, the 11 glass compositions produced (Table 3.1) were nominated as a low solubility form ($\geq$ 40 mol% CaO), and a high solubility form (< 40 mol% CaO).

Table 3.1 Ternary phosphate based glass compositions considered for the initial biocompatibility assessment

For practical and time scale considerations, CaO was added at an increment of 2 mol% (30, 32, 33...etc) so that the number of glass compositions to be investigated was reduced.

	Precursor content (mol%)		
Glass Code	**P_2O_5**	**CaO**	**Na_2O**
$(CaO)_{0.30}$-$(Na_2O)_{0.20}$-$(P_2O_5)_{0.50}$	50	30	20
$(CaO)_{0.32}$-$(Na_2O)_{0.18}$-$(P_2O_5)_{0.50}$	50	32	18
$(CaO)_{0.34}$-$(Na_2O)_{0.16}$-$(P_2O_5)_{0.50}$	50	34	16
$(CaO)_{0.35}$-$(Na_2O)_{0.15}$-$(P_2O_5)_{0.50}$	50	35	15
$(CaO)_{0.36}$-$(Na_2O)_{0.14}$-$(P_2O_5)_{0.50}$	50	36	14
$(CaO)_{0.38}$-$(Na_2O)_{0.12}$-$(P_2O_5)_{0.50}$	50	38	12
$(CaO)_{0.40}$-$(Na_2O)_{0.10}$-$(P_2O_5)_{0.50}$	50	40	10
$(CaO)_{0.42}$-$(Na_2O)_{0.08}$-$(P_2O_5)_{0.50}$	50	42	8
$(CaO)_{0.44}$-$(Na_2O)_{0.06}$-$(P_2O_5)_{0.50}$	50	44	6
$(CaO)_{0.46}$-$(Na_2O)_{0.04}$-$(P_2O_5)_{0.50}$	50	46	4
$(CaO)_{0.48}$-$(Na_2O)_{0.02}$-$(P_2O_5)_{0.50}$	50	48	2

3.2 Experimental protocol

3.2.1 The CyQUANT assay

To determine the capacity of the relatively high solubility glass compositions (i.e. of $\leq$ 40 mol% CaO) to support initial non-specific cell adhesion (Section 6.7), MG-63 cells attachment at the early time points of 30, 120 and 180 min in culture were assessed. Cells were seeded onto discs containing 30, 35 and 40 mol% of CaO and the tissue culture plastic surfaces of the Optiplate was used as a control surface (Figure 3.1A)

As a limited stock of HTF cells was available, only HOB and HOF cells were used for this assay. Glass discs containing $\geq$ 40 mol% of CaO were placed in the 24-well Optiplates and seeded, as seen in Figure 3.1B, taking into account the inclusion of the non-seeded control discs. Due to the high number of glass compositions investigated and taking into consideration primary cell stock availability, cell density was evaluated at 3 day intervals at day 1, day 4 and day 7 in addition to the early time point of 180 min in culture. The cells were fixed and the nucleic acids were

fluorescently labelled and later quantified giving an indication of the corresponding cell density.

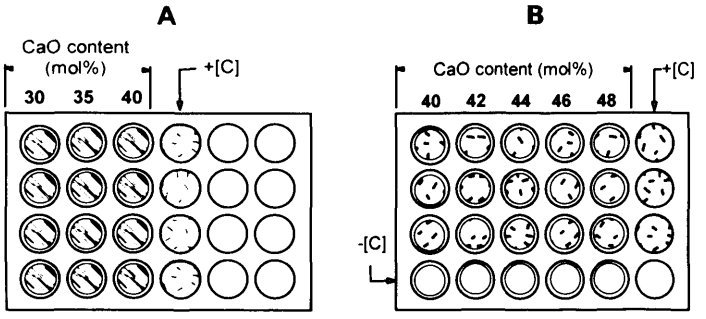

Figure 3.1 CyQUANT assay Optiplate configuration for (A), MG-63 cells and (B), Primary HOB and HOF cells

+[C] = positive cell seeded controls and; -[C] = negative non-seeded controls.

3.2.2 Scanning Electron Microscopy

Further to the CyQUANT assay, evaluating MG-63 cell attachment on ternary glass compositions containing 30-40 mol% CaO took place using SEM. This however was conducted at 24 h time point, as opposed to the early time points adopted for the CyQUANT analysis (30, 120 and 180 min), in order to asses the attached cell morphology and detect any presence of cell spreading (Shieh, 2000). Accordingly, MG-63 cells were seeded on the glass discs, incubated for 24 h, then fixed and the samples were processed for SEM (see Section 2.6.2)

3.2.3 Fluorescence Immunocytochemistry

Following the use of MG-63 cells to assess the effect of monensin supplemented GM on ON cytoplasmic localisation (Section 2.7.3) HOB, HOF and HTF cells were seeded onto the glass discs of the compositional range 40-48 mol% CaO; and the poly-l-lysine treated control coverslips (fig 3.2.). In line with the time points selected for the CyQUANT assay, and at day1, day 4 and day 7 in culture, the cells were fixed

and indirectly labelled with the appropriate antibodies against markers of osteoblastic and fibroblastic phenotype activity(Section 6.2.2). HOB cells were investigated for BSP, ON and OP synthesis whilst, HOF and HTF cells were labelled against the enzyme Proline-4-Hydoxylase (P-4-H) using the 5B5 monoclonal antibody (Section 2.7.3). This was followed by the secondary; FITC (fluorescein isothiocyanate) conjugated antibody labelling.

To asses the attached cell morphology in relation to the seeded glass composition, a similar experimental procedure was conducted (Figure 3.2) and at time points at 24 h, day 4 and day 7 in culture, cells were fixed and directly labelled with Cy3 (carbocyanine 3) conjugated anti-vimentin antibody. Results were obtained using the Leica fluorescent microscope.

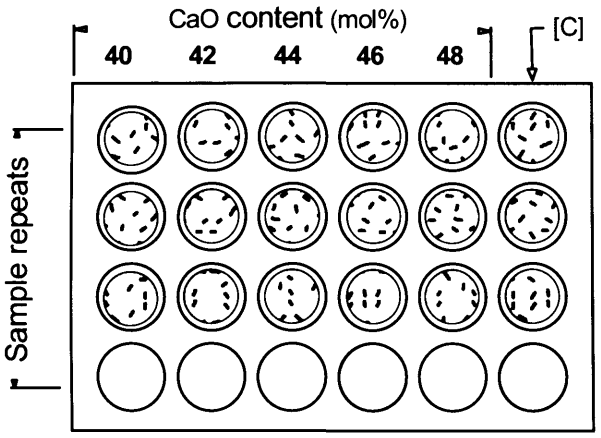

Figure 3.2 Fluorescent Immunocytochemistry assay 24-wellplate configuration

This configuration was adopted for each investigated antibody and at each time point. [C]= poly-l-lysine treated borosilicate control coverslips.

3.3 Results

3.3.1 Initial evaluation of biocompatibility: MG-63 cell attachment to the highly soluble glass compositions

When compared to the control surface, and by fluorescent quantification of nucleic acids, glass discs of 30 and 35 mol% CaO supported less cell attachment after 30 min in culture (Figure 3.3A).At 120 min time point, and on all glass compositions, cell density was less than that on the control surface (Figure 3.3B). However and after 180 min in culture, glasses containing 40 mol% CaO supported significantly higher cell attachment than those of the lower CaO content. Furthermore, cell attachment rates to the 40 mol% glass surface matched those of the tissue culture plastic c control (Figure 3.3C).

Using SEM and after 24 h in culture, only $(CaO)_{0.4}$-$(Na_2O)_{0.1}$-$(P_2O_5)_{0.5}$ glass discs exhibited a clear, well distributed, cell attachment across the entire disc surface (Figures 3.4A and B). In comparison, fewer cells remained attached to compositions with lower calcium content (Figure 3.4D) and no cells were attached to discs containing 30, 32 and 34 mol% of CaO (Table 3.2). All glasses containing less that 40 mol % CaO exhibited a fissured and irregular appearance of the disc surface as demonstrated by Figure 3.4C and 3.4D. This might be an indication of these glasses undergoing rapid surface degradation thus compromising cell attachment.

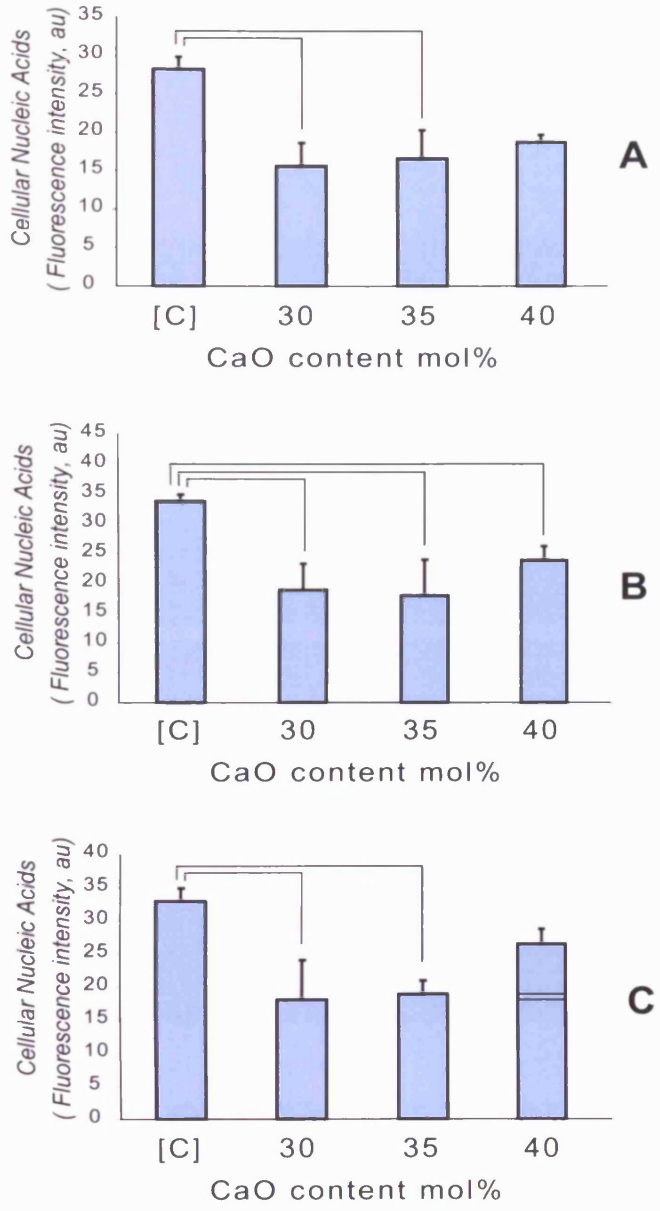

Figure 3.3 CyQUANT evaluation of MG-63 cell density on ternary glass discs

After 30 min (A), 120 min (B) and 180 min in culture(C). Significantly different values ($p<0.05$) are indicated using square brackets and dashed lines across the graph bars. [C]= Tissue culture plastic control surface. (au)= Fluorescence intensity arbitrary unit. (n= 4; error bars +SD)

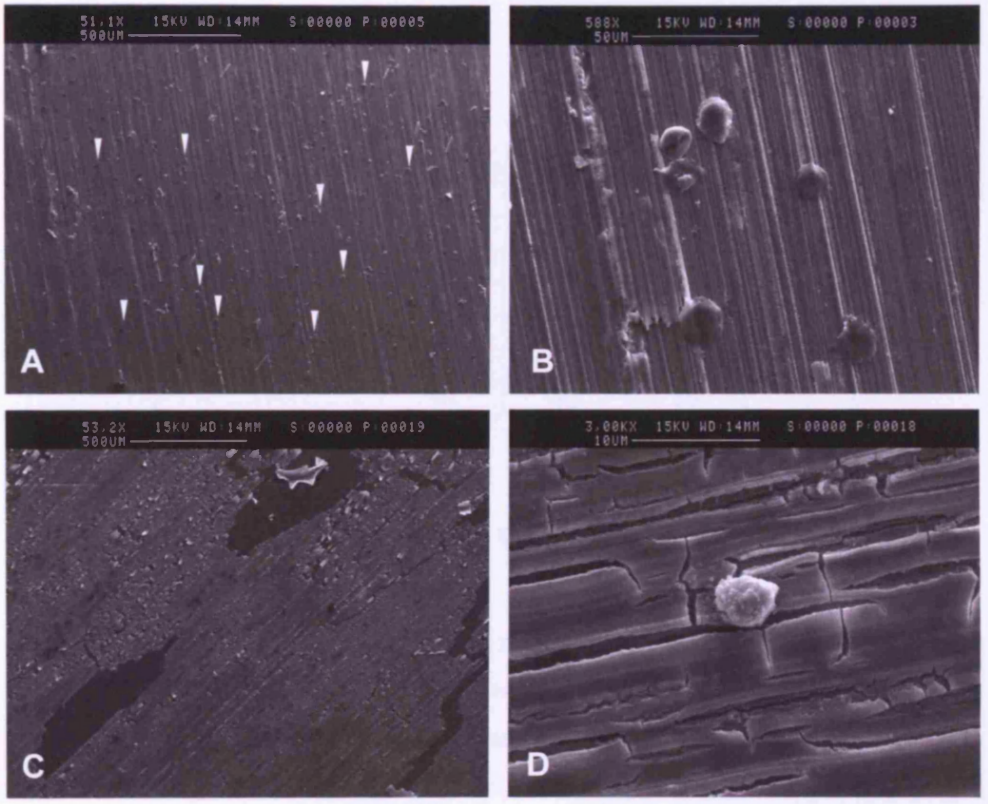

Figure 3.4 Scanning electron micrographs of MG-63 cells seeded on ternary glass discs

A (attached MG-63 cells marked by white arrow heads) and B showing $(CaO)_{0.4}$-$(Na_2O)_{0.1}$-$(P_2O_5)_{0.5}$ glass composition (51,1 and 588 magnification respectively). C and D showing $(CaO)_{0.36}$-$(Na_2O)_{0.14}$-$(P_2O_5)_{0.5}$ glass composition (53,2 and 300 magnification respectively).

Table 3.2 An evaluation of MG63 cell attachment after 24 h in culture on glass surfaces of various compositions

(-) indicates that no cells were present on the disc surface; (-/+) indicates the presence of few isolated cells with an irregular distribution pattern on the disc surface and; (+) indicates the clear presence of cell populations distributed regularly on the disc surface.

	Precursor content (mol%)			Cell Attachment
Glass Code	P_2O_5	CaO	Na_2O	MG63
$(CaO)_{0.30}$-$(Na_2O)_{0.20}$-$(P_2O_5)_{0.50}$	50	30	20	-
$(CaO)_{0.30}$-$(Na_2O)_{0.18}$-$(P_2O_5)_{0.50}$	50	32	18	-
$(CaO)_{0.34}$-$(Na_2O)_{0.16}$-$(P_2O_5)_{0.50}$	50	34	16	-
$(CaO)_{0.36}$-$(Na_2O)_{0.14}$-$(P_2O_5)_{0.50}$	50	36	14	-/+
$(CaO)_{0.38}$-$(Na_2O)_{0.12}$-$(P_2O_5)_{0.50}$	50	38	12	-/+
$(CaO)_{0.40}$-$(Na_2O)_{0.10}$-$(P_2O_5)_{0.50}$	50	40	10	+

3.3.2 Characterisation of primary cell phenotype

The inclusion of monensin salt in GM resulted in the localisation of ON in the cytoplasmic vesicles of MG-63 cells seeded on the control coverslips (Section 2.7.3). Subsequently, positive staining of ON was detected at 24 h in culture as seen from figure 3.5A. negative results were obtained from MG-63 cells seeded in normal GM as only background staining was detected (Figure 3.5B). Accordingly, all samples were incubated for 24 h in 1 μm monensin salt containing GM prior to immunocytochemistry processing.

In order to characterise primary cell populations, cells were seeded on the poly-l-lysine treated control surfaces and labelled with their respective phenotypic activity markers. This was also conducted to provide the template against which, cell phenotype maintenance on the ternary glass compositions could be assessed.

HOB cells expressed intracellular punctate staining for BSP, ON and OP as shown in Figures 3.6A, 3.6B and 3.6C, respectively. This positive staining was predominant throughout the population suggesting a homogenous culture of osteoblasts. Only background fluorescence was detected from the negative control cells, i.e. cells treated with 10% denatured donkey serum albumin as a polyclonal primary antibody

substitute (Figure 3.6D). This may be attributed to a degree of non-specific binding of both the primary, polyclonal antibodies and the secondary, FITC-conjugated antibody (Section 2.7.1.2). Cy3 conjugated anti-vimentin staining (Figure 3.6E) indicated well-spread cell morphology and an extensive intermediate filament vimentin network..

Similarly, HOF cell population expressed positive staining for prolyl-4-hydroxylase (Figure 3.7A) and similar results were obtained for HTF cells (Figure 3.7B). For both HOB and HTF cells, mouse IgG1 labelled monoclonal control cells exhibited neither positive, nor background staining when excited at the same intensity and duration as the positively labelled cells (Section 2.9) thus confirming the specificity of the positive staining. These cells also exhibited well-spread morphology with extensive cytoplasmic processes (Figure 3.7C and D).

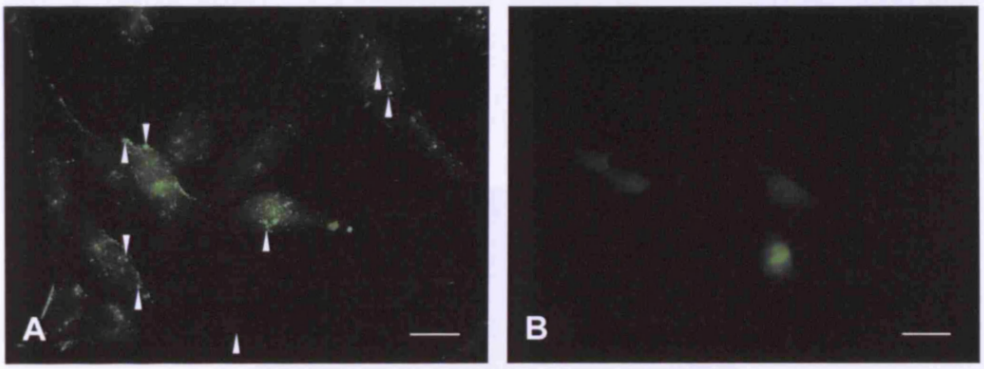

Figure 3.5 X63 objective Leica DMIRB fluorescent microscope images of MG-63 cells cultured on 13 mm borosilicate coverslips at 24 h time point

(A) Punctate FITC staining (white arrow heads) for ON following 24 h incubation in 1 μM monensin salt supplemented GM. (B) Background staining of FITC in cells seeded in normal GM (i.e. without monensin). Scale bar = 20μm.

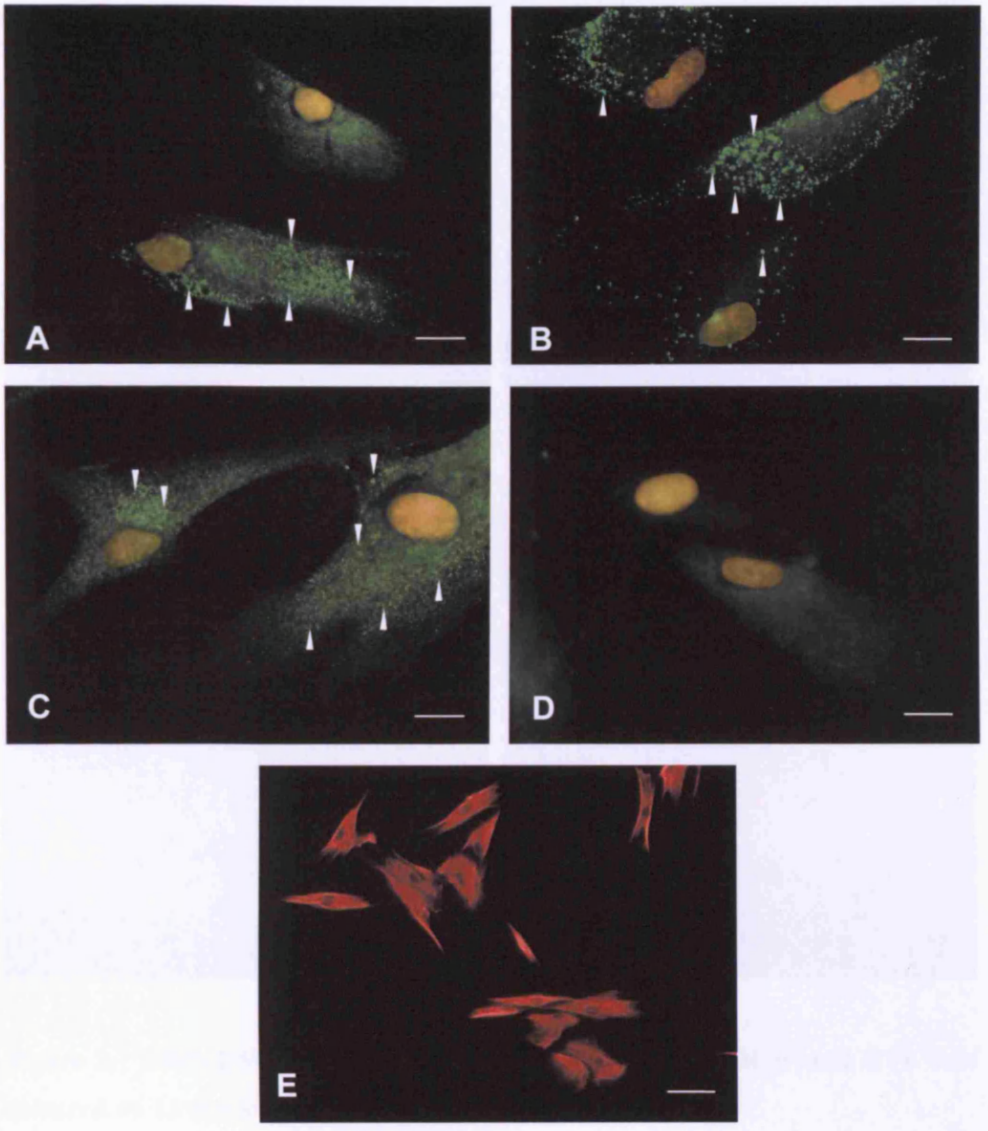

Figure 3.6 Leica DMIRB fluorescent microscope images of HOB cells cultured on 13 mm borosilicate coverslips at 24 h time point

Punctate FITC staining (white arrow heads) for BSP (A), ON (B), OP (C) (green colour, X63 objective, scale bar = 20μm). Negative control cells labelled using 10% denatured donkey serum albumin showing background staining (D). Red Cy3 anti-vimentin staining of intermediate cytoskeletal filaments (E and D) (red colour, X20 objective, scale bar = 50μm).Where applicable, nuclei are labelled with the DNA-binding dye DAPI (yellow).

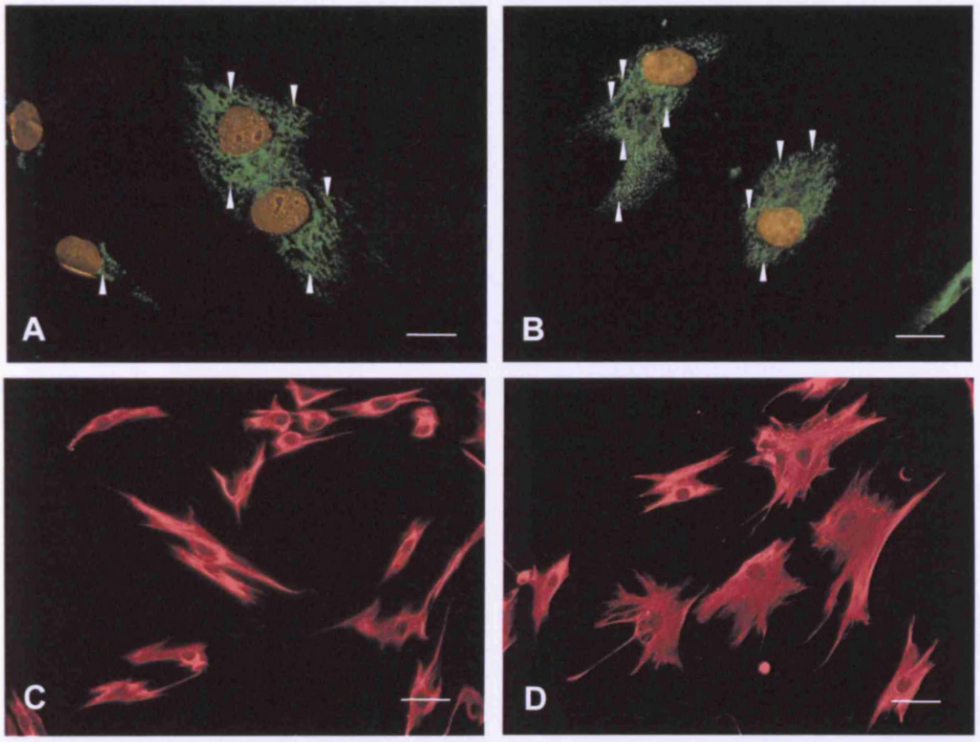

Figure 3.7 Leica DMIRB fluorescent microscope images of HOF and HTF cells cultured on 13 mm borosilicate coverslips at 24 h time point

Punctate FITC staining (white arrow heads) for 5B5 in HOF cells (A), and HTF cells (B) (green colour, X63 objective, scale bar = 20μm). Red Cy3 anti-vimentin staining of intermediate cytoskeletal filaments in HOF cells (C), and HTF cells (D) (red colour, X20 objective, scale bar = 50μm).Where applicable, nuclei are labelled with the DNA-binding dye DAPI (yellow).

3.3.3 Evaluation of ternary glasses biocompatibility: Craniofacial Osteoblasts

3.3.3.1 Preservation of cell phenotype

The HOB phenotype characteristics, through bone associated protein synthesis, were clearly expressed in culture on the glass containing 48 mol% CaO. This was demonstrated by the presence of cytoplasmic vesicles containing BSP (Figure 3.8), ON (Figure 3.9) and OP (Figure 3.10) at all time points in culture. It is clear that an adequate degree of cell spreading as the main criteria required to attain protein production, therefore, positive results were mainly obtained from cells cultured on the 48 mol% CaO content glass compositions.

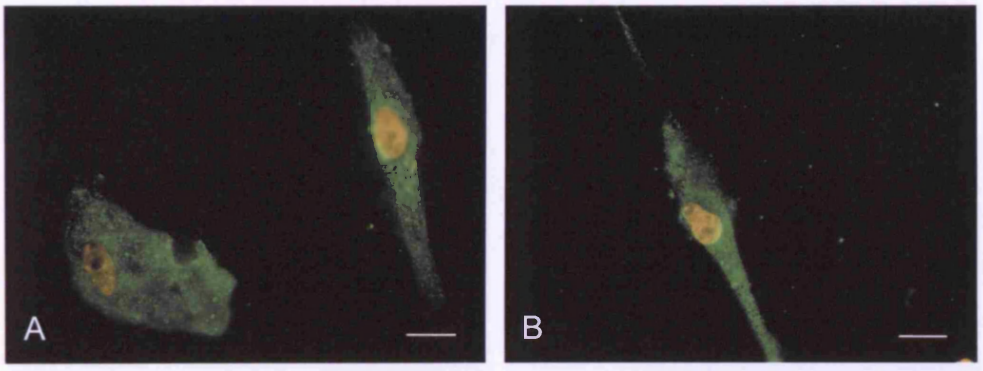

Figure 3.8 X63 objective Leica DMIRB fluorescent microscope images of HOB cells Labelled for BSP

Punctate green (FITC) staining for BSP in HOB cells cultured on $(CaO)_{0.48}$-$(Na_2O)_{0.02}$-$(P_2O_5)_{0.5}$ glass composition after 24 h (A) and 7 days (B) in culture. Nuclei are labelled with the DNA-binding dye DAPI (yellow). Cells incubated in for 24 h in 1 μM monensin prior to the fixing process. Scale bar = 20μm.

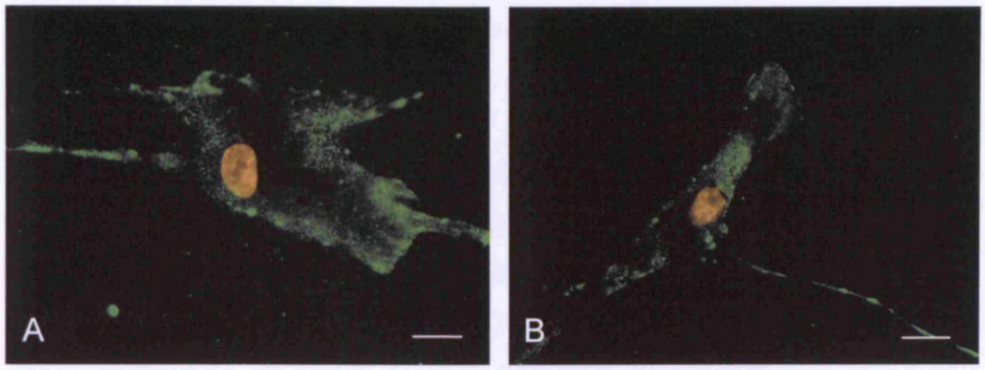

Figure 3.9 X63 objective Leica DMIRB fluorescent microscope images of HOB cells Labelled for ON

Punctate green (FITC) staining for ON in HOB cells cultured on $(CaO)_{0.48}$-$(Na_2O)_{0.02}$-$(P_2O_5)_{0.5}$ glass composition after 24 h (A) and 7 days (B) in culture. Nuclei are labelled with the DNA-binding dye DAPI (yellow). Cells incubated in for 24 h in 1 μM monensin prior to fixing process. Scale bar = 20μm.

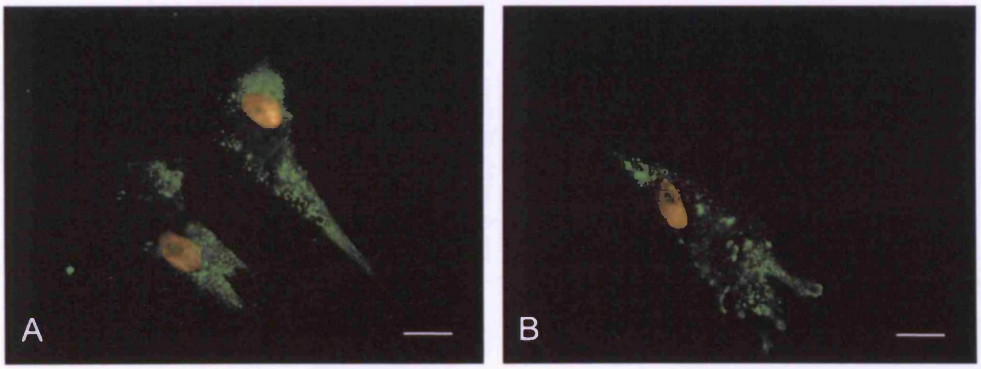

Figure 3.10 X63 objective Leica DMIRB fluorescent microscope images of HOB cells Labelled for OP

Punctate green (FITC) staining for OP in HOB cells cultured on $(CaO)_{0.48}$-$(Na_2O)_{0.02}$-$(P_2O_5)_{0.5}$ glass composition after 24 h (A) and 7 days (B) in culture. Nuclei are labelled with the DNA-binding dye DAPI (yellow). Cells incubated in for 24 h in 1 μM monensin prior to fixing process. Scale bar = 20μm.

3.3.3.2 Cell morphology and attachment patterns

After 24 h in culture, HOB cells were present on all glass discs. Rounded cell morphology remained predominant on glasses with lower calcium content (Figure 3.11A), whilst a degree of cell spreading was observed on the composition of 48 mol% CaO content (Figure 3.11B) when compared to the control cells (Figure 3.11C). At day 4 a similar pattern was noticed (Figures 3.11D and E) with cells retaining spread morphology on higher calcium containing compositions. By day 7 only composition $(CaO)_{0.48}$-$(Na_2O)_{0.02}$-$(P_2O_5)_{0.5}$ supported cell adhesion however, the rounded morphology of the attached cells became more conspicuous (Figure 3.11G and 3.11H) compared with the spread appearance of the control surface seeded cells (Figure 3.11I). Cell numbers, through visual observation and in correspondence with the CyQUANT evaluation of cell density (see Section 3.3.3.3), were highest on the 48 mol% CaO containing glass composition.

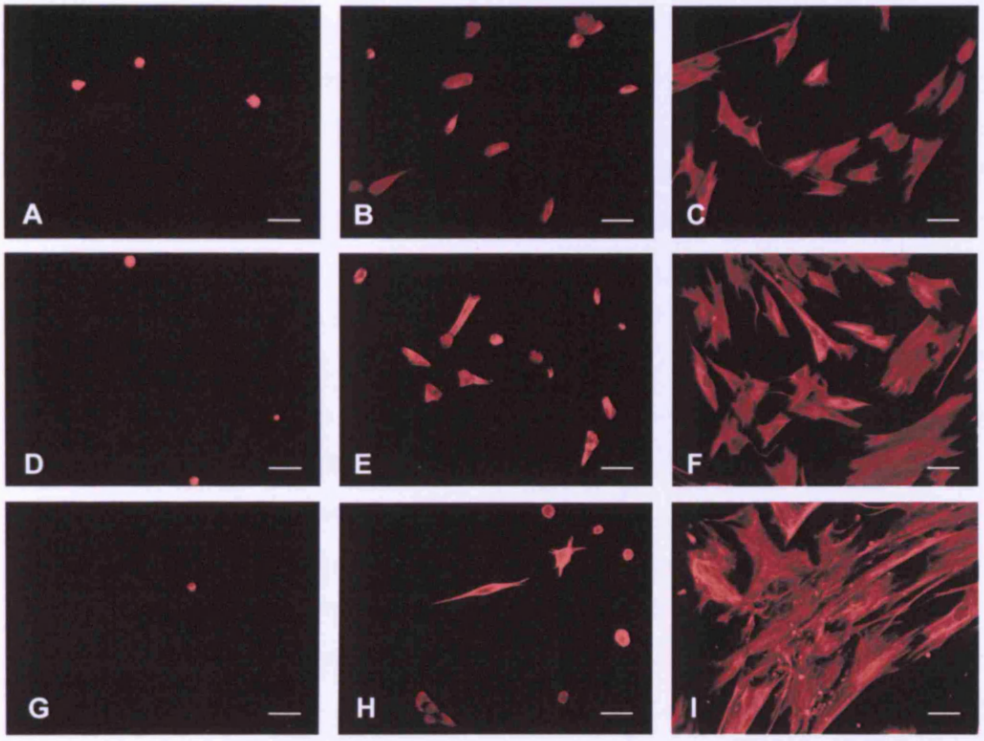

Figure 3.11 HOB cell morphology on ternary glass compositions

X20 objective Leica DMIRB fluorescence micrographs of HOB cells (i) cultured on $(CaO)_{0.4}$-$(Na_2O)_{0.1}$-$(P_2O_5)_{0.5}$ glass (A), $(CaO)_{0.48}$-$(Na_2O)_{0.02}$-$(P_2O_5)_{0.5}$ glass (B) and borosilicate coverslips (C) after 24 h in culture, (ii) cells cultured on $(CaO)_{0.4}$-$(Na_2O)_{0.1}$-$(P_2O_5)_{0.5}$ glass (D), $(CaO)_{0.48}$-$(Na_2O)_{0.02}$-$(P_2O_5)_{0.5}$ glass (E) and borosilicate coverslips (F) after 4 days in culture and (iii) cells cultured on $(CaO)_{0.4}$-$(Na_2O)_{0.1}$-$(P_2O_5)_{0.5}$ glass (G), $(CaO)_{0.48}$-$(Na_2O)_{0.02}$-$(P_2O_5)_{0.5}$ glass (H) and borosilicate coverslips (I) after 7 days in culture. Cells stained with anti-vimentin cy3 conjugated antibody (red). Scale bar = 20μm.

3.3.3.3 Cell survival and proliferation

As seen from figure 3.12, and using the CyQUANT analysis of the attached cell density, only HOB cells seeded on glass compositions containing 44 and 48 mol% CaO underwent considerable increase in density ($p<0.05$) by day 4 in culture. No further increase was noticed, however, by day 7 in culture. No proliferation pattern was associated with 40, 42 and 46 mol% CaO containing discs over time in culture. Cells seeded on the tissue culture plastic control surfaces exhibited considerable population growth, starting at day 1 time point, as a function of time in culture. Comparing density data for cells seeded on different glass compositions at each time point revealed that after 3 h in culture, no significant differences in density were present among cells seeded on all glass compositions (Figure 3.13A). By day 1, however, significantly fewer cells attached to the glass compositions of 40, 42 and 44 CaO content than those higher on CaO compositions (46 and 48 mol% CaO) where differences in the attached cell numbers against the control surfaces were insignificant (Figure 3.13B). By day 4 in culture, all glass compositions accommodated less attached cells than the control surface nonetheless, higher cell density was present on glass discs containing 44 and 48 mol% CaO in comparison with the 40 mol% CaO composition (Figure 3.13C). Similarly, and at day 7 time point, more cells attached to the control surfaces than to the glass discs of all compositions. Moreover, and as seen at day 1 and day 4 time points, more cells remained attached to the 48 mol% containing glass discs than to the lower on calcium, 40 mol% CaO containing, glass composition.

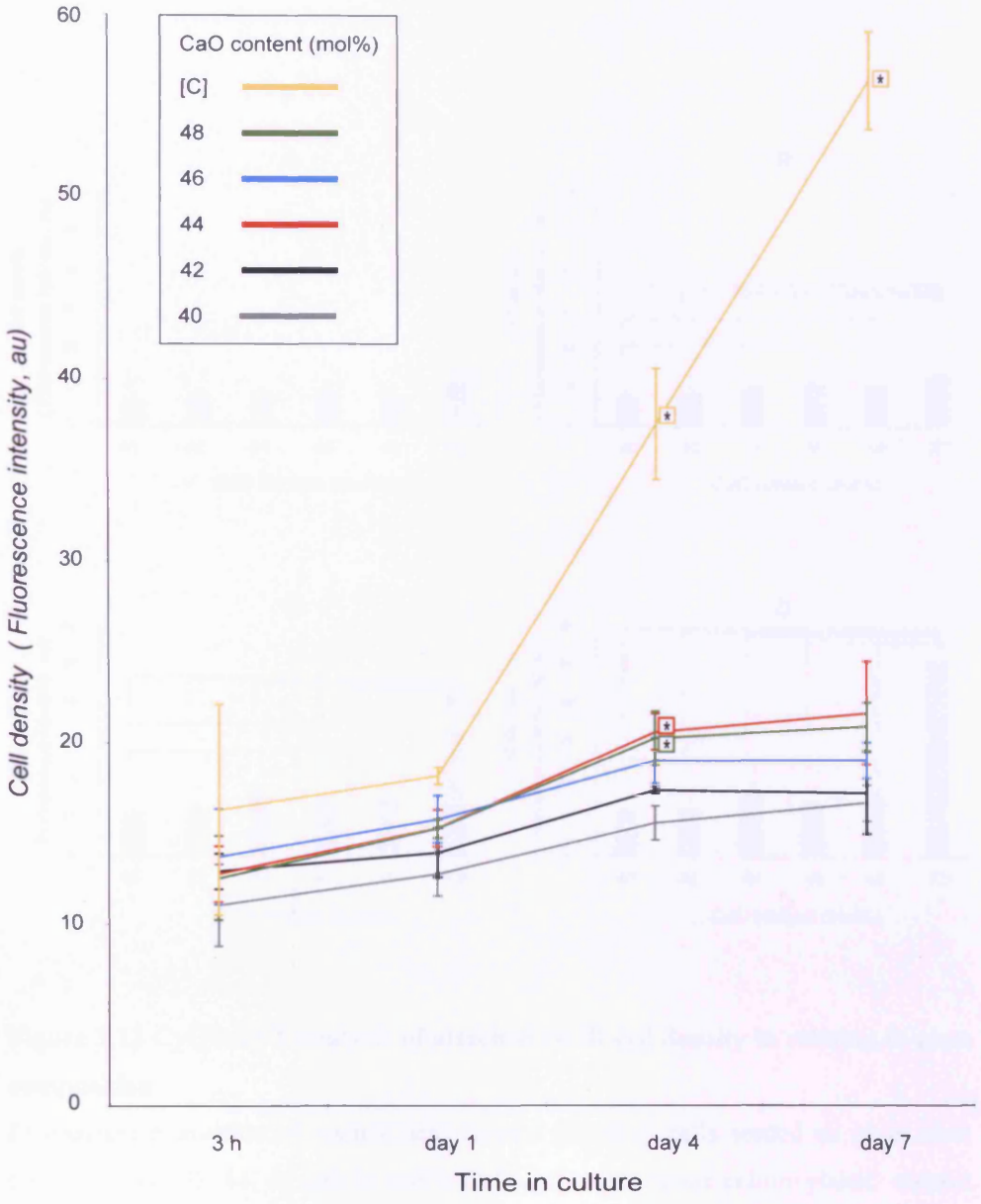

Figure 3.12 CyQUANT analysis of attached HOB cell survival and proliferation
Fluorescent evaluation of nucleic acid content for HOB cells seeded on glass discs containing 40, 42, 44, 46 and 48 mol% CaO and on the tissue culture plastic control surfaces ([C]) at 3 h, day 1, day 4 and day 7 in culture. For each composition, (*) indicates a significant (p<0.05) increase in cell density over time in culture. Data obtained by measuring the CyQUANT GR dye intensity using the Fluroskan Ascent plate reader. au = Fluorescence intensity arbitrary unit. (n = 3; error bars +/-SD)

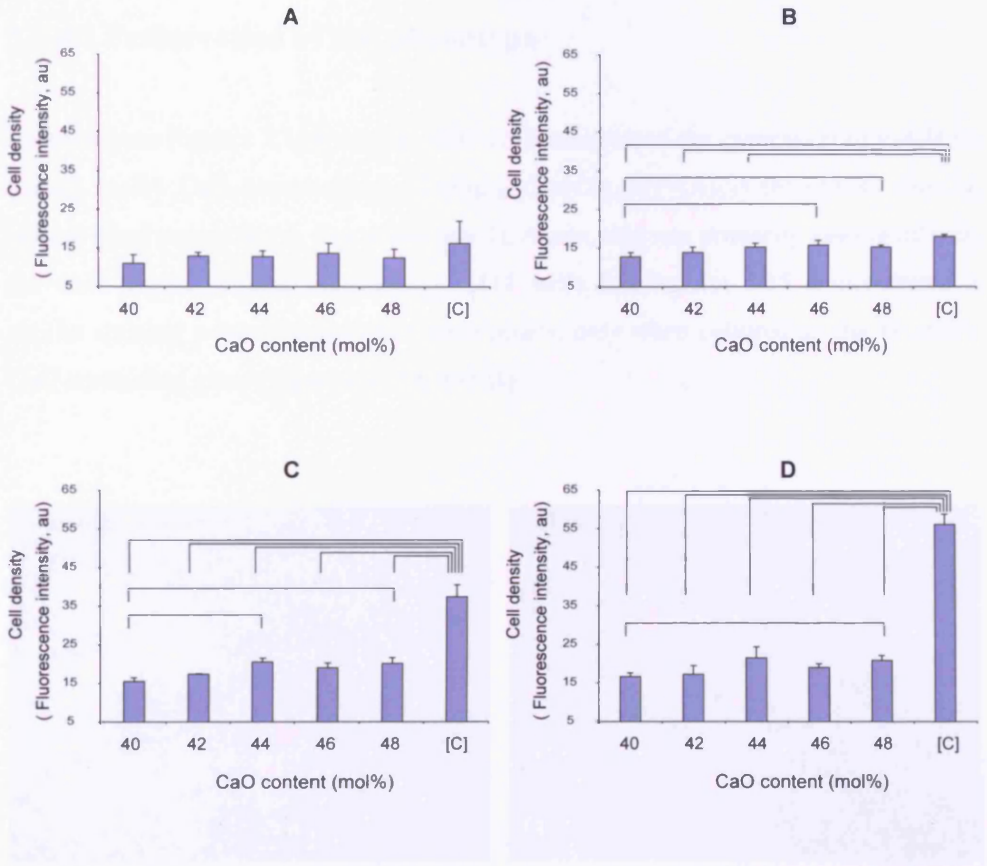

Figure 3.13 CyQUANT analysis of attached HOB cell density in relation to glass composition

Fluorescent evaluation of nucleic acid content for HOB cells seeded on glass discs containing 40, 42, 44, 46 and 48 mol% CaO and on the tissue culture plastic control surfaces ([C]) at 3 h (A), day 1 (B), day 4 (C) and day 7 (D) in culture. Significant differences in fluorescence values obtained from cells seeded on different glass compositions, at each time point, are linked using horizontal brackets (⊓). Data obtained by measuring the CyQUANT GR dye intensity using the Fluroskan Ascent plate reader. (au), Fluorescence intensity arbitrary unit. (n= 3; error bars +/-SD)

3.3.4 Evaluation of ternary glasses biocompatibility: Oral and tendon fibroblasts

3.3.4.1 Preservation of cell phenotype

As seen from Figures 3.14A and B, HOF cells maintained the expression of P-4-H on the 48 mol% CaO composition ($(CaO)_{0.48}$-$(Na_2O)_{0.02}$-$(P_2O_5)_{0.5}$) throughout time in culture (time points day 1, day 4 and day 7). Again, this was primarily associated with the well spread cellular morphology. HTF cells labelled for 5B5 demonstrated a similar staining pattern, at the same time points, only when cultured on the 48 mol% CaO containing glass (Figures 3.15A and B)

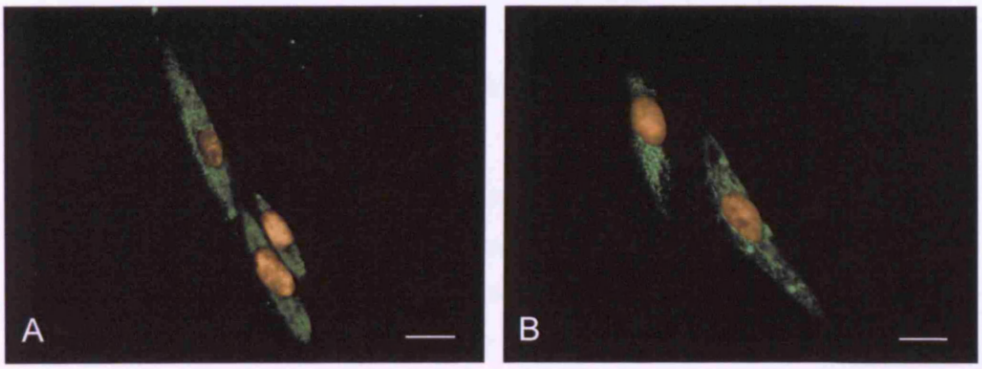

Figure 3.14 X63 objective Leica DMIRB fluorescent microscope images of HOF cells Labelled against P-4-H

Punctate green (FITC) staining for 5B5 in HOF cells cultured on $(CaO)_{0.48}$-$(Na_2O)_{0.02}$-$(P_2O_5)_{0.5}$ glass composition after 1 day (A) and 7 days (B) in culture. Nuclei are labelled with the DNA-binding dye DAPI (yellow). Scale bar = 20μm.

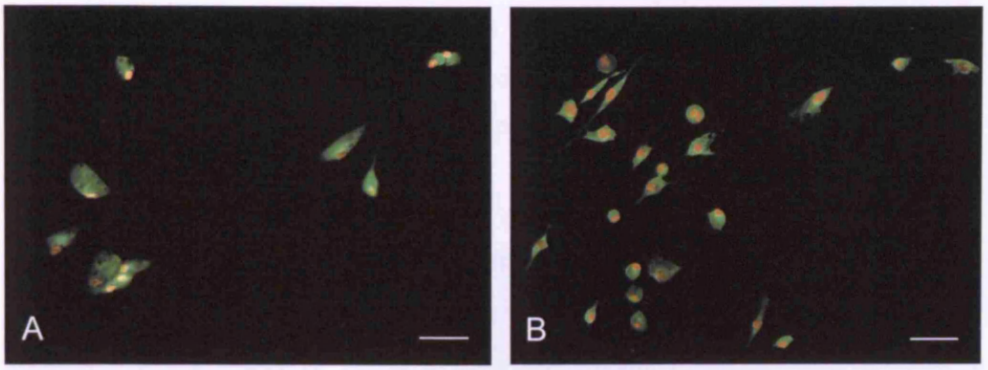

Figure 3.15 X20 objective Leica DMIRB fluorescent microscope images of HTF cells Labelled against P-4-H

Punctate green (FITC) staining for 5B5 in HTF cells cultured on $(CaO)_{0.48}$-$(Na_2O)_{0.02}$-$(P_2O_5)_{0.5}$ glass composition after 1 day (A) and 7 days (B) in culture. Nuclei are labelled with the DNA-binding dye DAPI (yellow). Scale bar = 50μm.

3.3.4.2 Cell morphology and attachment patterns

All glass compositions, at all time points, appeared to accommodate the adhesion and survival of HOF cells and, with the exception of day 4 in culture, no significant differences in cell density were visually detected on different substrates. However, the nature of cell adhesion varied considerably depending on the glass composition used. At 1 day attachment patterns for cells cultured on all glasses (Figure 3.16A and B) were relatively close to those seen on the control surfaces (Figure 3.16C). By day 4 increased numbers of cells were noted on all compositions. Whilst cells on the lower calcium containing glass composition $(CaO)_{0.4}$-$(Na_2O)_{0.10}$-$(P_2O_5)_{0.5}$ exhibited round morphology (Figure 3.16D), more cells were present on composition $(CaO)_{0.48}$-$(Na_2O)_{0.02}$-$(P_2O_5)_{0.5}$ (Figure 3.16E) with cells maintaining a spread appearance in comparison with that of the control cells (Figure 3.16F). At day 7, cells on the lower calcium-containing composition (Figure 3.16G) were rounded in comparison to the cells on composition $(CaO)_{0.48}$-$(Na_2O)_{0.02}$-$(P_2O_5)_{0.5}$ which, clearly, retained a well spread appearance (Figure 3.16H; control Figure 3.16I).

Vimentin filament staining in HOF cells revealed greater cell numbers related to the highest calcium containing glass composition, i.e. 48 mol% CaO at 24 h, day 4 and

day 7 as seen from Figures 3.17A, B and C respectively. At X40 objective magnification, HTF cells revealed a spread morphology, on the 48 mol% CaO glass composition (Figure 3.17D, E and F), approximating that of the control cells at all three time points (Figure 3.17G, H and I).

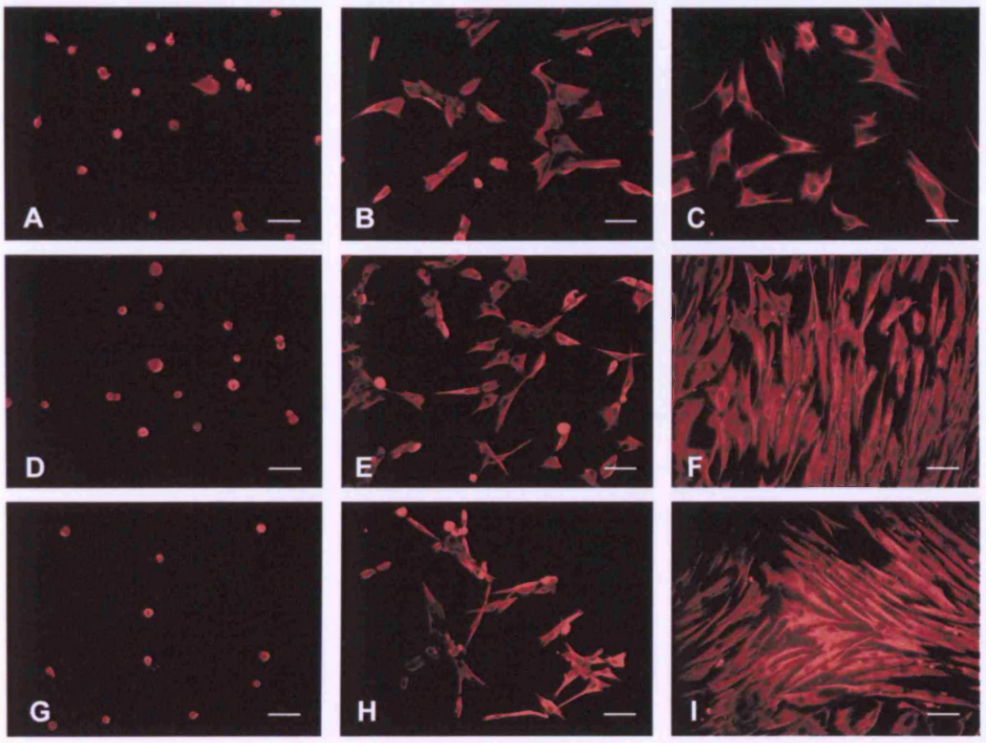

Figure 3.16 HOF cell Morphology on ternary glass compositions

X20 objective Leica DMIRB fluorescence micrographs of HOF cells (i) cultured on $(CaO)_{0.4}$-$(Na_2O)_{0.1}$-$(P_2O_5)_{0.5}$ glass (A), $(CaO)_{0.48}$-$(Na_2O)_{0.02}$-$(P_2O_5)_{0.5}$ glass (B) and borosilicate coverslips (C) after 1 day in culture, (ii) cells cultured on $(CaO)_{0.4}$-$(Na_2O)_{0.1}$-$(P_2O_5)_{0.5}$ glass (D), $(CaO)_{0.48}$-$(Na_2O)_{0.02}$-$(P_2O_5)_{0.5}$ glass (E) and borosilicate coverslips (F) after 4 days in culture and (iii) cells cultured on $(CaO)_{0.4}$-$(Na_2O)_{0.1}$-$(P_2O_5)_{0.5}$ glass (G), $(CaO)_{0.48}$-$(Na_2O)_{0.02}$-$(P_2O_5)_{0.5}$ glass (H) and borosilicate coverslips (I) after 7 days in culture. Cells stained with anti-vimentin cy3 conjugated antibody (red). Scale bar = 50μm.

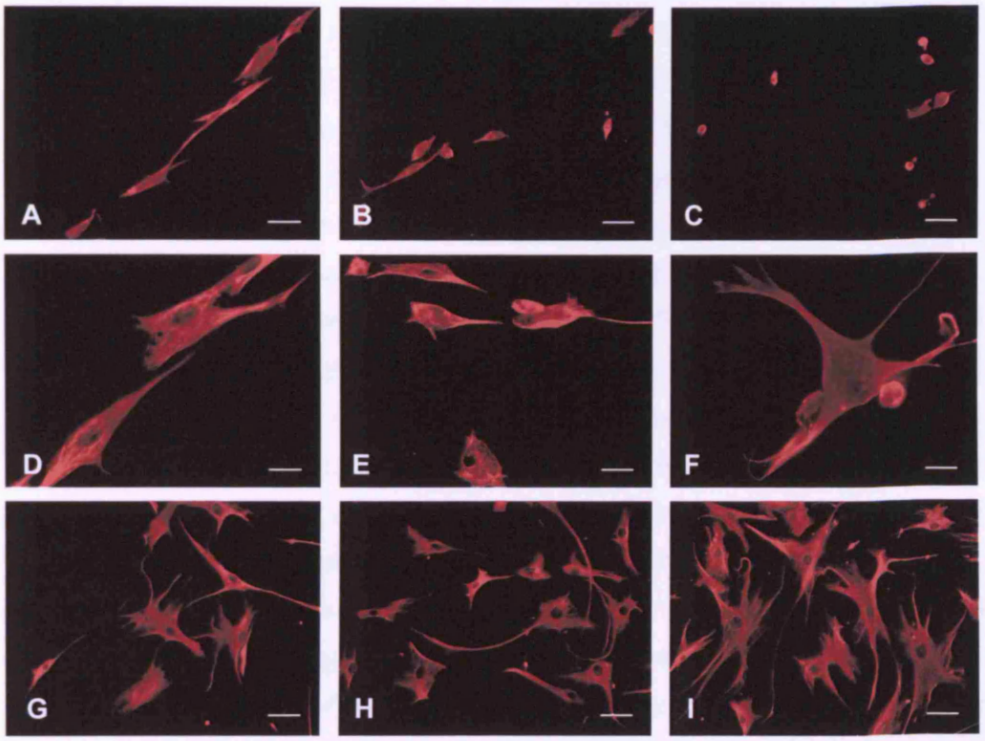

Figure 3.17 HTF cell Morphology on ternary glass compositions

HTF cells stained with anti-vimentin cy3 conjugated antibody. (i) X20 objective Leica DMIRB fluorescence micrographs of cells cultured on $(CaO)_{0.48}$-$(Na_2O)_{0.02}$-$(P_2O_5)_{0.5}$ glass composition after 1 day (A), 4 days (B) and 7 days (C) in culture (Scale bar = 50μm).and (ii) X40 objective fluorescence micrographs of HTF cells cultured on $(CaO)_{0.48}$-$(Na_2O)_{0.02}$-$(P_2O_5)_{0.5}$ glass composition after 1 day (G), 4 days (H) and 7 days (I) in culture (Scale bars = 25μm) cells cultured on borosilicate coverslips after 24 h (D), 4 days (E) and 7 days (F) in culture.

3.3.4.3 Cell survival and proliferation

Measuring the CyQUANT GR dye fluorescence intensity revealed a significant increase in HOF cell density, between days 1 and 4 in culture, on all seeded glass compositions except the 40 mol% CaO containing discs (Figure 3.18). This trend was reversed however as by day 7, a significant decline in cell numbers was observed on all seeded discs. Similar to the results obtained for HOB cells (Section 3.3.3.3), a clear proliferation pattern was associated with cells seeded on the control tissue culture plastic surfaces from day 1 onwards. After 3 h in culture, as seen from Figure 3.19A, similar density values were obtained for HOF cells attached to discs of all the compositions investigated together with the control surfaces. At day 1, the attached cell density values for all glass compositions were significantly lower than those of the control surfaces with the exception of the 42 mol% CaO containing glass composition (Figure 3.19B). By day 7, fewer cells attached to the 40, 42, 44 and 46 mol% CaO content glass compositions than to the tissue culture plastic control however, 48 mol% CaO content glass discs supported cell attachment at levels similar to those on the control surfaces and significantly higher than those on the 40, 42 and 44 glass compositions (Figure 3.19C). Eventually, and by day 7 in culture, cell density values on discs of all compositions were significantly lower than those established for tissue culture plastic (Figure 3.19D).

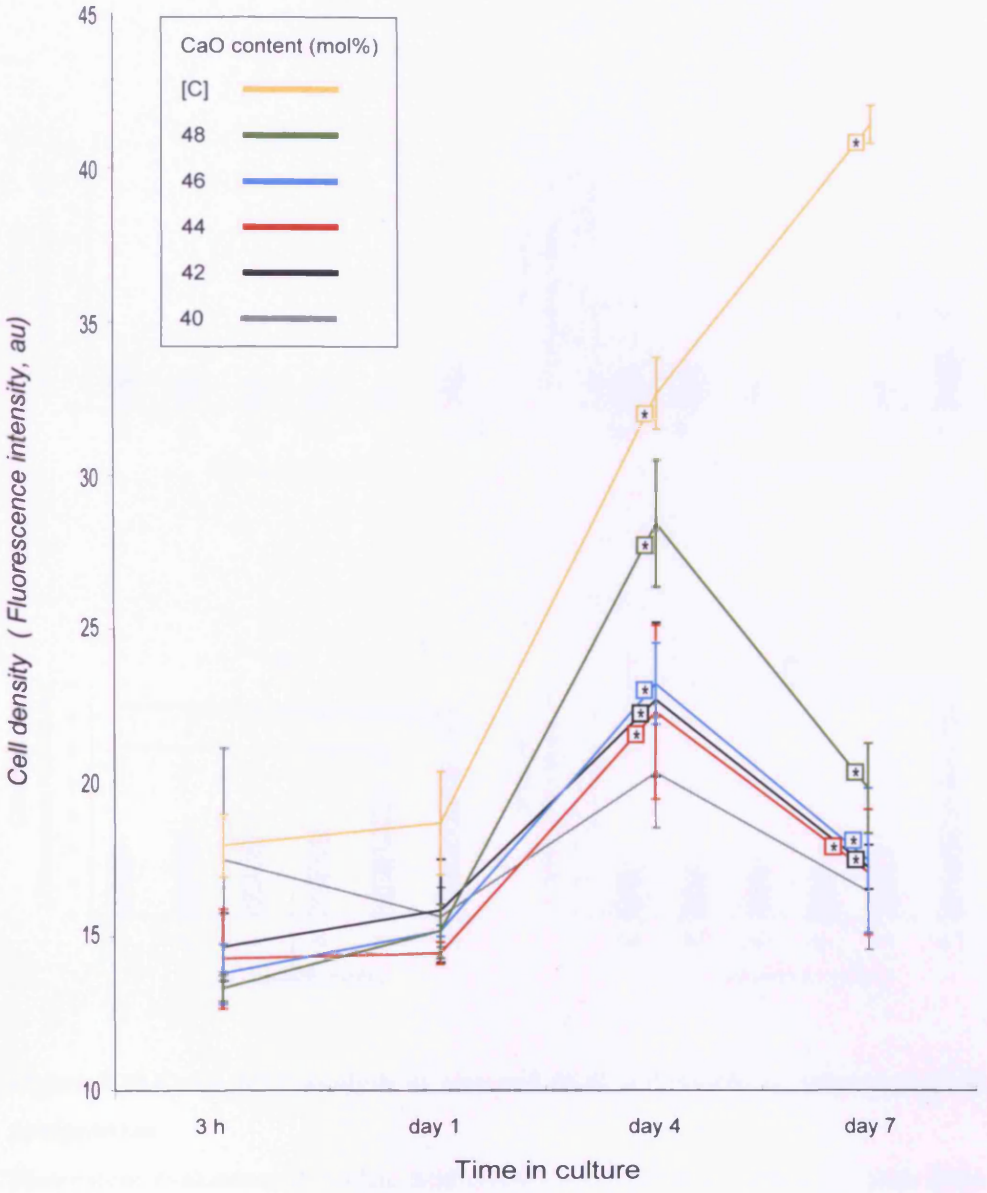

Figure 3.18 CyQUANT analysis of attached HOF cell survival and proliferation Fluorescent evaluation of nucleic acid content for HOF cells seeded on glass discs containing 40, 42, 44, 46 and 48 mol% CaO and on the tissue culture plastic control surfaces ([C]) at 3 h, day 1, day 4 and day 7 in culture. For each composition, (*) indicates a significant ($p<0.05$) increase in cell density over time in culture. Data obtained by measuring the CyQUANT GR dye intensity using the Fluroskan Ascent plate reader. au = Fluorescence intensity arbitrary unit. (n = 3; error bars +/-SD)

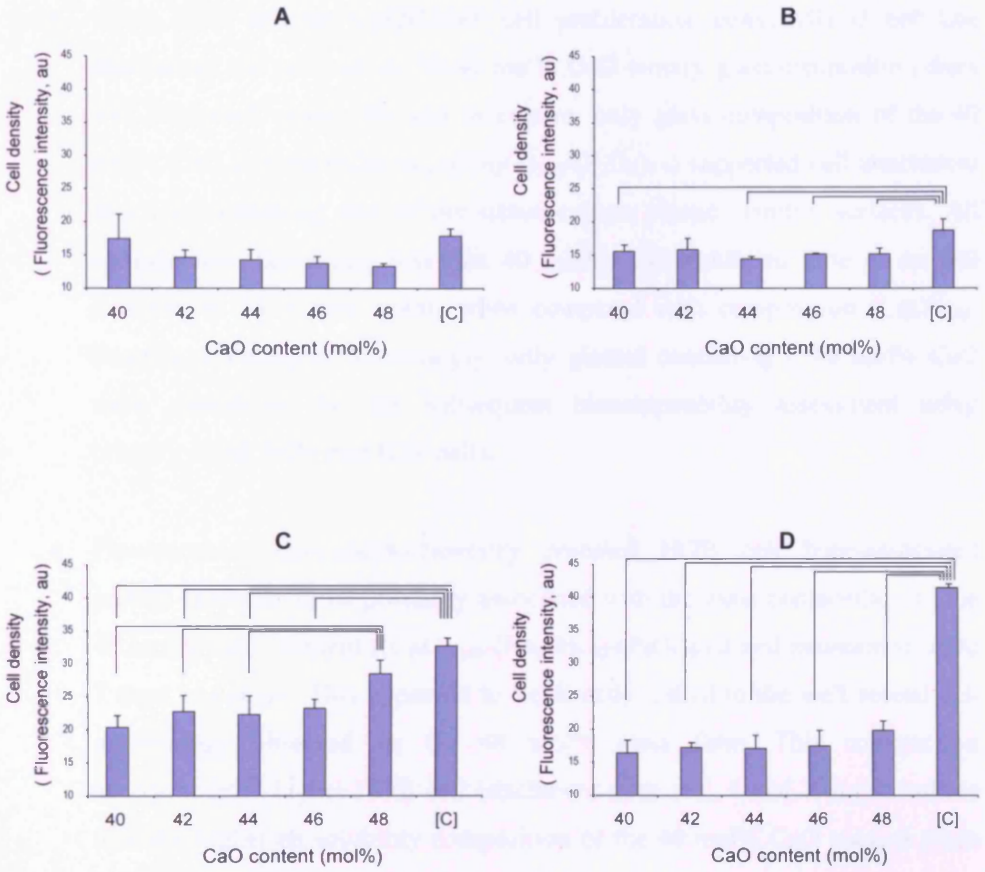

Figure 3.19 CyQUANT analysis of attached HOF cell density in relation to glass composition

Fluorescent evaluation of nucleic acid content for HOF cells seeded on glass discs containing 40, 42, 44, 46 and 48 mol% CaO and on the tissue culture plastic control surfaces ([C]) at 3 h (A), day 1 (B), day 4 (C) and day 7 (D) in culture. Significant differences in fluorescence values obtained from cells seeded on different glass compositions, at each time point, are linked using horizontal brackets (⊓). Data obtained by measuring the CyQUANT GR dye intensity using the Fluroskan Ascent plate reader. (au), Fluorescence intensity arbitrary unit. (n= 3; error bars +/-SD)

3.4 Summary

- Using SEM and the CyQUANT cell proliferation assay, MG-63 cell line attachment and survival on 30-40 mol% CaO ternary glass composition discs was evaluated. After 180 min in culture, only glass composition of the 40 mol% CaO content ($(CaO)_{0.40}$-$(Na_2O)_{0.02}$-$(P_2O_5)_{0.5}$) supported cell attachment at a level matching that of the tissue culture plastic control surfaces. All compositions containing less that 40 mol% CaO exhibited little or no cell survival, at 24 h time point, when compared with composition $(CaO)_{0.40}$-$(Na_2O)_{0.10}$-$(P_2O_5)_{0.50}$. Accordingly, only glasses containing $\geq$ 40 mol% CaO were considered for the subsequent biocompatibility assessment using primary HOB, HOF and HTF cells.

- Fluorescence immunocytochemistry revealed HOB cell bone-associated protein synthesis to be primarily associated with the glass composition of the 48 mol% CaO content ($(CaO)_{0.48}$-$(Na_2O)_{0.02}$-$(P_2O_5)_{0.50}$) and maintained up to 7 days in culture. This appeared to be directly linked to the well spread cell morphology observed on the 48 mol% glass form. This composition accommodated higher HOB cell attachment rates at 1, 4 and 7 day in culture than the higher on solubility composition of the 40 mol% CaO content when cell density was fluorescently quantified. No significant cell proliferation pattern was observed however in comparison with the tissue culture plastic control except for 44 and 48 mol% CaO content compositions. This proliferation pattern was limited to day 4 in culture.

- Up to 7 days in culture, HOF and HTF phenotype associated P-4-H synthesis, together with a well spread *in vitro* appearance, was clearly expressed and maintained exclusively on the 48 mol% glass discs as confirmed by fluorescent labelling. Using the CyQUANT analysis, HOF cell density was also higher on this composition (48 mol% CaO), at day 4 in culture, than on glasses containing 40, 42 and 44 mol% CaO however, and starting at day 4, a decrease in the attached cell density occurred over time in culture.

- As primary cell survival, functional *in vitro* morphology and phenotype protein synthesis appeared to be directly linked to the glass solubility profile, with the least soluble glass forms expressing the highest biocompatibility features, glass compositions of the 46 and 48 CaO content ($(CaO)_{0.46}$-$(Na_2O)_{0.04}$-$(P_2O_5)_{0.5}$ and $(CaO)_{0.48}$-$(Na_2O)_{0.02}$-$(P_2O_5)_{0.50}$) were elected for glass fibre fabrication and the fibre scaffold biocompatibility assessment. The lack of cell proliferation on these compositions however, highlighted the necessity of further optimising glass solubility by generating quaternary glass forms.

CHAPTER FOUR
RESULTS TWO

4.1 Introduction

Glass fibres of various diameters can be produced by varying the fibre drum rotational speeds. By increasing the rotational speed, glass fibres of smaller diameters can be produced (Ahmed et al., 2004). In terms of biocompatibility, the optimal fibre diameter was determined by evaluating HOB and HOF attachment and survival on the 48 mol% CaO containing ternary glass fibres generated at 3 different rotational speeds. Subsequently, solubility profiles and average fibre diameters of quaternary glass fibre forms were evaluated (Table 4.1). Cell survival, proliferation rates and maintenance of morphology on these fibres were established. The most biocompatible quaternary glass composition was later utilised for implementing the co-culture scaffold design to asses the feasibility of interface formation and the subsequent cell behaviour.

Table 4.1 Quaternary glass fibre compositions used for biocompatibility testing

	Precursor content (mol%)			
Glass Code	**P_2O_5**	**CaO**	**Na_2O**	**F_2O_3**
$(CaO)_{0.46}$-$(Na_2O)_{0.03}$-$(Fe_2O_3)_{0.01}$-$(P_2O_5)_{0.50}$	50	46	3	1
$(CaO)_{0.46}$-$(Na_2O)_{0.02}$-$(Fe_2O_3)_{0.02}$-$(P_2O_5)_{0.50}$	50	46	2	2
$(CaO)_{0.46}$-$(Na_2O)_{0.01}$-$(Fe_2O_3)_{0.03}$-$(P_2O_5)_{0.50}$	50	46	1	3

4.2 Experimental protocol

4.2.1 Scaffold Preparation

4.2.1.1 Ternary glass fibre system

The rotational speeds 800, 1200 and 1600 r/min were selected to produce fibres of the composition $(CaO)_{0.48}$-$(Na_2O)_{0.02}$-$(P_2O_5)_{0.5}$ as attempts to generate fibres at a speed lower than 800 r/min were unsuccessful. When increasing the CaO precursor content, higher melting temperatures are required if glass formation is to take place(Section 2.2.4). Accordingly, the combined fibre formation and glass phase transition processes can be induced when the prompt cooling of the fibre precursor can be guaranteed. At slower rotational speeds the fibre precursor is cooled at a lower rate, at the crucible outlet, and the transition from the liquid to the solid state of the mater occurs through the crystallisation phase (Section 2.2.1). Fibre production from glass compositions of 40-48 mol% CaO content was therefore constantly interrupted, by crystallisation, at slow rotational rates. Based on the previous work conducted by our group, fibre diameters were theoretically estimated as seen from Table 4.2 (Ahmed et al., 2004a). The fibre scaffold alignment, via the stepper motor function, took into consideration the presence of 5-10 μm fixed distance between adjacent fibres (Section 2.2.5). The scaffolds were also arranged so that fibre configuration took a monolayer mesh form, for both HOB and HOF cells, to maximise the substrate surface as at this stage, the rate and maintenance of HOB and HOF attachment to the glass fibre form are unknown.

Table 4.2 Estimated fibre diameter at various drum rotational speeds

The stepper motor control frequency was accordingly adjusted so that a hypothetical gap of 5- 10 μm is maintained between adjacent fibres.

Estimated fibre diameter (μm)	Drum Rotational speed (r/ min)	Stepper motor control frequency (Hz)
10- 15	1600	0.15
15- 20	1200	≈ 0.19
20- 25	800	0.2

4.2.1.2 Quaternary glass fibre system

Quaternary glass production was based on modifying the ternary composition $(CaO)_{0.46}$-$(Na_2O)_{0.04}$-$(P_2O_5)_{0.5}$. This composition was chosen as it was, among the ternary glass compositions investigated in chapter 3, second only to glass composition $(CaO)_{0.48}$-$(Na_2O)_{0.02}$-$(P_2O_5)_{0.5}$ (of the 48 mol% CaO content) in terms of biocompatibility and secondly, the molar structure of this glass permitted the inclusion of up to 3 mol% of F_2O_3 of at the expense of reducing the Na_2O content. Fibre scaffolds were produced using 1, 2 and 3 mol% F_2O_3 quaternary glass compositions and, as means of comparison, the corresponding ternary 46 mol% CaO containing composition. Fibres were drawn at 800 r/min rotational speed and aligned following fibre diameter characterisation, with a 0 (nil) μm inter-fibre separating gap so the substrate seeded surface could be maximised and the loss of seeded cells can be prevented. A monolayer mesh and a unidirectional parallel fibre arrangement were produced to seed HOB, and HOF cells respectively.

The quaternary glass composition of the 3 mol% Fe_2O_3 content ($(CaO)_{0.46}$-$(Na_2O)_{0.01}$-$(Fe_2O_3)_{0.03}$-$(P_2O_5)_{0.50}$) was used to produce the co-culture scaffold with the fibres aligned as above.

4.2.2 Glass fibre characterisation

Following epoxy resin embedding; resin block cutting and polishing, the average fibre diameter for each quaternary glass composition was determined (Section 2.4.2).

Weight loss for each glass fibre composition was obtained by subtracting the dry fibre bundle weight, at the appropriate time point, from the weight of the starting material, i.e. 100 mg. Composition related dissolution weight loss values, at days 1, 4, 7 and 10 were accordingly obtained following fibre bundles incubation in GM. This was conducted to establish the *in vitro* solubility trend for the 3 quaternary glass fibre compositions (1, 2 and 3 mol% F_2O_3 content); and the corresponding $(CaO)_{0.46}$-$(Na_2O)_{0.04}$-$(P_2O_5)_{0.5}$ ternary glass fibre form. Additionally, the average hourly weight loss value for each glass composition, and at all 4 time points, was calculated to determine the effect of F_2O_3 inclusion on the glass solubility profile.

For SEM, glass fibres of the 46 mol% CaO content ternary, and 3 mol% Fe_2O_3 quaternary compositions were produced at 800 r/min and processed as described in Section 2.4.3.

4.2.3 Cell density evaluation

The direct cell count method was used to evaluate HOB and HOF cell attachment, survival and proliferation through visualising the propidium iodide labelled nuclei.
Cell survival in relation to the seeded fibre diameter, using the ternary 48 mol% CaO glass composition, was accordingly established by obtaining adherent cell numbers at days 1, 4 and 7 in culture.
1, 2 and 3 mol% F_2O_3 quaternary, and 46 mol% CaO ternary, cell seeded glass fibre scaffolds were fixed at days 1, 7 and 14 in culture and the glass composition related cell survival, and proliferation patterns, were similarly evaluated.

4.2.3 Immunocytochemistry

By immunolabelling the intermediate cytoskeletal filaments with Cy3 conjugated anti-vimentin antibody, the maintenance and nature of cell morphology was assessed. Thus, cells seeded on glass fibres of the quaternary 2 and 3 mol% F_2O_3 were fixed and stained at days 14 and 21 in culture; fibre scaffolds mounted in the Citifluor mounting solution and the samples subsequently examined under the fluorescence microscope.

4.2.4 The CellTracker™ assay

To maintain normal cellular physiology and reduce potential artefacts, the concentration of the 5-chloromethylfluorescein diacetate dye should be kept as low as possible however; its use at low concentrations may reduce the efficacy and the *in vitro* lifetime of the assay. To determine the appropriate concentration of the CMFDA dye so that primary human cells could retain both viability and fluorescence, HOF cells were labelled with 5, 10 and 15 μM concentrations of the green CMFDA dye as detailed in Section 2.8. The cells were then incubated with non-labeled cells in 24 wellplates and observed at days 1, 2 and 3 using the fluorescence microscope.

Co-culture scaffolds were prepared using the $(CaO)_{0.46}$-$(Na_2O)_{0.01}$-$(Fe_2O_3)_{0.03}$-$(P_2O_5)_{0.50}$ fibre composition and HOF cells, pre-labelled with the optimal concentration of CMFDA, were seeded on one side of the separation barrier. Subsequently, HOB cells were seeded and the scaffolds were processed for fluorescent microscopy at days 1, 2 and 3 time points (also see chapter 2).

4.3 Results

4.3.1 Cell attachment and survival in relation to fibre diameter

4.3.1.1 Craniofacial osteoblasts

As seen from Figures 4.1A, B and C, HOB cell attachment was visualised on fibres of all diameters at 24 h time point however, less cells were seen attached to fibres drawn at 1600 r/min. By day 4 in culture, a decline in cell numbers was associated with both, 1200 and 1600 r/min generated fibres (Figure 4.1D, E and F). At day 7 time point, cell survival was only associated with fibres drawn at 800 r/min (Figure 4.1G).

Visual observation of cell attachment and survival patterns was confirmed by data analysis (Figure 4.2). At 24 h, HOB cell attachment values were significantly higher on fibres drawn at 800 r/min than those of cells adhered to both, 1200 and 1600 r/min drawn fibres. By day 4, no differences in cell numbers were present among all seeded scaffolds however, a significant decrease in cell density occurred on the 800 r/min produced fibres. This decrease in cell numbers continued in culture up until day 7.

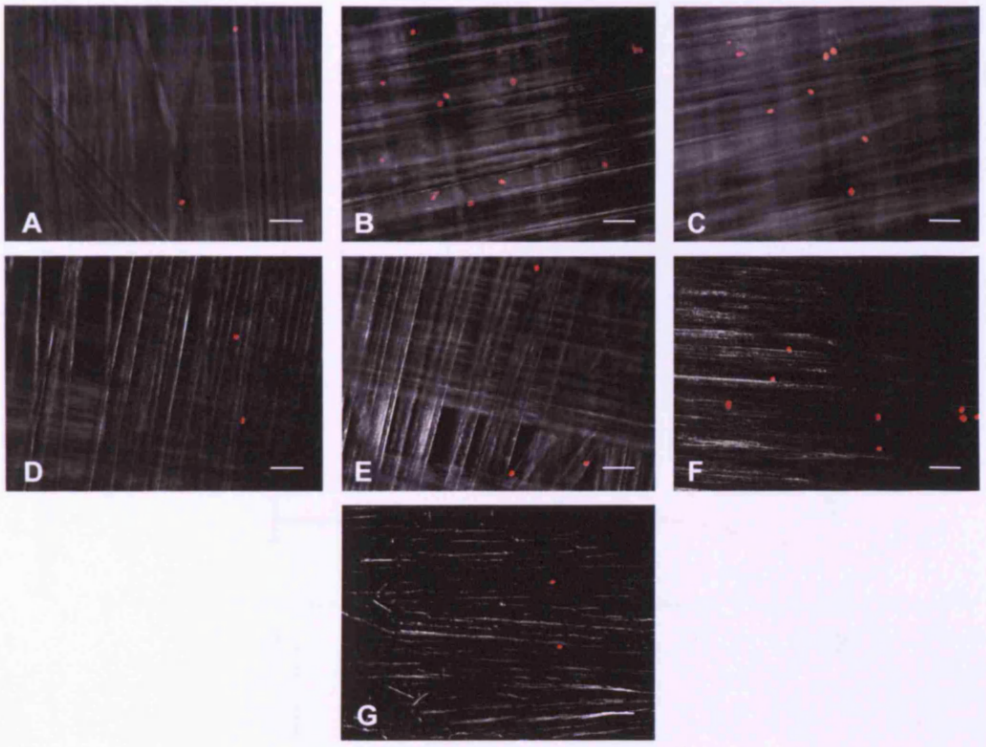

Figure 4.1 HOB cell attachment and survival on ternary glass fibres of various diameters

X20 objective Leica DMIRB fluorescence micrographs of HOB cells cultured on $(CaO)_{0.48}$-$(Na_2O)_{0.02}$-$(P_2O_5)_{0.50}$ glass fibres drawn at (A and D)1600 r/min, (B and E) 1200 r/min and (C, F and G) at 800 r/min. Samples were fixed, and processed for fluorescence immunocytochemistry at (A, B and C) 24 h, (D,E and F) day 4 and (G) day 7 time points. Nuclei are labelled with the DNA-binding dye, PI (Red). Scale bar = 50μm.

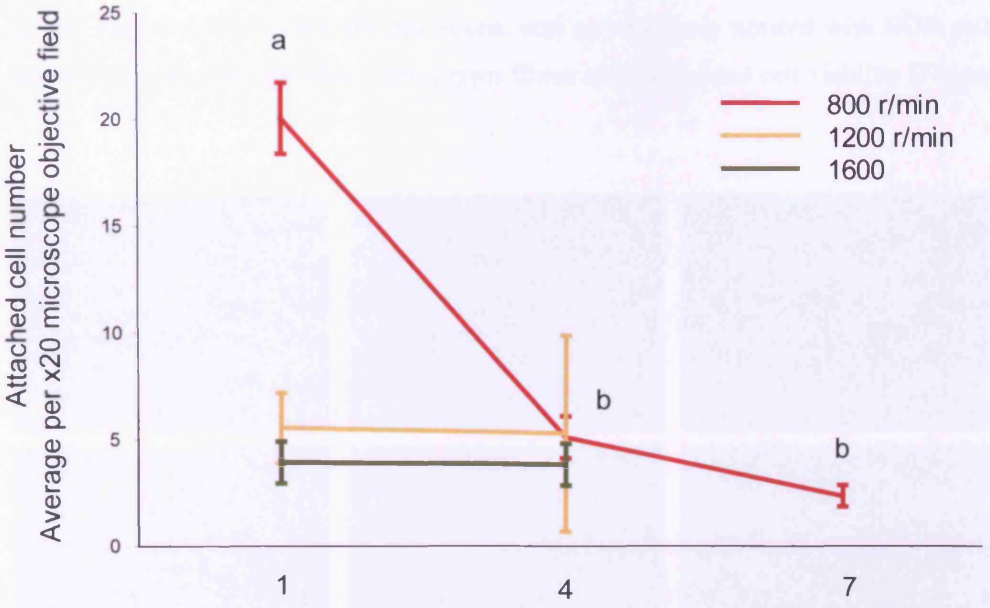

Figure 4.2 HOB cell attachment and survival on fibres of various diameters

Cells were cultured on $(CaO)_{0.48}$-$(Na_2O)_{0.02}$-$(P_2O_5)_{0.50}$ glass fibres drawn at 1600,1200 and 800 r/min. For each time point, (a) indicates significant (p<0.05) differences in cell density on various fibre diameter profiles. (b) indicates significant (p<0.05) differences in cell density, over time in culture, for cells seeded on the 800 r/min drawn fibres. Results were obtained via direct microscopic counting of the PI stained nuclei. No cell survival was present on the 1200 and 1600 r/min drawn fibres at day 7 in culture. (n= 3; error bars +/-SD)

4.3.1.1 Oral fibroblasts

HOF cell attachment on all seeded scaffolds, irrespective of fibre diameter profiles, was maintained at 24 h in culture (Figure 4.3A, B and C). The same trend, and as seen form Figures 4.3D, E and F; was noticed by the forth day in culture nonetheless, signs of scaffold degradation were seen associated with the 1200 and 1600 r/min produced fibres(Figure 4.3D and E). By day seven, and as previously noticed with HOB cell survival pattern, only the 800 r/min drawn fibres accommodated cell viability (Figure 4.3G).

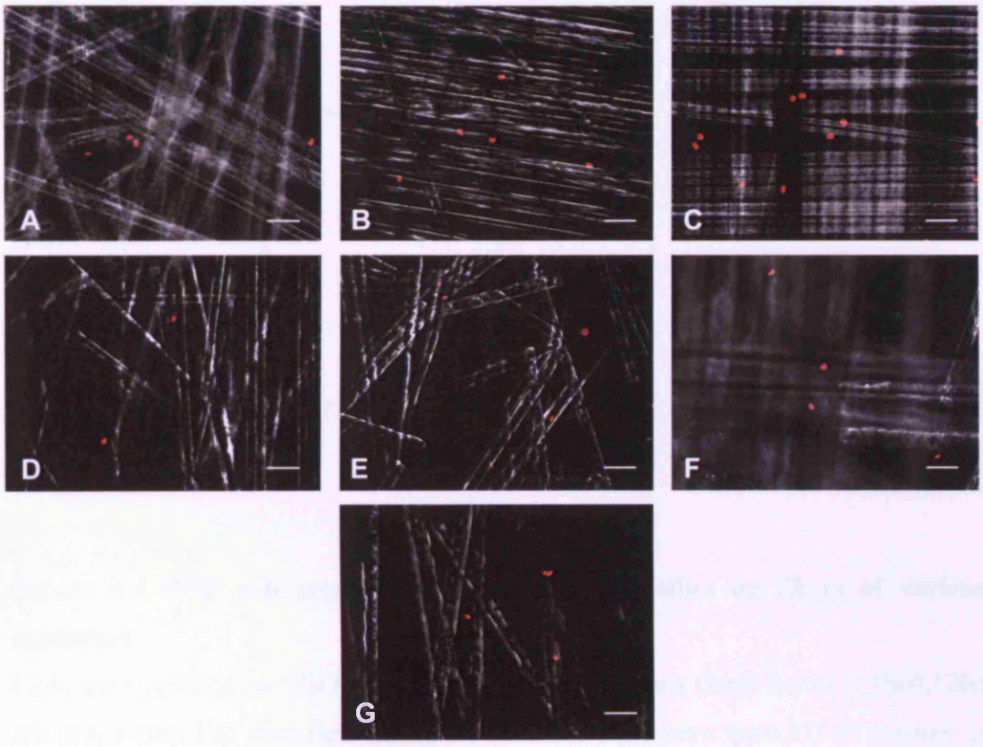

Figure 4.3 HOF cell attachment and survival on ternary glass fibres of various diameters

X20 objective Leica DMIRB fluorescence micrographs of HOB cells cultured on $(CaO)_{0.48}$-$(Na_2O)_{0.02}$-$(P_2O_5)_{0.50}$ glass fibres drawn at (A and D)1600 r/min, (B and E) 1200 r/min and (C, F and G) at 800 r/min. Samples were fixed, and processed for fluorescence immunocytocemistry at (A, B and C) 24 h, (D,E and F) day 4 and (G) day 7 time points. Nuclei are labelled with the DNA-binding dye, PI (Red). Scale bar =50μm.

Analysis of direct cell count values, at 24 h time point, established no significant differences in cell density in relation to fibre diameter (Figure 4.4.). A different result, however, was obtained at day 4 as more cells were maintained on the 800 r/min drawn fibres. Nonetheless, and despite the absence of cell number decrease on these fibres, no significant cell growth took place over time in culture.

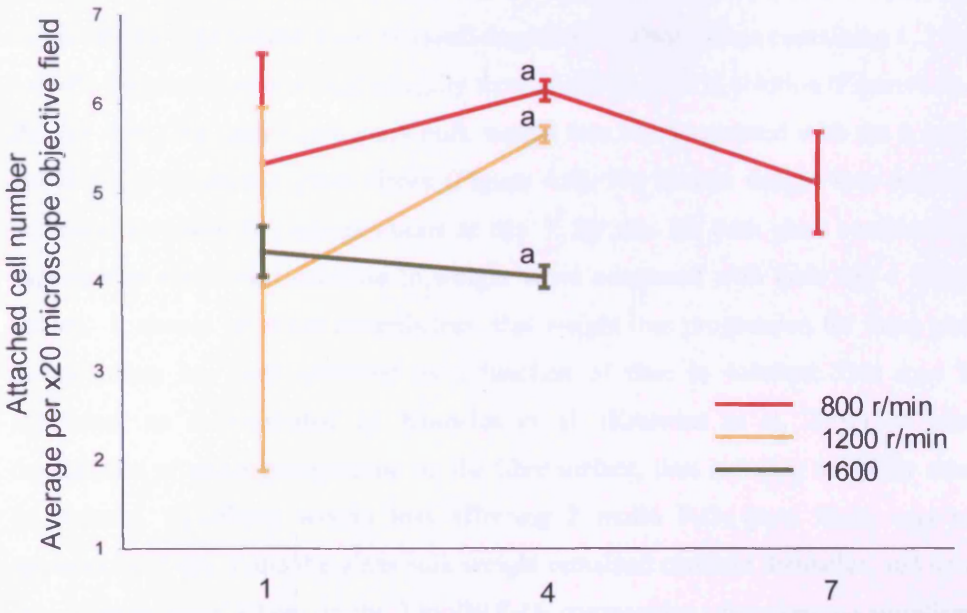

Figure 4.4 HOF cell attachment and survival profiles on fibres of various diameters

Cells were cultured on $(CaO)_{0.48}$-$(Na_2O)_{0.02}$-$(P_2O_5)_{0.50}$ glass fibres drawn at 1600,1200 and 800 r/min. For each time point, (a) indicates significant (p<0.05) differences in cell density on various fibre diameter profiles. Results were obtained via direct microscopic counting of the PI stained nuclei. No cell survival was present on the 1200 and 1600 r/min drawn fibres at day 7 in culture. (n= 3; error bars +/-SD)

4.3.2 Quaternary glass fibre characterisation

4.3.2.1 Solubility profiles

To insure consistency of nomenclature, fibres of the 46 mol% CaO content ternary composition are referred to as 0 mol% F_2O_3 containing throughout.

When conducting the solubility test, and by day 4 in solution, 0 mol% F_2O_3 fibre compositions experienced clear physical degradation whilst fibres containing 1, 2 and 3 mol% F_2O_3 retained physical integrity throughout the time in solution (Figure 4.5).

By day 4 in GM, significant glass bulk weight loss was associated with the 0 and 1 mol% F_2O_3 containing glass fibres (Figure 4.6). No further weight loss occurred however, for these two compositions at day 7. By day 10, both glass compositions experienced significant decrease in weight when compared with their day 4 weight values. It should be noted nevertheless, that weight loss progression for these glass compositions has been inhibited as a function of time in solution. This may be attributed, as demonstrated by Knowles et al. (Knowles et al, 2001), to glass degradation products precipitation on the fibre surface, thus reducing solubility rates.

In contrast, significant weight loss affecting 2 mol% F_2O_3 glass fibres was not apparent until day 7 and the glass bulk weight remained constant thereafter, and up to day 10 in solution. Fibres on the 3 mol% F_2O_3 composition underwent no significant weight loss until the last designated time point, at day 10 in GM.

In order to determine the exact effect of Fe_2O_3 inclusion on glass solubility trends the hourly weight loss for each glass composition was calculated. For each composition, and at each time point, weight loss was divided by the number of forming hours (1 day = 24 h). The mean of the values, at the 4 time points, was then obtained as the hourly weight loss. As expected, and in line with each composition degradation profile, F_2O_3 acted as a solubility inhibitor. Moreover, increasing F_2O_3 content lead to the corresponding exponential decrease in solubility (Figure 4.7).

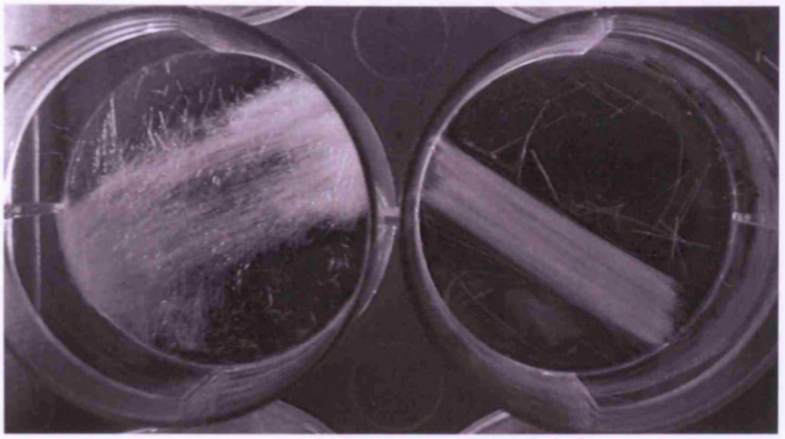

Figure 4.5 Light photograph of glass fibres during solubility profiling

0 mol% F_2O_3 containing fibre bundle (left well); and 1 mol% F_2O_3 containing fibre bundle (right well) at day 4 in GM. Experiment conducted in 6 wellplates.

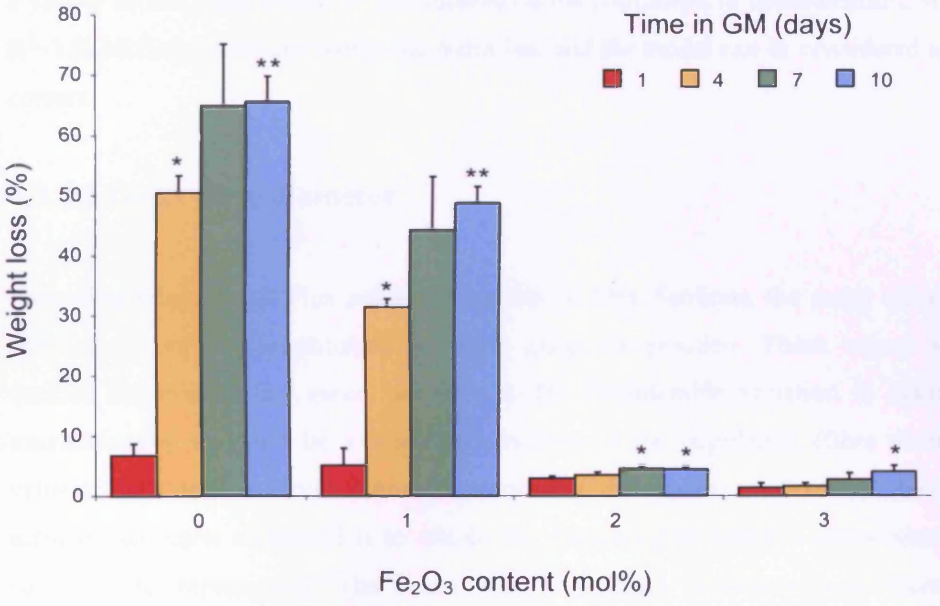

Figure 4.6 glass fibre weight loss rates for various compositions and at different time points

Significant increases in weight loss over time in GM are indicated by (*). (**) is significantly higher than (*). (n= 3; error bars +SD)

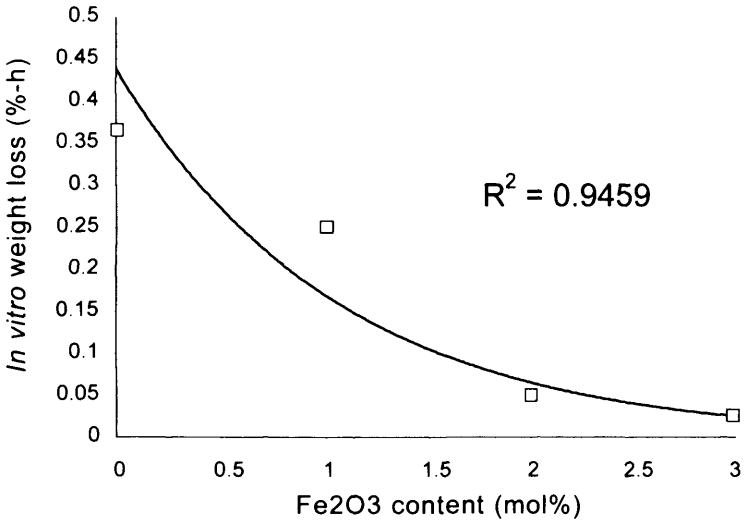

Figure 4.7 Glass solubility rates as a function of F_2O_3 content

Trend line graph. The hourly weight loss value for each composition is represented by a yellow square (data point). R^2 (R-Squared) is the coefficient of determination. When R^2=1.0, all data points are within the trend line and the model can be considered to be correct.

4.3.2.2 Glass fibre diameter

Following Image-Pro® Plus software analysis of fibre Sections, the mean value for fibre diameters was established for each glass composition. These values were verified however as the mean, and due to the considerable variation in diameter measurements, may not be a true representative of the population (fibre diameter values). This was achieved through performing descriptive analysis on the data obtained for each composition to obtain the frequency at which various diameter values were represented. The mean was considered legitimate, and therefore representative of a population, when the mean value fell within the most frequently present data range at 95% confidence level. Accordingly, and for all glass compositions investigated, the mean values have been shown to be representative of the 800 r/ min drawn fibres diameter (Figure 4.8). The average diameters for 1, 2 and 3 mol% were 30.040, 30.606 and 29.362 μm respectively. This also data confirmed that fibre diameter was relatively independent from glass composition range; as the

fibre drawing speed appeared to be the main factor in determining fibre diameter values. The mean value of 30.0026 (≈ 30) μm was thus adopted throughout the work.

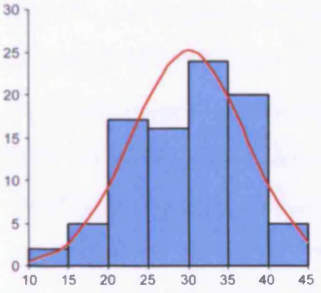

A

Composition (Fe_2O_3 content)	1 mol% Fe_2O_3
Mean value (μm)	30.040
95% CI (mean confidence level)	28.554- 31.525
Diameter range (lowest to highest, μm)	15.274- 42.166

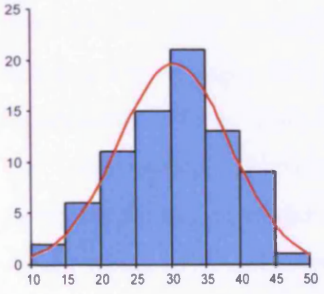

B

Composition (Fe_2O_3 content)	2 mol% Fe_2O_3
Mean value (μm)	30.626
95% CI (mean confidence level)	28.839- 32.413
Diameter range (lowest to highest, μm)	14.607- 44.781

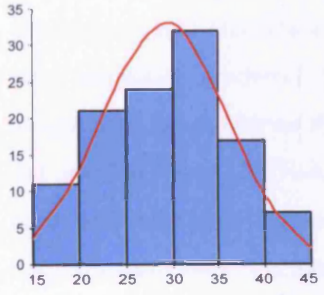

C

Composition (Fe_2O_3 content)	3 mol% Fe_2O_3
Mean value (μm)	29.362
95% CI (mean confidence level)	28.104- 30.620
Diameter range (lowest to highest, μm)	16.656- 41.925

Figure 4.8 Analysis of fibre diameter values frequency for each glass composition A descriptive continuous analysis of data. Frequency histograms of diameter data values for glass compositions $(CaO)_{0.46}$-$(Na_2O)_{0.03}$-$(Fe_2O_3)_{0.01}$-$(P_2O_5)_{0.50}$ (top graph), $(CaO)_{0.46}$-$(Na_2O)_{0.02}$-$(Fe_2O_3)_{0.02}$-$(P_2O_5)_{0.50}$ (centre graph) and, $(CaO)_{0.46}$-$(Na_2O)_{0.01}$-$(Fe_2O_3)_{0.03}$-$(P_2O_5)_{0.50}$ (bottom graph). **For all graphs; *(Y)* Axis, frequency of diameter range and *(X)* Axis, Fibre diameter (μm).** The distribution curve (superimposed red line) for each graph illustrates the extent of normality in data distribution. Data analysed and graphs generated using SPSS for Microsoft Windows.

4.3.2.3 Glass fibre surface topography evaluation

As revealed by SEM and at low magnification, fibre compositions $(CaO)_{0.46}$-$(Na_2O)_{0.01}$-$(Fe_2O_3)_{0.03}$-$(P_2O_5)_{0.50}$ (Figure 4.9A) and $(CaO)_{0.46}$-$(Na_2O)_{0.04}$-$(P_2O_5)_{0.50}$ (Figure 4.9B) exhibited visually smooth surfaces with no apparent surface patterns. At higher magnification, no particular surface topographical features were evident for both $(CaO)_{0.46}$-$(Na_2O)_{0.01}$-$(Fe_2O_3)_{0.03}$-$(P_2O_5)_{0.50}$ (Figure 4.9C) and $(CaO)_{0.46}$ - $(Na_2O)_{0.04}$-$(P_2O_5)_{0.50}$ (Figure 4.9D) glass fibre compositions however, the presence of white dots on the SEM image (Figures 4.9C and D, white arrow heads) might be related to a particular surface topography pattern. The SEM related white dot phenomenon is a manifestation of secondary electron (SE) production at low accelerating voltages and is strongly related to surface topography(Borovsky and Suszcynsky, 1991). This is caused by an incident SEM electron impacting some of the lower energy electrons (usually in the K-shell) of an atom in the specimen resulting in the ionization of the electron in the specimen atom (Borovsky and Suszcynsky, 1991). This ionized secondary electron then leaves the atom releasing a small kinetic energy detected by the scanning microscope. Each incident electron can produce several secondary electrons. Due to their extremely low energy however, only secondary electrons that are very near the glass surface (<10nm) can exit the sample and be examined (Suszcynsky and Borovsky, 1992). Accordingly, the white dot presence may be linked to nano-scale elevations on the glass surface. This, however, must be the subject of further confirmation in future work using higher SEM magnification rates. Furthermore and as seen in Figures 4.9C and D, the appearance and distribution of the white dots show slight variations between the ternary and quaternary glass fibre surfaces. This might be glass composition related and must also be investigated in future work.

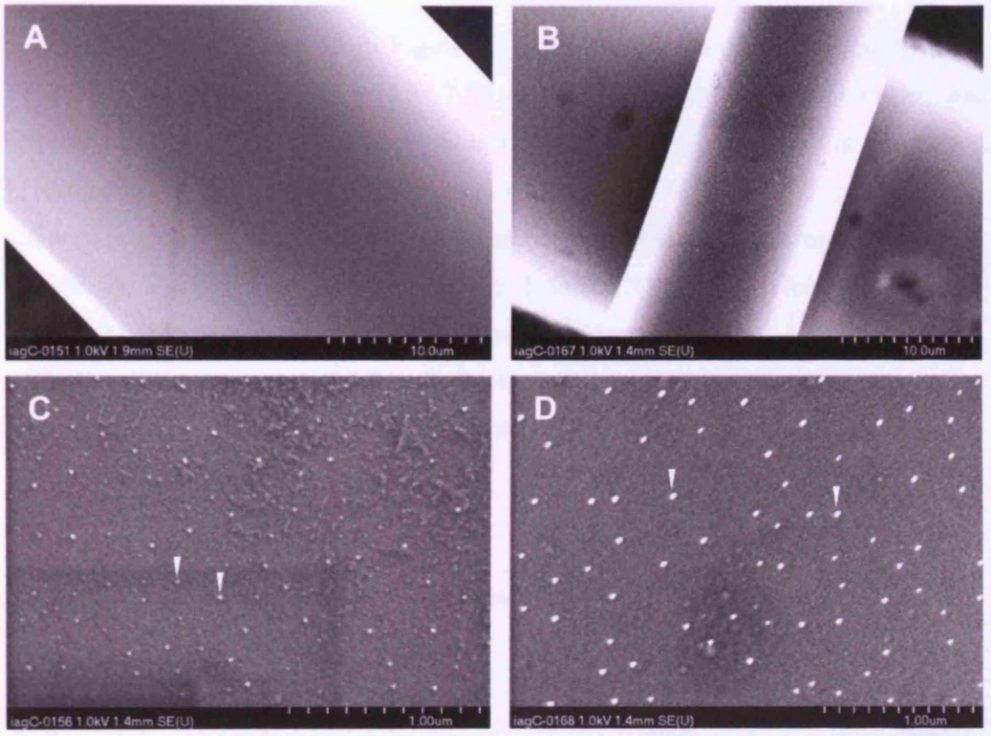

Figure 4.9 SEM micrographs of ternary and quaternary glass fibre surfaces

Hitachi S-4700II field emission scanning electron microscope images of glass fibre surfaces of quaternary, 3 mol% Fe_2O_3 containing glass composition (A and C, X6.932 x 10^3 and X86.892 x 10^3 respectively) and ternary, 46 mol% CaO containing glass composition (B and D, X6.075 x 10^3 and X63.958 x 10^3 respectively).

Secondary electron production related white dots are marked by white arrow heads (C and D)

4.3.3 Biocompatibility of quaternary glass fibres: Craniofacial osteoblasts

4.3.3.1 Cell survival and proliferation

As expected, and as seen from Figure 4.10., no cells were present on the 0 mol% Fe_2O_3 ternary glass fibres by day 7 in culture. A similar pattern however, was observed on the mol% Fe_2O_3 glass fibre form as cell survival ceased at the second investigated time point. Cell presence was maintained on the 2 mol% Fe_2O_3 containing glass fibres nonetheless, no significant proliferation occurred over time in culture. Analysis of cell density on the 3 mol% Fe_2O_3 fibre forms revealed a significant increase in the adherent cell numbers between days 7 and 14 thus, thus indicating the occurrence of cell growth. Also, and by day 14, cells were present at a significantly greater density on the 3 mol% Fe_2O_3 fibres than that on the 2 mol% Fe_2O_3 containing glass.

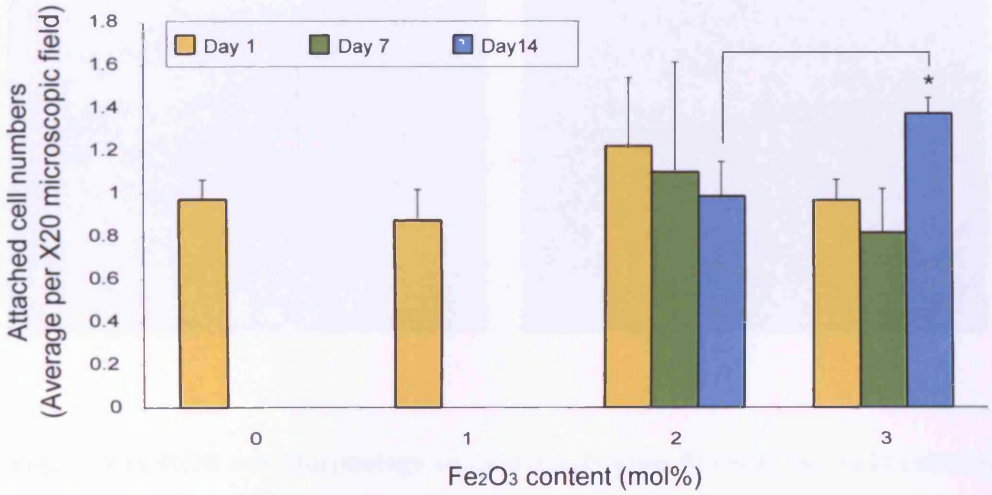

Figure 4.10 HOB cell survival and proliferation on quaternary glass fibres generated at 800 r/min

(*) indicates a significantly higher cell density on a glass composition at one time point. Significant differences in cell density on one glass composition as a function of time in culture are connected using square brackets. (n= 3; error bars +SD).

4.3.3.2 Maintenance of cell morphology

Fluorescence microscopy evaluation of the fibre scaffold samples, for the day 14 time point, revealed the prescence of cell attachment on both, 2 (Figure 4.11.A and B)and 3 (Figures 4.11C and D) mol% Fe_2O_3 containing, glass fibres. Adherent cells exhibited a well spread morphology and were oriented parallel to the fibres axes (Figure 4.11).

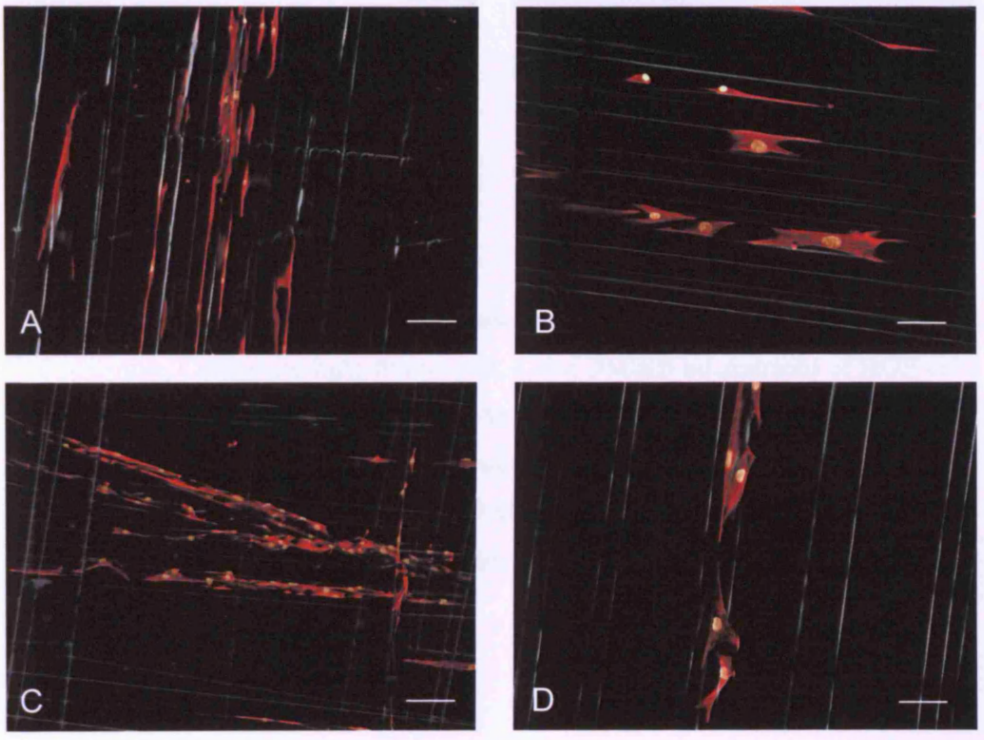

Figure 4.11 HOB cell Morphology on quaternary glass fibres at day 14 in culture
Composite light-fluorescent Leica DMIRB micrographs of HOB cells cultured on 2 mol% Fe_2O_3 glass fibres (A and B; X10 and X20 objective respectively) and 3 mol% Fe_2O_3 glass fibres (A and B; X10 and X20 objective respectively). The cytoskeleton was labelled with Cy3 conjugated anti vimentin antibody. Nuclei were labelled with the DNA-binding dye DAPI (yellow). Glass fibres were pseudo coloured (light green). Scale bars, X10 objective = 100, X20 objective = 50

By day 21, a noticeable increase in cell numbers was observed and dense HOB populations were present on both glass fibre compositions. Cell morphology and orientation patterns were also retained as seen from Figure 4.12.

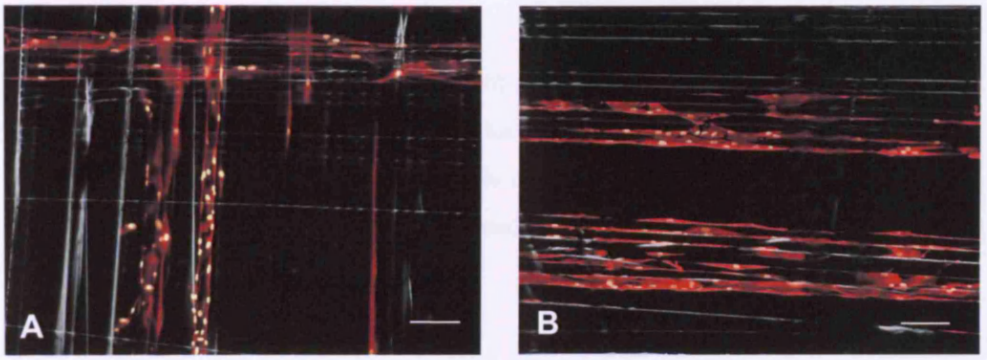

Figure 4.12 HOB cell Morphology on quaternary glass fibres at day 21 in culture X10 objective, Composite light-fluorescent, Leica DMIRB micrographs of HOB cells cultured on 2 mol% Fe_2O_3 glass fibres (A) and 3 mol% Fe_2O_3 glass fibres (B). The cytoskeleton was labelled with Cy3 conjugated anti vimentin antibody. Nuclei were labelled with the DNA-binding dye DAPI (yellow). Glass fibres were pseudo coloured (light green).). Scale bar = 100μm.

4.3.4 Biocompatibility of quaternary glass fibres: Oral fibroblasts

4.3.4.1 Cell survival and proliferation

As previously observed for HOB cells, no HOF cells remained attached to the 0 and 1 mol% Fe_2O_3 containing glass fibres by day 7 in culture. Cell attachment was preserved on the 2 mol% Fe_2O_3 albeit with no significant, time associated population growth. On the other hand, and on the 3 mol% Fe_2O_3 fibres, a significant increase in cell density occurred by day 14 where this density was of significantly greater value, at the same time point, than that of cells seeded on 2 mol% Fe_2O_3 fibres (Figure 4.13).

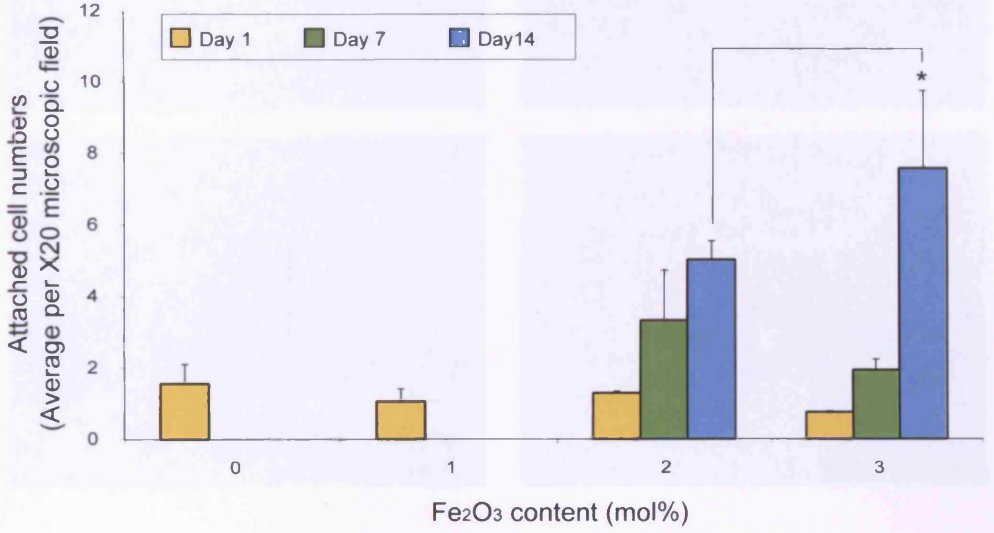

Figure 4.13 HOF cell survival and proliferation on quaternary glass fibres generated at 800 r/min

(*) indicates a significantly higher cell density on a glass composition at one time point. Significant differences in cell density on one glass composition as a function of time in culture are connected using square brackets. (n= 3; error bars +SD).

4.3.4.2 Maintenance of cell morphology

Florescent Cy3 conjugated staining of the vimentin intermediate filaments revealed, and at day 14 in culture, a well spread appearance of the adherent HOF cells (Figure 4.14). This was associated with both glass fibre compositions (2 and 3 mol% Fe_2O_3 containing)

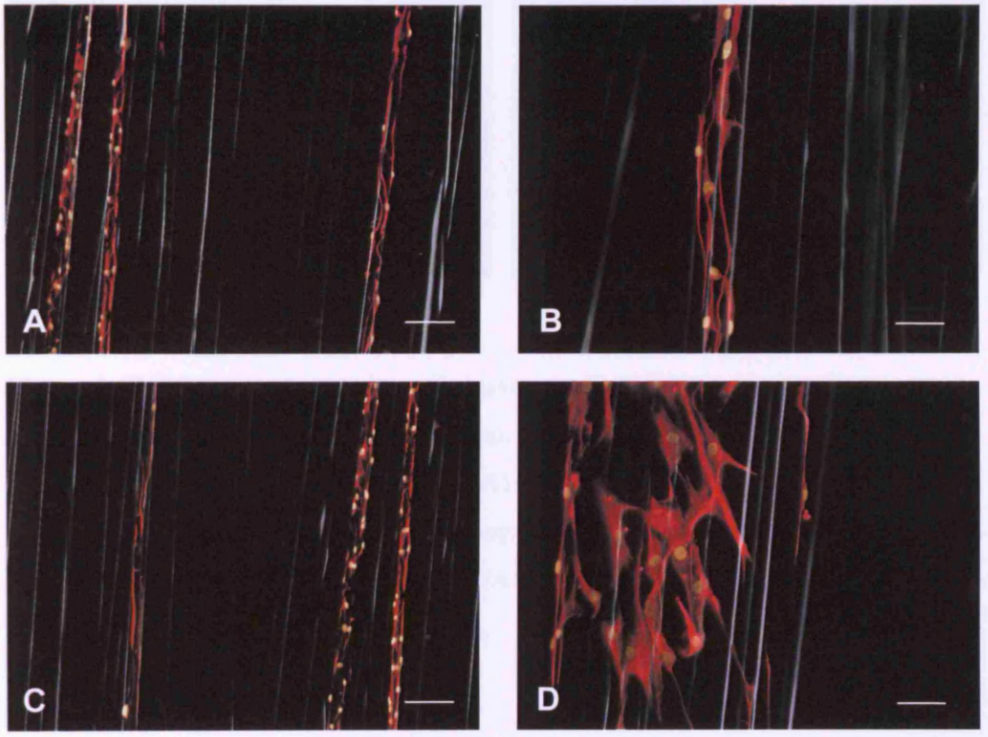

Figure 4.14 HOF cell Morphology on quaternary glass fibres at day 14 in culture
Composite light-fluorescent Leica DMIRB micrographs of HOF cells cultured on 2 mol% Fe_2O_3 glass fibres (A and B; X10 and X20 objective respectively) and 3 mol% Fe_2O_3 glass fibres (A and B; X10 and X20 objective respectively). The cytoskeleton is labelled with Cy3 conjugated anti vimentin antibody. The cytoskeleton was labelled with Cy3 conjugated anti vimentin antibody. Nuclei were labelled with the DNA-binding dye DAPI (yellow). Glass fibres were pseudo coloured (light green). Scale bars, X10 objective = 100μm, X20 objective = 50μm

Similarly, and by day 21, well spread morphology was maintained on both glass compositions and a clear increase in cell density, compared to that of the earlier time point, was present (Figure 4.15). Greater cell density was noticed however, by the visual evaluation of the entire scaffold, on the 3 mol% Fe_2O_3 glass fibres.

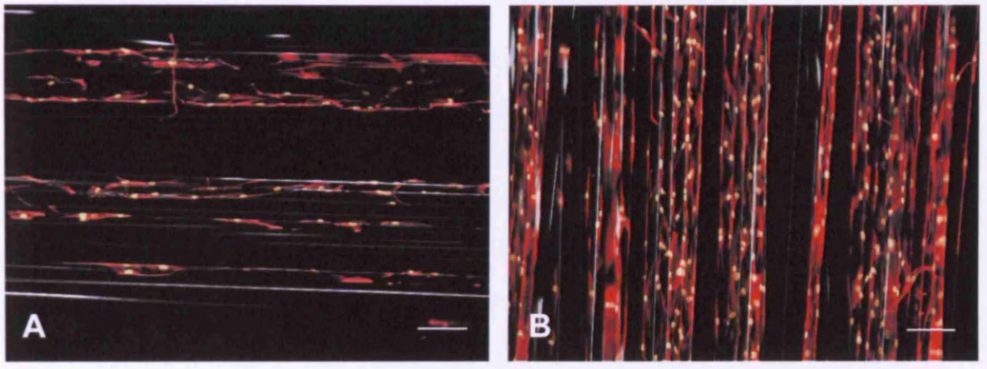

Figure 4.15 HOF cell Morphology on quaternary glass fibres at day 21 in culture
X10 objective, Composite light-fluorescent, Leica DMIRB micrographs of HOF cells cultured on 2 mol% Fe_2O_3 glass fibres (A) and 3 mol% Fe_2O_3 glass fibres (B). The cytoskeleton was labelled with Cy3 conjugated anti vimentin antibody. Nuclei were labelled with the DNA-binding dye DAPI (yellow). Glass fibres were pseudo coloured (light green). Scale bar = 100μm.

4.3.5 Co-culture evaluation

To maintain fluorescence up to 72 h in culture with a minimum impact on HOF cell function, the optimal concentration of CMFDA dye was determined at 10 μM (Figure 4.16). This concentration of CMFDA was subsequently used to perform fluorescent co-culture population differentiation.

Despite an applied separation space of 300 μm, initial examination of the co-culture at day 1 revealed the acellular zone, between the two populations, to be approximately of 2800-2000 μm wide. This could be attributed to mechanical agitation, during manual barrier removal, disrupting adherent cells situated at close proximity to the partitioning structure. By day 3, and as seen from Figure 4.17, marked cell migration resulted in reducing the separating space to an approximate distance of a 1000 μm.

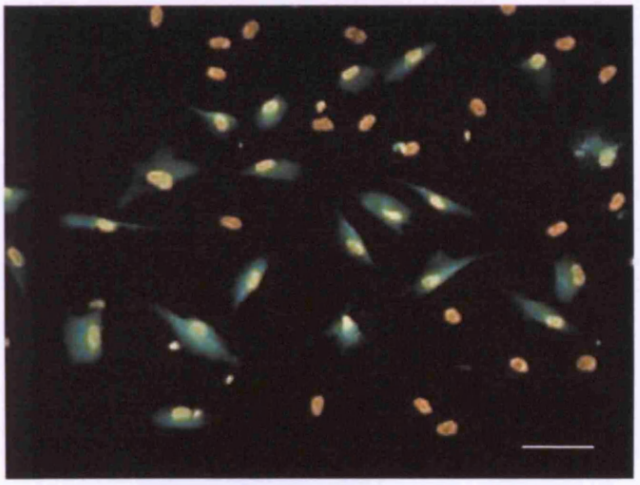

Figure 4.16 X20 objective Leica DMIRB fluorescence micrographs of HOF cells labelled with CellTracker™ dye

A mixed labelled (green cytoplasm and yellow nuclei) and unlabelled (yellow nuclei only) HOB population at 24 h in culture. Cells were seeded on 24-wellplate control surfaces and CMFDA used at 10 μM. Nuclei were stained with the DNA-binding dye DAPI. Scale bar = 50μm.

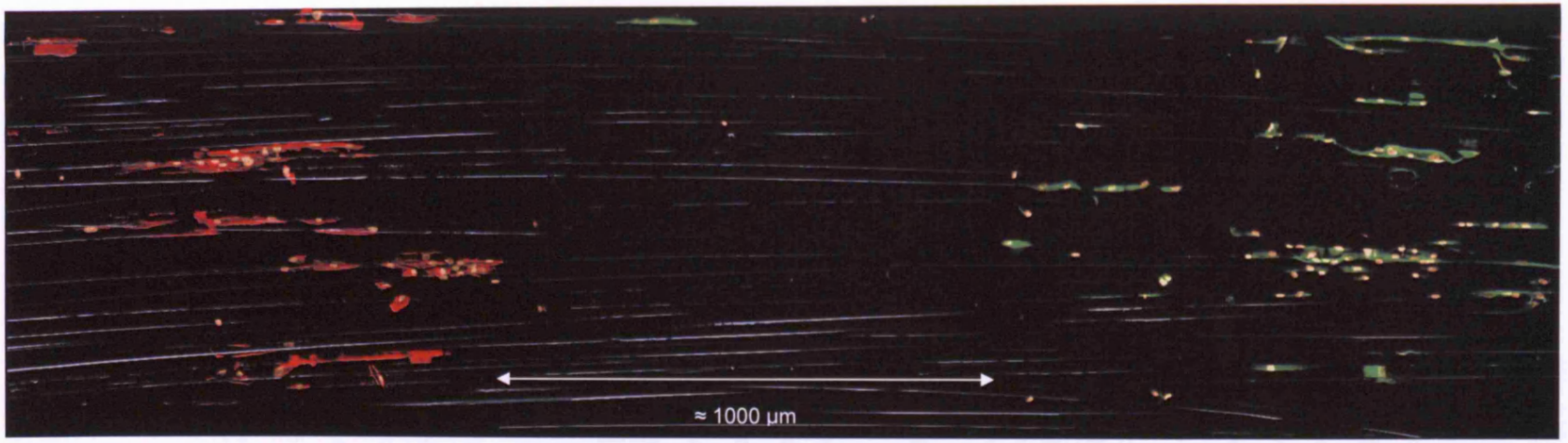

Figure 4.17 X10 objective fluorescent microscope image of HOB and HOF cells in co-culture

HOB cells (red anti-vimentin, left side) and HOF cells (Green CMFDA live dye, right side) seeded on $(CaO)_{0.46}$-$(Na_2O)_{0.01}$-$(Fe_2O_3)_{0.03}$-$(P_2O_5)_{0.50}$ glass fibres after 3 days in culture. This composite light-fluorescnet micrograph was composed from 3 adjacent microscope field images. Glass fibres were pseudo coloured (Light green). The nuclei were labelled with DAPI (yellow).

4.4 Summary

- The optimal diameter fibre range supporting cell attachment and survival on the ternary composition of the 48 mol% CaO ($(CaO)_{0.48}$-$(Na_2O)_{0.02}$-$(P_2O_5)_{0.50}$), has been determined to be approximately 30 μm and related to the fibre fabrication rotational speed of 800 r/min. Fibres generated at higher speeds, and thus of smaller diameter, failed to sustain cell attachment and exhibited signs of structural degradation by day 4 following incubation in GM. Even at the largest diameter values, 48 mol% CaO containing ternary fibres were incapable of supporting cell proliferation, as a decrease in seeded cell density was observed over time suggesting the unsuitability if these glasses, in their fibre form, as scaffolds for the long-term support of tissue regeneration.

- 1, 2 and 3 mol% Fe_2O_3 quaternary glass fibres, produced at 800 r/min, have been characterised in terms of solubility, diameter and surface topography and it has been established, that increasing Fe_2O_3 resulted in decreasing the solubility rate of the glass. It has also been concluded that the average diameter value of 30 μm can be adopted when performing controlled fibre alignment during scaffold production. No specific glass surface topographical features were visible as fibres exhibited a relatively smooth surface however; SE production was detected and might be related to the presence of nano-scale surface patterns.

- Using $(CaO)_{0.46}$-$(Na_2O)_{0.04}$-$(P_2O_5)_{0.50}$ ternary glass fibres as control, cell survival and proliferation was assessed on the quaternary glass fibre scaffolds where analysis of direct cell count has revealed, that only 2 and 3 mol% Fe_2O_3 containing glass fibres supported cell attachment up to 14 days in culture. Furthermore, a clear proliferation pattern, for both HOB and HOF cell types, was associated with composition $(CaO)_{0.46}$-$(Na_2O)_{0.01}$-$(Fe_2O_3)_{0.03}$-$(P_2O_5)_{0.50}$ (of the 3 mol% Fe_2O_3 content).

- Cells seeded on fibres of both glass compositions, of 2 and 3 mol% Fe_2O_3 content, exhibited a well spread *in vitro* morphology and this appearance was preserved up to 21 days in culture.

- The co-culture scaffold design, as a precursor for the *in vitro* regeneration of the hard-soft tissue enthesis, has been successfully implemented using $(CaO)_{0.46}$-$(Na_2O)_{0.01}$-$(Fe_2O_3)_{0.03}$-$(P_2O_5)_{0.50}$ glass fibre scaffold.

- Glass fibres of the 2 and 3 mol% Fe_2O_3 quaternary compositions ($(CaO)_{0.46}$-$(Na_2O)_{0.02}$-$(Fe_2O_3)_{0.02}$-$(P_2O_5)_{0.50}$ and $(CaO)_{0.46}$-$(Na_2O)_{0.01}$-$(Fe_2O_3)_{0.03}$-$(P_2O_5)_{0.50}$), generated at 800 r/min rotational speed, have therefore exhibited considerable *in vitro* biocompatibility with no apparent negative impact on cell survival and morphology. This biocompatibility however, must be further confirmed through evaluating maintenance of differentiated function of the seeded cells.

CHAPTER FIVE

RESULTS THREE

5.1 Introduction

By conducting qPCR experiments, HOB and HOF differentiated commitment to the hard and soft tissue ECM maintenance and turnover, on 2 and 3 mol% Fe_2O_3 glass fibre compositions, has been evaluated through assessing gene expression and regulation. These two quaternary glass compositions were selected as they supported, in their fibre form and produced at 800 r/ min rotational velocity, the attached cell survival and proliferation up to 14 days in culture and maintained a well spread cytoskeletal morphology up to 21 days in culture (Chapter 4).

qPCR analysis was also conducted to investigate the effect of extrinsic factor inclusion on the *in vitro* cell-scaffold interaction following supplementing the HOB cell culture with osteogenesis inducing medium; and changes in HOB differentiation were evaluated.

The impact of medium and waste perfusion on cell function, following the use of the open flow laminar bioreactor, has also been established.

5.2 Experimental protocol

5.2.1 Assessment of glass fibre biocompatibility

The 2 and 3 mol% Fe_2O_3 containing quaternary glass fibres were arranged as monolayer mesh and parallel unidirectional scaffold configurations and seeded with HOB and HOF cells, respectively at a 3.2 x 10^4 cell density. At days 14 and 21, HOB cell maintenance of differentiation was evaluated by quantifying gene expression levels for ON (Osteonectin; also termed SPARC), Cbfa-1 (core binding factor alpha 1 subunit isoform; also termed RUNX2) and COL-1 (Collagen Type I). On the other hand, and at the same time points, HOF cell related gene regulation was quantified through analysing COL1A1 (collagen type I alpha polypeptide 1 subunit) and P4HA3 (proline 4-hydroxylase alpha polypeptide III subunit) expression levels. The cells seeded scaffolds were placed in 50 mm Petri dishes and control cells were grown in 24 wellplates.

5.2.2 Stimulation of HOB culture mineralisation

Cultures of HOB cell seeded fibre scaffolds, of the 2 and 3 mol% Fe_2O_3 compositions, were supplemented with GM containing 50 μg/ ml ascorbic acid and 10 mM β-glycerophosphate (both from Sigma-Aldrich). The chemicals were prepared into working solutions using dH_2O and filtered twice using 0.2 μm syringe filters prior to the *in vitro* application. Following total RNA extraction at days 14 and 21, transcription levels for ON, Cbfa-1 and COL1A1 were quantified. The scaffold culture was maintained in 50 mm petri dishes and control cells were grown in 24 wellplates.

5.2.3 The laminar flow system setup

HOB and HOF cells were seeded on $(CaO)_{0.46}$-$(Na_2O)_{0.01}$-$(Fe_2O_3)_{0.03}$-$(P_2O_5)_{0.50}$ fibre scaffolds for 7 days after which, scaffolds were transferred into the flow chamber. This process took place in the tissue culture hood using sterile forceps. Firstly, the rubber tubes connected to the cell inlet and outlet were blocked using stainless steel

tube clamps. Next, the flow chamber was filled with 5 ml of GM; the cell seeded scaffold transferred from the petri dish; and the glass cover was applied and secured using the rubber O-ring. Finally, the chamber was placed inside the incubator and connected to the system, the clamps carefully removed and the flow process initiated by operating the roller pump.

Cells were subjected to 2 flow rates at 19.413 x 10^{-3} ml/s (at near zero shear stress, described throughout as flow rate I); and at 9.707 x 10^{-3} ml/s (50 % of the near zero shear stress associated flow value, described throughout as flow rate II). Due to the open nature of the flow, and the relatively high GM consumption, the experimental procedure was restricted to 8 h as continuous attendance, particularly overnight, was practically unattainable. It has been shown in various studies that detectable changes in gene expression, in animal and human cells, were induced following an 8 h exposure to flow culture conditions (Hilsey et al, Frangos et al). Cells seeded under static conditions (i.e. in petri dishes), and on the same scaffold configuration and composition, were used as controls.

5.2.3 Quantification of gene expression and regulation

For all experiments, and at the appropriate time points, adherent cells were lysed and total RNA extracted and verified for quality. cDNA was produced and labelled with the appropriate TaqMan® probes complimentary to the genes to be investigated (Figure 5.1.) (Section 2.10.5). HOB cells were labelled with TaqMan® probes for ON, Cbfa-1 and COL1A1 (product codes Hs00277762_m1, Hs00231692_m1 and Hs00164004_m1 respectively, Applied Biosystems). HOF cells were labelled with TaqMan® probes for P4HA3 and COL1A1 (product codes Hs00420085_m1 and Hs00164004_m1 respectively, Applied Biosystems). The ABI PRISM® 7300 Sequence Detection System was subsequently used to conduct at an assay volume of 25 µl per well and for 40 thermal cycles. Expression of the house keeping gene encoding 18S rRNA (TaqMan® probe Hs99999901_s1, Applied Biosystems) was used as a control to compare transcription levels of the various genes, at different time points and under the various culture conditions.

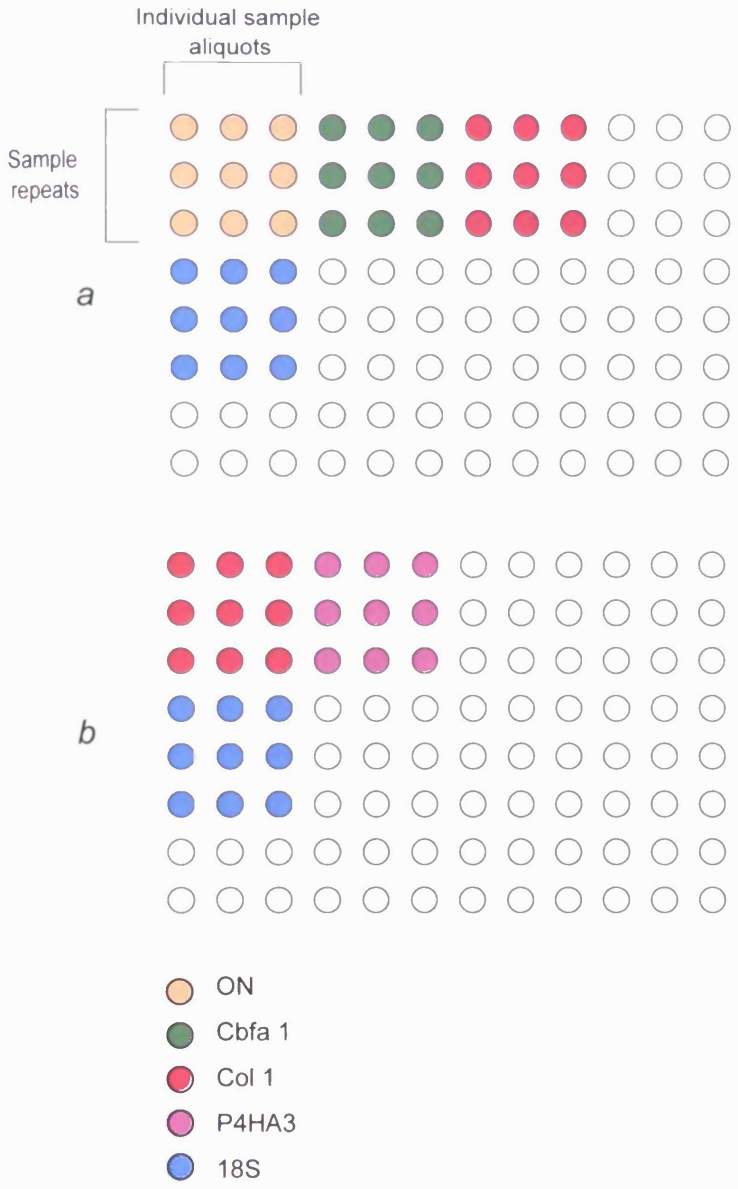

Figure 5.1 qPCR 96 wellplate assay configuration for HOB (*a*) and HOF (*b*) used throughout the experimental work

5.3 Results

5.3.1 Maintenance of differentiation

5.3.1.1 Craniofacial osteoblasts

At day 14 in culture, no significant difference in ON transcription was present between the cells seeded on the cells seeded on fibres of both, 2 and 3 mol% Fe_2O_3 compositions (Figure 5.2a). Scaffold-associated ON transcription levels were also similar to those of the control surface seeded cells. By day 21, ON gene transcription was up-regulated as a function of time in culture in HOB cells seeded on the 3 mol% Fe_2O_3 glass composition to a level matching that of the control cells. Cells seeded on the 2 mol% Fe_2O_3 fibres expressed significantly lower quantities of ON mRNA when compared to the control cells.

Quantification of PCR products for Cbfa-1 cDNA levels, at day 14, revealed equal expression among cells seeded on the two glass compositions and the control surface. By day 21 however, Cbfa-1 regulation was lower against the control in cells cultured on the 2 mol % Fe_2O_3 composition than those adhered to the 3 mol % Fe_2O_3 fibres where Osteocalcin synthesis matched that of the control cells (Figure 5.2b).

The COL1A1 gene was expressed at higher levels in control cells, at day 14 time point, than in cells seeded on the scaffolds of both quaternary glass compositions (Figure 5.3). Despite no changes in COL1A1 gene regulation against time in culture, COL1A1 mRNA synthesis was significantly lower in cells seeded on the 2 mol% Fe_2O_3 glass fibres compared to that of the control seeded HOB cells at day 21. In contrast, 3 mol % Fe_2O_3 seeded cells expressed similar levels of COL1A1 transcription compared to those of the control.

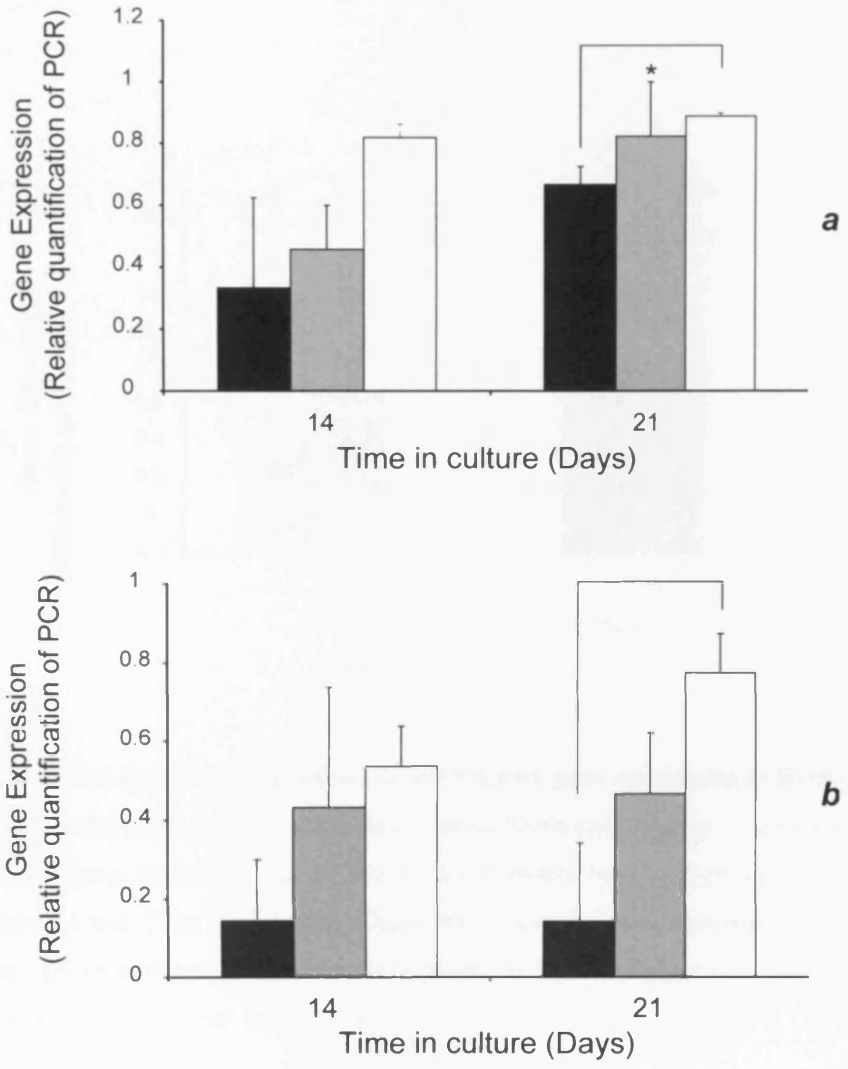

Figure 5.2 Relative quantification of ON (a) and Cbfa-1 (b) gene expression

HOB cells were seeded on 2 mol% Fe_2O_3 glass fibres (black bars), 3 mol% Fe_2O_3 glass fibres (gray bars), and tissue culture plastic (white bars) and processed for qPCR at days 14 and 21 in culture. (*) indicates significant gene up-regulation on one surface against time. Significant differences in gene expression for cells seeded on various surfaces, and at each time point, are linked using square brackets. ($p<0.05$). (*$n=3$, error bars +SD*)

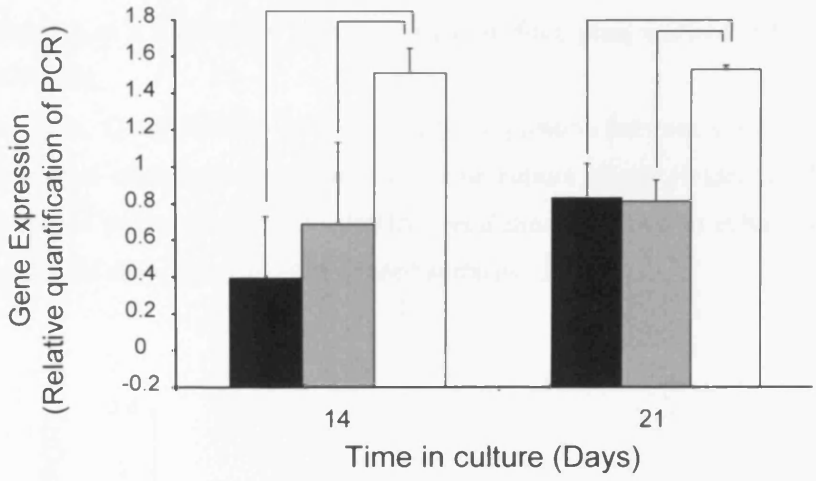

Figure 5.3 Relative quantification of COL1A1 gene expression in HOB cells

Cells were seeded on 2 mol% Fe_2O_3 glass fibres (black bars), 3 mol% Fe_2O_3 glass fibres (gray bars), and tissue culture plastic (white bars) and processed for qPCR at days 14 and 21 in culture. Significant differences in gene expression for cells seeded on various surfaces, and at each time point, are linked using square brackets ([and]). ($p<0.05$). (*$n=3$, error bars +SD*)

5.3.1.2 Oral fibroblasts

Analysis of HOF cells cDNA amplification at day 14 revealed similar cellular expression of COL1A1 on the 2 and 3 mol % Fe_2O_3 glass and the control surfaces (Figure 5.4). At day 21 in culture, regulation of COL1A1 was equally expressed by the seeded fibroblasts on all surfaces. No changes in COL1A1 gene regulation occurred, as a function of time in culture, in fibre glass scaffold and control seeded HOF cells.

Similarly, Quantification of P4HA3 gene regulation between cells seeded on both glass fibre compositions and control tissue culture plastic yielded similar results at both time points (Figure 5.5). P4HA3 regulation, overtime in culture, exhibited no significant changes on all HOF seeded surfaces.

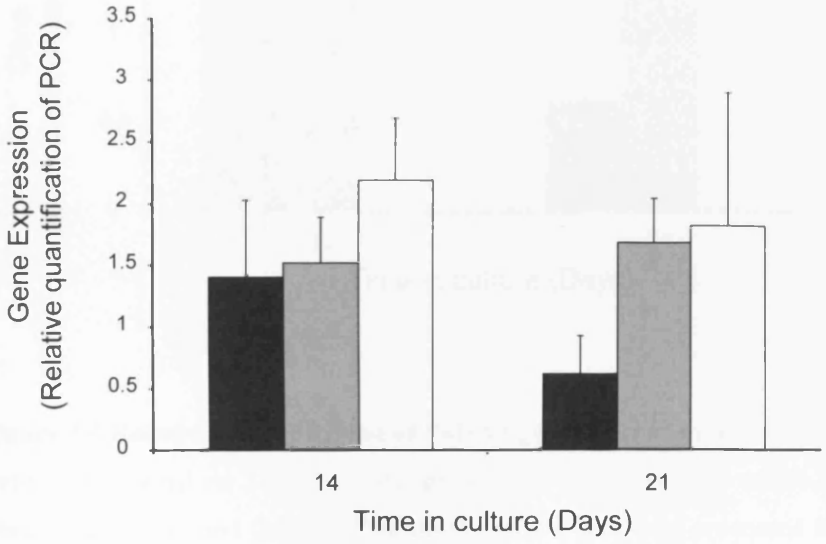

Figure 5.4 Relative quantification of COL1A1 gene expression in HOF cells

Cells were seeded on 2 mol% Fe_2O_3 glass fibres (black bars), 3 mol% Fe_2O_3 glass fibres (gray bars), and tissue culture plastic (white bars) and processed for qPCR at days 14 and 21 in culture. (*n=3, error bars +SD*)

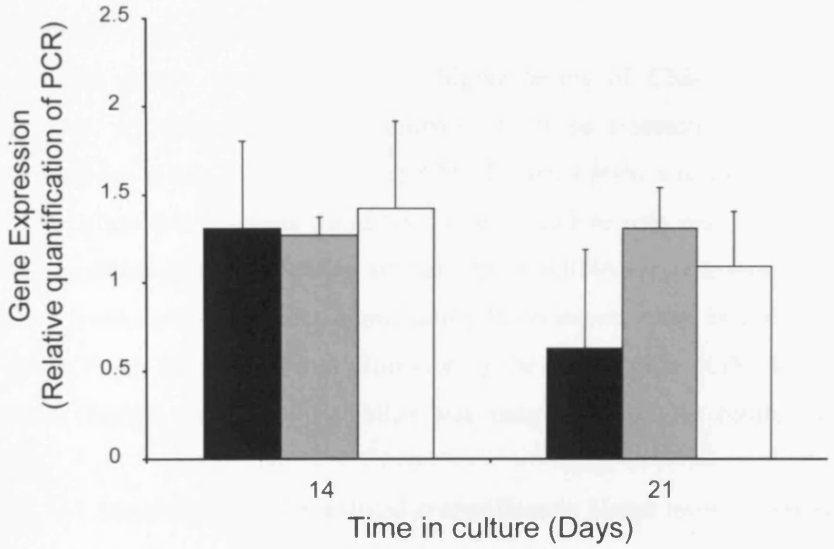

Figure 5.5 Relative quantification of P4HA3 gene expression in HOF cells

Cells were seeded on 2 mol% Fe_2O_3 glass fibres (black bars), 3 mol% Fe_2O_3 glass fibres (gray bars), and tissue culture plastic (white bars) and processed for qPCR at days 14 and 21 in culture. (*n=3, error bars +SD*)

5.3.2. Gene regulation: Induction of osteogenesis

As seen from Figure 5.6a, Cells seeded on the control surfaces expressed significantly higher levels of ON mRNA than those seeded on the glass fibres of either 2 or 3 mol% Fe_2O_3 compositions. However, the inclusion of ascorbic acid and β-glycerophosphate in the medium induced up-regulation of ON expression in the control and fibre seeded HOB cells for both glass compositions as revealed by PCR quantification at day 21. This up-regulation also resulted in increasing ON expression, in cells seeded on 2 and 3 mol% Fe_2O_3 fibre composition, to levels similar to those expressed by the control cells.

A similar pattern was observed as higher levels of Cbfa-1 transcription were expressed, by the control cells compared to those associated with both scaffold compositions at day 14 (Figure 5.6b). Cbfa-1 transcription was up-regulated however, on both glass compositions throughout time in culture with cells seeded on 3 mol% Fe_2O_3 containing fibres, yielding similar Cbfa-1 mRNA levels to those of the control. Cbfa-1 transcription remained significantly lower nevertheless, in cells seeded on the 2 mol% Fe_2O_3 fibres, than that expressed by the control cells. It should also be noted that no changes in Cbfa-1 regulation was associated with the control seeded HOB cells.

COL1A1 transcription was regulated at significantly higher levels by the control cells than those seeded on the fibre scaffolds at day 14 time point however, 3 mol% Fe_2O_3 seeded HOB cells expressed higher level of COL1A1 than those associated with the 2 mol% Fe_2O_3 containing fibres (Figure 5.7.). Unlike the results obtained under normal (non-osteogenic) GM culture conditions, COL1A1 was up-regulated on both scaffold compositions as indicated by qPCR analysis at day 21. Again, control cells have been shown to yield higher COL1A1 mRNA quantities than those produced by the scaffolds seeded cells.

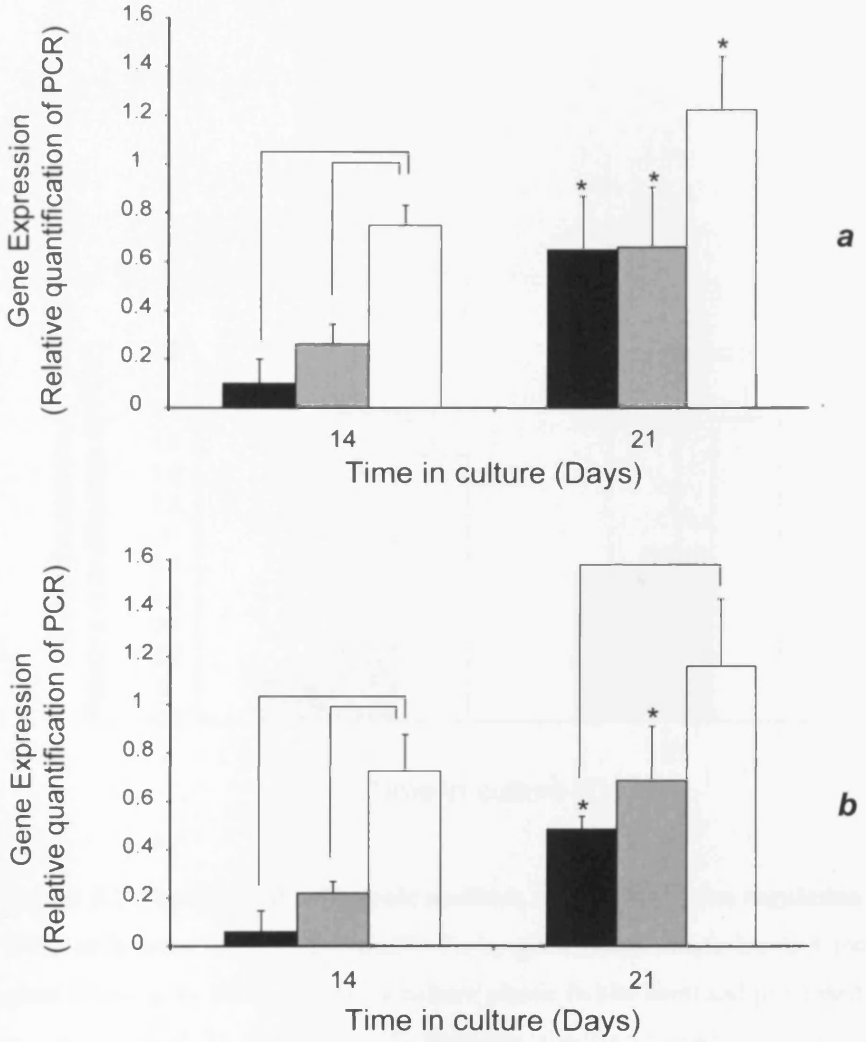

Figure 5.6 The effect of osteogenic medium on ON and Cbfa-1 gene regulation

HOB cells were seeded on 2 mol% Fe_2O_3 glass fibres (black bars), 3 mol% Fe_2O_3 glass fibres (gray bars), and tissue culture plastic (white bars) and processed for qPCR at days 14 and 21 in culture. (*) indicates significant gene up-regulation on one surface against time. Significant differences in gene expression for cells seeded on various surfaces, and at each time point, are linked using square brackets. ($p<0.05$). (*$n=3$, error bars +SD*)

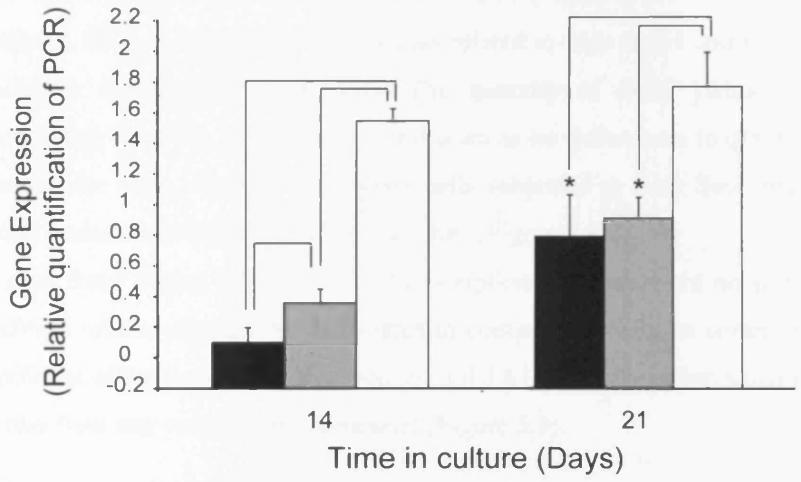

Figure 5.7 The effect of osteogenic medium on COL1A1 gene regulation

HOB cells were seeded on 2 mol% Fe_2O_3 glass fibres (black bars), 3 mol% Fe_2O_3 glass fibres (gray bars), and tissue culture plastic (white bars) and processed for qPCR at days 14 and 21 in culture. (*) indicates significant gene up-regulation on one surface against time. Significant differences in gene expression for cells seeded on various surfaces, and at each time point, are linked using square brackets. ($p<0.05$). (*$n=3$, error bars +SD*)

5.3.3 Gene regulation: The effect of flow culture conditions

5.3.3.1 Craniofacial osteoblasts

ON gene expression has exhibited insignificant differences in HOB cells subjected to both, I and II flow rates for 8 h. Also, no significant differences in ON transcription rates, when compared to the cells incubated under static culture conditions, were registered in the cells exposed to flow conditions (Figure 5.8a).

Similarly, Cbfa-1 mRNA synthesis yields related to flow rates I and II, appeared to be similar in the seeded HOB cells. The quantity of these yields also appeared independent from the flow culture conditions as no differences in qPCR results were obtained for gene expression between cells subjected to both flow rates, and those seeded under static culture condition control (Figure 5.8b).

As seen from Figure 5.9, COL1A1 transcription has underwent no significant, flow condition related changes for both rates in comparison with the control cells, and no significant differences were observed in COL1A1 gene expression when the effects to the two flow rate values were compared (Figure 5.9).

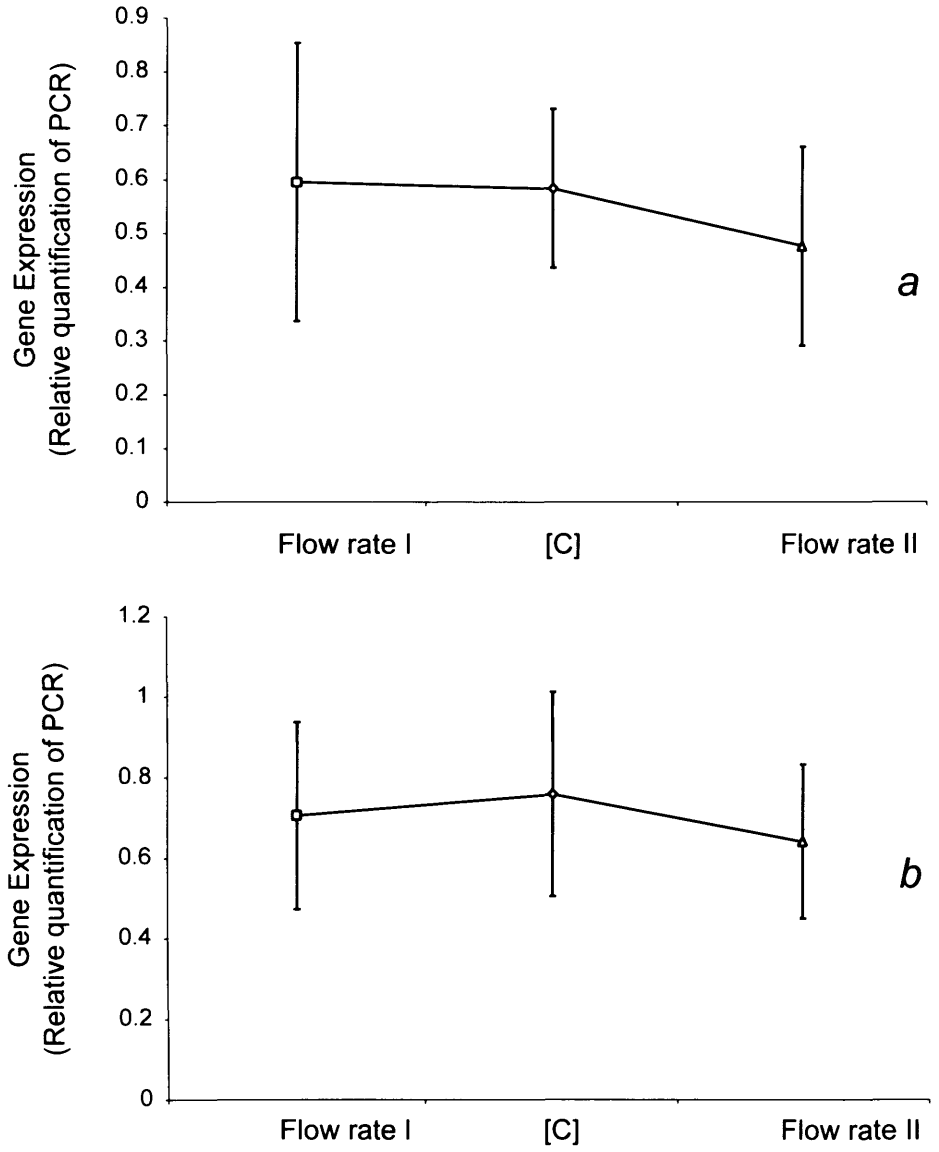

Figure 5.8 The effect of laminar GM flow on ON and Cbfa-1 gene transcription qPCR analysis results for ON (*a*) and Cbfa-1 (*b*) gene expression. HOB cells were seeded on $(CaO)_{0.46}$-$(Na_2O)_{0.01}$-$(Fe_2O_3)_{0.03}$-$(P_2O_5)_{0.50}$ glass fibre scaffolds for 7 days, subjected to laminar flow at 19.413 x 10^{-3} ml/s (Flow rate I) and 9.707 ml/ s x 10^{-3} (Flow rate II) for 8 h. cells seeded under static culture conditions were used as controls ([C]). (*n=3, error bars +/-SD*)

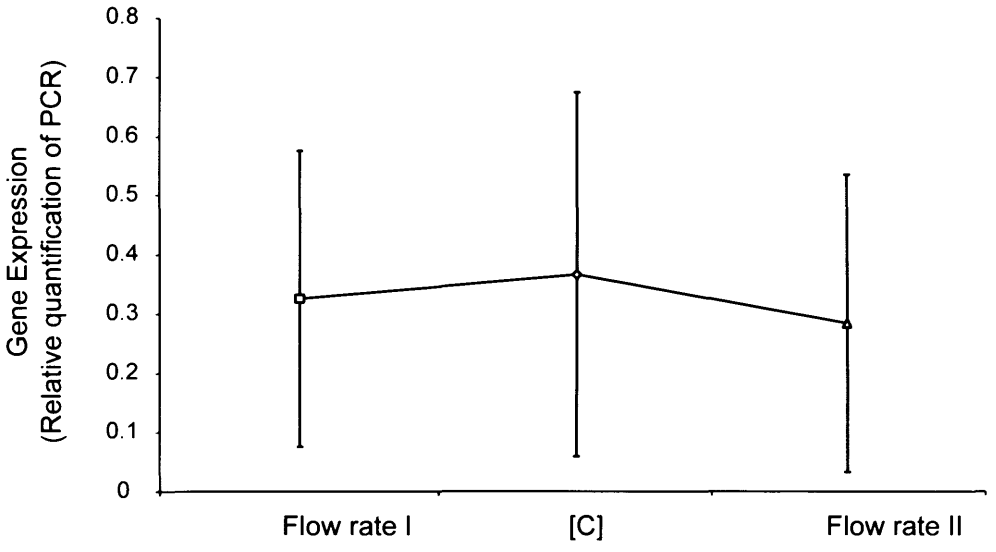

Figure 5.9 The effect of laminar GM flow on COL1A1 gene transcription in HOB cells

qPCR analysis results of HOB cells seeded on $(CaO)_{0.46}$-$(Na_2O)_{0.01}$-$(Fe_2O_3)_{0.03}$-$(P_2O_5)_{0.50}$ glass fibre scaffolds for 7 days, subjected to laminar flow at 19.413 x 10^{-3} ml/s (Flow rate I) and 9.707 x 10^{-3} ml/ s (Flow rate II) for 8 h. Cells seeded under static culture conditions were used as controls ([C]). (*n=3, error bars +/-SD*)

5.3.3.2 Oral fibroblasts

COL1A1 gene expression levels in HOF cells subjected, for 8 h, to flow rate I matched those of the control as no significant differences were obtained (Figure 5.10). At the higher flow rate I however, COL1A1 mRNA synthesis was down-regulated ensuing the 8 h flow application as quantification of PCR products revealed significantly lower COL1A1 expression values in comparison with both, cells exposed to flow rate I and the control cells.

On the other hand, and when assessing P4HA3 gene expression, no significant changes in gene expression were induced by either flow rate in comparison with the control and COL1A1 transcription rates, related to each flow value, were insignificantly different when compared (Figure 5.11).

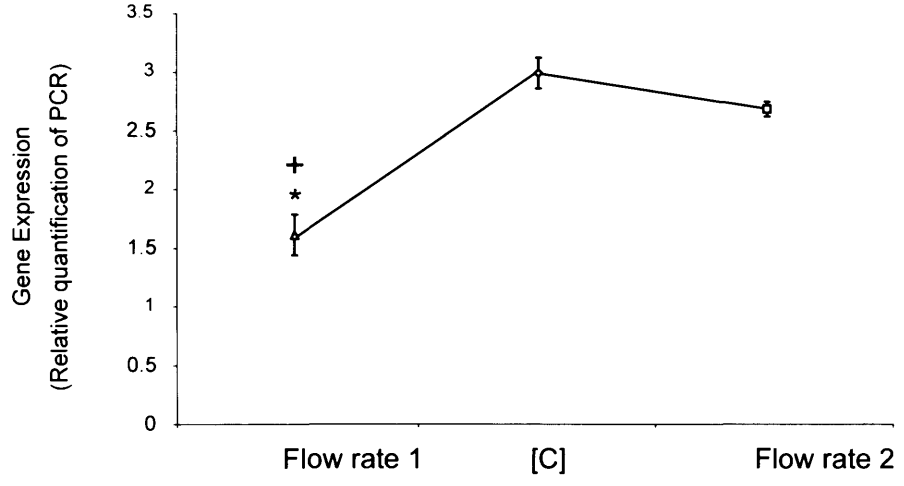

Figure 5.10 The effect of laminar GM flow on COL1A1 gene transcription in HOF cells

qPCR analysis results of HOF cells seeded on $(CaO)_{0.46}$-$(Na_2O)_{0.01}$-$(Fe_2O_3)_{0.03}$-$(P_2O_5)_{0.50}$ glass fibre scaffolds for 7 days, subjected to laminar flow at 19.413 x 10^{-3} ml/s (Flow rate I) and 9.707 x 10^{-3} ml/ s (Flow rate II) for 8 h. Cells seeded under static culture conditions were used as controls ([C]). (*) indicates significantly different gene transcription values between flow subjected, and control cells. (+) indicates significantly different gene transcription values between cells subjected to different flow rates. *($p<0.05$) ($n=3$, error bars +/-SD)*

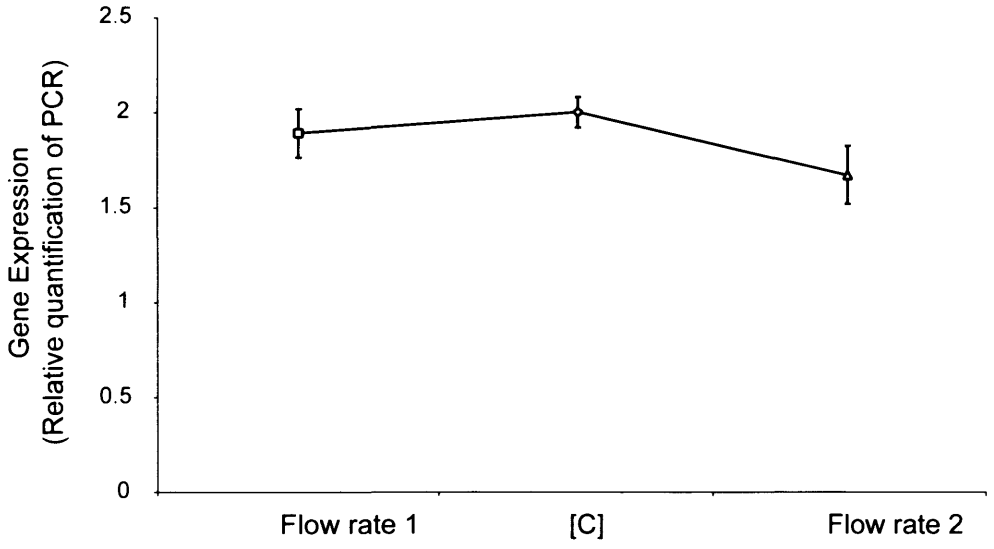

Figure 5.11 The effect of laminar GM flow on P4HA3 gene transcription in HOF cells

qPCR analysis results of HOF cells seeded on $(CaO)_{0.46}$-$(Na_2O)_{0.01}$-$(Fe_2O_3)_{0.03}$-$(P_2O_5)_{0.50}$ glass fibre scaffolds for 7 days, subjected to laminar flow at 19.413 x 10^{-3} ml/s (Flow rate I) and 9.707 x 10^{-3} ml/ s (Flow rate II) for 8 h. Cells seeded under static culture conditions were used as controls ([C]). (*n=3, error bars +/-SD*)

5.4 Summary

- Compared to the tissue culture seeded control cells, HOB cell differentiation have been maintained on the glass fibre scaffolds of the $(CaO)_{0.46}$-$(Na_2O)_{0.01}$-$(Fe_2O_3)_{0.03}$-$(P_2O_5)_{0.50}$ composition as no impact on HOB commitment to the bone ECM maintenance resulted from the use of these glasses as substrates. Quantification of PCR for ON and Cbfa-1 cDNA revealed gene expression levels closely approximating those of control cells at all investigated time points, with ON gene transcription up-regulated as a function of time in culture. COL1A1 mRNA synthesis was also expressed at similar levels, after 21 days in culture, on the scaffold and control surfaces.

- HOF cell commitment to the ECM turnover also appeared to have been preserved on glass fibres of 2 and 3 mol% fe_2O_3 content. No significant differences in COL1A1 and P4HA3 gene transcription levels on theses glasses were observed, at all time points, when compared the control surfaces.

- The inclusion of osteogenic supplements in the HOB cell culture GM resulted in up-regulating all the investigated genes on fibres of both 2 and 3 mol% fe_2O_3 compositions bringing ON transcription levels in particular, and on both glass compositions, to closely match those of the control. This has highlighted the important role of extrinsic factors in enhancing scaffold associated *in vitro* morphogenesis of tissue.

- Subjecting $(CaO)_{0.46}$-$(Na_2O)_{0.01}$-$(Fe_2O_3)_{0.03}$-$(P_2O_5)_{0.}50$ fibre scaffold seeded HOB cells to flow conditions, at 19.413 x 10^{-3} and 9.707 x 10^{-3} ml/ s, induced no significant changes in ON, Cbfa-1 and COL1A1 gene expression in relation to both flow rates and in comparison to the static cell culture conditions.

- Compared to control and 19.413 x 10^{-3} flow subjected cells, COL1A1 gene ascription was significantly lower in HOF cells exposed to the 9.707 x 10^{-3} ml/s flow rate. P4HA3 transcription on the other hand appeared to be

unaffected by the application of medium perfusion at either flow rate and in comparison with to control.

CHAPTER SIX

DISCUSSION

6.1 Introduction

The use of artificial materials in the fields of medicine and biology has been the subject of rapidly increasing interest and continuous development in recent years. Concurrently, the multidisciplinary research field of tissue engineering underwent considerable advances in utilising such artificial substances as biocompatible and bioactive templates (or scaffolds) for regenerating deficient tissue structures with the aim of overcoming the disadvantages of conventional therapeutical practices.

In order to apply the principles of tissue engineering to generate the hard-soft tissue interfaces, as an alternative cell transplantation strategy dealing with the clinical problems of ligament/ tendon disease and injury (Section 1.2), an *in vitro* cell-scaffold interaction must be promoted so that the morphogenesis of histologically, biomechanically and genetically compatible tissue units can be induced using the patient's own differentiated site specific or mesenchymal stem cells.

It is clear, nonetheless, that the scaffold constituting material must possess biocompatible properties permitting cell attachment and viability with no adverse effect on cell phenotype characteristics and function. Furthermore, this material must allow the long-term maintenance of the adherent cell differentiated function whereby the turnover of the newly synthesized matrix can be sustained. The material should also be soluble in a controllable manner corresponding to the *in vitro* morphogenesis and, if necessary, the rate of the in vivo maturity and integration of the hybrid tissue. Again, the biocompatibility of the soluble material is of extreme importance as inflammatory, toxic or immunogenic reactions to the in vivo degradation of the material should be of limited, short term and containable scope.

As outlined in section 1.8, numerous polymeric biodegradable substances are currently undergoing extensive assessment as fibre scaffold materials for tissue engineering. Whether naturally derived (collagen, fibrinogen, hyaluronic acid) or synthetic (PLLA, PGA, PLAGA), several reports have demonstrated the promising potential of these substances in supporting bone, ligament and tendon tissue regeneration (Burg et al., 2000; Holy et al., 2000; Novikova et al., 2003). Mechanically however, polymers are inherently weak and structural reinforcement into composites is often a requirement. Moreover, the release of the synthetic form degradation products has been shown to be associated with the induction of an acute

inflammatory response which may, potentially, hinder the critically important in vivo integration of the implanted hybrid tissue (van et al., 1994; Meikle et al., 1994; Martin et al., 1996; Winet and Bao, 1997; Holy et al., 2000).

As several reports have suggested, soluble phosphate based glasses may fulfil the benchmark criteria of biocompatibility and can be considered for *in vitro* evaluation as scaffold forming materials (Section 1.9.2). Furthermore, these glasses were frequently described as bioactive promoting the formation of biological bonding, vital for the implant integration to both hard and soft tissues (Hench, 1998). These glasses can be produced with controllable degradation profiles and, in the form of fibres, can be fabricated into three dimensional scaffolds of suitable shape and volume matching those of the tissue structure to be replaced (Ahmed et al., 2004a; Ahmed et al., 2004b). Fibres generated from phosphate glass species have also been shown to possess considerable tensile strength that may aid in withstanding the mechanical forces in an in vivo environment (Pahler and Bruckner, 1982; Lin et al., 1994).

This study therefore assessed the short term biocompatibility of these ternary glasses, of the generic form, in terms of HOB, HOF and HTF cell attachment, survival, morphology and maintenance of phenotype. Subsequently, and based on the most biocompatible ternary compositions, quaternary Fe_2O_3 containing glass fibre scaffolds were produced and evaluated for biocompatibility.

The role of extrinsic factors in enhancing *in vitro* tissue formation has also been investigated through inducing scaffold associated osteoblast differentiation, and the application of flow culture conditions. A contiguous co-culture scaffolding system, seeded with both HOB and HOF cells, has also been devised.

6.2 Biocompatibility of ternary glass compositions

6.2.1 Introduction

Studies conducted at the EDI laboratories have demonstrated that substrates obtained from the ternary form of these glasses, particularly those of 30 mol% CaO content, have resulted in no negative impact on osteoblastic differentiation (Salih et al., 2000). Accordingly, This study evaluated the short term biocompatibility of ternary glass compositions containing 30-48 mol% CaO, and of the generic form $(CaO)_{0.x}$-$(Na_2O)_{0.y}$-$(P_2O_5)_{0.5}$, in terms of HOB, HOF and HTF cell attachment, survival, morphology and maintenance of phenotype with the aim of determining the most suitable composition, or compositions, for biocompatible scaffold production. The solubility of these glasses is controlled by the presence of CaO and as concluded by previous reports, increasing CaO content decreases the corresponding glass solubility rates (Franks et al., 2000; Knowles et al., 2001; Franks et al., 2001). The ternary glasses investigated in this study therefore ranged from the high on solubility, 30 mol% CaO containing composition to the low on solubility, 48 mol% CaO containing glass.

6.2.2 Cell attachment and survival

The survival of anchorage-dependent cells such as HOB, HOF and HTF is strongly dependant on the appropriate cell attachment to the substrate surface. The presence and nature of this attachment greatly influences essential cellular mechanisms such as protein synthesis, proliferation, differentiation, migration and apoptosis (Richman et al., 2005). Accordingly, scaffold constituting materials must permit functional cell attachment within the 24-48 h following cell seeding (Baèáková et al., 2004).

Initial experiments using the CyQUANT cell density assay revealed, after 180 min in culture, considerably lower MG-63 cell density on ternary glass discs containing < 40 mol% CaO than that on the 40 mol % CaO content where cell density matched that of the control surface(figure 3.3). This result was visually confirmed, using SEM, as these compositions of ≤ 38 mol% CaO content supported little or no cell attachment (figure 3.4, table 3.2). It is probable, and due to the high solubility of these glasses,

that surface degradation (figure 3.4 C and D) hindered the efficient deposition of ECM molecules required for functional cell attachment thus causing the induction apoptosis in the seeded cell population. On the other hand, the lack of cell survival on the highly soluble glasses may be attributed to higher levels of Na cation release into the culture environment. Recent work investigating a 50 mol% P_2O_5 ternary glass composition has shown that Na^+ ion release was proportionate to the rate of glass degradation (Ahmed et al., 2004b). For 30, 35 and 40 mol% CaO containing compositions, Na^+ ion release levels at day 7 in solution were approximately 65, 40 and 25 PPM (parts per million: unit of concentration by weight) respectively. Several studies have suggested that higher concentrations of Na^+ result in the alkalization of the local environment (increased pH levels), thus negatively affecting cell viability (Jonasova et al., 2002).

In contrast, and as observed by fluorescence microscopy, the 40 to 48 mol% glass compositional range supported HOB, HOF and HTF cell survival up to 7 days in culture. However, visual observation revealed higher levels of adherent cells on the 48 mol% CaO glass in comparison with the control surfaces and at all time points. This was confirmed when conducting CyQUANT analysis as significantly higher levels of nucleic acid content for the seeded HOB cells (at time points day 1, 4 and 7) (Figure 3.13), and HOF cells (Figure 3.19), were associated with the glass composition containing 48 mol% CaO when compared to the higher on solubility, 40 mol% CaO glass form.

The seeded cell viability therefore is clearly dependent on the glass composition and in this respect, the least soluble glasses containing 48 mol% CaO emerged as the most biocompatible by means of supporting cell attachment and short term survival.

6.2.3. Cell morphology and phenotype

The nature and extent of cell attachment, as determined by cell morphology, are important factors in assessing the biocompatibility of the scaffold constituting material in terms of both adhesivity and cytotoxicity. Following cell attachment, reorganization of actin microfilaments results in initiating various intracellular signalling mechanisms influencing major cellular events such as proliferation, differentiation, protein synthesis and survival. For anchorage-dependant cells, a well

spread attachment is vital for cell division and population growth whilst an impaired round (spherical) attachment will invariably lead to cell death (Dubin-Thaler et al., 2004). The soluble scaffold material should therefore provide adequate surface adhesion to support a well-spread morphology, the maintenance of which, is indicative of the lack of degradation product toxicity. Morphological evaluation of both osteoblasts and fibroblasts revealed rounded cell morphology on lower CaO containing glass surfaces in particular that of the 40 mol% CaO content whilst on higher CaO containing glass compositions, mainly that of the 48 mol% CaO content, a considerable proportion of the cell population exhibited a well-spread morphology of a conformation resembling that of the cells seeded on control surfaces.

A well spread cytoskeleton is also important in maintaining the phenotypic function of the cell (Lim et al., 2004). The cell phenotype Is the functional outcome of its differentiated commitment to perform specific tasks as, for example, the osteoblastic phenotype Is expressed by the cell ability to synthesize and induce the mineralisation of the bone ECM. This study evaluated the maintenance of HOB, HOF and HTF phenotype by assessing, via immunocytochemistry, the ability of the seeded cells to synthesize the ECM proteins required to maintain both hard and soft tissues.

HOB cells were characterized and the maintenance of their phenotype on the ternary, 40 to 48 % CaO containing, glasses was evaluated through immunolabelling the bone associated noncollagenous proteins (NCPs): BSP, ON and OP. BSP accounts for 15 % of the NCPs present in bone and has been shown to play an active role in bone ECM remodelling and osteoblast differentiation. OP is also implicated in bone remodelling through inhibiting nucleation and HA crystal growth. Moreover, both BSP and OP are bone specific and both contain RGD motif peptide sequences and actively engage in receptor-mediated cell binding to the bone ECM (Hing, 2004). As a nucleator, ON has the capacity to bind to Ca^{+} and collagen types I and V, thus initiating the process of heterogeneous nucleation necessary for bone mineralisation (Section 1.6.3.2). Studies have also suggested a role for ON in regulating cell-matrix interactions (Hing, 2004). In a pattern similar to that of the control cells, and providing that cell spreading was present, synthesis of bone associated proteins BSP, ON and OP by HOB cells cultured on the highest calcium containing glass composition, i.e. 48 mol% CaO, was observed at all time points and up to 7 days in culture (figures 3.8, 3.9 and 3.10).

The HOF and HTF phenotype was characterized by the 5B5 antibody labelling to detect the production of P-4-H, the enzyme vital for procollagen molecule assembly

and collagen synthesis (Section 1.6.3.3). Several studies have suggested the use of the 5B5 as a marker for fibroblastic activity(Bosseloir et al., 1994; Ohtsubo et al., 2000; Ulf et al., 2002). HOF and HTF cells seeded on the 48 mol% CaO containing glass composition were capable of synthesising P-4-H, at all time points, as the presence of positive punctate staining for P-4-H was conformed by fluorescence immunostaining (Figures 3.14 and 3.15). Again, this was only associated with the presence of a well spread cytoskeleton (Figures 3.16 and 3.17).

6.2.4 Cell proliferation

The fully differentiated cell is post proliferative, i.e. with a suppressed capacity to divide, hence the reciprocal relationship between differentiation and proliferation (Aparicio et al., 2002). When primary, fully differentiated cells are isolated from tissue the population gradually undergoes dedifferentiation and becomes more committed to cell division. This process is caused by the lack of biochemical and biomechanical inducers of cell differentiation in the cell culture environment (Cervenkova et al., 2001). Cell proliferation however, is an important step in inducing *in vitro* tissue morphogenesis as a high level of cell density is required for the adequate cell invasion of the scaffold to take place (Itoh et al., 2001). Once this has been achieved and the appropriate cell density has been reached, multi-dimensional cell-cell interactions will result in population redifferentiation and the subsequent tissue formation (Holmes, 2002). Redifferentiation can also be induced following the cell interaction with the newly formed ECM and by providing the appropriate stimuli to the cell-scaffold culture environment, e.g. mechanical load or growth factors (Sage, 2001; Cancedda et al., 2003).

As revealed by the CyQUANT analysis, and despite supporting cell survival and phenotype, no significant cell proliferation and population growth was established on the least soluble, 46 and 48 mol% CaO containing, glass compositions (Figures 3.12 and 3.18).

The extent and nature of cell attachment to substrates is critical for the ensuing cell population growth (Cowles et al., 2000). Therefore, and due to the soluble nature of the glass, it is probable that the sufficient attachment necessary to ensure proliferation has not been permitted.

The least soluble ternary glass compositions, particularly of the 48 mol% CaO content, supported cell attachment and survival up to 7 days in culture where a significant proportion of the seeded population exhibited a well spread morphology.
The biocompatibility of these glasses appeared to be directly linked to solubility as when cell survival and well spread morphology have been supported, no toxic effect of glass degradation products were apparent as phenotypic protein expression of the seeded cells had been maintained. Glass compositions $(CaO)_{0.48}$–$(Na_2O)_{0.02}$–$(P_2O_5)_{0.5}$ and $(CaO)_{0.46}$–$(Na_2O)_{0.04}$–$(P_2O_5)_{0.5}$, of the 46 and 48 mol% CaO respectively, were therefore elected as base compositions for glass fibre production. However, and due to the lack of the seeded cell proliferation, the solubility of these glasses had to be further controlled by introducing a fourth precursor into the glass formulation.

6.3 The glass fibre system

6.3.1 Introduction

The architectural properties of the scaffold must take into consideration the anatomical nature of the tissue to be generated. Therefore, and as the main objective of this study was to asses the potential use of phosphate based glasses as biocompatible scaffolds for engineering the hard-soft tissue interface, a fibre-based structure may present an ideal scaffold system. Glass fibres provide a contiguous matrix onto which, both cellular components of the interface can be seeded (i.e. osteoblasts and fibroblasts). Additionally, these fibres can easily be moulded to fit the defect area to be repaired.
The use of fibre-based constructs has been evaluated in numerous studies as scaffolds for tissue regeneration. Naturally derived fibre systems (collagen and elastin) have been investigated for vascular regeneration (Buijtenhuijs et al., 2004; Buttafoco et al., 2006). Bioactive glasses, particularly Bioglass® 45S5, have also been considered as fibre based systems for peripheral nerve and bone repair with promising potential (Clupper et al., 2004; Bunting et al., 2005).

6.3.2 The effect of fibre diameter on cell attachment and viability

Surface geometry and morphological characteristics of the biocompatible scaffold greatly influence the seeded cell viability and behaviour (Salgado et al., 2004). For example, pore size variations in porous scaffold constructs yield variable surface characteristics firstly, by increasing or decreasing the surface area available for cell attachment and secondly, by producing different surface topography patterns. This has been shown, in numerous studies, to have a direct implication on the seeded cell viability, migration and proliferation (Laurencin et al., 1999; Stangl et al., 2001; O'Brien et al., 2005). In this regard however, little information is available on the effect fibre diameter may exert on the biocompatibility of fibre-form scaffold systems. As detailed in Section 2.2.4, phosphate based glass fibres can be produced at various diameters depending on the drum rotational speed. Morphologically, fibres of various diameters differ in their surface area and surface curvature and subsequently, fibres of larger diameters are characterised by a larger surface area and less surface curvature. On 48 mol % CaO containing ternary glass fibres, HOB cell attachment pattern and viability were proportionate to the seeded fibre diameter where fibres drawn at 800 r/ min, i.e. of the largest diameters, accommodated higher numbers of attached cells than those of smaller diameters after 24 h in culture (figures 4.1 and 4.2). Over time, and despite a reduction in the attached cells number, only the 800 r/min produced fibres supported the survival of HOB cells up to 7 days. Similarly, HOF cells survival was directly linked to fibre diameter and at day 7 time point, no cells were present on the fibres generated at 1200 and 1600 r/ min (Figures 4.3 and 4.4).

These results are in line with recent findings by Spallazzi et al. where it has been shown that chondrocyte adhesion to microspheres was affected by the surface curvature of the material. In fact, an increased curvature resulted in significantly delaying cell spreading on the substrate (Spalazzi et al., 2003). It had been also suggested, that fibre curvature influenced tendon fibroblast morphology and orientation on synthetic polymer scaffold materials (Ricci et al., 1984). The drum rotational speed of 800 r/min was therefore adopted for quaternary glass fibre production henceforth.

6.3.3 Glass fibre structural modification

Despite maintaining attachment, morphology and phenotype, cells seeded onto ternary phosphate based glasses exhibited no significant proliferation trends over time in culture. As the biocompatibility of phosphate based glasses appeared to be directly affected by the glass solubility (Section 3.4), the ternary glass form was modified into a less soluble quaternary form by adding Fe_2O_3 as a fourth precursor. The inclusion of Fe_2O_3 as a network modifier has been shown to strengthen the glass network structure and to significantly reduce solubility (Lin et al., 1994; Ahmed et al., 2004a). This might be attributed to the replacement of P–O–P bonds (Figure 1.13) in the glass by Fe–O–P bonds, and to the strong cross-linking of the phosphate chains by the iron ions (Ahmed et al., 2004a). In a study by Lin et al., the addition of Fe_2O_3 resulted in the production of phosphate based glass fibres of reduced solubility, increased fibre tensile strength and enhanced glass transition temperature (Lin et al., 1994). Quaternary Iron-phosphate glass fibres evaluated at the EDI have been shown to be of considerable biocompatibility as scaffolds for muscle tissue engineering (Ahmed et al., 2004a; Shah et al., 2005).

In this study, quaternary iron-phosphate glass fibres of 1, 2 and 3 mol% Fe_2O_3 content (generic form $(CaO)_{0.46}$-$(Na_2O)_{0.0x}$-$(Fe_2O_3)_{0.0y}$-$(P_2O_5)_{0.50}$) were produced using the ternary glass of the 46 mol% CaO content as a base composition. This ternary composition was chosen as it permitted the addition of up to 3 mol% Fe_2O_3 into the glass network. As expected, solubility measurements have shown that increasing the Fe_2O_3 significantly decreased the corresponding glass dissolution rate (Figures 4.6 and 4.7)

6.3.4 Cell viability, proliferation and morphology

Following direct cell count experiments it appeared that all three quaternary glass compositions, and the control 46 mol% CaO containing ternary form, supported cell attachment to the fibre surface at day 1 in culture for both HOB and HOF cell types (Section 4.3.4). However, and beyond the initial time point investigated, cell survival was only retained on glass fibres containing 2 and 3 mol% Fe_2O_3 (compositions $(CaO)_{0.46}$-$(Na_2O)_{0.02}$-$(Fe_2O_3)_{0.02}$-$(P_2O_5)_{0.50}$ and $(CaO)_{0.46}$-$(Na_2O)_{0.01}$-$(Fe_2O_3)_{0.03}$-$(P_2O_5)_{0.50}$) where the presence of a viable cell population was detected up to 14 days

in culture (figures 4.10 and 4.13). Again, the capacity of the glass to retain cell attachment appeared to be directly linked to its solubility profile and as can be seen from Figure 4.6, 2 and 3 mol% Fe_2O_3 containing glasses were the least soluble among the compositions investigated.

More importantly, a significant increase in cell density for both cell types, and over time in culture, was associated with the 3 mol% Fe_2O_3 glass composition $(CaO)_{0.46}$-$(Na_2O)_{0.01}$-$(Fe_2O_3)_{0.03}$-$(P_2O_5)_{0.50}$ suggesting that the substrate properties necessary for cell proliferation have been fulfilled. This result was verified by fluorescence microscopy as after 21 days in culture where considerable proportions of the surfaces of the examined scaffolds were invaded by dense populations of HOB and HOF cells. This was, as expected, mainly associated with the 3 mol% Fe_2O_3 fibre composition (figures 4.12 and 4.14).

The adhered cells exhibited a well spread morphology across the entire seeded population where cell spreading was parallel to the fibre axes. Similar work has reported the presence of this particular form of cytoskeletal orientation on fibre substrates and it has been suggested, that cell spreading occurred in the favourable plane along the fibre axis rather than the highly curved fibre circumference (Ricci et al., 1984). This orientation may also become reinforced by the scaffold configuration where the constituting fibres are arranged with minimum inter-fibre distances, and the formation of pseudo grooves between adjacent fibres may occur. On grooved substrates, the geometrical distribution of focal adhesions influences the reorganisation of microtubules and actin filaments where subsequent cell spreading and migration are oriented parallel to the groove direction (Oakley and Brunette, 1993).

As a soluble material, the 3 mol% Fe_2O_3 containing quaternary composition has demonstrated excellent surface adhesivity by permitting ECM adhesion molecules adsorption and the subsequent cell attachment, spreading and proliferation with no apparent cytotoxicity in terms of cell morphology and population growth. This on the other hand has highlighted the advantageous surface properties of these glasses, as high levels of cell adhesivity have been provided without the need for surface modification. In comparison, most synthetic polymers are naturally hydrophobic so that adsorbed adhesion proteins become rigid and integrin receptor recognition-resistant. Accordingly, the use of these materials as biocompatible scaffolds is often dependent on increasing surface hydrophilia (wettability) by various methods such as

ion bombardment, ultraviolet light irradiation and plasma glow discharge (Khang et al., 1997; Baèáková et al., 2004).

6.3.5 Maintenance of cell differentiation

Further to evaluating the seeded cell long term viability and proliferation, the biocompatibility of the quaternary glass compositions, in terms of cytotoxicity, was verified by assessing the maintenance of cell differentiation. Therefore, and as detailed in Section 5.2.1, qPCR experiments were used to quantify mRNA transcription levels associated with the regulation of HOB and HOF cell differentiated function in synthesising, and maintaining, the ECM associated with each cell type. It has also been established whether ECM turnover related gene transcription has been up-regulated by the presence of any bioactive influence of the glass. Soluble calcium phosphate containing bioceramics and glasses are frequently described as class *A* bioactive materials as possessing firstly; conductive properties by permitting cell migration from, and the binding of adjacent tissue in vivo and secondly; an inductive effect, i.e. activating the cellular processes necessary for tissue formation (Hench, 1998; Gunatillake and Adhikari, 2003). In a study by Knabe et al., primary human osteoblasts were seeded onto a Ca_2-$KNa(PO_4)_2$ based biodegradable scaffold material and it has been shown that the presence of this substrate significantly enhanced gene expression for COL-I, ALP, OP, OC and ON when compared with tricalcium phosphate substrates (Knabe et al., 2005).

COL-I synthesis by HOB cells is essential for ECM formation and maintenance (see chapter one) whilst ON synthesis, and as previously mentioned in this chapter, is indicative of active involvement in ECM mineralisation. Also, the expression and regulation of osteocalcin (OC) transcription factor encoding gene, Cbfa1, is truly indicative of osteoblastic function as osteocalcin is synthesised when remodelling of the bone ECM is activated (Karsenty, 2000). OC, termed bone Gla (gamma-carboxyglutamate) protein, is the most abundant transmembrane protein in bone forming approximately 20% of the total NCPs. OC acts as a potent inhibitor of mineralisation by suppressing nucleation and crystal growth of HA (Hauschka et al., 1989; Hing, 2004).

The transcriptions of ON and Cbfa-1 were activated and maintained on 3 mol% Fe_2O_3 glass composition ($(CaO)_{0.46}$-$(Na_2O)_{0.01}$-$(Fe_2O_3)_{0.03}$-$(P_2O_5)_{0.50}$) over time in culture

with mRNA synthesis levels, for both genes and at day 14 and 21 time points, matching those of the control cells. Furthermore, ON gene expression was up-regulated as a function of time in culture and no similar trend was associated with the control cells. This may suggest that the presence of the phosphate glass fibres resulted in enhancing osteoblastic differentiation by stimulating HOB cell engagement in ECM nucleation. On the other hand, no changes were observed in Cbfa gene expression against time in culture. This might be attributed to the fact cbfa-1 transcription is closely related to OC synthesis and as a late marker of osteoblastic activity, OC transcription is normally up-regulated following bone ECM mineralisation and maturation, during the bone remodelling phase (Franceschi and Iyer, 1992; Xiao et al., 1998). COL1A1 (encoding collagen type I alpha-1 polypeptide chains) gene regulation was also maintained and at the most advanced time point, similar COL1A1 mRNA synthesis levels were exhibited by the control and the 3 mol% Fe_2O_3 glass seeded cells.

HOF cell differentiation was also maintained, on both 2 and 3 mol% glass compositions and at all the time points investigated (Figures 5.4 and 5.5). The capacity of scaffold seeded HOF cells to deposit and maintain soft tissue ECM by synthesising, and assembling, COL-I molecules (Figure 1.10) remained intact when compared with that of the control cells as indicated by qPCR analysis of COL1A1 gene expression.

It is worth considering that the control tissue culture polystyrene is treated in a variety of ways to increase wettability by incorporating various anionic groups into the surface, thus providing the optimum environment for initial non-specific cell adhesion, protein adsorption, integrin-mediated attachment and the subsequent cell spreading and function (Scolaro et al., 2005). It is therefore significant, taking into consideration the glass solubility and the highly curved surface geometry, that 3 mol% Fe_2O_3 glass fibre scaffolds maintained HOB and HOF differentiation in a similar manner to that of the control surfaces.

6.4 Extrinsic factor inclusion: The affect on cell function

As detailed in section 1.7.5, designing cell-scaffold culture systems for tissue repair must take into consideration the various extracellular components such as matrix proteins (e.g. NCPs and proteoglycans) and soluble factors (e.g. growth factors, hormones and vitamins). In vito induction of tissue morphogenesis must also utilise the use of bioreactor systems so that mechanical stimuli, medium diffusion and wate remocal can all delivered to the culture environment.

6.4.1 Induction of osteogenesis: enhancing scaffold associated osteoblast differentiation

As described in Sections 1.6.2.4 and 1.6.2.5, in vivo bone ECM formation and mineralisation is a highly organised process sequentially involving (i) preosteoblast differentiation into osteoblasts; (ii) the synthesis and deposition of the collagen matrix by the differentiated cells and; (iii) the HA nucleation and ECM calcification. Despite being primarily mediated by osteoblastic action, this process is regulated and greatly dependent on the presence of The application of tissue engineering strategies must therefore address the inclusion of these factors when attempting to induce *in vitro* bone morphogenesis.

As previously demonstrated (Section 4.3.3), glass fibre composition $(CaO)_{0.46}$-$(Na_2O)_{0.01}$-$(Fe_2O_3)_{0.03}$-$(P_2O_5)_{0.50}$ exhibited excellent scaffold material properties and it is hence important, that mineralised tissue formation is induced by providing the appropriate cell-scaffold culture environment.

Ascorbic acid (AA, Vitamin C) induces the *in vitro* differentiation of embryonic stem cells into osteoblasts(zur Nieden et al., 2003). In the differentiated osteoblast, AA transport into the cell is conducted by a Na^+ dependent protein, SVCT1 (sodium-dependent vitamin-C transporter 1) whose up-regulation is induced by dexamethasone. AA has been shown to up-regulate gene expression for Type I procollagen and stimulate collagen synthesis (Franceschi and Iyer, 1992). AA also plays a major role in regulating mineralised ECM remodelling by influencing OC production. OC synthesis is triggered by the action of OSE2 (osteocalcin gene 2 promoter) which, in turn, is activated by the interaction between AA and Osf2 (OC transcription factor, encoded by Cbfa1 gene) and the *in vitro* addition of AA therefore,

has resulted in up-regulating OC transcription rate (Franceschi and Iyer, 1992; Xiao et al., 1998).

In this study, 2 and 3 mol% Fe_2O_3 containing glass fibre scaffold cultures were supplemented with AA and the ensuing effects on HOB differentiation were evaluated. The culture was also supplemented with β-glycerophosphate as a source of the organic phosphate necessary for HA nucleation and crystal growth(Beck, Jr. et al., 2000).

As a result (Figures 5.6 and 5.7), gene expression for COL1A1, ON and Cbfa-1 was up-regulated on both glass compositions against time in culture suggesting that the scaffold seeded HOB cell capacity to synthesise collagen; and regulate the mineralisation of bone ECM had been significantly enhanced. This trend was not associated with HOB cells seeded in normal GM, i.e. with no osteogenesis inducing factors, thus emphasising the importance of using such factors to induce scaffold associated bone formation.

6.4.2 The effects of flow culture conditions

The application of suitable bioreactor systems is of extreme importance in enhancing the mass transfer of medium to the cell-scaffold, by continuous flow perfusion, and in order to provide the efficient removal of scaffold acidic degradation by-products should these be present (Park, 2002).Under static culture conditions, the inadequate diffusion of oxygen, nutrients and waste into three-dimensional cell seeded scaffolds may hinder tissue formation. This is frequently manifested as cell survival, growth and ECM deposition is limited to surface areas of such scaffold structures (Botchwey et al., 2001; Salgado et al., 2004).

It has been reported by Holtorf et al., that the application of flow perfusion on three-dimensional titanium mesh scaffold cultures induced osteoblast differentiation by up regulating ALP and OP expression; enhancing cell population growth; and increasing the rate of ECM mineralisation (Holtorf et al., 2005). Several similar studies, aiming at generating various tissue types, utilised the use of scaffold-associated flow perfusion systems all of which, resulted in enhancing *in vitro* tissue formation (Grabowski et al., 1993; Navarro et al., 2001; Park, 2002; Radisic et al., 2004). It has also been shown that the *in vitro* mechanical strain imposed by fluid induced shear stresses can influence both the differentiation and the matrix remodelling capacity of

bone, tendon and ligament cells (Frangos et al., 1987; Hillsley and Frangos, 1997; Hung et al., 1997; van Griensven et al., 2003). Accordingly, and as this study aimed primarily at assessing the affect of medium perfusion on cell differentiation, the lamellar flow rate was regulated such that the flow related shear stress was kept at a minimum value (see Section 5.2.3).

Following exposure to the two flow rate values at 19.413 x 10^{-3} ml/s and 9.707 10^{-3} ml/s, and for 8 h in culture, no changes in HOB differentiation were detected, on the 3 mol% Fe_2O_3 glass fibres and for both flow rates, when compared to the static culture control cells (Figures 5.8 and 5.9). Expression of the HOF cells P4HA3 gene also appeared unaffected by the application of medium flow (figure 5.11). COL1A1 gene expression however was down-regulated in response to the higher flow rate of 19.413 x 10^{-3} ml/s (Figure 5.10). This may indicate that medium perfusion, at the higher flow rate, exerted a mechanical influence on the seeded HOF population.

These results further confirmed the lack of cytotoxicity of glass composition $(CaO)_{0.46}$-$(Na_2O)_{0.01}$-$(Fe_2O_3)_{0.03}$-$(P_2O_5)_{0.50}$ as no significant differences in Cbfa-1, ON and COL-I gene expression were noticed between cells seeded under static and the flow conditions of 8 h duration where glass degradation products were continuously removed. Furthermore, these results also validated the flow system configuration, and the lamellar nature of the flow, by demonstrating its capacity of delivering mass medium perfusion whilst maintaining cell differentiation at the lower flow rate value (9.707 10^{-3} ml/s). This system can therefore be applied when the diffusion of medium is critical for maintaining more complex, larger volume, cell-scaffold cultures.

6.5 Contiguous HOB-HOF co-culture implementation

The inadequacies imposed by the limited and functionally inferior integration of surgically inserted grafts, where the reconstruction of tissue entheses is required (Section 1.5.1) , have accentuated the importance of developing scaffold systems capable of accommodating the formation of such interfaces. Not only will this approach permit the functional morphogenesis of the interface; the in vivo fusion of each graft component to the corresponding tissue type will also significantly enhance the implant success.

The concept of generating the hard-soft tissue interface can be implemented in the form of a co-culture seeded scaffold system. For example, such systems have been

assessed for the *in vitro* induction of osteochondral interface formation where osteoblasts and chondrocytes were seeded, in co-culture, on three-dimensional scaffolds of various compositions (Spalazzi et al., 2003; Elisseeff et al., 2005).

It is important to recognise, however, and when applicable to generating osteoligamentous and osteotendinous interfaces, that fibroblasts exhibit higher proliferation and DNA synthesis rates in culture than those of the osteoblasts and consequently, a co-culture of the two cell types will invariably become predominated by the fibroblastic population (Shin et al., 2004). It has been shown that as a result of fibroblast predominance, the capacity of the co-cultured osteoblastic cells to regulate ECM formation and mineralisation was inhibited (Ogiso et al., 1991; Ogiso et al., 1992). It is vital therefore, that initial development of each tissue component is independently granted via a scaffold configuration that permits, and maintains, the separate seeding of each cell type. Such a configuration is also necessary to allow the separate supplementation of the extrinsic factors specific to each cell type.

This study has investigated the feasibility of producing a co-culture scaffolding system using a continuous, 3 mol% Fe_2O_3 containing, glass fibre arrangement separately seeded with HOB and HOF cells and as seen form Figure 4.16, the use of the separation barrier resulted in creating a clear, well defined, separation zone between the two populations. Once significant ECM formation specific to each tissue type has occurred, this barrier could be removed so that HOB and HOF interaction across the interface may take place.

6.6 Quaternary Phosphate based fibre scaffolds: Future work

The 3 mol% Fe_2O_3 containing, phosphate glass fibre system devised in this study have fulfilled the criteria required to support the initial phase of cell-scaffold interaction in a cell transplantation process that may lead, ultimately, to *in vitro* tissue generation (Figure 6.1). This system can therefore be further evaluated and developed so that tangible tissue formation can take place.

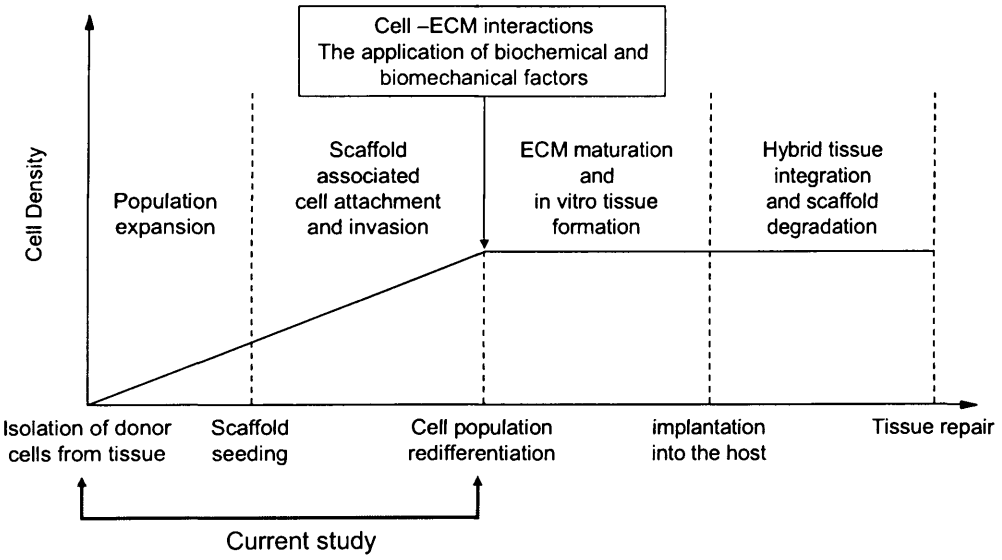

Figure 6.2 The sequence of events involved in the cell transplantation approach for inductive tissue regeneration

Despite the seeded cells exhibiting an intact ability to regulate collagen gene transcription, collagen synthesis and the fibre scaffold ability to support matrix formation and the rate of this formation must be assessed through the use of SEM, immunohistochemistry and protein biochemistry (western blot analysis).

Throughout this work, cell attachment and morphology have been evaluated as major indicators of biocompatibility. Functional cell attachment to substrates, following the initial non-specific attachment, is integrin receptor mediated (Richman et al., 2005) (Figure 6.2). This type of adhesion occurs as a result of the cell membrane integrin receptors (transmembrane glycoproteins) binding to the ECM molecules that might have adsorbed on the substrate surface from the cell culture medium. Following

integrin binding to ECM adhesion molecule, integrin receptors are clustered with other molecules into adhesion structures termed focal adhesions or focal contacts. These focal adhesions play a major role in influencing essential cellular mechanisms such as protein synthesis, proliferation, differentiation, migration and apoptosis (Richman et al., 2005). It is important, therefore, that future studies evaluate the capacity of the quaternary phosphate glasses to permit ECM adhesion molecules adsorption by, for example, X-Ray Photoelectron Spectroscopy (Satriano et al., 2005). The distribution and conformation of focal adhesions should also be investigated, using SEM for example (Richards et al., 2001), and related to further possible structural enhancement of the glasses.

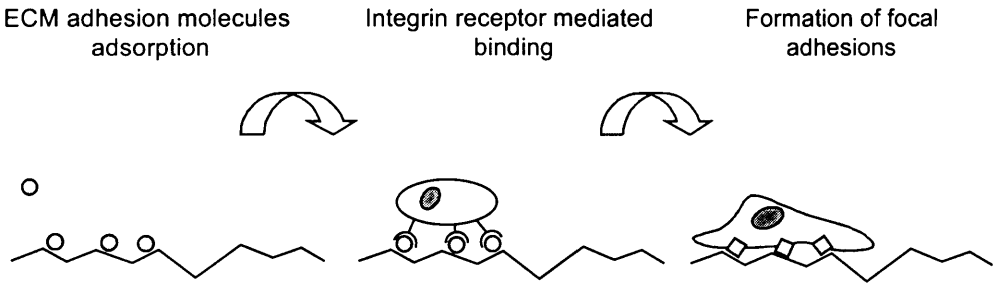

Surface properties influencing adhesivity:

Wettability
Electrical charge
Roughness
Topography
Cristallinity
PH
Porosity
Solubility
Carbon, amin or oxygen groups

Figure 6.1 Integrin mediated cell adhesion to biocompatible substrates

Simulating the in vivo environment should also be further promoted through developing a culture system within which the extrinsic factors critical for tissue formation such as mechanical loading, shear stresses and tissue growth factors can be comprehensively included.

As for the scaffold properties, the mechanical capacity of the fibres to withstand *in vitro* stresses will greatly influence, following in vivo implantation, the subsequent

clinical strategy determining, for instance, the nature and longevity of the implant site immobilisation. The mechanical properties of the fibres, particularly tensile strength should therefore be quantitatively evaluated using, for example, tensile testing devices so that improving the scaffold strength and resistance may be considered. The ability to produce complex three-dimensional scaffold configurations, of shape and volume fitting that of the structure to be replaced, should also be addressed. Expanding on the preliminary findings in this study (Section 4.3.2.3), an in depth analysis of the fibre surface topography must also be carried out as the presence of specific surface patterns play an important role in influencing cell attachment(Webster et al., 1999).

The co-culture arrangement can be further enhanced whereby chondrocytes may also be included to fully implement the hard-soft tissue interface structure, i.e. bone, fibrocartilage and ligament/tendon (Section 1.6.4). This arrangement must also permit the initial separate administration of extrinsic factors specific to each cell type.

Once tissue morphogenesis has been successfully induced, the tissue-scaffold complex must be applied in an animal model so that an insight can be gained into establishing a linear relationship between the in vivo integration of the engineered tissue and the scaffold degradation trend. This is also important to establish the efficiency and duration of the implant integration process; the capacity of the scaffold of bioactively bonding to the adjacent tissue; and the presence of any inflammatory and immune responses by the host.

For the clinical application of inductive tissue engineering to become a reality, tissue replacement units must be provided on demand and within a reasonable frame of time and the above processes therefore, must be coordinated within a strategy where rapid *in vitro* tissue formation can take place.

6.8 Conclusion

This study has utilised for the first time, at the time of writing this thesis, the use of non-silica phosphate based glass fibres as a primary human osteoblast-fibroblast seeded system with the potential application for the hard soft-tissue interface regeneration. Additionally, the capacity of these scaffolds to accommodate a contiguous, segregated and well defined co-culture system has also been explored for the first time.

Quaternary phosphate based glass fibres, produced at 800 r/min rotational speed, of the composition $(CaO)_{0.46}$-$(Na_2O)_{0.01}$-$(Fe_2O_3)_{0.03}$-$(P_2O_5)_{0.50}$ have been shown to possess excellent properties as primary human osteoblast and fibroblast seeded fibre scaffold for the inductive, *in vitro*, tissue engineering of the hard-soft tissue interface.

These 3 mol% iron oxide containing fibres exhibited firstly, sufficient surface adhesivity to support cell attachment and functional, well spread, morphology and secondly, high biocompatibility by maintaining the long term cell viability, proliferation and expression of the cell differentiated function. It is of considerable significance that these properties were present in these glasses in their basic form without the need for post-production structural modification.

This work has also demonstrated the feasibility of devising a cell-scaffold culture system where the extrinsic biochemical and biomechanical factors, necessary for *in vitro* tissue formation, can be included. The application of an osteogenic medium environment promoted the expression of scaffold associated osteoblastic differentiation in terms of ECM synthesis and remodelling. Medium and waste perfusion within the cell-scaffold complex have also been delivered to enhance tissue formation with no negative impact, at a certain flow rate, on cell differentiation by using an open circuit, lamellar flow, bioreactor.

These scaffolds have also been configured to accommodate a co-culture system onto which, the cellular components of the hard-soft tissue enthesis can be separately seeded whereby the anatomical nature of such an interface can be imitated.

Appendix

1. Reagents and Kit

Cell culture

D-MEM	Invitrogen, Paisley, UK.
DMSO	Sigma-Aldrich, Dorset, UK.
Fetal calf serum	Invitrogen, Paisley, UK.
PBS (sterile, Ca^{2+}/Mg^{2+}free)	Invitrogen, Paisley, UK.
Penicillin	Invitrogen, Paisley, UK.
Streptomycin	Invitrogen, Paisley, UK.
Trypsin-EDTA	Invitrogen, Paisley, UK.

Immunocytochemistry

AF2 antifadent	Citifluor Ltd., London, UK.
Anti-vimentin IgG1, clone V9	Sigma-Aldrich, Dorset, UK.
BSP polyclonal IgG1	Dr. L. Fisher, NIH, Bethesda, USA.
CellTracker™ green	Invitrogen, Paisley, UK.
DAPI	Sigma-Aldrich, Dorset, UK.
Donkey serum albumin	Serotec, Oxford, UK.
FITC-conjugated donkey anti-mouse IgG	Jackson ImmunoResearch, USA.
FITC-conjugated donkey anti-rabbit IgG	Jackson ImmunoResearch, USA.
Methanol (grade 99.9 %)	BDH, Manchester, UK.
Mouse IgG1 (monoclonal negative control)	Dako Ltd., Cambridge, UK.
ON polyclonal IgG1	Dr. L. Fisher, NIH, Bethesda, USA
OP polyclonal IgG1	Dr. L. Fisher, NIH, Bethesda, USA.
P-4-H monoclonal IgG1, Clone 5B5	Dako Ltd., Cambridge, UK.
Triton-X100	Sigma-Aldrich, Dorset, UK.

Quantitative Polymerase chain reaction

ABI PRISM™ Optical Adhesive Covers	Applied Biosystems, Cheshire, UK.
Assays-on-Demand™ Gene Expression assay Mix (including TaqMan® probes)	
Hs00164004_m1	Applied Biosystems, Cheshire, UK.
Hs00164004_m1	Applied Biosystems, Cheshire, UK.
Hs00231692_m1	Applied Biosystems, Cheshire, UK.
Hs00277762_m1	Applied Biosystems, Cheshire, UK.
Hs00420085_m1	Applied Biosystems, Cheshire, UK.
Hs99999901_s1	Applied Biosystems, Cheshire, UK.
Ethanol	BDH, Manchester, UK.
High Capacity cDNA Archive kit	Applied Biosystems, Cheshire, UK.
RNeasy Mini Kit	Qiagen Ltd., W Sussex, UK.
TaqMan Universal PCR Master Mix	Applied Biosystems, Cheshire, UK.
β-mercaptoethanol	Sigma-Aldrich, Dorset, UK.
Optical 96-Well Reaction Plates	Applied Biosystems, Cheshire, UK.

Cell density evaluation

Propidium iodide	Sigma-Aldrich, Dorset, UK.
CyQUANT Cell Proliferation Assay Kit	Invitrogen, Paisley, UK.

Glass substrate/scaffold production and characterisation

$CaCo_3$	BDH, Manchester, UK.
NaH_2Po_4	BDH, Manchester, UK.
P_2O_5	BDH, Manchester, UK.
Fe_2O_3	BDH, Manchester, UK.
SpeciFix-20 resin kit	Struers Ltd., Glasgow, UK.
RTV 118 silicone	Techsil Ltd. Warwickshire, UK.
Cyanoacrylate gel (01-06854)	Henkel UK Ltd., Hertfordshire, UK.
MD polishing cloth (Largo, DAC, NAP)	Struers Ltd., Glasgow, UK.
DP-suspension (1,3 and 9 μM)	Struers Ltd., Glasgow, UK.

2. Media and Solutions

Growth Medium (GM)

	For 500 ml
89% DMEM	455 ml
10% FCS	50 ml
1% Penicillin/streptomycin	5 ml

Freezing Medium

	For 1 ml
90% FCS	900 µl
10% DMSO	100 µl

DAPI

	For 1000 µl
DAPI stock solution (in DMSO)	1 µl
PBS	999 µl

Propidium iodide

	For 1000 µl
PI stock solution (in DMSO)	1 µl
PBS	999 µl

Secondary antibody non-specific blocking solution

	For 10 ml
Donkey serum albumin	1 ml
PBS	9 ml

Polyclonal antibody negative control

	For 10 ml
FCS	1 ml
PBS	9 µl

0.25% Triton-X 100

	For 100 ml
Triton-X 100	2.5 ml of a 1% stock solution
dH2O	97.5 ml

CyQUANT GR dye

	For 20 ml
dH2O	19 ml
CyQUANT cell lysis buffer	1 ml
CyQUANT GR stock solution	1:400 of the above

cDNA preparation (High Capacity cDNA Archive kit)

	For 60 µl reaction volume
10X Reverse Transcription Buffer	6 µl
25X dNTPs	2.4 µl
10X random primers	6 µl
MultiScribe™ Reverse Transcriptase	3 µl
Nuclease-free H2O	12.6 µl
RNA solution (in Nuclease-free H2O)	30 µl

qPCR reaction sample

	For 25 µl reaction volume
TaqMan Universal PCR Master Mix (2X)	12.5 µl
20X Assays-on-Demand™ Gene Expression Assay Mix	1.25 µ
Nuclease-free H_2O	8.75 µl
cDNA	2.5 µl

3. Antibody concentrations

Antibody	Function	Diluent	Concentration
BSP	Primary polyclonal	PBS	1:100
Cy3-conjugated α-vimentin/cloneV9	Primary monoclonal	PBS	1:300
FITC-conjugated donkey α -mouse	Secondary monoclonal	PBS	1:200
FITC-conjugated donkey α-rabbit	Secondary polyclonal	PBS	1:200
Mouse IgG1	Monoclonal negative control	PBS	1:50
ON	Primary polyclonal	PBS	1:100
OP	Primary polyclonal	PBS	1:100
α-P-4-H/clone 5b5	Primary monoclonal	PBS	1:50

4. Equipment

ABI PRISM® 7300 SD System	Applied Biosystems, Cheshire, UK..
Dicor furnace	Dentsply, Surrey, UK.
Glass fibre rig	Eastman Dental Institute, London, UK.
IPS-12 multi-speed roller pump	Sotax, Basel, Switzerland.
Leica DM-IRB inverted microscope	Leica Microsystems UK Ltd., Bucks, UK
Fluroskan Ascent plate reader	Labsystems, Helsinki, Finland.
RTF 1500 furnace	Carbolite, Derbyshire, UK.
Shellab 2123-2 incubator	Sheldon INC., OR, USA.
Testbourne diamond saw	Testbourne Ltd., Hampshire, UK.
Ultrospec 2000 UV spectrophotometer	Pharmacia Biotech, Cambridge, UK.

5. Software

- Fluorescence microscopy image acquisition, pseudo colouring and composition:

Leica FW4000 software Leica Microsystems UK Ltd., Bucks, UK.

- Glass fibre diameter measurement/ image analysis:

Image-Pro® Plus software4.0	Media Cybernetics UK, Berkshire, UK.

- qPCR data acquisition and relative quantification:

7300 SDS software	Applied Biosystems, Cheshire, UK.

- Raster to vector image conversion:

Autotrace 0.31.1 (open source)	www.sourceforge.org

- Statistical analysis:

SPSS for windows (release 11)	SPSS UK Ltd. , Surrey, UK.

- Vector image generation

Inkscape SVG editor 0.42 (open source)	www.sourceforge.org

- 3D image generation:

Truespace 3.2	Caligari Corporation, CA, USA.

References

Ahmad,M., McCarthy,M.B., and Gronowicz,G. (1999). An *in vitro* model for mineralisation of human osteoblast-like cells on implant materials. Biomaterials *20*, 211-20.

Ahmed,I., Collins,C.A., Lewis,M.P., Olsen,I., and Knowles,J.C. (2004). Processing, characterisation and biocompatibility of iron-phosphate glass fibres for tissue engineering. Biomaterials *25*, 3223-3232.

Ahmed,I., Lewis,M., Olsen,I., and Knowles,J.C. (2004). Phosphate glasses for tissue engineering: Part 2. Processing and characterisation of a ternary-based P2O5-CaO-Na2O glass fibre system. Biomaterials *25*, 501-507.

Alberto,P.L. (2004). Guided tissue regeneration in jaw reconstruction: Review and applications. Journal of Oral and Maxillofacial Surgery *62*, 89.

Alsberg,E., Hill,E.E., and Mooney,D.J. (2001). Craniofacial tissue engineering. Crit Rev Oral Biol Med *12*, 64-75.

Alsberg,E., Kong,H.J., Hirano,Y., Smith,M.K., Albeiruti,A., and Mooney,D.J. (2003). Regulating Bone Formation via Controlled Scaffold Degradation. J Dent Res *82*, 903-908.

Aparicio,C., Gil,F.J., Planell,J.A., and Engel,E. (2002). Human-osteoblast proliferation and differentiation on grit-blasted and bioactive titanium for dental applications. J. Mater. Sci. Mater. Med. *13*, 1105-1111.

Armitage,G.C., Avery,J.K., Bhaskar,S.N., Hand,A.R., Johnson,M.C., Melcher,A.H., Kapur,S.P., Sharawy,M., Stern,I.B., Sulik,K.K., Ten Cate,A.R., Vidic,B., and Yaeger,J.A. (1990). Orban's oral histology and embryology. (St. Louis: Mosby).

Aviles,A.J., Theodorou,S., Sekosen,M., Schraufnagel,D., and Ramasastry,S. (2004). Challenging Alexis Carrel: a study in alternate microvascular techniques. Neurol Res *26*, 809-15.

BAÈÁKOVÁ,L., FILOVÁ,E., RYPÁÈEK,F., ŠVORÈÍK,V., and STARÝ,V. (2004). Cell Adhesion on Artificial Materials for Tissue Engineering. Physiol. Res. *53*, S35-S45.

Bakker,D.P., van der Plaats,A., Verkerke,G.J., Busscher,H.J., and van der Mei,H.C. (2003). Comparison of Velocity Profiles for Different Flow Chamber Designs Used in Studies of Microbial Adhesion to Surfaces. Appl Environ Microbiol *69*, 6280-6287.

Baksh,D., Song,L., and Tuan,R.S. (2004). Adult mesenchymal stem cells: characterization, differentiation, and application in cell and gene therapy. J Cell Mol Med *8*, 301-16.

Beck,G.R., Jr., Zerler,B., and Moran,E. (2000). Phosphate is a specific signal for induction of osteopontin gene expression. Proc. Natl. Acad. Sci. U. S. A *97*, 8352-8357.

Becker,D. (1990). [Function-related reconstruction of chronic syndesmosis ruptures by implantation of a dacron ligament]. Beitr Orthop Traumatol *37*, 551-61.

Benjamin,M., Bollow,M., Braun,J., Brandt,J., Braun,J., Braun,J., Sieper,J., Burgos-Vargas,R., Claudepierre,P., De Vlam,K., Veys,E., Eulderink,F., Fassbender,H.-G., Fitzgerald,O., Francois,R., Haupl,T., Sittinger,M., Heinegard,D., Khan,M.A., Kriegsmann,J., Gay,S., Leirisalo-Repo,M., Mcgonagle,D., Olivieri,I., Sieper,J., Braun,J., Zhang,Y., and Poole,A.R. (2000). Anatomy and biochemistry of entheses. Ann Rheum Dis *59*, 995-999.

Berg,E.E. (1992). Intrinsic healing of a patellar tendon donor site defect after anterior cruciate ligament reconstruction. Clin Orthop Relat Res 160-3.

Birk,D. and Trelstad,R. (1986). Extracellular compartments in tendon morphogenesis: collagen fibril, bundle, and macroaggregate formation. J. Cell Biol *103*, 231-240.

Buijtenhuijs,P., Buttafoco,L., Poot,A.A., Daamen,W.F., van Kuppevelt,T.H., Dijkstra,P.J., De Vos,R.A.I., Sterk,L.M.T., Geelkerken,B.R.H., Feijen,J., and Vermes,I. (2004). Tissue engineering of blood vessels: characterization of smooth-muscle cells for culturing on collagen-and-elastin-based scaffolds. Biotechnology and Applied Biochemistry *39*, 141-149.

Boden,S.D. (1999). Bioactive factors for bone tissue engineering. Clin Orthop Relat Res S84-S94.

Boleti,H., Ojcius,D.M., and Dautry-Varsat,A. (2000). Fluorescent labelling of intracellular bacteria in living host cells. Journal of Microbiological Methods *40*, 265-274.

Borovsky,J.E. and Suszcynsky,D.M. (1991). Reduction of secondary-electron yields by collective electric fields within metals. PHYSICAL. REVIEW. A *43*, 1433-1440.

Bosseloir,A., Heinen,E., Defrance,T., Bouzhazha,F., Antoine,N., and Simar,L.J. (1994). Moabs MAS516 and 5B5, two fibroblast markers, recognize human follicular dendritic cells. Moabs MAS516 and 5B5, two fibroblast markers, recognize human follicular dendritic cells *42*, 49-54.

Botchwey,E.A., Pollack,S.R., Levine,E.M., and Laurencin,C.T. (2001). Bone tissue engineering in a rotating bioreactor using a microcarrier matrix system. J Biomed Mater Res *55*, 242-253.

Braddock,M., Houston,P., Campbell,C., and Ashcroft,P. (2001). Born again bone: tissue engineering for bone repair. News Physiol Sci *16*, 208-213.

Brekke,J.H. and Toth,J.M. (1998). Principles of tissue engineering applied to programmable osteogenesis. J Biomed Mater Res *43*, 380-398.

Bring,D.K.I., Heidgren,M.L., Kreicbergs,A., and Ackermann,P.W. (2005). Increase in sensory neuropeptides surrounding the Achilles tendon in rats with adjuvant arthritis. J Orthop Res *23*, 294-301.

Brown,T.D. (2000). Techniques for mechanical stimulation of cells *in vitro*: a review. J Biomech *33*, 3-14.

Bruder,S.P. and Fox,B.S. (1999). Tissue engineering of bone. Cell based strategies. Clin Orthop Relat Res S68-S83.

Bunting,S., Di Silvio,L., Deb,S., and Hall,S. (2005). Bioresorbable glass fibres facilitate peripheral nerve regeneration. The Journal of Hand Surgery: Journal of the British Society for Surgery of the Hand *30*, 242-247.

Burg,K.J., Porter,S., and Kellam,J.F. (2000). Biomaterial developments for bone tissue engineering. Biomaterials *21*, 2347-2359.

Buttafoco,L., Kolkman,N.G., Engbers-Buijtenhuijs,P., Poot,A.A., Dijkstra,P.J., Vermes,I., and Feijen,J. (2006). Electrospinning of collagen and elastin for tissue engineering applications. Biomaterials *27*, 724-734.

Cancedda,R., Dozin,B., Giannoni,P., and Quarto,R. (2003). Tissue engineering and cell therapy of cartilage and bone. Matrix Biol. *22*, 81-91.

Cervenkova,K., Belejova,M., Vesely,J., Chmela,Z., Rypka,M., Ulrichova,J., Modriansky,M., and Maurel,P. (2001). Cell suspensions, cell cultures, and tissue slices--important metabolic *in vitro* systems. Biomed. Pap. Med. Fac. Univ Palacky. Olomouc. Czech. Repub. *145*, 57-60.

Charvet,J.L., Cordes,J.A., and Alexander,H. (2000). Mechanical and fracture behavior of a fiber-reinforced bioabsorbable material for orthopaedic applications. J Mater Sci Mater Med *11*, 101-109.

Choksey,A., Soonawalla,D., and Murray,J. (1996). Repair of neglected achilles tendon ruptures with Marlex mesh. Injury *27*, 215-217.

Choueka,J., Charvet,J.L., Alexander,H., Oh,Y.O., Joseph,G., Blumenthal,N.C., and LaCourse,W.C. (1995). Effect of annealing temperature on the degradation of reinforcing fibers for absorbable implants. J Biomed Mater Res *29*, 1309-15.

Claudepierre,P. and Voisin,M.C. (2005). The entheses: histology, pathology, and pathophysiology. Joint Bone Spine *72*, 32-7.

Clover,J. and Gowen,M. (1994). Are MG-63 and HOS TE85 human osteosarcoma cell lines representative models of the osteoblastic phenotype? Bone *15*, 585-591.

Clupper,D.C., Gough,J.E., Embanga,P.M., Notingher,I., Hench,L.L., and Hall,M.M. (2004). Bioactive evaluation of 45S5 bioactive glass fibres and preliminary study of human osteoblast attachment. Journal of Materials Science: Materials in Medicine *15*, 803-808.

Coleman,B.D., Khan,K.M., Maffulli,N., Cook,J.L., and Wark,J.D. (2000). Studies of surgical outcome after patellar tendinopathy: clinical significance of methodological deficiencies and guidelines for future studies. Scandinavian Journal of Medicine and Science in Sports *10*, 2-11.

Comley,A.S. and Krishnan,J. (1999). Donor site morbidity after quadriceps tendon harvest for rotator cuff repair. Aust N Z J Surg *69*, 808-10.

Cook,J.L. and Khan,K.M. (2001). What is the most appropriate treatment for patellar tendinopathy? Br J Sports Med *35*, 291-294.

Cook,J.L., Khan,K.M., and Purdam,C. (2002). Achilles tendinopathy. Br J Sports Med *7*, 121-130.

Cooper,J.A., Lu,H.H., Ko,F.K., Freeman,J.W., and Laurencin,C.T. (2005). Fiber-based tissue-engineered scaffold for ligament replacement: design considerations and *in vitro* evaluation. Biomaterials *26*, 1523-1532.

Cortes,Z.E. and Maloney,M.D. (2004). Anterior cruciate ligament reconstruction in osteogenesis imperfecta: a case report. Am J Sports Med *32*, 1317-1322.

Cowles,E.A., Brailey,L.L., and Gronowicz,G.A. (2000). Integrin-mediated signaling regulates AP-1 transcription factors and proliferation in osteoblasts. J. Biomed. Mater. Res. *52*, 725-737.

Croteau,S., Rauch,F., Silvestri,A., and Hamdy,R.C. (1999). Bone morphogenetic proteins in orthopedics: from basic science to clinical practice. Orthopedics *22*, 686-95.

Culav,E.M., Clark,C.H., and Merrilees,M.J. (1999). Connective tissues: matrix composition and its relevance to physical therapy. Phys Ther *79*, 308-19.

De Luca,A., Pierno,S., Natuzzi,F., Franchini,C., Duranti,A., Lentini,G., Tortorella,V., Jockusch,H., and Camerino,D.C. (1997). Evaluation of the Antimyotonic Activity of Mexiletine and Some New Analogs on Sodium Currents of Single Muscle Fibers and on the Abnormal Excitability of the Myotonic ADR Mouse. J Pharmacol Exp Ther *282*, 93-100.

Descamps,O.S., Leysen,X., Van Leuven,F., and Heller,F.R. (2001). The use of Achilles tendon ultrasonography for the diagnosis of familial hypercholesterolemia. Atherosclerosis *157*, 514-518.

Dhore,C.R., Cleutjens,J.P., Lutgens,E., Cleutjens,K.B., Geusens,P.P., Kitslaar,P.J., Tordoir,J.H., Spronk,H.M., Vermeer,C., and Daemen,M.J. (2001). Differential expression of bone matrix regulatory proteins in human atherosclerotic plaques. Arterioscler. Thromb. Vasc. Biol *21*, 1998-2003.

Doschak,M.R. and Zernicke,R.F. (2005). Structure, function and adaptation of bone-tendon and bone-ligament complexes. J Musculoskelet Neuronal Interact *5*, 35-40.

Dressler,M.R., Butler,D.L., and Boivin,G.P. (2005). Effects of age on the repair ability of mesenchymal stem cells in rabbit tendon. J Orthop Res *23*, 287-293.

Dubin-Thaler,B.J., Giannone,G., Dobereiner,H.G., and Sheetz,M.P. (2004). Nanometer analysis of cell spreading on matrix-coated surfaces reveals two distinct cell states and STEPs. Biophys. J. *86*, 1794-1806.

Ducheyne,P. and Qiu,Q. (1999). Bioactive ceramics: the effect of surface reactivity on bone formation and bone cell function. Biomaterials *20*, 2287-2303.

Elisseeff,J., Puleo,C., Yang,F., and Sharma,B. (2005). Advances in skeletal tissue engineering with hydrogels. Orthodontics and Craniofacial Research *8*, 150-161.

Eriksson,K., Anderberg,P., Hamberg,P., Olerud,P., and Wredmark,T. (2001). There are differences in early morbidity after ACL reconstruction when comparing patellar tendon and semitendinosus tendon graft. A prospective randomized study of 107 patients. Scandinavian Journal of Medicine and Science in Sports *11*, 170-177.

Evans,R.D., Perkins,V.C., Henry,A., Stephens,P.E., Robinson,M.K., and Watt,F.M. (2003). A tumor-associated {beta}1 integrin mutation that abrogates epithelial differentiation control. J. Cell Biol. *160*, 589-596.

Federman,S., Miller,L.M., and Sagi,I. (2002). Following matrix metalloproteinases activity near the cell boundary by infrared micro-spectroscopy. Matrix Biology *21*, 567-577.

Fenwick,S.A., Hazleman,B.L., and Riley,G.P. (2002). The vasculature and its role in the damaged and healing tendon. Arthritis Res *4*, 252-260.

Ferguson,M.W. and O'Kane,S. (2004). Scar-free healing: from embryonic mechanisms to adult therapeutic intervention. Phil. Trans. R Soc. B Biol. Sci *359*, 839-850.

Forriol,F. and Shapiro,F. (2005). Bone development: interaction of molecular components and biophysical forces. Clin. Orthop. Relat Res. 14-33.

Fisher,L.W., Stubbs III,J.T., and Young,M.F. (1995). Antisera and cDNA probes to human and certain animal model bone matrix noncollagenous proteins. Acta Orthopaedica Scandinavica, Supplement *66*, 61-65.

Franceschi,R.T. and Iyer,B.S. (1992). Relationship between collagen synthesis and expression of the osteoblast phenoType In MC3T3-E1 cells. Journal Of Bone And Mineral Research: The Official Journal Of The American Society For Bone And Mineral Research *7*, 235-246.

Frangos,J.A., McIntire,L.V., and Eskin,S.G. (1987). Shear stress induced stimulation of mammalian cell metabolism. Biotechnol. Bioeng. *32*, 1053-1060.

Frank,C.B. (2004). Ligament structure, physiology and function. J Musculoskelet Neuronal Interact *4*, 199-201.

Franks,K., Abrahams,I., Georgiou,G., and Knowles,J.C. (2001). Investigation of thermal parameters and crytallisation in a ternary CaO-Na2O-P2O5-based glass system. Biomaterials *22*, 497-501.

Franks,K., Abrahams,I., and Knowles,J.C. (2000). Development of soluble glasses for biomedical use Part I: *in vitro* solubility measurement. J. Mater. Sci. Mater. Med. *11*, 609-614.

Fujihara,K., Kotaki,M., and Ramakrishna,S. (2005). Guided bone regeneration membrane made of polycaprolactone/calcium carbonate composite nano-fibers. Biomaterials *26*, 4139-4147.

Gabriella,D., V, Berlingieri,M.T., Visconti,R., Castellone,M.D., Viglietto,G., Baldassarre,G., Zannini,M., Bellacosa,A., Tsichlis,P.N., Fusco,A., and Santoro,M. (2000). Akt/Protein Kinase B Promotes Survival and Hormone-independent Proliferation of Thyroid Cells in the Absence of Dedifferentiating and Transforming Effects. Cancer Res *60*, 3916-3920.

Gay,C.V., Gilman,V.R., and Sugiyama,T. (2000). Perspectives on osteoblast and osteoclast function. Poult. Sci. *79*, 1005-1008.

Gibbs, P. Is glass solid or liquid? 1996. Department of Mathematics, University of California, USA.
Ref Type: Report

Goh,J.C., Ouyang,H.W., Teoh,S.H., Chan,C.K., and Lee,E.H. (2003). Tissue-engineering approach to the repair and regeneration of tendons and ligaments. Tissue Eng *9 Suppl 1:S31-44.*, S31-S44.

Gosline,J., Lillie,M., Carrington,E., Guerette,P., Ortlepp,C., and Savage,K. (2002). Elastic proteins: biological roles and mechanical properties. Philos Trans R Soc Lond B Biol Sci *357*, 121-32.

Gough,J.E., Christian,P., Scotchford,C.A., and Jones,I.A. (2003). Long-term craniofacial osteoblast culture on a sodium phosphate and a calcium/sodium phosphate glass. J Biomed Mater Res A *66A*, 233-240.

Gough,J.E., Christian,P., Scotchford,C.A., Rudd,C.D., and Jones,I.A. (2002). Synthesis, degradation, and *in vitro* cell responses of sodium phosphate glasses for craniofacial bone repair. J Biomed Mater Res A *59*, 481-489.

Grabowski,E.F., Zuckerman,D.B., and Nemerson,Y. (1993). The functional expression of tissue factor by fibroblasts and endothelial cells under flow conditions. Blood *81*, 3265-3270.

Grinnell,F. (1994). Fibroblasts, myofibroblasts, and wound contraction. J Cell Biol *124*, 401-404.

Grzesik,W.J., Frazier,C.R., Shapiro,J.R., Sponseller,P.D., Robey,P.G., and Fedarko,N.S. (2002). Age-related changes in human bone proteoglycan structure. Impact of osteogenesis imperfecta. J. Biol. Chem. *277*, 43638-43647.

Gugala,Z. and Gogolewski,S. (2002). Healing of critical-size segmental bone defects in the sheep tibiae using bioresorbable polylactide membranes. Injury *33*, 71-76.

Gunatillake,P.A. and Adhikari,R. (2003). Biodegradable synthetic polymers for tissue engineering. Eur Cell Mater *5*, 1-16.

Hakkinen,L.A.R.I., Uitto,V.J., and Larjava,H.A.N.N. (2000). Cell biology of gingival wound healing. Periodontology 2000 *24*, 127-152.

Harakas,N.K. (1984). Demineralized bone-matrix-induced osteogenesis. Clin Orthop Relat Res 239-51.

Hauschka,P.V., Lian,J.B., Cole,D.E., and Gundberg,C.M. (1989). Osteocalcin and matrix Gla protein: vitamin K-dependent proteins in bone. Physiol Rev. *69*, 990-1047.

Haverstick,D.M., Heady,T.N., Macdonald,T.L., and Gray,L.S. (2000). Inhibition of Human Prostate Cancer Proliferation *in vitro* and in a Mouse Model by a Compound Synthesized to Block Ca2+ Entry. Cancer Res *60*, 1002-1008.

Hayem,G. (2001). Tenology: a new frontier. Joint Bone Spine *68*, 19-25.

Hench,L.L. (1998). Biomaterials: a forecast for the future. Biomaterials *19*, 1419-23.

Herrington,L., Wrapson,C., Matthews,M., and Matthews,H. (2005). Anterior Cruciate Ligament reconstruction, hamstring versus bone-patella tendon-bone grafts: a systematic literature review of outcome from surgery. The Knee *12*, 41-50.

Hillsley,M.V. and Frangos,J.A. (1997). Alkaline phosphatase in osteoblasts is down-regulated by pulsatile fluid flow. *60*, 48-53.

Hing,K.A. (2004). Bone repair in the twenty-first century: biology, chemistry or engineering? Philos. Transact. A Math. Phys. Eng Sci. *362*, 2821-2850.

Hokugo,A., Kubo,Y., Takahashi,Y., Fukuda,A., Horiuchi,K., Mushimoto,K., Morita,S., and Tabata,Y. (2004). Prefabrication of vascularized bone graft using guided bone regeneration. Tissue Eng *10*, 978-86.

Holmes,T.C. (2002). Novel peptide-based biomaterial scaffolds for tissue engineering. Trends Biotechnol. *20*, 16-21.

Holtorf,H.L., Jansen,J.A., and Mikos,A.G. (2005). Flow perfusion culture induces the osteoblastic differentiation of marrow stroma cell-scaffold constructs in the absence of dexamethasone. J. Biomed. Mater. Res. A *72*, 326-334.

Holy,C.E., Shoichet,M.S., and Davies,J.E. (2000). Engineering three-dimensional bone tissue *in vitro* using biodegradable scaffolds: investigating initial cell-seeding density and culture period. J. Biomed. Mater. Res. *51*, 376-382.

Hughes,L.C., Archer,C.W., and ap Gwynn,I. (2005). The ultrastructure of mouse articular cartilage: Collagen orientation and implications for tissue functionality. A polarised light and scanning electron microscope study and review. Euro. Cells. Mater *9*, 68-84.

Hung,C.T., Allen,F.D., Pollack,S.R., Attia,E.T., Hannafin,J.A., and Torzilli,P.A. (1997). Intracellular Calcium Response of ACL and MCL Ligament Fibroblasts to Fluid-Induced Shear Stress. Cellular Signalling *9*, 587-594.

Irwin,C.R., Myrillas,T.T., Traynor,P., Leadbetter,N., and Cawston,T.E. (2002). The role of soluble interleukin (IL)-6 receptor in mediating the effects of IL-6 on matrix metalloproteinase-1 and tissue inhibitor of metalloproteinase-1 expression by gingival fibroblasts. J Periodontol *73*, 741-747.

Itoh,H., Aso,Y., Furuse,M., Noishiki,Y., and Miyata,T. (2001). A honeycomb collagen carrier for cell culture as a tissue engineering scaffold. Artif. Organs *25*, 213-217.

Jarvinen,M., Jozsa,L., Kannus,P., Jarvinen,T.L., Kvist,M., and Leadbetter,W. (1997). Histopathological findings in chronic tendon disorders. Scand J Med Sci Sports *7*, 86-95.

Jonasova,L., Muller,F.A., Helebrant,A., Strnad,J., and Greil,P. (2002). Hydroxyapatite formation on alkali-treated titanium with different content of Na+ in the surface layer. Biomaterials *23*, 3095-3101.

Jozsa,L., Reffy,A., Balint,B.J., and Demel,Z. (1981). Involvement of tendons in inherited diseases. Acta Paediatr Acad Sci Hung *22*, 293-298.

Kader,D., Saxena,A., Movin,T., and Maffulli,N. (2002). Achilles tendinopathy: some aspects of basic science and clinical management. Br J Sports Med *36*, 239-249.

Kadler,K.E., Holmes,D.F., Trotter,J.A., and Chapman,J.A. (1996). Collagen fibril formation. Biochem J *316 (Pt 1)*, 1-11.

Kannus,P. (2000). Structure of the tendon connective tissue. Scand J Med Sci Sports *10*, 312-320.

Karsenty,G. (2000). Role of Cbfa1 in osteoblast differentiation and function. Semin Cell Dev Biol *11*, 343-346.

Kartus,J., Ejerhed,L., Sernert,N., Brandsson,S., and Karlsson,J. (2000). Comparison of traditional and subcutaneous patellar tendon harvest. A prospective study of donor site-related problems after anterior cruciate ligament reconstruction using different graft harvesting techniques. Am J Sports Med *28*, 328-35.

Kartus,J., Lindahl,S., Stener,S., Eriksson,B.I., and Karlsson,J. (1999). Magnetic Resonance Imaging of the Patellar Tendon After Harvesting Its Central Third: A Comparison Between Traditional and Subcutaneous Harvesting Techniques. Arthroscopy: The Journal of Arthroscopic & Related Surgery *15*, 587-593.

Kartus,J., Movin,T., and Karlsson,J. (2001). Donor-site morbidity and anterior knee problems after anterior cruciate ligament reconstruction using autografts. Arthroscopy: The Journal of Arthroscopic & Related Surgery *17*, 971-980.

Kato,Y.P., Dunn,M.G., Zawadsky,J.P., Tria,A.J., and Silver,F.H. (1991). Regeneration of Achilles tendon with a collagen tendon prosthesis. Results of a one-year implantation study. J Bone Joint Surg Am *73*, 561-74.

Khang,G., Jeon,J.H., Lee,J.W., Cho,S.C., and Lee,H.B. (1997). Cell and platelet adhesions on plasma glow discharge-treated poly(lactide-co-glycolide). Biomed. Mater. Eng *7*, 357-368.

Kim,S.G., Akaike,T., Sasagaw,T., Atomi,Y., and Kurosawa,H. (2002). Gene expression of Type I and Type III collagen by mechanical stretch in anterior cruciate ligament cells. Cell Struct Funct *27*, 139-44.

Kimura,A., Aoki,M., Fukushima,S., Ishii,S., and Yamakoshi,K. (2003). Reconstruction of a defect of the rotator cuff with polytetrafluoroethylene felt graft. Recovery of tensile strength and histocompatibility in an animal model. J Bone Joint Surg Br *85-B*, 282.

Kjaer,M., Langberg,H., Miller,B.F., Boushel,R., Crameri,R., Koskinen,S., Heinemeier,K., Olesen,J.L., Dossing,S., Hansen,M., Pedersen,S.G., Rennie,M.J., and Magnusson,P. (2005). Metabolic activity and collagen turnover in human tendon in response to physical activity. J Musculoskelet Neuronal Interact *5*, 41-52.

Kjaer,M.I.C.H. (2004). Role of Extracellular Matrix in Adaptation of Tendon and Skeletal Muscle to Mechanical Loading. Physiol. Rev *84*, 649-698.

Knabe,C., Stiller,M., Berger,G., Reif,D., Gildenhaar,R., Howlett,C.R., and Zreiqat,H. (2005). The effect of bioactive glass ceramics on the expression of bone-related genes and proteins *in vitro*. Clinical Oral Implants Research *16*, 119-127.

Knowles,J.C., Franks,K., and Abrahams,I. (2001). Investigation of the solubility and ion release in the glass system K2O- Na2O-CaO-P2O5. Biomaterials *22*, 3091-3096.

Knott,L., Tarlton,J.F., and Bailey,A.J. (1997). Chemistry of collagen cross-linking: biochemical changes in collagen during the partial mineralization of turkey leg tendon. Biochem. J. *322*, 535-542.

Kramer,I., Wibulswas,A., Croft,D., and Genot,E. (2003). Rheumatoid arthritis: targeting the proliferative fibroblasts. Prog Cell Cycle Res *5:59-70.*, 59-70.

Langer,R. and Vacanti,J.P. (1993). Tissue engineering. Science *260*, 920-6.

Laurencin,C.T., Ambrosio,A.M.A., Borden,M.D., and Cooper,J.A. (1999). Tissue Engineering: Orthopedic Applications. Annual Review of Biomedical Engineering *1*, 19-46.

Lee,C.H., Singla,A., and Lee,Y. (2001). Biomedical applications of collagen. Int J Pharm *221*, 1-22.

Lemkin,P.F., Myrick,J.M., Lakshmanan,Y., Shue,M.J., Patrick,J.L., Hornbeck,P.V., Thornwal,G.C., and Partin,A.W. (1999). Exploratory data analysis groupware for qualitative and quantitative electrophoretic gel analysis over the Internet-WebGel. Electrophoresis *20*, 3492-3507.

Lim,J.Y., Liu,X., Vogler,E.A., and Donahue,H.J. (2004). Systematic variation in osteoblast adhesion and phenotype with substratum surface characteristics. J. Biomed. Mater. Res. A *68*, 504-512.

Lin,S.T., Krebs,S.L., Kadiyala,S., Leong,K.W., LaCourse,W.C., and Kumar,B. (1994). Development of bioabsorbable glass fibres. Biomaterials *15*, 1057-1061.

Lin,T.W., Cardenas,L., and Soslowsky,L.J. (2004). Biomechanics of tendon injury and repair. J Biomech *37*, 865-877.

Linder,L.H., Sukin,D.L., Burks,R.T., and Haut,R.C. (1994). Biomechanical and histological properties of the canine patellar tendon after removal of its medial third. Am J Sports Med *22*, 136-42.

Lodish,H., Berk,A., Zipursky,L.S., Matsudaira,P., Baltimore,D., and Darnell,J. (2004). Molecular cell biology. (New York: W.H. Freeman).

Lygoe,K.A., Norman,J.T., Marshall,J.F., and Lewis,M.P. (2004). alphav integrins play an important role in myofibroblast differentiation. Wound Repair and Regeneration *12*, 461-470.

Mackie,E.J. (2003). Osteoblasts: novel roles in orchestration of skeletal architecture. The International Journal of Biochemistry & Cell Biology *35*, 1301-1305.

Maffulli,N. (1999). Rupture of the Achilles tendon. J Bone Joint Surg Am *81*, 1019-36.

Maffulli,N., Moller,H.D., and Evans,C.H. (2002). Tendon healing: can it be optimised? Br J Sports Med *36*, 315-316.

Mancini,M., Anderson,B.O., Caldwell,E., Sedghinasab,M., Paty,P.B., and Hockenbery,D.M. (1997). Mitochondrial Proliferation and Paradoxical Membrane Depolarization during Terminal Differentiation and Apoptosis in a Human Colon Carcinoma Cell Line. The Journal of Cell Biology *138*, 449-469.

Martin,C., Winet,H., and Bao,J.Y. (196). Acidity near eroding polylactide-polyglycolide *in vitro* and in vivo in rabbit tibial bone chambers. Biomaterials *17*, 2373-2380.

Martinek,V., Latterman,C., Usas,A., Abramowitch,S., Woo,S.L., Fu,F.H., and Huard,J. (2002). Enhancement of tendon-bone integration of anterior cruciate ligament grafts with bone morphogenetic protein-2 gene transfer: a histological and biomechanical study. J Bone Joint Surg Am *84-A*, 1123-1131.

Matsumoto,F., Trudel,G., Uhthoff,H.K., and Backman,D.S. (2003). Mechanical Effects of Immobilization on the Achilles' Tendon. Arch Phys Med Rehabil *84*, 662-667.

Meikle,M.C., Papaioannou,S., Ratledge,T.J., Speight,P.M., Watt-Smith,S.R., Hill,P.A., and Reynolds,J.J. (1994). Effect of poly DL-lactide--co-glycolide implants and xenogeneic bone matrix-derived growth factors on calvarial bone repair in the rabbit. Biomaterials *15*, 513-521.

Misof,K., Landis,W.J., Klaushofer,K., and Fratzl,P. (1997). Collagen from the osteogenesis imperfecta mouse model (oim) shows reduced resistance against tensile stress. J Clin Invest *100*, 40-45.

Mitchell,B. and Sharma,R. (2004). Embryology : an illustrated colour text. (Edinburgh ; New York: Churchill Livingstone).

Mooney,D.J., Mazzoni,C.L., Breuer,C., McNamara,K., Hern,D., Vacanti,J.P., and Langer,R. (1996). Stabilized polyglycolic acid fibre-based tubes for tissue engineering. Biomaterials *17*, 115-124.

Mollenhauer,H.H., James Morre,D., and Rowe,L.D. (1990). Alteration of intracellular traffic by monensin; mechanism, specificity and relationship to toxicity. Biochimica et Biophysica Acta (BBA) - Reviews on Biomembranes *1031*, 225-246.

Navarro,F.A., Mizuno,S., Huertas,J.C., Glowacki,J., and Orgill,D.P. (2001). Perfusion of medium improves growth of human oral neomucosal tissue constructs. Wound Repair Regen *9*, 507-512.

Navarro,M., Ginebra,M.-P., Clement,J., Salvador,M., Gloria,A., and Planell,J.A. (2003). Physicochemical Degradation of Titania-Stabilized Soluble Phosphate Glasses for Medical Applications. Journal of the American Ceramic Society *86*, 1345-1352.
Nelson,D.L. and Cox,M.M. (2004). Principles of Biochemistry. (New York: W. H. Freeman).

Ng,B.H., Chou,S.M., Lim,B.H., and Chong,A. (2004). Strain rate effect on the failure properties of tendons. Proc. Instn Mech. Engrs *218*, 203-206.

Nistor,L. (1981). Surgical and non-surgical treatment of Achilles Tendon rupture. A prospective randomized study. J Bone Joint Surg Am *63*, 394-9.

Novikova,L.N., Novikov,L.N., and Kellerth,J.O. (2003). Biopolymers and biodegradable smart implants for tissue regeneration after spinal cord injury. Curr Opin Neurol *16*, 711-5.

Noth,U., Osyczka,A.M., Tuli,R., Hickok,N.J., Danielson,K.G., and Tuan,R.S. (2002). Multilineage mesenchymal differentiation potential of human trabecular bone-derived cells. J. Orthop. Res. *20*, 1060-1069.

O'Brien,F.J., Harley,B.A., Yannas,I.V., and Gibson,L.J. (2005). The effect of pore size on cell adhesion in collagen-GAG scaffolds. Biomaterials *26*, 433-441.

O'Connor,F.G., Howard,T.M., Fieseler,C.M., and Nirschl,R.P. (1997). Managing Overuse Injuries: A Systematic Approach. Phys Sports Med *25*.

Oakes,B.W. (2004). Orthopaedic tissue engineering: from laboratory to the clinic. Med J Aust *180*, S35-S38.

Oakley,C. and Brunette,D.M. (1993). The sequence of alignment of microtubules, focal contacts and actin filaments in fibroblasts spreading on smooth and grooved titanium substrata. J. Cell Sci. *106*, 343-354.

Ogiso,B., Hughes,F.J., Davies,J.E., and McCulloch,C.A. (1992). Fibroblastic regulation of osteoblast function by prostaglandins. Cell Signal. *4*, 627-639.

Ogiso,B., Hughes,F.J., Melcher,A.H., and McCulloch,C.A. (1991). Fibroblasts inhibit mineralised bone nodule formation by rat bone marrow stromal cells *in vitro*. J Cell Physiol *146*, 442-450.

Ohtsubo,R., Matsui,M., Horiguchi,H., Ogata,T., Fujiwara,M., Nagasawa,T., and Kamma,H. (2000). Characterization of a human cell line derived from liposarcoma tissue: is the beta subunit of prolyl 4-hydroxylase specific for a fibroblastic phenoType In culture cells? *In vitro* Cell Dev Biol Anim *36*, 217-221.

Oliveira,A. and Reis,R. (2004). Pre-mineralisation of starch/polycrapolactone bone tissue engineering scaffolds by a calcium-silicate-based process. Journal of Materials Science: Materials in Medicine *15*, 533-540.

Ornitz,D.M. (2005). FGF signaling in the developing endochondral skeleton. Cytokine & Growth Factor Reviews *16*, 205-213.

Pahler,G. and Bruckner,R. (1982). Mechanical Properties and Structural Aspects of Binary Phosphate Glass Fibres. Journal of Non-Crystalline Solids *85*, 105-126.

Park,T.G. (2002). Perfusion culture of hepatocytes within galactose-derivatized biodegradable poly(lactide-co-glycolide) scaffolds prepared by gas foaming of effervescent salts. J. Biomed. Mater. Res. *59*, 127-135.

Proctor,C.S., Jackson,D.W., and Simon,T.M. (1997). Characterization of the repair tissue after removal of the central one-third of the patellar ligament. An experimental study in a goat model. J Bone Joint Surg Am *79*, 997-1006.

Radisic,M., Yang,L., Boublik,J., Cohen,R.J., Langer,R., Freed,L.E., and Vunjak-Novakovic,G. (2004). Medium perfusion enables engineering of compact and contractile cardiac tissue. Am J Physiol Heart Circ Physiol *286*, H507-H516.

Ricci,J.L., Gona,A.G., Alexander,H., and Parsons,J.R. (1984). Morphological characteristics of tendon cells cultured on synthetic fibers. J. Biomed. Mater. Res. *18*, 1073-1087.

Richards,R.G., Stiffanic,M., Owen,G.R., Riehle,M., Ap Gwynn,I., and Curtis,A.S.G. (2001). Immunogold labelling of fibroblast focal adhesion sites visualised in fixed material using scanning electron microscopy, and living, using internal reflection microscopy. Cell Biology International *25*, 1237-1249.

Richman,G.P., Tirrell,D.A., and Asthagiri,A.R. (2005). Quantitatively distinct requirements for signaling-competent cell spreading on engineered versus natural adhesion ligands. Journal of Controlled Release *101*, 3-12.

Roolker,W., Patt,T.W., van Dijk,C.N., Vegter,M., and Marti,R.K. (2000). The Gore-Tex prosthetic ligament as a salvage procedure in deficient knees. Knee Surg Sports Traumatol Arthrosc *8*, 20-25.

Sagarriga Visconti,C., Kavalkovich,K., Wu,J., and Niyibizi,C. (1996). Biochemical analysis of collagens at the ligament-bone interface reveals presence of cartilage-specific collagens. Arch Biochem Biophys *328*, 135-42.

Sage,E.H. (2001). Regulation of interactions between cells and extracellular matrix: a command performance on several stages. J. Clin. Invest. *107*, 781-783.

Sage,H., Vernon,R., Funk,S., Everitt,E., and Angello,J. (1989). SPARC, a secreted protein associated with cellular proliferation, inhibits cell spreading *in vitro* and exhibits Ca+2-dependent binding to the extracellular matrix. J. Cell Biol. *109*, 341-356.

Salgado,A.J., Coutinho,O.P., and Reis,R.L. (2004). Bone tissue engineering: state of the art and future trends. Macromol. Biosci. *4*, 743-765.

Salih,V., Franks,K., James,M., Hastings,G.W., Knowles,J.C., and Olsen,I. (2000). Development of soluble glasses for biomedical use Part II: the biological response of human osteoblast cell lines to phosphate-based soluble glasses. J. Mater. Sci. Mater. Med. *11*, 615-620.

Salih,V., Franks,K., James,M., Hastings,G.W., Knowles,J.C., and Olsen,I. (2000). Development of soluble glasses for biomedical use Part II: the biological response of human osteoblast cell lines to phosphate-based soluble glasses. J Mater Sci Mater Med *11*, 615-20.

Salih,V., Knowles,J.C., O'Hare,M.J., and Olsen,I. (2001). Retroviral transduction of alveolar bone cells with a temperature- sensitive SV40 large T antigen. Cell Tissue Res *304*, 371-376.

Sambrook,P., Schrieber,L., and Ellis,A. (2001). The Musculoskeletal System: Basic Science and Clinical Conditions. Churchill Livingstone).

Sanchis-Alfonso,V., Lopez,A., Monteagudo-Castro,C., and Rosell-Sastre,E. (1999). Healing of the patellar tendon donor defect created after central-third patellar tendon autograft harvest. Knee Surg Sports Traumatol Arthrosc *7*, 340-348.

Satriano,C., Manso,M., Gambino,G.L., Rossi,F., and Marletta,G. (2005). Adsorption of a cell-adhesive oligopeptide on polymer surfaces irradiated by ion beams. Biomed Mater Eng *15*, 87-99.

Schliephake,H. (2002). Bone growth factors in maxillofacial skeletal reconstruction. Int J Oral Maxillofac Surg *31*, 469-484.

Scolaro,E.J., Ames,R.P., and Brittingham,A. (2005). Growth-Phase Dependent Substrate Adhesion in Crithidia fasciculata. The Journal of Eukaryotic Microbiology *52*, 17-22.

Scott,J.E. (2003). Elasticity in extracellular matrix 'shape modules' of tendon, cartilage, etc. A sliding proteoglycan-filament model. J. Physiol. *553*, 335-343.

Scott,J.E. (2004). Our shape is elastic, modular and held together by carbohydrate strings. Physiology News 22-24.

Shah,R., Sinanan,A.C., Knowles,J.C., Hunt,N.P., and Lewis,M.P. (2005). Craniofacial muscle engineering using a three-dimensional phosphate glass fibre construct. Biomaterials *26*, 1497-1505.

Shane Croughan,M., Sayre,H.S., and Wang,D.I.C. (1988). Viscous reduction of turbulent damage in animal cell culture. Biotechnol. Bioeng. *60*, 48-53.

Shieh,M. (2000). Control of Bone Cell Functions on Three-Dimensional Tissue Engineering Scaffolds. The MIT Biology Undergraduate Journal *3*, 195-204.

Shin,H., Zygourakis,K., Farach-Carson,M.C., Yaszemski,M.J., and Mikos,A.G. (2004). Attachment, proliferation, and migration of marrow stromal osteoblasts cultured on biomimetic hydrogels modified with an osteopontin-derived peptide. Biomaterials *25*, 895-906.

Sikavitsas,V.I., Temenoff,J.S., and Mikos,A.G. (2001). Biomaterials and bone mechanotransduction. Biomaterials *22*, 2581-2593.

Sommerfeldt,D.W. and Rubin,C.T. (2001). Biology of bone and how it orchestrates the form and function of the skeleton. Eur. Spine J *10 Suppl 2:S86-95.*, S86-S95.

Song,E.K., Rowe,S.M., Chung,J.Y., Moon,E.S., and Lee,K.B. (2004). Failure of osteointegration of hamstring tendon autograft after anterior cruciate ligament reconstruction. Arthroscopy *20*, 424-428.

Soon,M., Neo,C.P., Mitra,A.K., and Tay,B.K. (2004). Morbidity following anterior cruciate ligament reconstruction using hamstring autograft. Ann Acad Med Singapore *33*, 214-9.

Spalazzi,J.P., Dionisio,K.L., Jiang,J., and Lu,H.H. (2003). Osteoblast and chondrocyte interactions during coculture on scaffolds. IEEE Eng Med. Biol. Mag. *22*, 27-34.

Stangl,R., Rinne,B., Kastl,S., and Hendrich,C. (2001). The influence of pore geometry in cp Ti-implants--a cell culture investigation. Eur. Cell Mater. *2:1-9.*, 1-9.

Steenbrugge,F., Verdonk,R., Vorlat,P., Mortier,F., and Verstraete,K. (2001). Repair of chronic ruptures of the anterior cruciate ligament using allograft reconstruction and a ligament augmentation device. Acta Orthop Belg *67*, 252-8.

Suszcynsky,D.M. and Borovsky,J.E. (1992). Modified Sternglass theory for the emission of secondary electrons by fast-electron impact. PHYSICAL. REVIEW. A *45*, 6424-6428.

Tall,A.R., Small,D.M., and Lees,R.S. (1978). Interaction of collagen with the lipids of tendon xanthomata. J Clin Invest *62*, 836-846.

Termine,J.D., Kleinman,H.K., Whitson,S.W., Conn,K.M., McGarvey,M.L., and Martin,G.R. (1981). Osteonectin, a bone-specific protein linking mineral to collagen. Cell *26*, 99-105.

Thamaraiselvi,T.V. and Rajeswari,S. (2004). Biological Evaluation of Bioceramic Materials - A Review. Trends Biomater. Artif. Organs *18*, 9-17.

Thomas,G.J., Poomsawat,S., Lewis,M.P., Hart,I.R., Speight,P.M., and Marshall,J.F. (2001). alphavbeta6 Integrin Upregulates Matrix Metalloproteinase 9 and Promotes Migration of Normal Oral Keratinocytes. Journal of Investigative Dermatology *116*, 898-904.

Thompson,I.D. and Hench,L.L. (1998). Mechanical properties of bioactive glasses, glass-ceramics and composites. Proc. Instn Mech. Engrs *212*, 127-136.

Toledo-Pereyra,L.H. and Lopez-Neblina,F. (2003). Xenotransplantation: a view to the past and an unrealized promise to the future. Exp Clin Transplant *1*, 1-7.
Ulf,A., Julia,P., Guido,H., and Anja,S. (2002). Minocycline does not alter collagen Type I metabolism of dermal fibroblasts in culture. Arch Dermatol Res *294*, 103-108.

Scott,J.E. (2003). Elasticity in extracellular matrix 'shape modules' of tendon, cartilage, etc. A sliding proteoglycan-filament model. J. Physiol. *553*, 335-343.

Scott,J.E. (2004). Our shape is elastic, modular and held together by carbohydrate strings. Physiology News 22-24.

Uo,M., Mizuno,M., Kuboki,Y., Makishima,A., and Watari,F. (1998). Properties and cytotoxicity of water soluble Na2O-CaO-P2O5 glasses. Biomaterials *19*, 2277-2284.

Vacanti,J.P., Langer,R., Upton,J., and Marler,J.J. (1998). Transplantation of cells in matrices for tissue regeneration. Adv Drug Deliv Rev *33*, 165-182.

van Beurden,H.E., Von den Hoff,J.W., Torensma,R., Maltha,J.C., and Kuijpers-Jagtman,A.M. (2005). Myofibroblasts in palatal wound healing: prospects for the reduction of wound contraction after cleft palate repair. J. Dent. Res. *84*, 871-880.

Van Griensven,M., Zeichen,J., Skutek,M., Barkhausen,T., Krettek,C., and Bosch,U. (2003). Cyclic mechanical strain induces NO production in human patellar tendon fibroblasts - a possible role for remodelling and pathological transformation. Experimental and Toxicologic Pathology *54*, 335-338.

Van Kampen,C.L. (1994). Biomechanics of synthetic augmentation of ligament reconstructions. Clinical Materials *15*, 23-27.

Van Sliedregt,A., Knook,M., Hesseling,S.C., Koerten,H.K., de Groot,K., and van Blitterswijk,C.A. (1992). Cellular reaction on the intraperitoneal injection of four types of polylactide particulates. Biomaterials *13*, 819-24.

Van Sliedregt,A., van Loon,J.A., van der Brink,J., de Groot,K., and van Blitterswijk,C.A. (1994). Evaluation of polylactide monomers in an *in vitro* biocompatibility assay. Biomaterials *15*, 251-6.

Van,S.A., van Loon,J.A., van der,B.J., de,G.K., and van Blitterswijk,C.A. (1994). Evaluation of polylactide monomers in an *in vitro* biocompatibility assay. Biomaterials *15*, 251-256.

Verdonschot N, van Hal CT, Schreurs BW, Buma P, Huiskes R, and Slooff TJ (2001). Time-dependent mechanical properties of HA/TCP particles in relation to morsellized bone grafts for use in impaction grafting. J Biomed Mater Res.

Vogelin,E., Jones,N.F., Huang,J.I., Brekke,J.H., and Toth,J.M. (2000). Practical illustrations in tissue engineering: surgical considerations relevant to the implantation of osteoinductive devices. Tissue Eng *6*, 449-460.

Wan,Y., Yang,J., Yang,J., Bei,J., and Wang,S. (2003). Cell adhesion on gaseous plasma modified poly-(-lactide) surface under shear stress field. Biomaterials *24*, 3757-3764.

Webster,T.J., Siegel,R.W., and Bizios,R. (1999). Osteoblast adhesion on nanophase ceramics. Biomaterials *20*, 1221-1227.

Weintraub,W. (2003). The nature of tendons and ligaments. In Tendon And Ligament Healing: A New Approach to Sports and Overuse Injury, W.Weintraub, ed. Paradigm Publications), pp. 11-50.

Weiss,L. (1983). Cell and tissue biology : a textbook of histology. (Baltimore: Urban & Schwarzenberg).

Wen,H.B., de Wijn,J.R., Cui,F.Z., and de Groot,K. (1998). Preparation of calcium phosphate coatings on titanium implant materials by simple chemistry. J Biomed Mater Res *41*, 227-36.

Wiedmann-Al-Ahmad,M., Gutwald,R., Lauer,G., Hubner,U., and Schmelzeisen,R. (2002). How to optimize seeding and culturing of human osteoblast-like cells on various biomaterials. Biomaterials *23*, 3319-3328.

Wieslander,A.P., Nordin,M.K., Hansson,B., Baldetorp,B., and Kjellstrand,P.T. (1993). *In vitro* toxicity of biomaterials determined with cell density, total protein, cell cycle distribution and adenine nucleotides. Biomater. Artif. Cells Immobilization Biotechnol. *21*, 63-70.

Winet,H. and Bao,J.Y. (1997). Comparative bone healing near eroding polylactide-polyglycolide implants of differing crystallinity in rabbit tibial bone chambers. J. Biomater. Sci. Polym. Ed *8*, 517-532.

Winslow, T. Stem Cells: Scientific Progress and Future Research Directions. 2001. Maryland, Department of Health and Human Services, USA. Ref Type: Report

Wolfe,J. and Bryant,G. (1999). Freezing, Drying, and/or Vitrification of Membrane-Solute-Water Systems. Cryobiology *39*, 103-129.

Wolfman,N.M., Hattersley,G., Cox,K., Celeste,A.J., Nelson,R., Yamaji,N., Dube,J.L., DiBlasio-Smith,E., Nove,J., Song,J.J., Wozney,J.M., and Rosen,V. (1997). Ectopic Induction of Tendon and Ligament in Rats by Growth and Differentiation Factors 5,á6,áand 7,áMembers of the TGF-beta Gene Family. J. Clin. Invest. *100*, 321-330.

Wredmark,T. and Engstrom,B. (1993). Five-year results of anterior cruciate ligament reconstruction with the Stryker Dacron high-strength ligament. Knee Surg Sports Traumatol Arthrosc *1*, 71-5.

Xiao,G., Wang,D., Benson,M.D., Karsenty,G., and Franceschi,R.T. (1998). Role of the alpha2-integrin in osteoblast-specific gene expression and activation of the Osf2 transcription factor. The Journal Of Biological Chemistry *273*, 32988-32994.

Xinmin,L., Jaejung,K., Jian,Z., Weikuan,G., and Richard,Q. (2005). Use of signal thresholds to determine significant changes in microarray data analyses. Genet. Mol. Biol *28*, 191-200.

Xynos,I.D., Hukkanen,M.V., Batten,J.J., Buttery,L.D., Hench,L.L., and Polak,J.M. (2000). Bioglass 45S5 stimulates osteoblast turnover and enhances bone formation *In vitro*: implications and applications for bone tissue engineering. Calcif Tissue Int *67*, 321-329.

Yasuda,K., Kondo,E., Ichiyama,H., Tanabe,Y., and Tohyama,H. (2005). Surgical and biomechanical concepts of anatomic anterior cruciate ligament reconstruction. Operative Techniques in Orthopaedics *15*, 96-102.

Zelzer,E. and Olsen,B.R. (2003). The genetic basis for skeletal diseases. Nature *423*, 343-348.

Zhang,G., Young,B.B., Ezura,Y., Favata,M., Soslowsky,L.J., Chakravarti,S., and Birk,D.E. (2005). Development of tendon structure and function: Regulation of collagen fibrillogenesis. J Musculoskelet Neuronal Interact *5*, 5-21.

Zur Nieden,N.I., Kempka,G., and Ahr,H.J. (2003). *In vitro* differentiation of embryonic stem cells into mineralized osteoblasts. Differentiation *71*, 18-27.

Available online at www.sciencedirect.com
SCIENCE DIRECT®
Biomaterials 25 (2004) 2283–2292
Biomaterials
www.elsevier.com/locate/biomaterials

Soluble phosphate glasses: in vitro studies using human cells of hard and soft tissue origin

Malak Bitar[a], Vehid Salih[b,*], Vivek Mudera[a], Jonathan C. Knowles[a], Mark P. Lewis[a]

doi:10.1016/j.biomaterials.2003.08.054

JOURNAL OF MATERIALS SCIENCE: MATERIALS IN MEDICINE 16 (2005) 1131–1136

Soluble phosphate glass fibres for repair of bone-ligament interface

M. BITAR, J. C. KNOWLES, M. P. LEWIS, V. SALIH*

0957–4530